School of Design and the Built Environment

Automatic 3D Reconstruction for As-built Underground Utilities

Yang Su

0000-0002-6290-2128

This thesis is presented for the Degree of
Doctor of Philosophy
of
Curtin University

June 2024

Declaration

To the best of my knowledge and belief this thesis contains no material previously published by any other person except where due acknowledgment has been made.

This thesis contains no material which has been accepted for the award of any other degree or diploma in any university.

Signature:

Date: June 18th 2024

(left blank)

Acknowledgement

First and foremost, I extend my deepest appreciation to my esteemed supervisors, Associate Professor Brad Carey, Professor Peng Wu, Dr. Jun Wang, Professor Xiangyu Wang and Dr. Danqi Li. Their exceptional mentorship, boundless knowledge, and unwavering dedication have been the cornerstone of my academic journey. Their insightful feedback, constructive criticism, and continuous encouragement have challenged me to push my boundaries and strive for excellence. I am profoundly grateful for their patient guidance, which has shaped my research and enriched my understanding of the subject.

I am also indebted to my dedicated colleagues and fellow researchers, Yongze Song, Junxiang Zhu, Chengke Wu, Rui Jiang, Wenchi Shou, Yuan Yao, who have shared their expertise, insights, and camaraderie throughout this academic odyssey. The intellectual exchange and collaborative spirit within our research group have been invaluable in shaping my ideas and expanding my horizons. Their friendship and willingness to engage in stimulating discussions have created a vibrant academic environment that I am honoured to have been a part of.

This study would not be possible without the financial support from the Linkage Projects of Australian Research Council (LP180100222). And I wish to extend my sincere gratitude to the esteemed colleagues within the School of Design and Built Environment, notably including Dr. Swapan, whose invaluable assistance greatly facilitated both my academic pursuits and personal endeavors at Curtin University.

Finally, to my loving family, I extend my heartfelt gratitude for their unwavering support, love, and understanding. Their belief in my abilities has been my constant source of motivation, and their sacrifices have allowed me to focus on my studies and research with unwavering determination. Thank you, mom. Thank you, dad. Thank you, my dear wife Sunny. Thank you for being my rock, my confidante, and my biggest cheerleader.

(left blank)

Abstract

Underground utilities (UUs), such as water and sewage pipes, gas, and oil pipelines, and communications and data cables, are important infrastructures for ensuring the operation of various essential functions of a city. Up-to-date and accurate three-dimensional (3D) reconstruction, which includes the reconstruction of the horizontal position, depth, and topological information of the UU target, is the cornerstone for informed decision making in each stage of the UU life-cycle asset management, such as UU planning and (re)development, ownership management, construction, safety management, and operation and maintenance (O&M). However, obtaining an accurate 3D reconstruction has always been considered as a challenging task.

In non-destructive scenarios, where the pipeline is under the soil cover, obtaining accurate results for the UU 3D reconstruction task is often difficult. In engineering practice, the most popular UU 3D information detection method is ground-penetrating radar (GPR), which can efficiently and stably reconstruct most metal and non-metal utilities by identifying the hyperbolic apex in GPR B-scan images. However, existing image-processing methods are highly sensitive to noise information in the input, and the precision of the output results is inadequate. In recent years, although deep-learning based object detection method can improve the stability of recognition, it still faces the problem of error accumulation due to the decomposition of the apex localisation into two sub-problems of bounding box detection and hyperbola fitting, which affects the precision of UU positioning.

In exposed scenarios, asset managers and technicians can inspect the pipeline in the maintenance, repair, or installation phase, but it is still very difficult to accurately reconstruct the UU target under low-light conditions, such as dusk and night. In existing studies, image-based 3D reconstruction and laser scanning have proven to be effective and promising for reconstruction. However, the effectiveness of the laser-scanning method depends heavily on the device itself and is expensive to use. Image-based 3D reconstruction methods benefit from lower equipment costs as they utilize standard photographic equipment, which is generally less expensive and more readily

available than specialized laser scanners. Additionally, these methods require less specialized training for personnel, further reducing overall project costs compared to the 3D laser scanning method. However, the reconstruction effectiveness is greatly reduced under low-light conditions. The important issue of improving the UU image-based 3D reconstruction performance under low-light conditions remains unresolved.

The collection of UU topological information is an essential task in 3D reconstruction. The topological connection between the pipeline (or cable) nodes is related to the transportation and connectivity functions of the UU network. However, obtaining accurate topological information, owing to the age of installations or imprecise records, is often difficult. In existing studies, the traditional manual inspection method is primarily used to obtain missing data; however, this method is expensive and inefficient. Additionally, there are studies using imputation or machine-learning methods to predict the missing attribute information in the UU network; however, these methods cannot perform tasks related to the completion of topological relations. Alternative low-cost and accurate methods are required for the completion of topology information.

To address the above problems, this study develops a novel approach for improving the 3D reconstruction accuracy of UUs at different stages and supplying missing topology information. First, an end-to-end UU localisation (EUUL) deep-learning model using GPR B-scan data is proposed and validated. It adopts a key point-regression mode instead of the box-fitting mode that realises end-to-end learning and trains the model. An anchor-free structure with a lightweight backbone is applied to the EUUL model to improve the processing time. To manage the noise interference of the UU positioning data, a channel attention mechanism is added to the EUUL model, so that the model can focus on key task features to ensure precision. The experimental results with real-site GPR data demonstrate that the proposed EUUL model achieves a significant localisation precision of 97.01% and an inference speed of 125 fps. These results outperform existing mainstream models, namely YOLOv3 (91.67%, 82 fps) and Faster region convolutional neural networks (R-CNNs) (65.52%, 20 fps). This

indicates that the proposed method effectively enhances the precision of GPR interpretation, while concurrently reducing the processing time. Second, a zero-reference deep-learning model for low-light image enhancement of UU 3D reconstruction (ZDE3D) is proposed and validated. ZDE3D improves the 3D reconstruction performance of low-light images using an unsupervised loss-function design without paired or unpaired training datasets. Field experiments confirm that ZDE3D can effectively increase the quantity of sparse reconstruction point clouds by an average of 13.19% compared to the reconstruction output based on original low-light images. Additionally, the reconstruction accuracy achieves a significant value of 98.58%. This demonstrates that the proposed method can effectively enhance 3D reconstruction in low-light working environments without compromising reconstruction accuracy. Third, this thesis introduces the UUs topology-completion (UUTC) model based on the application of graph convolutional network (GCN) techniques. A comprehensive evaluation of the proposed model is conducted by performing a series of experiments using a real wastewater network database in France. This evaluation employs five prominent GCN models, focusing on the missing rates of topological data. The experimental results demonstrate that the average topological relationship completeness ratio of the proposed UUTC model reached 85.33%, which surpasses the performance of the existing mainstream methods (GCN 76.78%, ChebGCN 76.37%, SAGEGCN 79.37%, GTAGCN 80.85%, and TAGCN 79.44%). The proposed method is effective in enhancing the accuracy of UU topological information completion, thereby assisting stakeholders in making informed decisions.

The theoretical contributions of this study are twofold. First, the proposed EUUL model overcomes the error accumulation problem in the UU localisation task based on GPR B-scan images in existing research. Second, the ZDE3D model integrates domain knowledge into unsupervised deep learning, which improves the effectiveness of image-based UU 3D reconstruction under low-light conditions. This study has several practical implications. First, a more accurate as-built UU 3D reconstruction can effectively improve project safety management. Personal injuries and property losses caused by accidental damage to pipelines can be avoided by accurately predicting the

location of the utilities. Second, unnecessary costs can be reduced using a more accurate as-built UU 3D reconstruction model. The number of design and construction changes will be significantly reduced, thereby avoiding cost losses due to congestion and rework. Third, convenient topological relationship prediction can effectively reduce the time required to obtaining all project topological data and improve management efficiency. The proposed approach can provide a more systematic and precise assessment of UU network topology relationships. This is beneficial for shortening the preliminary survey time for new construction UU and maintenance projects.

Table of contents

List of figures

List of tables

List of abbreviations

ACC	Accuracy
AE	Acoustic Emission
AP	Average Precision
AMELIA	Multiple Imputations of Incomplete Multivariate Data
ANNs	Artificial Neural Networks
AI	Artificial Intelligence
AR	Augmented Reality
AUC	Area Under Curve
AVM	Alkali Vapour Magnetometer
BA	Bundle Adjustment
CAT	Cable Avoidance Tool
ChebGCN	Chebyshev Graph Convolutional Network
CSP	Cross-Stage Partial
CPU	Central Processing Unit
CSVM	Convolutional Support Vector Machine
CNN	Convolutional Neural Network
CT-GNN	Cross-Task Graph Neural Network
CV	Computer Vision
DGL	Deep Graph Library
DT	Decision Trees
DT	Destructive Technologies
DT	Digital Twins
ECA	Efficient Channel Attention

ELU	Exponential Linear Unit
EMI	Electromagnetic Induction
EUUL	End-to-end Underground Utility Localisation
FAST	Features from Accelerated Segment Test
FM	Flux-gate Magnetometer
FN	False Negative
FP	False Positive
FPR	False-Positive Rates
fps	Frames per Second
GAN	Generative Adversarial Network
GATGCN	Graph Attention Graph Convolutional Network
GCN	Graph Convolutional Network
GIS	Geographic Information Systems
GPR	Ground-Penetrating Radar
GPS	Global Position System
HDR	High-Dynamic Range
HT	Hough Transform
ICP	Iterative Closest Point
IMPSEQ	Sequential Imputation for missing values
IMU	Inertial Measurement Unit
IRMI	Iterative Robust Model-based Imputation
IRT	Infrared Thermography
KNN	K-Nearest Neighbour
LLNet	Low-light Image Enhancement
LSTM	Long Short-Term Memory
MLP	Multilayer Perceptron
MTU	Mapping the Underworld
MVS	Multi-View Stereo

NDT	Non-Destructive Technologies
NNs	Neural Networks
O&M	Operation and Maintenance
PCA	Principal Component Analysis
PCL	Pipe and Cable Locator
PnP	Point-n-Points
PPM	Proton Precession Magnetometer
PSMNet	Pyramid Stereo Matching Network
ReLU	Rectified Linear Unit
RFID	Radio-Frequency Identification
RGB	Red Green Blue
RGB-D	Red Green Blue-Depth
ROC	Receiver Operating Characteristic
R-CNN	Region-Convolutional Neural Network
SAGEGCN	Structure-Aware Deep Graph Convolutional Networks
SEM	Similarity Extraction Module
SFM	Structure from Motion
SIFT	Scale-Invariant Feature Transform
SQUID	Superconducting Quantum Interference Device
SSD	Single Shot MultiBox Detector
SURF	Speeded Up Robust Features
SVM	Support Vector Machine
TAGCN	Topology Adaptive Graph Convolutional Networks
TM	Template Matching
TN	True Negative
ToF	Time of Fly
TP	False Positive
TPR	True Positive Rate

UU	Underground Utilities
UUDM	Underground Utility Data Model
UUTC	Underground Utilities Topology Completion
UUOI	Underground Utility Occupation Index
UWDT	Underground World Digital Twin
VR	Virtual Reality
vSLAM	visual Simultaneous Localisation and Mapping
WDSs	Water Distribution systems
WWP	Wastewater Treatment Plants
YOLO	You Only Look Once
YOLOv3	You Only Look Once version 3
Zero-DCE	Zero-Reference Deep Curve Estimation
ZDE3D	Zero-reference Deep-Learning Model for the Low-light Image Enhancement of Underground Utilities 3D Reconstruction

List of publications

A. Journal paper (* corresponding author)

1. **Su, Y.,** Wang, J*., Li, D., Wang, X., Hu, L., Yao, Y., & Kang, Y. (2023). End-to-end deep learning model for underground utilities localisation using GPR. Automation in Construction, 149, 104776.

2. **Su, Y.,** Wang, J*., Wang, X., Hu, L., Yao, Y., Shou, W., & Li, D. (2023). Zero-reference deep learning for low-light image enhancement of underground utilities 3D reconstruction. Automation in Construction, 152, 104930.

3. **Su, Y.,** Wang, J*., Wang, X., Yao, Y., & Shou, W. (2023). 3D reconstruction in underground utilities. Automation in Construction, 156, 105100.

4. **Yang Su,** Jun Wang*, Peng Wu, Chengke Wu, Aobo Yue, Wenchi Shou. (2023). Automatic Completion of Underground Utility Topologies Using Graph

Convolutional Networks. Journal of Computing in Civil Engineering. (Under Review)

B. Journal paper (* corresponding author)

1. **Yang, Su.,** Qian, Jia., Yuan Yao., Jun Wang*****. (2022). A review of GPR application on underground utilities: limitations and the best performance. World Building Conference 2022 (Melbourne, Australia).

Chapter 1 : Introduction

1.1 Background

Underground utilities (UUs) play a pivotal role in supporting modern urban life, as they are an essential component of urban infrastructure (Yan et al., 2021; Yan et al., 2019; Meijer et al., 2022). The UU infrastructure is continuously transporting water, electricity, gas, and other essential resources that support urban life globally, while also collecting and disposing pollutants generated by residents' daily activities. Based on their specific functions, the common types of UUs can be classified, as shown in Table 1-1.

Table 1-1 Common underground utilities (UUs) and functions

No.	Categories	Functions
1	Water supply pipes	Transporting potable water from treatment plants or wells to residential, commercial, and industrial properties for drinking, cooking, cleaning, and other uses.
2	Sewer pipes	Transporting wastewater and sewage from residential, commercial, and industrial properties to wastewater treatment plants for processing and treatment.
3	Stormwater drainage pipe	Collecting and transporting rainwater and other surface runoff to prevent flooding and erosion in streets and public areas.
4	Gas pipelines	Transporting natural or propane gas to residential, commercial, and industrial properties for heating and cooking purposes.
5	Electrical cables	Transporting electrical power from

No.	Categories	Functions
		substations to homes and businesses for lighting, heating, cooling, and operating electrical equipment.
6	Telecommunications cables	Providing voice and data communication services, such as telephone, internet, and video conferencing, to homes and businesses.
7	Fibre optic cables	Providing high-speed internet, telephone, and cable-TV services to homes and businesses.
8	Heating and cooling pipelines	Transporting hot or cold water or steam for heating, cooling, or process applications.
9	Fuel pipelines	Transporting liquid or gaseous fuels, such as gasoline, diesel, or propane, to fuel stations or industrial facilities.

UUs are typically invisible when used. Creating an accurate, up-to-date, and comprehensive three-dimensional (3D) reconstruction (digital 3D representation of as-built UUs) has become one of the most important priorities for infrastructure life-cycle management, such as ownership management, land acquisition, planning and (re)development, construction recording, operation and maintenance (O&M), and safety management. All these activities require an accurate 3D representation of the UU. 1) Ownership management. As the urban population continues to increase worldwide, the density and complexity of UU distribution are also increasing. In an invisible underground space, pipe networks of different ownership types are often intertwined. The as-built 3D reconstruction can intuitively and visually help managers clarify their scope of ownership and avoid disputes. 2) Land acquisition. Before implementing an above-ground construction project, it is necessary to obtain a thorough inventory of the UUs within the area it occupies to ensure that there is no

design function interference. During this process, management efficiency is greatly improved if all stakeholders have an accurate 3D representation model in the target area. 3) Planning and (re)development. Whether in a completely new UU or reconstruction and expansion project, an accurate 3D reconstruction model is the basic information required for the design plan. Accurate and complete as-built information can effectively avoid design errors and claims, thereby reducing project costs. 4) Safety management. Accidents where pipelines are accidentally damaged during UU construction occur occasionally. According to the US Pipeline and Hazardous Materials Safety Administration (2021), 12,505 pipeline accidents have occurred between 2001 and 2020, resulting in 270 fatalities, 1,176 injuries, and $9.95 billion in property losses. According to an investigation report released by the Underground Pipeline Professional Committee of the China Urban Planning Association (2022), 737 underground-pipeline damage accidents occurred in China from October 2019 to September 2020, resulting in 166 fatalities, an increase of 130.14% from the previous year. 5) O&M. During O&M, a reliable UU 3D-reconstruction model can help managers rapidly locate fault locations and reduce management costs. A reliable UU 3D-reconstruction model enables managers to quickly pinpoint the exact location of faults without the need for disruptive and time-consuming ground excavation, thereby minimizing the need for extensive physical inspections and reducing the time and labor typically required to diagnose and resolve faults.

The 3D reconstruction of UUs can be divided into three parts according to their demands: non-destructive reconstruction, exposed reconstruction, and topology reconstruction.

Non-destructive reconstruction. In most UU 3D-reconstruction scenarios, pipelines are covered by soil layers, and special equipment is required for positioning under non-excavatable conditions to map out a 3D model of the target area. Non-destructive reconstructions commonly used in engineering practice include ground-penetrating radar (GPR), radio-frequency identification (RFID), electromagnetic induction (EMI), acoustic emission (AE), thermography, and IMU-based system methods. What is

common among these methods is that without excavation, the signal difference generated by physical signals, such as electromagnetic waves, sound waves, and thermal radiation passing through the target UU area, is used for positioning analysis. Considering the most popular GPR method as an example, it uses the propagation law of high-frequency electromagnetic waves in different media to realise the non-destructive reconstruction of underground pipe networks. Figure 1-1 shows the generation principle of a GPR B-scan hyperbola in a UU 3D-reconstruction scene. First, the transmitting antenna sends an electromagnetic-wave signal to the UU. Subsequently, the signal formed by the UU is received by the receiving antenna. When the GPR passes through a position directly above the UU object (such as at the time of T_1), the antenna can receive the signal reflected by the UU in the shortest duration; therefore, the distance between the UU and GPR device recorded in the B-scan image is the shortest (S_1) for the same signal propagation speed. When the GPR is at other target positions (e.g. at the time of T_0 and T_2), the receiving antenna can similarly obtain the signal formed by the reflection of the UU target. However, the distance between the GPR and the target (denoted by S_0 and S_2, respectively) is larger than that of S_1; consequently, the distance between the UU and GPR devices recorded in the B-scan image will be larger. Therefore, the radar signal shows a shape resembling a hyperbola (lower half) in the B-scan image. Based on the above characteristics, the position of the UU can be obtained by detecting the hyperbola area and searching for its apex (the red point in the right section of Figure 1-1).

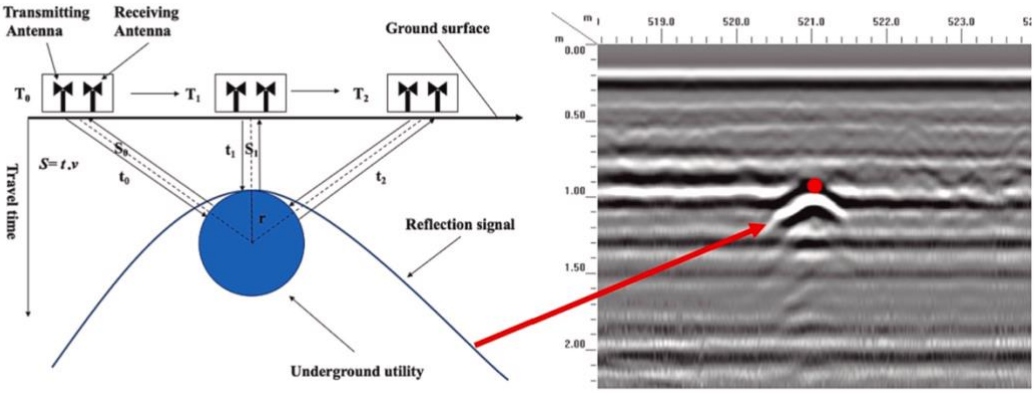

Figure 1-1 Schematic of the working principle of ground-penetrating radar

Exposed reconstruction. In some stages, underground facilities can be temporarily exposed, such as when pipeline installation is completed (before covering the soil) and during pipeline excavation repair and maintenance. In these scenarios, technologies other than non-destructive reconstruction are required to perform exposed reconstruction on UU. Currently, the most common exposed reconstruction (or destructive reconstruction) technologies include laser scanning and photogrammetry (image-based 3D reconstruction): 1) Laser-scanning technology uses laser radar equipment to scan the exposed UU surface from multiple angles to form point-cloud model information for 3D reconstruction. As shown in Figure 1-2, the laser-scanning method can rapidly establish accurate surface information features. The reconstruction process includes emitting laser beams, scanning the target surface to obtain point-cloud data, and pre-processing the acquired point-cloud data, including denoising, sampling, and registration operations. The purpose is to remove unnecessary noise points in the point cloud to facilitate further registration or measurement operations on the point cloud. The final step is to convert the point-cloud data into a 3D model. 3D-reconstruction algorithms include voxel-based, surface-based, and image-based methods. 2) The photogrammetry (image-based 3D reconstruction) method uses pictures or video stream data to collect image information from different angles of the same scene to generate a 3D model. The reconstruction process primarily uses image matching, triangulation, and beam method techniques to extract 3D coordinate information of the object, before converting it into a 3D model. Compared with the laser-scanning method, the photogrammetry method based on image data has a lower cost of obtaining data and is more convenient. Only a consumer-grade smartphone is needed to complete the reconstruction task quickly. More importantly, the photogrammetry method can record important attributes, such as the material and colour of the target, while collecting 3D spatial coordinate information. In contrast, the laser-scanning method can only collect spatial information. Figure 1-2 shows the steps and effects of UU 3D reconstruction using laser scanning and photogrammetry, respectively.

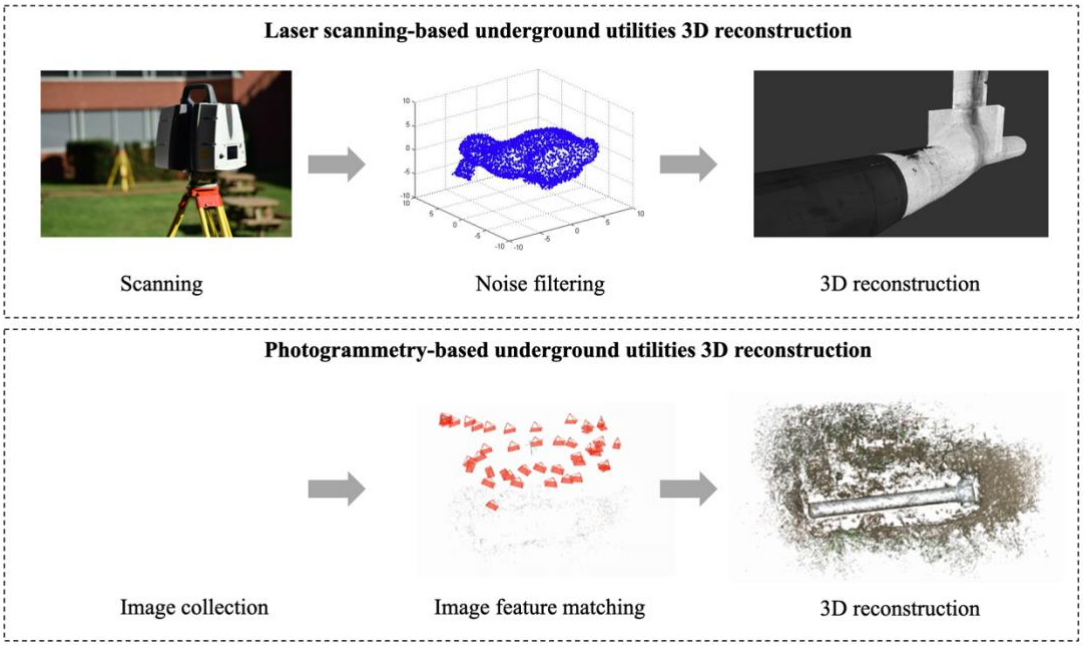

Figure 1-2 Steps and effects of UU 3D reconstruction using laser scanning and photogrammetry

Topology reconstruction. Topological information (interconnection relationship between pipelines) is necessary to fully demonstrate the UU network. Relying solely on the facilities' surface, the 3D model cannot accurately describe the real structure of the UU. However, neither non-destructive nor exposed reconstruction can detect the connection relationship between pipelines. The current main UU topological relationship reconstruction methods in engineering practice include: 1) Traditional manual method. Traversing the manhole and other facilities in the target area according to existing drawing records or combining GPR with manual inspection is still the mainstream method. This method has the advantage of accurate inspection; however, the costs of labour, equipment, and time are extremely high. 2) Database completion. Because a pipeline network is a complete system with practical significance, the topological relationship between various pipeline parts can be inferred from the observed partial information. Specifically, the inference of unknown topological relationships can be realised through imputation, machine learning, and graphs. Although the database completion method requires a certain amount of known information, it is highly effective in engineering practice. This is because, in most

cases, the pipeline network in the target area is not completely independent but exists as a part of the overall pipeline network. Therefore, the data-driven topology-completion method has a significant cost advantage, particularly for large-scale data scenarios.

An overview of this thesis is presented in Figure 1-3. The research was based on the 3D reconstruction key stages mentioned above (non-destructive, exposed, and topological), addressing specific engineering scenario requirements, and ultimately creating a more effective UU 3D reconstruction model. It is important to note that this thesis focuses exclusively on a detailed examination of the region outlined by the red dashed box in Figure 1-3. The roles of other areas lie in forming a comprehensive 3D reconstruction technical roadmap but are not the primary focus of this research.

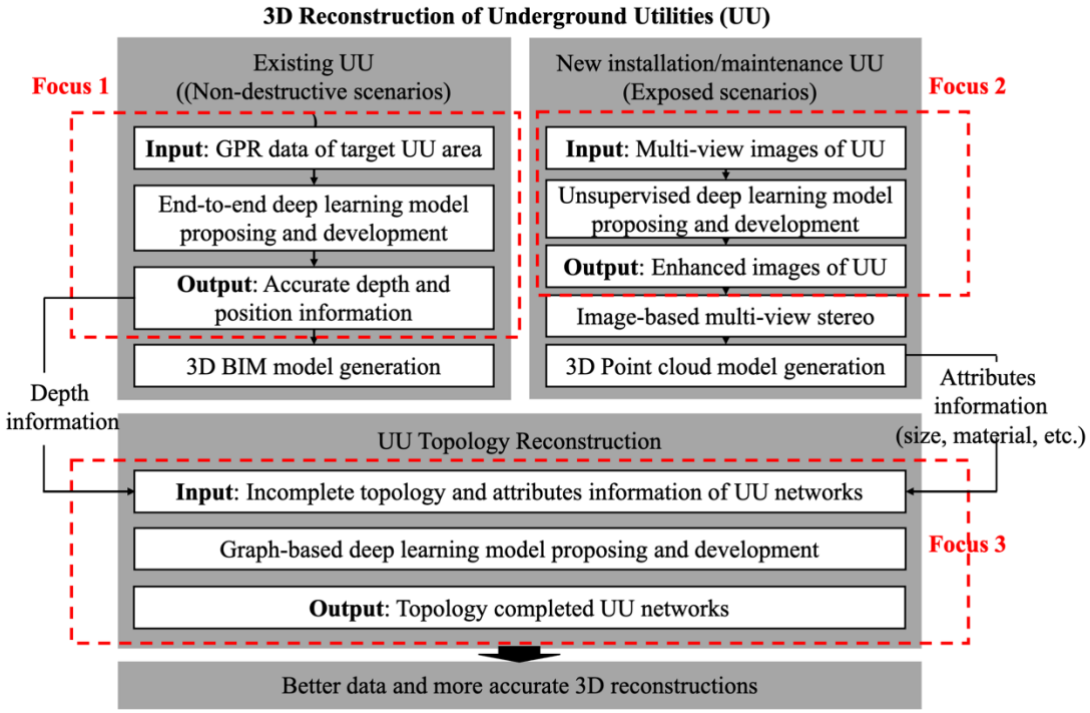

Figure 1-3 Study Overview

1.2 Problem statement

As cities continue to expand, the difficulty of managing the full life-cycle of UUs is also increasing. In response to the complex combination of infrastructure, water pipes, power supply, and storage space that crisscross underground spaces, countries have

proposed their own digital underground space representations to improve the management efficiency of UUs. In 2012, the UK University of Birmingham and other research institutions jointly proposed a project called MTU (Mapping the Underworld (University of Birmingham et al., 2012)) – which seeks to develop the means to locate, map in 3-D, and record using a single shared multi-sensor platform – the position of all buried utility assets without excavation. In 2017, the Singapore Land Authority, in collaboration with the Singapore-ETH Centre, developed a system called Imagining a digitally enabled future (Yan et al., 2021) for the digital twins of UUs to complement the 3D maps of the country and facilitate integrated planning and development. In Phase 1, it planned and identified what would be required in the roadmap to develop a coherent national subsurface utility mapping strategy. Starting in 2019, it embarked on a second phase, bringing the roadmap to life and supporting the ecosystem to generate and deliver accurate and complete digital data to stakeholders. Beginning in January 2022, Digital Underground has entered its third phase, and Singapore has the potential to become the world's leading laboratory for underground mapping.

However, the current 3D reconstruction of as-built UUs remains challenging in terms of providing accurate 3D representations for practice scenarios. The detailed problems are summarised below.

1.2.1 Inadequate research attention for UU 3D reconstruction

Various 3D reconstruction techniques have been widely applied to UUs. However, existing studies have the following limitations. 1) Some researchers reviewed the development process of 3D reconstruction technology and analysed some technical details of 3D reconstruction but only focused on the 3D reconstruction technology itself and ignored the application of technology in engineering context. For example, the works of Mark (2010), Hao et al. (2012), and Yu et al. (2021) provide comprehensive summaries of the principles of various technologies. However, they do not fully explore the characteristics and limitations of technology applications in engineering, such as the scalability of these technologies in large-scale infrastructure projects, their adaptability to varying environmental conditions, and the accuracy and

reliability of the data in complex urban settings. 2) Other review studies were published several years ago, therefore, have not captured recent technological advancements. For example, a summary of UU positioning technology and requirements was conducted by the US Federal Laboratory in 2000 (Federal Laboratory Consortium, 2000). Metje et al. (2007) summarised the MTU technology, and Liu and Kleiner (2013) reviewed underground exploration technology for water pipes. Therefore, these studies are not sufficiently specific and comprehensive for the field of UU 3D reconstruction and cannot guide the selection of UU 3D reconstruction technology in engineering practice. 3) There is also a need for research that systematically analyse various 3D reconstruction technologies using factors such as cost, accuracy, compatibility with existing systems, and operational feasibility to determine the most effective solution for specific needs.

1.2.2 Inefficient UU localisation precision in GPR interpretation

GPR, the most popular non-destructive method, has been widely applied in UU 3D reconstruction tasks. However, UU localisation based on B-scan images is challenging for the following reasons: 1) Owing to the electromagnetic-wave principal characteristics of GPR, the generation process of B-scan images is affected by various interference factors from the environment, such as electrical installations and tree roots, as well as from the device (Lei et al., 2019; Singh et al., 2013; Adouane et al., 2021). These noise sources further complicate the UU target recognition. 2) Unlike other GPR detection tasks, such as reinforcement localisation in concrete structures (Wang et al., 2020; Liu et al., 2020; Ahmed et al., 2020), UUs are buried deeper, composed of various material types, and surrounded by a more complex environment. The limitations of the task object are likely to deteriorate B-scan image quality.

The B-scan image generated by GPR must be analysed by domain experts to obtain accurate position information pertaining to the UU. UU localisation in GPR B-scan images is highly subjective and significantly depends on expert knowledge and engineering experience. Although many studies have been conducted to improve the automation of GPR B-scan data interpretation, the following limitations remain. First,

conventional methods involve complex processing steps that render them highly susceptible to environmental noise and yield unstable precision performance (Maas et al., 2013; Harkat et al., 2016; Sagnard et al., 2016). Second, existing deep-learning methods separate a problem into two sub-problems: box detection and hyperbola fitting (Lei et al., 2019; Harkart et al., 2019; Hou et al., 2021a; Zong et al., 2019). This allows the problem's solution to be obtained only from the local optimal solutions of the sub-problems and not the global optimal solution. In UU localization using GPR, deep learning methods typically divide the problem into sub-problems (the box detection and hyperbola fitting), each solved for what seems best within their limited scope, termed as "local solutions." However, this step-by-step approach can miss the overall best solution—or "global solution"—for the entire dataset, leading to errors and suboptimal performance when these local solutions are combined. Furthermore, this step-by-step solution results in greater error accumulation, which affects the UU localisation precision.

1.2.3 Inefficient image-based reconstruction performance under low-light scenarios

To date, there are two main technical routes for UU 3D reconstruction: image-based 3D reconstruction and laser scanning (Pătrăucean et al., 2015). Image-based 3D reconstruction utilises multi-view 2D image data to restore the UU target spatial information (Döner et al., 2011; Yan et al., 2018). Laser scanning collects 3D spatial information of the UU surface through the Time of Fly (ToF), which is the time interval between the transmission and reception of pulses (Bosché et al., 2015; Wang et al., 2021a). However, laser-scanning devices are often limited by high holding costs, training costs, and poor convenience. As an alternative method, image-based 3D reconstruction requires only an inexpensive camera or even a mobile phone camera to obtain accurate 3D information. In addition, there are no pre-training preparation requirements or investments before the operation.

However, image-based 3D reconstruction performance still has challenges in harsh conditions, such as a low-light environment during the evening or mid-night. During

the construction of UUs, the lighting conditions must be improved owing to the depth factor. In the O&M update scenarios of UU, repairs and updates are often required in the shortest possible time, making it unavoidable to perform 3D reconstruction in scenes with poor lighting or even at night. Under low-light conditions, the degree of recognition of the object surface texture decreases, reducing the quantity and quality of the generated point clouds (Roncella et al., 2021; Pozo et al., 2019; Burdziakowski et al., 2021). To overcome these difficulties, existing studies have primarily focused on conventional image-processing algorithms to enhance reconstruction performance. The limitations of such methods are that many parameters must be manually input by practitioners, and these methods are highly subjective (Guidi et al., 2014; Lu et al., 2012). With the development of deep learning, several models have been applied to enhance low-light images using paired training datasets (low-light input images and ideal reference output images) (Wei et al., 2018; Lore et al., 2017). Nevertheless, it cannot be directly used to enhance low-light images for a better 3D reconstruction outcome, as it is difficult to obtain paired training data and reference data (referring to the low-light images and paired ideal reference images that could be used for 3D reconstruction) to supervise the training progress. Even with access to the required dataset, the reconstruction outcome is still unreliable, as it is heavily dependent on the chosen reference images and practitioners' experience. In addition, few studies have incorporated the characteristics of as-built UU scenarios into the conditions for image optimisation.

1.2.4 Inefficient UUs topology-completion accuracy

Efficient and low-cost solutions for the completion of missing data in UU topology information are still lacking. The traditional method, which is also the most widely used method in engineering practice, is to detect the connection relationship between pipelines using GPR (Birkenfeld, 2010; Skartados et al., 2019), PipeProbe (Lai et al., 2010), or other manual methods, such as manhole inspection (Alejo et al., 2019). Although this approach can achieve high accuracy, it requires substantial human labour and expensive resources. Some studies have transformed the missing data-completion

problem of general UU attributes (diameter, material, water level, etc.) into an imputation problem. They used traditional imputation algorithms: single, linear regression-based, and three multiple imputations (Davey et al., 2009; Little et al., 2019; Von et al., 2004; Graham et al., 2012; Templ et al., 2011); machine-learning methods: principal component analysis (PCA) (Gangopadhyay et al., 2005); K-nearest neighbour (KNN) (Woldesellasse et al., 2021); decision trees (Barros et al., 2012); and neural networks (NNs) (Bishop, 1995) to accurately predict missing values. However, imputation cannot be used to predict the topological relationships.

1.3 Scope and aim/objectives

To address these issues, this study aims to improve the data-collection process and accuracy of the data used in the 3D reconstruction of as-built UUs. By obtaining better data and more accurate 3D reconstructions, the management decision making of UU operation maintenance rehabilitation and renewal can be improved. To achieve the aim of having more accurate and reliable 3D reconstructions, four objectives were established.

Objective 1: To identify research topics, trends, and limitations of automatic 3D reconstruction for as-built UUs. This thesis first identified existing mainstream 3D reconstruction technologies and analysed their advantages, disadvantages, and best performance. Second, the application research of various technologies was summarised from the perspective of engineering practice. Third, a decision-making framework for selecting 3D reconstruction technologies was proposed to improve the management efficiency of the UU life-cycle.

Objective 2: To develop a novel GPR-based as-built UU localisation deep-learning model for non-destructive scenarios. An end-to-end UU localisation (EUUL) deep-learning model using GPR B-scan data was proposed. First, unlike other deep-learning UU localisation methods, the EUUL model adopts the key point-regression mode instead of the box-fitting mode to realise end-to-end learning and train the model. Second, an anchor-free structure that does not rely on predefined anchor boxes to detect objects, with a lightweight backbone (CSPDarknet53), was applied to the EUUL

model to improve speed. Unlike traditional models that use anchors as reference points for bounding box predictions, anchor-free models predict the center points of objects directly. It increases the accuracy by allowing the model to dynamically adjust to the shape and size of the objects being detected without being constrained by preset anchors. And the computational overhead was also reduced by eliminating the need for calculating and adjusting multiple anchor boxes. Finally, to manage the noise interference of the UU positioning data, a channel attention mechanism was added to the EUUL model, such that the model focused on key features in the task to ensure precision.

Objective 3: To develop a novel unsupervised image-based 3D reconstruction model for the low-light 3D reconstruction of as-built UUs for exposed scenarios. A zero-reference (unsupervised) deep-learning model for low-light image enhancement for UU 3D reconstruction (ZDE3D) was proposed. This model was trained without a given reference sample image; that is, no paired or unpaired data were required in the training process. The enhancement of the UU 3D reconstruction performance was achieved by loss functions, where the design was based on 3D reconstruction principles and pixel-wise restricted relationships between the input and output images. Therefore, the influence of subjective parameter settings in the optimisation process can be avoided to the maximum extent, and the performance of UU 3D reconstruction in a low-light environment can be simply and effectively improved.

Objective 4: To develop a graph convolutional network (GCN)-based topology-completion model for as-built UUs. A GCN-based UU topology-completion (UUTC) model was proposed in this thesis. The model can extract UU attributes and topology features simultaneously and combine the correlation between the pipeline network topology relationship and attribute features to effectively complement the missing topology information. To verify the superiority of the proposed model over the existing mainstream GCN model in the UU data-completion task, five mainstream control groups were modelled focusing on missing data rates. The actual wastewater pipeline database from Angers Metropolis, France, was used as the case study.

1.4 Significance

The up-to-date 3D reconstruction of UUs is essential for ensuring safety, cost-effectiveness, efficient planning, and timely facility maintenance management. However, obtaining an accurate UU 3D reconstruction model is affected by many factors, and it is still very difficult to reconstruct the topological relationship after obtaining the spatial model. This research addresses these issues by developing a novel GPR-based as-built UU localisation deep-learning model for non-destructive scenarios, improving the UU localisation precision. A novel unsupervised image-based 3D reconstruction model was developed to improve the low-light 3D reconstruction of the as-built UUs for exposed scenarios. Regarding topology reconstruction challenges, a GCN-based topology-completion model for as-built UUs can infer missing topological information. Accordingly, this study makes three main contributions.

(1) Improving the precision of current GPR-based UU localisation

This study contributes to the knowledge body by proposing an EUUL deep-learning model using GPR B-scan data. The prevailing deep-learning approaches decompose the problem into two distinct sub-problems, namely box detection and hyperbolic fitting (Lei et al., 2019; Harkart et al., 2019; Hou et al., 2021; Zong et al., 2019), which leads to the computation of the solution primarily from the local optimal of the sub-problems rather than the global optimal. Moreover, this incremental approach to problem solving results in greater error accumulation, impeding the precision of UU localisation. The proposed EUUL model transforms the UU positioning problem into an end-to-end problem, from B-scan images to pipeline hyperbolic fixed-point coordinates. Simultaneously, it reduces the interference of environmental noise on the data by adding an efficient channel attention (ECA) module to achieve a higher positioning precision. The proposed methods are validated in experiments with real GPR datasets, and the results show that the performance is superior to existing mainstream models in terms of precision, operating speed, and robustness.

(2) Improving the reconstruction performance of image-based UUs in a low-light environment

The proposed image-based UU reconstruction model is of considerable importance in both theory and practice. Previous image-based studies have focused on surface reconstruction of UU under normal illumination conditions. However, UU installation and maintenance projects have a short construction period and greatly impact residents' lives; therefore, low-light scenes such as evening or night are very common. This study proposed a zero-reference (unsupervised) deep-learning model for the low-light image enhancement of UU 3D reconstruction (ZDE3D). From a theoretical perspective, the proposed ZDE3D model compensates for low-light image enhancement based on unsupervised learning in existing research on low-light image 3D reconstruction blanks. From a practical perspective, the ZDE3D model obtains more matching point clouds under the same input conditions, which effectively improves the surface 3D reconstruction effect of UU scenes in low-light environments. Field experiment implementation confirmed that the capability of ZDE3D can significantly increase the quantity of sparse reconstruction point clouds while ensuring high model reconstruction accuracy. This study is crucial for enhancing and broadening the scope of image-based 3D reconstruction technology in UU scenarios.

(3) Improving the completion accuracy of graph-based UU topology information

This study makes a practical contribution by providing a graph convolutional network-based model (UUTC) for the UU topology completion task. Previous UU database completion studies have focused on common attributes such as material depth and diameter. However, the topological relationship is very important for UU 3D reconstruction, and a model reconstructed with the topological relationship can fully represent the pipeline function. The proposed deep-learning model uses a convolutional graph neural network to transform the topological relationship prediction task into an edge relationship classification task between pipeline nodes. Combined with the UUs' greater possibility of topological connections between similar pipelines, a graph-based supervised deep-learning model for UU topology database completion was developed. The UUTC model can quickly predict the UU topological relationship under different missing data conditions, which avoids expensive manual inspection costs and achieves fairly reliable prediction accuracy. In this study, a model verification experiment based on real wastewater data was conducted. Compared with five mainstream GCN models, the proposed UUTC showed the best topological relationship completion ability under different missing data rates. The development of

UUTC can effectively help stakeholders quickly understand the topological relationship of unknown areas and make more scientific management decisions.

1.5 Thesis structure

This thesis has seven chapters which are summarised below and in Figure 1-4.

Chapter 1 describes the background, research problems, aims, and objectives of this thesis, as well as the thesis structure.

Chapter 2 summarises the literature on the current 3D reconstruction technologies for UUs, GPR-based 3D reconstruction for UUs, image-based 3D reconstruction for UUs, and topology completion for as-built UUs.

Chapter 3 introduces the study's research methodology. It outlines the research philosophy that underpins research methods. The chapter then introduces the method for developing the GPR-based as-built UU localisation deep-learning model (EUUL), a method for developing a novel unsupervised image-based 3D reconstruction model (ZDE3D), and a method for developing the GCN-based topology information completion model.

Chapter 4 develops an EUUL deep-learning model using GPR B-scan data. The EUUL model includes a lightweight backbone (CSPDarknet53) for feature extraction of the input data, and the computational cost is reduced to improve the data processing efficiency of the model. An ECA module was used to reduce the interference of environmental noise by learning to adjust the weight distribution between different captured channels. A prediction module that directly predicts the pipe coordinate position to achieve end-to-end learning and reduce the localisation error caused by step-by-step learning. Detailed experimental results are summarised to compare the EUUL model with other popular models for GPR-based UU localisation.

Chapter 5 develops an unsupervised deep-learning model for low-light image enhancement for UU 3D reconstruction (ZDE3D). The proposed ZDE3D model enhances the image-based UU 3D reconstruction through the pixel-level unsupervised loss functions. The design of these loss functions also considers common low-light enhancement, the principle of photogrammetry, and the features of UU projects. Field experiments in different scenarios were conducted and analysed to validate the performance of the ZDE3D model. In addition, ablation experiments are conducted to verify the contribution of the proposed loss functions.

Chapter 6 develops a graph convolutional network-based UU topology-completion (UUTC) model. The UUTC model comprises of four main modules: input, similarity extraction module (SEM), convolution, and link prediction. The model takes the observed topological relationships and node attribute information of the UU network as input and aims to generate completed network topology relationship data as output. The experimental results show that the proposed model can effectively complete the UU topological relations (average precision of 85.33%) for different proportions of missing topological relations.

Chapter 7 concludes important findings in the thesis, highlights contributions and implications, discusses limitations of this research, and suggests future studies.

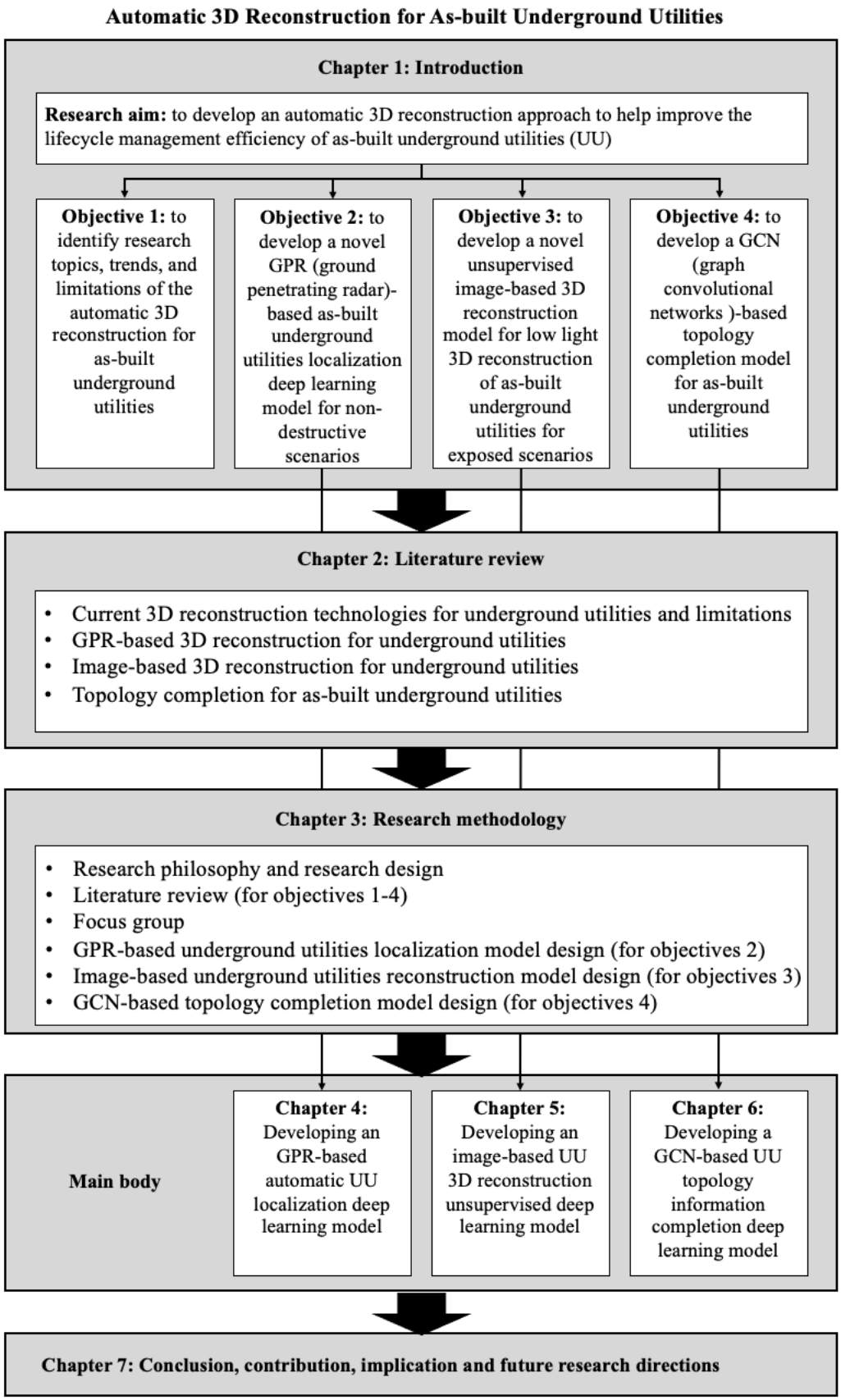

Figure 1-4 Thesis framework

Chapter 2 : Literature review

2.1 Current status of the UU 3D reconstruction

2.1.1 Review of the key technologies for 3D UU reconstruction

After years of development in the field of 3D reconstruction in underground engineering, many techniques and methods have been developed to achieve the goal of 3D reconstruction. This section summarises the essence and characteristics of the existing 3D reconstruction technology from a technical perspective. In Section 2.1, non-destructive technologies (NDT) for UU 3D reconstruction are introduced, whereas Section 2.2 reviews destructive technologies (DT), which are performed under the condition of excavation. Finally, Section 2.3 summarises the advantages and limitations of this technology.

2.1.1.1 Non-destructive technologies

2.1.1.1.1 GPR

GPR is one of the most common and efficient non-destructive 3D reconstruction techniques for UUs. This is essentially a method that uses antennas to transmit and receive high-frequency electromagnetic waves to detect the characteristics and distribution rules of matter inside the target area (Lai & Derobert, 2017; Zhao et al., 2017). In the UU scenario, GPR equipment is always used to scan the specified ground area (such as the section method, wide angle method, and transmitted wave method) to obtain the reflection characteristic data (mainly referring to B-scan images) of the underground hierarchy of the target area, and further analyse the location and characteristics of the pipeline according to the dielectric coefficient and waveform characteristics. Thus, a 3D model of the UU pipeline in the target areas was obtained with relevant engineering experience (Guo et al., 2009; Li et al., 2012; Maas et al., 2013; Jaw & Hashim, 2013; Zhang et al., 2016). In a recent study, Li et al. (2020a) reconstructed an underground-pipeline model fused with GPR and Camera in 2020, and the average localisation error was 4.47 centimetres. However, this approach is typically less accurate in engineering applications. There are two main reasons for this:

1) there are many disturbing factors (such as high-voltage line magnetic field, iron pipe corrosion products, and other factors (Hao et al., 2012; Pennock et al., 2010; Bai et al., 2020; Tosti et al., 2016)) in a complex real engineering environment; and (2) the final model reconstruction accuracy of this method relies heavily on manual experience, which requires a large amount of engineering experience in both GPR and UU engineering (Zhang et al., 2016).

2.1.1.1.2 RFID

RFID is a non-contact, fast information exchange, and storage technology realised by radio waves. However, in the reconstruction scenario of UUs, this technology generally requires binding RFID tags containing specific information during the construction of UUs. The signal strength reflection difference obtained at different distances is used to locate the depth and direction of pipelines, and is combined with engineering data, or GPR, and other methods to achieve 3D pipeline reconstruction (Sen et al., 2009; Hao et al., 2008; Zhang et al., 2017; Kumar et al., 2012). Compared with GPR, RFID technology has two major advantages: 1) This method can be used to overcome the problem of weak radar signals in plastic pipes (Zhang et al., 2017; North et al., 2010) when the surrounding soil has attenuation or the pipes and soil have similar electromagnetic characteristics, which is a good supplement to GPR technology. 2) The relatively low operating frequency (tens of kHz to tens of MHz) means that it has a greater coverage range than most pulsed GPR systems used for practical detection (hundreds to thousands of MHz). For example, Kumar (2012) developed an RFID-based 3D positioning model for underground assets and experimentally verified that the 3D reconstruction accuracy of the system was within ± 100 mm. However, the shortcomings of RFID technology are evident. First, its cost is high, and it is not easy to maintain, and replace after embedding. Second, the label is subjected to soil corrosion in an underground environment, which affects the reception of the signal (Zhang et al., 2017; Kumar et al., 2012).

2.1.1.1.3 Electromagnetic induction (EMI)

Electromagnetic induction (EMI) is a method used to locate and map UUs. The basic

assumption of this method is that, when the magnetic field peak is measured, the equipment position is directly above the UU (i.e., the horizontal position), and the buried depth of the pipeline can be estimated according to the signal strength. Electromagnetic technologies can be classified into active and passive modes (Lai et al., 2017; Jeong et al., 2004; Siu et al., 2019). In the active mode, a voltage was applied at the end of an underground metal pipe, and the position and depth of the pipe were determined by measuring the peak position and strength of the generated magnetic field. Passive means that the UU itself generates a certain magnetic field strength (such as a cable) through an ultrasensitive magnetic detection device to determine the depth of position and then generate a three-dimensional model of the UU. Magnetic technologies commonly used equipment that avoids cable avoidance tools (CATs), pipe and cable locators (PCLs), flux-gate magnetometers (FMs), proton precession magnetometers (PPMs), alkali vapour magnetometers (AVMs), and superconducting quantum interference devices (SQUIDs). (Jeong et al., 2004; Metje et al., 2020; Karaa et al., 2014). Magnetic technologies complement GPR detection and reconstruction methods because magnetic signals are less attenuated in wet soils with a higher clay content than in conventional GPR. The accuracy of this method was 3% in the range of 3 m, and 5% in the range of 3–5 m (Yan et al., 2019). Together with Geographic Information Systems (GIS), a promising storage technology for utility location and attribute data, these methods can achieve good 3D reconstruction (Karaa et al., 2014; Liu et al., 2012). However, this method is only effective for metal pipelines. Simultaneously, it is extremely difficult to apply when the underlying infrastructure conditions are complex (e.g. with multiple staggered metal pipelines) (Jeong et al., 2004; Siu et al., 2019). Therefore, the electromagnetic-technology-based UU reconstruction method still has a narrow application range.

2.1.1.1.4 Acoustic emission

AE methods involve using sensors, such as hydrophones, to detect and measure the acoustic signals generated by UUs. These methods can be used to locate and map various utilities, including pipes, cables, and other infrastructure (Khan et al., 2010;

Talmaki et al., 2013; Metcalf et al., 2020; University of Birmingham et al., 2012). AE methods detect sounds or vibrations generated by utilities as they operate. For example, the water flow in a pipe can generate a characteristic acoustic signal that can be detected and used to locate utilities. Similarly, the movement of electrical cables can generate an acoustic signal that can be detected and used to locate the cables. AE methods can be used to locate both metallic and non-metallic utilities, and they are often used in conjunction with other methods, such as EMI or GPR, to provide a more complete picture of the underground environment. Acoustic methods have the advantages of low acoustic attenuation and effective propagation in both solids and liquids (Smith et al., 2019; Volker et al., 2013). However, ultrasonic technologies also have some clear limitations, such as the dry and wet degree of the soil, hard surfaces (such as pipes under the surface of concrete), and rock roots near the target pipes and other pipes. These factors affect measurement results (Rachev et al., 2018; Muggleton et al., 2002; Leinov et al., 2015). This method can track pipelines buried less than 0.5 m (Metje et al., 2007) without noise interference.

2.1.1.1.5 Thermography

Thermography is a method by which the invisible infrared energy emitted by UUs is transformed into visible thermal images to obtain the location information of pipelines for 3D reconstruction modelling. The instrument commonly used in this method is infrared thermography (IRT), which comprises an infrared detector and optical imaging objective lens (Lagüela et al., 2018; Solla et al., 2016). The IRT data of the UU were acquired through the detection and measurement of the infrared radiation energy emitted by the target under examination and subsequently capturing the distribution pattern of the energy via the photosensitive component of the infrared detector. This thermal image corresponds to the thermal distribution field on the object's surface. This is similar to the acoustic and electromagnetic-wave methods, which can achieve trenchless reconstruction (Fan et al., 2005; Capozzoli et al., 2017). The most recent study in Singapore by Capozzoli et al. (2017) explored this approach. The thermography method provides an accurate distance between tubes. However, the

depth and characteristics of the surrounding media were not well defined (the pipeline depth in the experiment was only approximately 0.2 m). Therefore, thermography is a reliable method for NDT reconstructions. However, in other studies, the accuracy of this method must be clarified.

2.1.1.1.6 IMU-based system

An inertial measurement unit (IMU) is a sensor that records the speed, acceleration, and direction of rotation of its inertia. As one of the trenchless pipeline detection modelling methods in the UU scene, this method mainly records the velocity, rotation angle, and other parameters using an IMU sensor mounted on the robot equipment to obtain the depth and strike data of the pipeline, and finally draws a three-dimensional model of UUs (Hyun et al., 2010; Lee et al., 2011; Wang et al., 2012). The IMU method can obtain the most accurate 3D pipeline reconstruction data under non-destructive conditions. The general horizontal accuracy was 0.25% of the total pipeline length and the depth accuracy was 0.1% (Yan et al., 2019). In the latest study, Zhang et al. (2019b) reported that the maximum horizontal error was 0.10 m, and the maximum height error was only 0.04 m (5x6 m pipes with four joint sockets). It should be noted that low-cost IMU equipment was used in the research by Zhang et al. (2019b); therefore, the IMU method can achieve higher accuracy if cost factors are not considered. In addition, the IMU-based method also has the advantage of not being affected by the soil environment (e.g. soil composition and water content) and deep application depth. However, compared with other trenchless methods, the IMU method has the following limitations: 1) it is vulnerable to electromagnetic interference; 2) it cannot be used in working pipes (such as water pipes); and 3) solid pipes, such as cables, cannot be used. (Lee et al., 2011; Chowdhury et al., 2016; Reyes-Acosta et al., 2019). These defects lead to a status quo applicable to only a few scenarios.

2.1.1.2 Destructive technologies

2.1.1.2.1 laser scanning

Laser scanning has been widely used in the three-dimensional model reconstruction of

pipelines during the excavation stage (Duran et al., 2003; Stanić et al., 2017). This method is based on the principle of laser ranging, which collects the spatial position of the surface points of the target utility to form a three-dimensional model. Similar to total station technology, laser scanning also needs to be used in the scenario of pipeline exposure, which is characterised by its ability to obtain high-precision object surfaces in large-scale environments. Compared with other methods, the advantages of laser scanning are as follows: 1) it has the best automatic performance (Lee et al., 2013; Wang et al., 2022(a); Maalek et al., 2018); 2) it can realise model reconstruction with millimetre-level accuracy (Patel et al., 2010b; Wang et al., 2021a; Guo et al., 2020b); and 3) owing to the use of laser information acquisition, it has a strong anti-environmental interference ability and is suitable for large-scale three-dimensional reconstruction of UUs in an open environment (Patel et al., 2010b; Son et al., 2016). However, its fatal disadvantage is that it cannot be used in the pre-excavation phase, which significantly reduces the engineering practicability of the method. In addition, laser scanning alone can only reconstruct the spatial information of reconstructed objects, and it is not easy to obtain information other than the shape of the surface.

2.1.1.2.2 Photogrammetry

Photogrammetry is another method that can be performed only in open scenes. Photogrammetry refers to the technique of using optical sensors to record images of target objects and analyse object shapes and spatial positions using image features (Richard & Canberra, 2003). This technique was applied to the 3D reconstruction of pipeline utilities by Veldhuis and Vosselman (1998). Photogrammetry has the following advantages: 1) data collection is convenient, and only photos are required; 2) low cost of data acquisition equipment, a common digital camera (or even a mobile phone camera) can meet the requirements; and 3) on the basis of obtaining the spatial features of the target, RGB pixel information can also be obtained, which can be used for further analysis of the target object (Yılmaztürk et al., 2010; Maalek et al., 2021; Javadnejad et al., 2017; Lueke et al., 2011). However, similar to total station and laser scanning, photogrammetry can only be used for 3D reconstruction of UUs during

specific stages of pipeline exposure. However, compared to laser scanning, photogrammetry has three important characteristics: high accuracy, automation, and low cost. Therefore, it has evident engineering application potential (Javadnejad et al., 2017; Yang et al., 2021; Elkhrachy, 2021). In addition, existing research teams have combined photogrammetry, laser scanning, and GPR technology to perform 3D reconstruction tasks for UUs (Yan et al., 2019; Li et al., 2020a) and have shown great potential.

2.1.1.3 Summary

The above review shows that every 3D reconstruction technique, whether NDT or DT, is not a perfect choice for every scene. Figure 2-1 summarises the advantages and limitations of all types of mainstream 3D reconstruction technologies mentioned above, as well as the limitations and best performance reported in the current literature.

Scene	Type	Advantages	Limitations	Best Performance
Technologies – NDT	GPR	High reconstruction accuracy Adapt to various material targets Convenient operation	Difficult data analysis	Centimeter level accuracy can be realized
	RFID	Wide range of application depth Stable signal strength	Low reconstruction accuracy Labels are susceptible to corrosion	3D reconstruction accuracy between ± 100 mm
	Electromagnetic	Stable signal strength	Low reconstruction accuracy Mutual interference between multiple targets	3% in the range of 3 meters 5% in the range of 3 to 5 meters
	Acoustic	Signals propagate in various media Small signal attenuation	Low reconstruction accuracy Vulnerable to noise interference Small applicable depth range	Support the working range of 0 ~ 0.5m below the ground
	Thermography	Convenient operation	Low reconstruction accuracy Small applicable depth range Large temperature scenes only	Support the working range of 0 ~ 0.2m below the ground
	IMU-based system	Low cost High reconstruction accuracy	Small scope of application The operation is complicated	Horizontal accuracy: 0.25% of the total length of the pipeline Depth direction accuracy: 0.1% of the total depth
DT	Laser scanning	High reconstruction accuracy Simple operation	The operation is complicated High equipment cost	Millimeter level accuracy can be realized
	Photogrammetry	High reconstruction accuracy Low equipment cost Rich semantic information Simple operation	Vulnerable to light conditions	Centimeter level accuracy can be realized Rich semantic information

Figure 2-1 Limitations and best performance of 3D reconstruction technologies

In addition, multi-sensor fusion is an important implementation path in underground 3D reconstruction. It includes the following three types: 1) NDT + NDT. For example, when one PCL and GPR are used, the depth measurement accuracy error can reach 40% of the buried depth; when both are used, the depth measurement accuracy error can reach 15% of the buried depth (Yan et al., 2019). In addition, some studies have

integrated GPR technology and acoustic technology for the three-dimensional reconstruction of UU (Yan et al., 2019) or improved position accuracy through GPS (Khan et al., 2010; Šarlah et al., 2020; Li et al., 2016). 2) DT+DT: The first combines DT technology with GPS to improve the accuracy of the reconstructed position (Patel et al., 2010). In the other category, photogrammetry was combined with laser scanning to overcome the degenerate phenomenon in the absence of the geometric features of the laser method and the difficulty of improving accuracy when only the photogrammetry method was used (Lin et al., 2021; Ye et al., 2019). 3) NDT was integrated with DT variants. For example, GPR has been combined with visual simultaneous localisation and mapping (vSLAM) based on photogrammetry to establish a 3D reconstruction system for multi-pipeline groups (Li et al., 2020a). In addition, Virtual Reality (VR), Augmented Reality (AR), and other technologies have been used in 3D reconstruction to improve the display effect (Fenais et al., 2020; Childs et al., 2020) in recent years.

2.1.2 Review of the current applications of 3D reconstruction methods

Although categorised under the term 'UU 3D reconstruction methods', the techniques discussed above exhibit significant variations in their respective applicability to specific scenarios. Such differences in the implementation details can significantly influence the selection of appropriate engineering technology routes. As a result, this section reviews the present applications of 3D reconstructed models, as shown in Table 2-1, which may aid decision makers in identifying appropriate 3D reconstruction technologies or combinations based on their suitability for particular scenarios.

Table 2-1 Applications of the 3D reconstructed models

Stage	Classification	Category	Application Details
Before Construction	UU Inspection	GPR RFID EMI AE	Hebsur et al. (2013) utilised GPR technology for reconstructing the UUs of ancient cities to establish an information base for urban models.

Stage	Classification	Category	Application Details
		Thermography IMU-based system	Ristić et al. (2014) used GPR technology for identifying the subterranean structure of a flooding bank in Novi Sad, Serbia, as well as for delineating the geometry of man-made public utilities (pipelines). Deng et al. (2020) applied GPR technology to detect and reconstruct water supply pipelines in older communities of China. Additionally, in the same year, Cai et al. (2020) established a robust and accurate method for inventorying UUs by utilising GPR in conjunction with existing utility records as two independent sources of information.
	Network Planning	GPR RFID EMI AE Thermography IMU-based system	Mooney et al. (2010) used multi-channel ground-penetrating radar (GPR) to conduct three-dimensional reconstruction of underground cables in Yonkers, NY to verify the influence of this method on the design and planning of UU project and found many unknown public utilities that had major conflicts with the planned construction. Harbin et al. (2016) collected the required UU data to reduce existing pipeline and newly designed UUs and to plan by identifying potential expansion areas of the

Stage	Classification	Category	Application Details
			existing network at the University of Alabama. Zhang et al. (2020a) proposed the UU Occupation Index (UUOI) based on existing UUs, occupied underground space and space models for future use, which is used to provide abstract utility and space use information for the government's urban planning and development.
During Construction	Machine Guide	GPR EMI Laser scanning Photogrammetry	Talmaki et al. (2012) developed a comprehensive computing framework for real-time monitoring of construction activities in a concurrent 3D virtual world to reduce the possibility of accidental pipeline collision by excavators. Al-Bayati et al. (2019) Collected and analysed 11,160 damages in the state of North Carolina to reduce the risk for the damages to UUs while machine work. Tanoli et al. (2019) proposed a new approach to modelling UUs for machine navigation systems to provide visual guidance to operators and prevent accidental damage to underground pipes.
	3D record generating	Laser scanning Photogrammetry	Son et al. (2015) developed a fully automatic system for as-built pipeline 3D reconstruction based on laser technology.

Stage	Classification	Category	Application Details
			However, it may inaccurately segment a single pipeline into multiple parts due to occlusion. In 2017, Ahmad et al. (2017) proposed a modified global ICP (Iterative Closest Point) method for automatic 3D models recording of the UU. While promising, the adaptation for complex UU networks and its cost-effectiveness remains unexplored. Stylianidis et al. (2020) validated a new system (LARA) that integrates handheld and mobile devices for monitoring, recording, and managing utility-based geospatial data products and services. However, it depends on the accuracy of GIS data in network operators' databases, which can result in discrepancies between the virtual and actual positions of underground pipes.
After Construction	Asset management	GPR RFID EMI AE Thermography IMU-based system	Ortega et al. (2019) demonstrated an effective way to manage urban infrastructure by visualising underground infrastructure in an interactive 3D immersive environment. The dependence on the accuracy and precision of GIS data in network databases which can also lead to discrepancies between the virtual and actual

Stage	Classification	Category	Application Details
			positions of underground pipes. Yan et al. (2019) connected the UU 3D model to the government database of cadastral plots for land management in Singapore. And the study highlighted the lack of reliable, comprehensive, and accurate 3D data on underground utilities, which hampers effective urban planning and management of underground infrastructure. Yan et al. (2021) proposed UUDM (UU data model) to help ownership management, land acquisition, planning and (re)development of the UU based on his previous work.
	Defect Detection	GPR AE IMU-based system	Zhang et al. (2019a) developed a low-cost IMU and odometer integrated system that can effectively detect pipeline settlement with a depth accuracy of 0.11 m. However, underground utility companies are often reluctant to share accurate information about their existing utilities, which hinders effective urban planning and utility management due to missing historical as-built records and the unavailability of accurate utility data for governmental planning.

Stage	Classification	Category	Application Details
			Zhang et al. (2019b) verified the rapid and high-precision detection of pipelines based on internal images of pipelines and achieved good experimental results. While the primary limitation is the challenge of obtaining accurate and comprehensive internal damage and erosion data within urban drainage pipe networks due to the complex and irregular distribution of defects. Shokri et al. (2020) accurately mapped the old, corroded pipes in Malaysia. However, variations in soil electrical resistivity and moisture content can have the effect of reduced accuracy. Gunatilake et al. (2020) combined stereo vision with laser profiling realised the imperfections monitor of the pipe linings under unfavourable environmental condition.

2.1.2.1 Application before construction

Before UU construction, 3D reconstruction techniques, mainly NDT, were generally used in UU inspection and planning for unknown target areas.

2.1.2.1.1 UU inspection

However, urban UUs generally have explicit electronic or paper-based drawings. However, problems such as loss of records, failure to construct according to drawings,

and location changes owing to pipeline settlement pose a huge challenge to city management, especially in old urban areas. The non-destructive 3D reconstruction technique can reconstruct UU under completely unpredicted conditions at minimum cost. Obtaining the exact locations and depths of unknown utilities is crucial for urban management. Only with a clear grasp of the detailed underground location information of various types of pipelines can the government form a complete and effective asset-management system.

2.1.2.1.2 Network planning

The planning of UU networks is an important part of overall urban design and planning. Unreasonable UU network planning leads to wasting workforce and material resources, particularly when urban areas are to be developed. However, pipeline network planning is a systematic project that requires coordination. This project is fundamental to the reconstruction of the localisation and dimensions of various utilities. A clear 3D reconstruction of the UU can effectively avoid repeated network construction, reduce the construction cycle of utilities, and select the best layout path. The employment of UU in new urban development is driven by various factors, including the need for intensive utilisation of land resources, accessibility considerations, the desire to avoid the challenges faced by old cities, cultural and modernity concerns, and the aim of constructing intelligent, environmentally friendly, and sustainable urban spaces.

2.1.2.2 Application during construction

2.1.2.2.1 Machine guide

Mechanical excavation is essential in the construction of UU projects. Simultaneously, accidental damage to pipelines around other construction sites is the most important risk factor in implementing UU projects. In the case of accidental pipeline breakage, the project progress may be stalled, and traffic congestion around the site may occur. Serious casualties can occur (such as injuries caused by accidental gas-pipeline explosions). In this scenario, UU real-time 3D reconstruction can effectively solve the problem of the pipeline being destroyed and pipeline for construction machinery

(primarily excavators) to visualise construction guidance (Tanoli et al., 2019; Li et al., 2018b).

2.1.2.2.2 3D record generating

In the construction stage of a UU project, the UU's specific buried location, including its size or material, may change owing to various environmental factors. In such situations, UU 3D reconstruction technology (mainly DT) can effectively aid the construction and owner units form three-dimensional and reliable UU construction-information records. Laser scanning and photogrammetry satisfy this requirement in terms of accuracy and reconstruction speed. Compared with complex two-dimensional information recording, three-dimensional reconstruction helps managers quickly generate a clear and intuitive engineering record model, which can lay a good foundation for subsequent communication. Accurate electronic models and rich information (such as pipeline material, construction time, construction unit, and construction method attached to the 3D pipeline model) can effectively avoid the loss or defect in drawing information, which is conducive to the maintenance and management of UU throughout its life-cycle.

2.1.2.3 Application after construction

2.1.2.3.1 asset management (information exchange)

For UU managers, the most onerous task after the construction of UU is to manage a large number of underground invisible assets. As mentioned previously, the application of 3D reconstruction technology, such as coordinating resources, information sharing, and efficient communication between economic construction personnel and utility owners, provides great convenience. Related faculty objects can be easily identified.

2.1.2.3.2 Detection of pipe defects and settlement

The UU 3D reconstruction process also identifies the utility exceptions. Over time, congestion of all types, settlement, or congestion of utilities undertaking all types of tasks appear. Owing to the invisibility of utilities, these problems are often difficult for

managers to detect. However, these problems can be extremely damaging. The leakage of sewage pipelines seriously damages the ecological environment of the surrounding area and significantly impacts the surrounding residents. Leaks in water supply pipes can cause water shortages for many urban residents. Settling pipes are one of the main causes of road collapses. Moreover, pipeline congestion causes a task to strike completely. Each item consumes a large amount of government or private funding. Through various non-destructive 3D reconstruction techniques, defects in these buried utilities can be recognised.

2.1.3 Current challenges

From the perspective of engineering practice, this section summarises the core challenges that are often encountered in the process of UU 3D reconstruction through literature review and induction. We hope that a summary of these core issues will promote research in this field.

2.1.3.1 Accuracy

The first and most important challenge is the accuracy of 3D reconstruction. This problem refers to the accuracy challenge of 3D reconstruction models under the requirements of non-destructive scenes. The accuracy of UU 3D reconstruction can be summarised in terms of depth and size.

The depth of pipeline utilities is the most important information in the UU 3D reconstruction task. Unlike common 3D reconstruction tasks, the UU 3D reconstruction task cannot be easily explored because its location is below the surface, and the owner has clear and strict requirements on its spatial location. The spatial position of a pipeline is represented by its direction and depth. Information on pipeline direction is often easy to obtain. It only needs to determine the position of two points of the utilities (or more for curved utilities, such as cables) (Zhou et al., 2022; Jiang et al., 2019). However, accurate depth information is often obscured by the complex underground ambient noise (Zong et al., 2019; Hartshorn et al., 2022; Bach et al., 2017). Therefore, pipeline depth is the most important part of the 3D reconstruction of

UUs. Whether using GPR or other technical methods, the determination of pipeline depth under trenchless conditions is unsatisfactory (Karsznia et al., 2021; Oliver et al., 2020; Wu et al., 2019). According to various technologies and engineering reports, the judgement accuracy of pipeline depth is approximately 1/10 of the actual buried depth of the pipeline.

Another challenge in UU 3D reconstruction accuracy is the pipeline size. The diameter information often plays a key role in engineering practice, especially in 3D reconstruction projects of old utilities (Hashemi et al., 2011; Rashed et al., 2015). For example, Naghshbandi et al. (2021) reported in his study in 2021 that pipeline size often indicates important information such as their purpose and working state (whether there is aperture deformation). However, in current studies of non-destructive methods, accurate information on utility size is often unavailable (Yan et al., 2019; Mat Junoh et al., 2022).

2.1.3.2 Automation

The second challenge, the most popular in this field, is the automation of three-dimensional reconstruction of UUs. As can be seen from the summary of various techniques in Section 3, all non-destructive techniques need to be further processed to transform into the final three-dimensional models (Manataki et al., 2021; Chrysostomou et al., 2020; Cloete et al., 2020). However, only some automatic methods, such as laser scanning and photogrammetry, are suitable when pipelines are exposed during the construction or maintenance stages. Although the degree of automation in intermediate data processing for these non-destructive techniques varies, they all require many manual operations, even by experts with specialised knowledge. This greatly reduces the efficiency of the UU 3D reconstruction. Taking the most widely used and mature GPR method as an example, the translation of raw data output by GPR equipment mainly needs to go through: 1) Data conversion (i.e. raw data decoding, image conversion); 2) Data processing (i.e. noise filtering, frequency gain, etc.)3) Manual interpretation (i.e. judging a specific target situation using B-scan images) and other steps (Šarlah et al., 2020; Al-Nuaimy et al., 2000; Wang et al., 2020b;

Hou et al., 2021b), especially in the B-scan image interpretation stage, the staff require significant professional knowledge and years of engineering experience. In recent years, significant progress has been made in the field of automation (Feng et al., 2022; Jaufer et al., 2021; Son et al., 2021; Liu et al., 2023); however, achieving reliable automatic UU reconstruction without manual participation remains an open problem.

2.1.3.3 Semantic enrichment

The third main challenge is the semantic enrichment of the 3D model of the UU Project. In the process of 3D reconstruction of the underground, shareholders often want to know not only the geometric information of UUs, but also the semantic information of the entire system; that is, material, slopes, manufacturer, and ownership form the core information related to major economic benefits or safety indices that concern owners (Yan et al., 2021; Wang, 2021b; Lau et al., 2021). For example, Tanoli et al. (2019) reported that rich semantic information could significantly protect the personal safety of construction personnel (i.e., natural gas-pipeline systems) (Tanoli et al., 2019). Lau (2021) and De Coster et al. (2019) reported that pipeline leakage detection is feasible by three-dimensional pipeline reconstruction combined with other prior information. In addition, semantic information is an important part of the data in the maintenance management stage of UU during the entire life-cycle. Research on semantic information can significantly promote the intelligent process of UU engineering maintenance.

2.1.4 Potential research directions

2.1.4.1 Integration of artificial intelligence technologies and methods

From the perspective of 3D reconstruction technology, replacing human labour in the complicated 3D reconstruction of UU with artificial intelligence is inevitable. In recent years, with the continuous maturation and development of artificial intelligence (AI) technology, the integration of an increasing number of AI and 3D reconstruction technologies has provided excellent solutions for the 3D reconstruction and management of UUs (Cheng et al., 2020; Lee et al., 2020; Bilal et al., 2018). Currently,

research in this field is in its infancy. Among NDT technologies, GPR is the most promising. It has the features of fast and convenient use, a wide range of applications (i.e., metal and non-metal pipelines can be used (Yan et al., 2019; Prego et al., 2017)), and the data are uniform and sufficiently rich for data-driven methods. Therefore, it is suitable for use in combination with AI algorithms. Among DT technologies, the most promising is the automated and low-cost 3D reconstruction mode realised based on laser scanning and photogrammetry combined with AI technology (Maalek et al., 2021; Lin et al., 2021; Ye et al., 2019). Owing to the large-scale and long cycle of UU engineering scenes, such projects are generally highly sensitive to cost (Yan et al., 2021; Biersteker et al., 2021; Glass et al., 2019). Therefore, the 3D reconstruction of laser scanning and photogrammetry fusion at low cost may result in a huge development space.

2.1.4.2 Underground world digital twin

The underground placement of utility pipes and cables can be attributed to various factors, such as shielding against harm from surface activities, exposure to harsh weather, and structural reinforcement against differential movements. Despite these benefits, when it comes to conducting maintenance or establishing new service connections, the subterranean terrain poses a formidable challenge by impeding our ability to determine the location and nature of subsurface infrastructure.

Therefore, from a management perspective, virtual revisualisations of UU projects should be built. Span lifecycles may become the best way to solve most UU project problems. Once informed with sufficient data, such as geometric and semantic information, the underground world digital twin (UWDT) can be used to run simulations, study performance issues, and generate possible improvements to generate valuable insights, which can then be applied back to the original physical projects. This idea has been reflected in research worldwide (Saeed et al., 2019; Huang et al., 2021; Rogage et al., 2022). However, more research is needed to integrate existing scattered data acquisition, data processing, project practice, and other research. Thereafter, a complete underground system and standard decision-making pattern are

formed. In summary, the formation of digital records during the initial stages of the UU project forms the basis for implementing all the UWDT visions. An accurate reconstruction of as-built UUs is the first step in the UWDT.

2.2 GPR-based 3D reconstruction for UUs

Ground Penetrating Radar (GPR) is a prevalent non-destructive technique utilized extensively in urban utility (UU) 3D reconstruction tasks. Despite its widespread application, achieving high precision in UU localisation using GPR B-scan images presents several challenges: 1) Interference factors: GPR operates based on the propagation characteristics of electromagnetic waves, which are susceptible to various environmental interferences. These include electromagnetic disruptions from nearby electrical installations, physical obstructions like tree roots, and inherent noise from the GPR device itself (Lei et al., 2019; Singh et al., 2013; Adouane et al., 2021). Such disturbances can obscure or distort the B-scan images, complicating the recognition and accurate localisation of UU targets. 2) Complexity of underground environments: unlike tasks such as reinforcement localisation within concrete structures, UUs are typically buried deeper and consist of diverse materials, adding layers of complexity to the GPR detection process (Wang et al., 2020; Liu et al., 2020; Ahmed et al., 2020). These factors can degrade the quality of B-scan images, making it difficult to discern and accurately map the utilities.

The interpretation of B-scan images for precise UU localisation largely depends on the expertise and experience of domain experts. This requirement for specialist input highlights the subjectivity and variability in interpreting GPR data. Although numerous studies have aimed to enhance the automation of B-scan data analysis, two primary limitations persist: 1) Conventional methods' susceptibility to noise: traditional processing techniques for GPR data involve complex steps that are highly sensitive to environmental noise. This sensitivity often results in unstable precision, as the methods can yield varied outcomes depending on the ambient interference encountered during scans (Maas et al., 2013; Harkat et al., 2016; Sagnard et al., 2016). 2) Segmented approach of deep-learning methods: modern deep-learning strategies

typically divide the task into two stages: detecting bounding boxes around potential UU locations and fitting hyperbolic curves to these detections. While this segmented approach allows for tackling each sub-problem effectively, it also leads to potential error accumulation. Each stage generates errors that propagate to the next, compounding inaccuracies and affecting the overall precision of UU localisation (Lei et al., 2019; Harkart et al., 2019; Hou et al., 2021a; Zong et al., 2019).

These challenges underscore the need for developing more robust GPR analysis techniques that can mitigate the effects of environmental noise and provide a more holistic solution rather than relying on local optima obtained from subdivided problem-solving approaches.

2.2.1 Conventional image-processing methods for GPR UU localisation

In the early stages of GPR automated interpretation research, researchers primarily focused on using image-processing technologies to analyse image features to locate hyperbolas. The most used methods in these studies are the Hough transform (HT), template matching (TM), and edge detection, as listed in Table 2-2.

Table 2-2 Conventional image-processing methods for GPR UU localisation

Type	Title	Advantages	Limitations
Hough transform	Advanced image-processing technique for real-time interpretation of ground-penetrating radar images (Capineri, 1998)	Automatic processing involves minimal operator intervention; real-time recognition provides position and size information simultaneously.	Parameters must be manually set in advance; computing resources are required.
	Using pattern recognition to automatically localise	The Viola–Jones algorithm is applied to reduce the	Parameters must be manually set in advance;

Type	Title	Advantages	Limitations
	reflection hyperbolas in data from GPR (Maas et al., 2013)	computational resource requirement; it can be used in unprocessed radargrams.	sensitiveness to background noise.
	GPR hyperbola detection using scale-invariant feature transforms (Harkat et al., 2016)	Improved robustness compared with the previous Hough transform (HT) algorithm; execution time is only 1/4 of the original HT algorithm.	Parameters must be manually set in advance; vulnerability to colour images.
	GPR objects hyperbola region feature extraction (Rajiv et al., 2017)	Real-time detection realised; favourable accuracy and robustness performance compared with previous template-matching algorithms.	Parameters must be manually set in advance.
Template matching	Two fast buried pipe detection schemes in GPR images (Gamba et al., 2003)	High operating speed; detection of small targets is allowed; offline system training is allowed.	Parameters must be manually set in advance; sensitive to background noise.
	An approach for predicting the shape and size of a buried basic object on	Different shapes of actual buried object are tested.	Parameters must be manually set in advance.

Type	Title	Advantages	Limitations
	surface GPR system (Syambas et al., 2012)		
	Template-matching based detection of hyperbolas in ground-penetrating radargrams for buried utilities (Sagnard et al., 2016)	High operating speed; algorithm robustness is strengthened via the benefit of diverse polarisations.	Parameters must be manually set in advance; sensitive to background noise; no actual data are used for verification.
	Estimating geometrical parameters of cylindrical targets detected by GPR using template-matching algorithm (Ahmadi et al., 2017)	The algorithm robustness is strengthened via pre-processing and post-processing steps; automatic fitting of hyperbola is realised.	Complex pre-processing prior to system operation; parameters must be manually set in advance.
	Automatic localisation of gas pipes from GPR imagery (Terrasse et al., 2016)	Automatic real-time detection; effect of image background is reduced by detecting the correlation between a hyperbola dictionary and B-scan.	Parameters must be manually set in advance.
Edge detection	Automatic and fast detection of buried utilities positions and	High operating speed; low detection error; pipe position and soil	Noise filtering required; sensitive to non-removed

Type	Title	Advantages	Limitations
	estimation of soil permittivity using GPR (Ardekani et al., 2006)	permittivity are obtained simultaneously.	background clutters and high-frequency noise in horizontal dimension.
	A novel edge detection for buried target extraction after SVD-2D wavelet processing (Zheng et al., 2014)	False detection results are reduced via cross-correlation calculation of background and target signals; better robustness against noise.	Parameters must be manually set in advance; pre-processing required.
	Improving GPR imaging of the buried water utility infrastructure by integrating the multi-dimensional non-linear data decomposition technique into the edge detection (Chen et al., 2021)	The signal-to-noise ratio before edge detecting is increased using the multi-dimensional ensemble empirical mode decomposition algorithm.	The complexity of the calculation process with considerable labour prevents wider application; processed image may not fully express the original information.
	On the introduction of the Canny operator in an advanced imaging algorithm for real-time detection of	The detection speed is increased by eliminating unnecessary edge pixels from Canny-	Apexes of target hyperbolas cloud may be removed accidentally, which may result in

Type	Title	Advantages	Limitations
	hyperbolas in GPR data (Bugarinović et al., 2020)	processed data; localisation robustness is improved by removing horizontal reflections from road and soil layers.	localisation error; parameters must be manually set in advance.

2.2.1.1 HT

HT, which was first introduced by Duda and Hart (1972), is used for feature extraction in image analysis, computer vision, and digital image processing. In 1998, Capineri et al. (1988) first proposed a real-time method based on HT, which was used to detect straight lines and hyperbolas in B-scan images with errors of less than 7% and 2% in the pipe position and location, respectively. However, HT operations are time consuming and yield random results. The original HT algorithm for UU localisation has been improved over the years to address the time-consumption issue. In 2013, Maas et al. (2013) combined the Viola–Jones algorithm (Viola et al., 2004) with HT to significantly reduce the computation required for HT and enable its deployment on ordinary computers. In 2016, Harkat et al. (2016) proposed the application of a scale-invariant feature transform-based HT to detect hyperbolas in GPR B-scan data.

HT-based methods significantly reduce the calculation costs. However, these methods involve several manual steps and are difficult to apply to areas with significant noise interference, thus necessitating GPR pre-processing operations.

2.2.1.2 TM

TM is an image-processing technique that locates objects by matching image sections with templates. It requires only the discrimination of hyperbolas from the background instead of including all patterns (Ali et al., 2021). In 2003, Gamba et al. (2003) first implemented a TM approach for GPR data analysis, which allowed for rapid detection of GPR hyperbolas. A TM approach was used to locate and detect pipe signatures in

two perpendicular antenna polarisations (Sagnard & Tarel, 2016). The use of TM methods has expanded further (Syambas et al., 2012; Ahmadi et al., 2017; Terrasse et al., 2016).

However, in TM methods, several parameters must be manually adjusted for different target features (Sagnard et al., 2016). Therefore, achieving fully automated localisation via the TM requires considerable effort. Additionally, TM-based methods cannot accommodate the B-scan pollution caused by complex underground environments (Sagnard et al., 2016; Rajiv et al., 2017).

2.2.1.3 Edge detection

In general, the edges of an image provide the most information. In this regard, edge extraction can remove a significant amount of interference information and improve data processing efficiency. In 2006, Ardekani (2006) proposed a new edge-detection method for separating useful data from GPR images where the apex coordinates were precisely located. However, the auto-detection results contained a few errors, owing to the non-removed background clutter and high-frequency noise in the horizontal dimension. In 2014, Zheng et al. (2014) introduced a cross-correlation calculation to improve noise filtering. In 2020 and 2021, Chen et al. (2021) and Bugarinović et al. (2020) introduced enhanced edge-detection methods for GPR interpretation by embedding a Canny edge detector and using a multi-dimensional non-linear data decomposition technique.

However, the limitations of edge-detection methods are evident, including unsatisfactory processing of complex image data containing noise. Similar to other conventional methods, these methods require several parameters to be set in advance (Khan et al., 2021; Kaur et al., 2016).

2.2.2 Deep-learning-based GPR methods for UU localisation

In contrast to conventional methods, deep-learning-based methods directly learn high-dimensional features via convolutional operations from B-scan images, instead of selecting specific features and parameters (Ali et al., 2021; Amaral et al., 2022). NNs

were first applied to GPR data interpretation in 1995 (Molyneaux et al., 1995). A deep-learning method was developed for rebar size and depth detection by stacking three fully connected ANN layers using a back-propagation mechanism. In UUs localisation tasks, these deep-learning methods are primarily used to solve two problems: one is to detect the region (containing hyperbolic features) where the UUs are located in the GPR B-scan input image (Özkaya et al., 2021; De Coster et al., 2019; Kim et al., 2019b; Onyszko et al., 2021), and the other involves processing the hyperbola and obtaining its apex to specify the coordinates of the target (Lei et al., 2019; Harkat et al., 2018).

Deep-learning-based methods for UU localisation can be classified into two categories, that is, one-stage and two-stage methods, owing to developments in deep-learning object detection (Table 2-3).

2.2.2.1 Two-stage methods

In the two-stage method, the regions of interest (region proposal) are first identified and then used for classification. The earliest two-stage detector was the R-CNN (Girshick et al., 2014). Subsequently, similar two-stage NNs have been introduced based on the R-CNN, including the R-CNN series (fast R-CNN and Faster R-CNN) and SPPNet (Girshick, 2015; Ren et al., 2017; He et al., 2015). Hou et al. (2021a) and Li et al. (2021) developed and tested their R-CNN-based model using actual GPR B-scan images for automatic object signature detection and segmentation, respectively. Meanwhile, Lei et al. (2019), Pham et al. (2018), and Ko et al. (2019) applied the advanced fast R-CNN models. The accuracy of two-stage methods reported in existing studies is generally higher than 90%, and these methods can effectively locate pipeline targets in different scenarios. In addition to accuracy, previous studies have focused on reducing the computational resource requirements (Xiao et al., 2021; Jaufer et al., 2021) required for GPR interpretation to accommodate more complex construction scenarios.

However, such methods are relatively time consuming for two reasons: 1) The generation of region proposals, for example, via selective search in an R-CNN and a fast R-CNN or a region proposal network in a Faster R-CNN. 2) Object classification operations for each region proposal. Therefore, time consumption has become the most

significant obstacle in the implementation of two-stage methods. To achieve accurate localisation, hyperbola fitting is required after the UUs region detection.

2.2.2.2 One-stage methods

In the one-stage method, the class probability and position coordinate values of an object are determined without an area proposal. This affords a higher detection speed because the final result can be obtained immediately after a single detection (Amaral et al., 2022). Typical algorithms include the YOLO series (Redmon et al., 2016; Redmon et al., 2018), SSD (Liu et al., 2016), and RetinaNet (Lin et al., 2017). In 2019, Zong (2019) applied YOLOv3 to real-time localisation in a B-scan dataset. The experimental results showed that the average one-stage UU detection accuracy and recall rates exceeded 85%. In other studies, one-stage methods have been improved by applying K-means to select anchor boxes (Li et al., 2020b) or adding a penalty term to minimise the normalised distance (Zhang et al., 2021).

However, the accuracy of the one-stage method is lower than that of the two-stage method, even though the former is more advantageous in terms of the operating speed (Ali et al., 2021; Amaral et al., 2022). In addition, the accuracy of these methods may be further reduced in the presence of complex noise.

Table 2-3 Deep-learning-based GPR methods for UU localisation

Type	Title	Mode	Advantages	Limitations
Two-stage	Deep-learning-based subsurface target detection from GPR scans (Hou et al., 2021a)	box fitting	The anchor scheme design of R-CNN model is improved to obtain a better 'candidate box'. Transfer learning is performed to solve the problem of	The GPR dataset is extremely difficult to obtain, and the amount of data is insufficient. The features extracted by DL models are not intuitive; the validity depends on the quality

Type	Title	Mode	Advantages	Limitations
			insufficient GPR dataset.	of the root dataset, and the interpretability of the model is unsatisfactory.
	Research on hyperbola detection and fitting in GPR B-scan image (Xiao et al., 2021)	box fitting	The calculation cost is reduced significantly via randomised HT.	The error from mean-position hyperbola fitting is not considered.
	GPR-R-CNN: an algorithm of subsurface defect detection for airport runway based on GPR (Li et al., 2021)	box only	GPR B-scan two-dimensional information and C-scan three-dimensional features are fused based on the R-CNN model to improve the robustness.	Only hyperbola regions are detected; further hyperbola apex positioning to clarify pipeline location information is not mentioned.
	Deep-learning-based automatic hyperbola detection on GPR data for buried utility pipes mapping	Box only	The proposed model significantly reduces the probability of false-positive detection by improving the Faster R-CNN model.	Pre-processing required; only hyperbola regions are detected; further hyperbola apex positioning to clarify pipeline location is not

Type	Title	Mode	Advantages	Limitations
	(Jaufer et al., 2021)			mentioned.
	Automatic hyperbola detection and fitting in GPR B-scan image (Lei et al., 2019)	Box fitting	A new double cluster search estimation algorithm is proposed to separate the target point clusters and realise hyperbolic feature recognition for apex localisation.	Pre-processing required; error from mean-position hyperbola fitting is not considered.
	Performance analysis of detecting buried pipelines in GPR images using Faster R-CNN (Ko et al., 2019)	Box fitting	Few deep-learning models are compared with the Faster R-CNN model for pipeline localisation.	Owing to insufficient actual data, the data generated by the gprMax simulation software is used for model training and validation.
	Buried object detection from B-scan GPR data using faster-R-CNN (Pham et al., 2018)	Box only	The proposed Faster R-CNN-based deep-learning model requires only a small amount of actual data for training and can achieve better localisation accuracy than classical	Owing to insufficient actual data, the data generated by the gprMax simulation software are used for model training and validation. Only Hyperbola regions are detected; further

Type	Title	Mode	Advantages	Limitations
			machine-learning methods.	hyperbola apex positioning to clarify the pipeline location is not mentioned.
One-stage	Radar assessment of structural concrete using neural networks (NNs) (Molyneaux et al., 1995)	Box only	This study is the first to propose the application of artificial NNs for GPR image interpretation.	Only hyperbola regions are detected; further hyperbola apex positioning to clarify the pipeline location is not mentioned.
	A deep-learning approach for urban underground objects detection from vehicle-borne GPR data in real-time (Zong et al., 2019)	Box only	The constructed dataset is composed of different types of targets, including cables and metal/non-metal pipes; the small target recognition problem is solved using the YOLOv3 framework; the localisation speed is much higher than that of two-stage methods (16 fps).	Only hyperbola regions are detected; further hyperbola apex positioning to clarify the pipeline location is not mentioned.

Type	Title	Mode	Advantages	Limitations
	Real-time pattern recognition of GPR images with YOLO V3 implemented by TensorFlow (Li et al., 2020b)	Box only	The K-means algorithm is applied to select anchor boxes to improve the accuracy of positioning hyperbolic vertices; results from multiple experiments show that the proposed YOLOv3-based model offers significant positioning speed advantage (12 fps on a CPU).	Complex anchor point selection mechanism and low localisation accuracy; only hyperbola regions are detected; further hyperbola apex positioning to clarify the pipeline location is not mentioned.
	A GAN-based deep-learning framework for automatic subsurface object recognition from GPR data (Zhang et al., 2021)	Box only	A deep-learning framework based on generative adversarial networks is proposed to solve the problem of insufficient GPR data; the average localisation accuracy is higher than that of other one-stage	Only hyperbola regions are detected; further hyperbola apex positioning to clarify the pipeline location is not mentioned.

Type	Title	Mode	Advantages	Limitations
			methods.	
			Others	
	Residual CNN+ Bi-LSTM model to analyse GPR B-scan images (Özkaya et al., 2021)	Box only	Bidirectional long short-term memory is proposed to achieve better metric performances than those afforded by transfer learning models. Results of multiple experiments show that the proposed model yields superior recognition accuracy (*F1* score of 97.42%).	Only hyperbola regions are detected; further hyperbola apex positioning to clarify the pipeline location is not mentioned.
	Towards an improvement of GPR-based detection of pipes and leaks in water distribution networks (De Coster et al., 2019)	Box only	The proposed convolutional support vector machine (CSVM) network yields improved classification performance; the number of parameters in the	Most of the experimental data are generated using the gprMax simulator software; only hyperbola regions are detected; further hyperbola apex positioning to clarify the pipeline location is

Type	Title	Mode	Advantages	Limitations
			proposed CSVM models is considerably lower than that in pretrained CNN model.	not mentioned.
	Classifier design by a multi-objective genetic algorithm approach for GPR automatic target detection (Harkat et al., 2018)	Box only	A multi-objective genetic approach is used to design a radial basis function classifier that can achieve similar results but with much lower complexity.	Pre-processing required; GPR hyperbolas cannot be identified from an entire radiogram; only hyperbola regions are detected; further hyperbola apex positioning to clarify the pipeline location is not mentioned.
	A novel 3D GPR image arrangement for deep-learning-based underground object classification (Kim et al., 2019b)	Box only	The proposed model yields extremely low false-positive errors by combining B- and C-scan GPR images for model training;	Several pre-processing steps must be conducted manually; only hyperbola regions are detected; further hyperbola apex positioning to clarify the pipeline location is not mentioned.

Type	Title	Mode	Advantages	Limitations
	A new methodology for the detection and extraction of hyperbolas in GPR Images (Onyszko et al., 2021)	Box only	The proposed model demonstrates excellent robustness in noisy environments; the localisation recall rate is 100% in the experiments.	Pre-processing required; several pre-processing steps must be conducted manually; only hyperbola regions are detected; further hyperbola apex positioning to clarify the pipeline location is not mentioned.

In the table above, 'box only' indicates that the proposed model can only detect the bounding box area of the UUs hyperbolas. Meanwhile, 'box fitting' indicates that the proposed model can locate the accurate coordinates of the UUs hyperbola apex after the bounding box is detected.

2.2.2.3 Summary

The advantages of deep-learning methods, such as high automation and versatility, are evident. However, current deep-learning methods have the following limitations.

1) Box-fitting mode. The box-fitting mode was used in all the one- and two-stage methods to locate the hyperbola apexes, as shown in Figure 2-2. The location problem can be classified into two aspects: hyperbola region detection and hyperbola fitting (point location) (Ali et al., 2021; Zheng et al., 2014; Amaral et al., 2022). In some studies, the pre-processing of B-scan images had to be increased to remove noise. Consequently, the model could not adjust the parameters globally to obtain optimal weight results; thus, the localisation precision deteriorated. In these methods, the bounding box can only provide an approximation of the hyperbolic range in a B-scan image. In contrast, a hyperbola that represents the location of the UUs and the corresponding apex may exist in multiple potential hyperbolas within the bounding

box range. Different fitting processing methods yielded different hyperbolic results. The localisation error caused by the fitting has not been considered in previous studies.

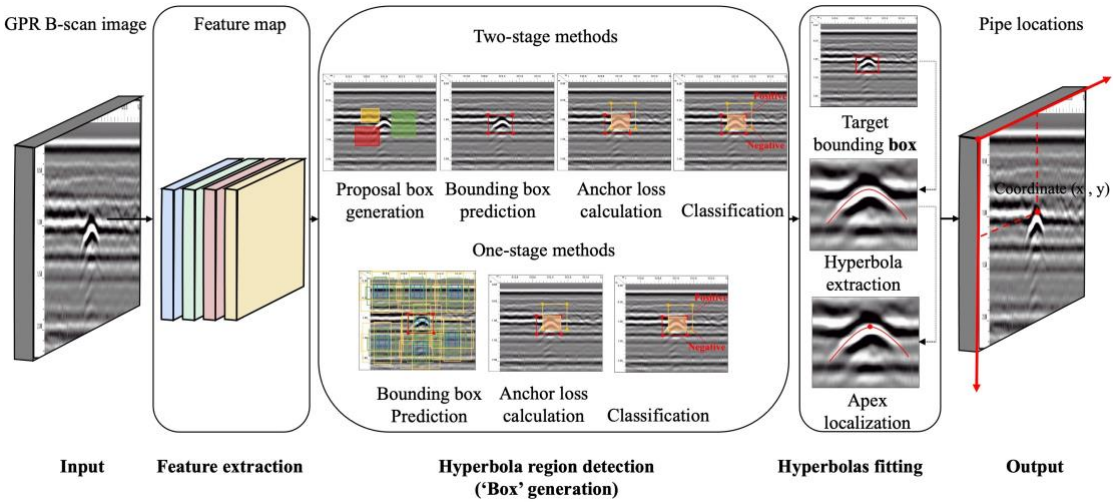

Figure 2-2 Overview of box-fitting mode

2) Dilemmas in anchor-based methods. The anchor-based method is currently used in all relevant studies, regardless of whether a one- or two-stage method is used. However, only a few target hyperbolas are present in the B-scan images. Setting many anchor boxes generates numerous simple samples, which substantially imbalance the populations of positive and negative samples. The two-stage method improved the positive and negative sample screening mechanisms but resulted in a significantly reduced operating speed.

3) Pre-processing. The B-scan image data obtained by GPR include all types of background noise, particularly in a complex fieldwork environment. Reducing noise interference through pre-processing increases the workload and renders it more difficult to realise a high degree of automation for UU localisation.

2.3 Image-based 3D reconstruction for UUs

Image-based 3D reconstruction is a pivotal technique in computer vision, widely utilized to capture the spatial attributes of objects from multiple images. This method supersedes traditional labor-intensive approaches, offering a cost-effective solution with broad applications in fields like construction monitoring, mining surveying, and medical diagnostics. Despite its extensive use, image-based 3D reconstruction faces

specific challenges when applied to underground utilities (UUs), particularly under varied lighting conditions.

The process of image-based 3D reconstruction involves two critical stages: sparse and dense reconstructions. Initially, sparse reconstruction focuses on extracting and matching features across different images to establish a relationship between camera perspectives and the object. This foundation is crucial as it involves detailed algorithms for feature point analysis, and methods such as Structure from Motion (SFM) for camera parameter estimation. The accuracy of this stage is paramount in determining the overall success of the 3D reconstruction. Following the sparse reconstruction, the dense reconstruction phase uses the sparse point cloud data to compute dense 3D point clouds. Techniques such as Multi-view Stereo (MVS) and voxel-based reconstruction play significant roles here. However, the effectiveness of these methods heavily depends on the initial sparse data quality, which can be compromised under suboptimal conditions (Guidi et al., 2014; Lu et al., 2012).

A major challenge for image-based UUs reconstruction is its sensitivity to lighting. Inadequate lighting conditions, such as those found in underground or nighttime environments, significantly hinder the ability to capture high-quality images. Poor lighting affects the detection and matching of features, leading to less reliable camera parameter estimation and, subsequently, inaccurate 3D models (Roncella et al., 2021; Pozo et al., 2019; Burdziakowski et al., 2021). The dependence on lighting is a substantial limitation, especially considering the critical nature of accurate UU mapping for maintenance and planning.

To address the lighting issue, significant research has been directed towards enhancing image quality in low-light conditions using both conventional methods (like histogram adjustments and white balance techniques) and advanced deep learning approaches. Despite these efforts, achieving consistent quality in image enhancement remains a challenge due to the subjective nature of manual adjustments and the dependence on empirical parameters, which can vary significantly between users and environments.

2.3.1 Image-based 3D reconstruction

Image-based 3D reconstruction is a popular topic in the field of computer vision (CV). It automatically captures the intuitive spatial information of objects from images, thus replacing the traditional modelling methods that are intrinsically labour intensive and low cost. For decades, image-based 3D reconstruction has been widely used in various fields, such as construction progress monitoring (Xue et al., 2021; Kropp et al., 2018), mining surveying and mapping (Ren et al., 2019), and medical diagnosis (Widya et al., 2021). This section reviews research on 3D reconstruction based on RGB images. RGB-D-type and single-image inputs were excluded because they cannot be applied to large-scale scenarios (Zollhöfer et al., 2018; Azinovic et al., 2021). Image-based 3D reconstruction restores the surface model of an object from multi-view images captured from various angles. This process includes two main steps: sparse and dense reconstruction, as shown in Figure 2-3.

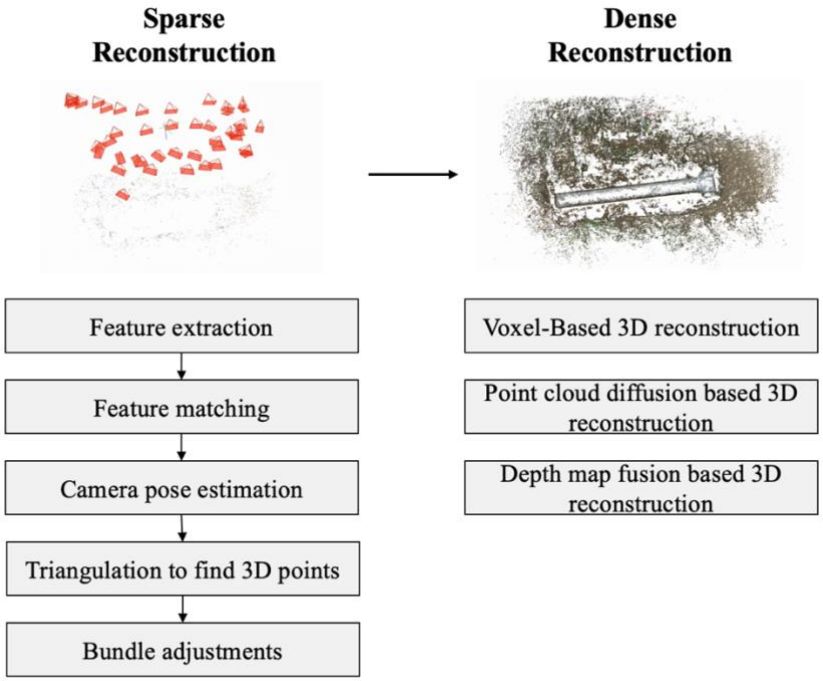

Figure 2-3 General pipeline of the image-based 3D reconstruction

2.3.1.1 Sparse reconstruction

Sparse reconstruction is the upstream core foundation of the image-based 3D

reconstruction task, which aims to determine the relationship between the shooting perspective of multiple-input RGB images and the target object. The three basic steps of sparse reconstruction are feature extraction, matching, and camera parameter estimation.

Extracting and matching (matching of the same point on an object from different angles) feature points (spots, corners, etc.) is the core basis for determining the performance of a 3D reconstruction. In 1999, Lowe (1999) proposed the renowned scale-invariant feature transform (SIFT) algorithm, which uses Euclidean distance to calculate the matching degree between feature points and subsequently improved it in 2004 (Lowe, 2004). In 2006, Bay (2006) and Rosten (2006) proposed speeded up robust features (SURF) and features from accelerated segment test (FAST) algorithms, which have less computation and robustness than SIFT. Subsequently, Rublee (2011) proposed a new ORB algorithm with rotation invariance based on BRIEF in 2010 (Calonder et al., 2010).

The camera parameter estimation process determines the position and orientation of the camera relative to the object using the correspondence between the pixel features of the 2D image and the target object. Structure from motion (SFM) (Hartley et al., 2003) is the most widely used methodology for estimating camera parameters using camera motion trajectories. The SFM was further developed into two main reconstruction modelling techniques: incremental reconstruction and global reconstruction (Jiang et al., 2020; Zhu et al., 2018). Incremental reconstruction involves triangulation and point-n-points (PnP), while applying partial bundle adjustment (BA) (Azzam et al., 2020; Jiang et al., 2020). In contrast, global reconstruction can obtain all camera poses and scene structures simultaneously and only requires BA once, but it is less robust (Schonberger et al., 2016).

2.3.1.2 Dense reconstruction

Dense reconstruction, as a downstream task in the process of 3D reconstruction, refers to the gradual calculation of dense 3D point clouds on the surface of scene objects based on the sparse point-cloud information obtained from sparse reconstruction (Ma

et al., 2018). Multi-view stereo (MVS) (Furukawa et al., 2015) is the core method for cross-image pixel matching in dense reconstruction and includes voxel-based dense reconstruction (Eigen et al., 2014; Choy et al., 2016), feature point growing (Lhuillier & Lin, 2005; Wu et al., 2010; Furukawa et al., 2010), and depth map fusion (Weder et al., 2020; Riegler et al., 2017).

2.3.2 3D reconstruction from low-light images

As mentioned above, sensitivity to lighting conditions is the main issue that image-based approaches for as-built UU records must address (Burdziakowski et al., 2021). Exposure is one of the most important factors for determining the quality of a photo. For example, in overexposed or underexposed areas, image details can be lost and colour-diluted. The core task of this study is to develop a low-light UU record model. Therefore, this section reviews the existing research on image enhancement for 3D reconstruction tasks in low-light environments.

2.3.2.1 Conventional methods

Conventional methods are still dominant in the relevant research to optimise the 3D reconstruction performance in a low-light environment, such as colour balance (Pascale, 2006; Ancuti et al., 2018), histogram distribution (Coltuc et al., 2006; Ibrahim et al., 2007), RGB to grey (Lu et al., 2012; Grundland et al., 2007), white balance (Grundland et al., 2007; Liu et al., 1995; Weng et al., 2005), and image content enhancement algorithms (MacDonald et al., 2014; Vedaldi et al., 2010). In 2013, Sohaib et al. (2013) developed an image-based system to extract useful 3D reconstruction information from images captured in various environments. In 2014, Guidi et al. (2014) and Ballabeni et al. (2015) utilised digital pre-processing and colour enhancement of high-dynamic range (HDR) imaging to improve automatic 3D reconstruction based on SFM and image matching. Santise et al. (2018) proposed a stereo photogrammetry system based on the time of exposure and degree of aperture of the shutter for low-light and night-time image analysis. The reconstruction of the rock mass surface in a low-light environment was realised. Alasal et al. (2018) and Aldeeb et al. (2018) used image enhancement technology, respectively, to increase

image contrast to improve the quality of 3D model construction. Kanellakis et al. (2019) developed an algorithm based on contrast-limited adaptive histogram equalisation (CLAHE), which achieves 3D image reconstruction in low-light environment by suppressing noise while enhancing image contrast. Yeh et al. (2021) proposed a robust system based on HDR technology to achieve object reconstruction in a low-light environment; however, this method requires RGB-D equipment.

All these studies would aid in obtaining better image-based 3D reconstruction performance. However, a common problem is that empirical input parameters are required for the modelling process, leading to the reconstruction performance being subject to the users' experience. For example, explicit and accurate thresholds must be assigned to parameters such as the brightness, contrast, histogram distribution, and white balance for processing.

2.3.2.2 Deep-learning methods

Image enhancement methods based on deep learning are constantly emerging algorithms (for example, Retinex-Net and LLNet) (Lu et al., 2012; Lore et al., 2017). However, studies of image enhancement for 3D reconstruction in low-light environments are limited. Tang et al. (2019) proposed a stereo matching reconstruction network based on the Pyramid Stereo Matching Network (PSMNet) and a reconstruction module for determining the characteristics of low-light level images. To mitigate serious and complex noise in low-light images, an image reconstruction module was added to the traditional stereo matching network for automatic denoising. Other methods have only been studied from the perspective of low-light image quality improvement without considering the content of 3D object reconstruction (Sobbahi et al., 2022). In 2018, LightenNet (Li et al., 2018a) was proposed for learning an image for illumination map translation using a conventional CNN. Subsequently, models (LowLightGAN (Kim et al., 2019a) and EnlightenGAN (Jiang et al., 2021)) based on generative adversarial networks (GANs) were introduced using synthetic DIV2K datasets (Agustsson et al., 2017). More recently, advanced zero-reference models (zero-DCE (Guo et al., 2020a), SCI (Ma et al., 2022), and (Zhang et al., 2020b)) have

been proposed to overcome the problem of matching the data for training.

The image enhancement method based on a deep-learning cloud avoids the manual parameter setting and selection process of the most appropriate conventional method, subject to various site conditions. However, it converts the low-light enhancement problem into the problem of finding the optimal mapping between the input images and target reference images, regardless of the site conditions. To solve this problem, paired or unpaired template ground-truth images (reference images) are required for model training supervision. In other words, the optimised target images (reference images) should be clarified in advance. Although this technique is much more convenient than conventional methods, it still fails to avoid the subjective impact of the 'template ground-truth images' leading to the limitations in the model learning. This is challenging to achieve because the collection of reference images is difficult.

2.3.2.3 Summary

Conventional methods introduce numerous human factors, making the 3D reconstruction process time consuming and highly subjective. Deep-learning methods can effectively avoid subjectivity in the 3D reconstruction process and realise real-time operation. However, applicable reference images are still inevitable for the model training of the supervision mechanism. The subjective parameters or rarely appropriate reference image settings of the above methods restrict the optimisation potential of low-light images, thereby disabling the deep-learning model for autonomous learning and adjustment. As a result, establishing an unrestricted deep-learning model with loose assumptions on reference images is essential to that no paired or unpaired data reference images as the 'ground truth' are needed in the training process.

2.3.3 Image-based UU 3D reconstruction

UUs are usually not exposed, but when depth, material, size, and other information are speculated through non-destructive techniques, such as GPR (Özkaya et al., 2021; De Coster et al., 2019), the best opportunity for UU documentation has been missed (Bureau of Transportation Statistics, 2016; Van et al., 2019; Wang et al., 2022b; Yan et

al., 2019). In the exposed stage (construction or maintenance), the image-based 3D reconstruction method showed remarkable advantages, such as fast speed, low cost, high precision, and no training required.

Image-based UU 3D reconstruction has demonstrated an infinite potential under normal lighting conditions. In an earlier study, Hu (2005) developed a 3D reconstruction system for UUs using photogrammetric methods and validated its effectiveness and cost advantage. Tulloch et al. (2006) proposed a mobile photogrammetric mapping system to map exposed utilities on construction sites in 2006. The system comprised a global positioning system (GPS), tablet computer, and high-quality camera (Nikon Coolpix 8800). Although the system had a slightly lower accuracy (absolute horizontal accuracy of 0.33 m), it still showed promising reconstruction cost advantages and ease of use. In 2021, smartphone-based photogrammetry was used for as-built 3D documentation during the open excavation replacement of water pipes in Denmark (Hansen et al., 2021a; Hansen et al., 2021b). In the most recent 2022 study, Yuen et al. (2022) proposed a low-cost 3D reconstruction system based on a digital camera and applied it to an actual engineering site. The efficiency and accuracy of the reconstruction have been widely recognised.

Although existing studies have recognised the limitations of illumination conditions in image-based UU 3D reconstruction, an effective solution has yet to be proposed. Hu (2005) and Tulloch et al. (2006) point out that the light condition of acquired image datasets is crucial to the reconstruction tasks. The blur image/video collected from real sites can lead to a sharp decline in the effect of the point-cloud reconstruction, which has been experimentally validated (Hansen et al., 2021a; Hansen et al., 2021b). Different camera image capture protocols using consumer-grade smartphones were examined by Yuen et al. (2022), but they needed to provide a reasonable plan to improve the quality of these inputs.

2.4 Topology completion for as-built UUs

In the management of underground utilities (UUs), the accurate completion of missing topology information remains a challenging task. Despite the critical need for efficient

solutions, current methods often fall short. Traditional techniques such as Ground Penetrating Radar (GPR) (Birkenfeld, 2010; Skartados et al., 2019), PipeProbe PipeProbe (Lai et al., 2010), and manual manhole inspections (Alejo et al., 2019), though widely used, are labor-intensive and costly. These methods, while precise, do not offer a scalable or cost-effective solution for widespread data collection.

To combat these issues, recent studies have shifted focus toward transforming the completion of general UU attributes—such as diameter, material, and water levels—into an imputation problem (Davey et al., 2009; Little et al., 2019; Von et al., 2004; Graham et al., 2012; Templ et al., 2011). Techniques including traditional single and linear regression-based imputation, as well as more sophisticated multiple imputation methods (e.g., AMELIA and IMPSEQ), along with machine learning strategies like Principal Component Analysis (PCA) (Gangopadhyay et al., 2005), K-Nearest Neighbour (KNN) (Woldesellasse et al., 2021), decision trees (Barros et al., 2012), and neural networks (Bishop, 1995) have been explored for their potential to accurately predict missing values. However, these imputation and machine learning methods are currently inadequate for predicting the complex topological relationships essential for comprehensive UU management.

This section aims to explore the existing gaps in these methodologies and discuss potential advancements that could enhance the accuracy and reduce the costs associated with topology completion in UU systems. By addressing these inefficiencies, we can better equip engineers and managers with the tools needed for effective UU lifecycle management.

2.4.1 Topology completion for UUs

Topology completion for UUs is important for full life-cycle management. However, missing data are common in UU scenarios. To solve this problem, the existing data-completion methods can be divided into traditional, imputation, machine-learning, and graph-based methods.

2.4.1.1 Traditional methods

The first reaction of most managers is to obtain relevant information and collect relevant data. Finding data backups or mutually corroborating data records from other relevant materials can partially solve the missing data problem to a certain extent. The use of GPR (Birkenfeld et al., 2010; Skartados et al., 2019; Zeng et al., 1997) or manual surveys (Lai et al., 2010; Alejo et al., 2019) is a common method for data completion. However, these methods can only be used in a very small target area, and their implementation costs increase rapidly as the volume of UU data that must be completed increases. In addition, large-scale pipeline network investigations are limited by factors, such as time and equipment.

2.4.1.2 Imputation

Unlike traditional methods, imputation completes the task of missing data through reasonable differences from a data-analysis perspective. Kabir et al. (2020) conducted a study on the efficacy of various imputation methods for completing the water network database. This study evaluated three single imputation methods, namely, mean imputation (Davey et al., 2009), median imputation (Little et al., 2019), and linear regression-based imputation (Von et al., 2004; Graham et al., 2012), as well as three multiple imputation methods: iterative robust model-based imputation (IRMI) (Templ et al., 2011), multiple imputations of incomplete multivariate data (AMELIA) (Honaker et al., 2011), and sequential imputation for missing values (IMPSEQ) (Verboven et al., 2007). The findings suggest that the IMPSEQ method demonstrated superior performance in terms of completing the missing values in the water network with biases of only −0.900, 2.100, 0.800, and −0.400 for the pipe age, diameter, number of valves, and number of service connections, respectively. In recent years, the imputation method has been used in pipeline damage prediction (Xu et al., 2021), water quality detection (Srebotnjak et al., 2012), and demand forecasting (Zanfei et al., 2022).

2.4.1.3 Machine-learning methods

Machine-learning methods predict missing values by learning the intrinsic structure and patterns of data. In 2017, a Gaussian process regression method (Samuelsson et

al., 2017) was applied to a wastewater treatment plant (WWTP) monitoring application scenario, and missing data in the flow-rate signal were accurately estimated. PCA was used to predict the dynamic variation in the potentiometric head in Bangkok (Gangopadhyay et al., 2005). Woldesellasse (Woldesellasse & Tesfamariam, 2021) carried out neural network construction based on algorithms such as *K*-Nearest Neighbour (KNN), AMELIA, and IMPSEQ (Batista & Monard, 2002; Honaker et al., 2011; Verboven et al., 2007) in his research to deal with incomplete and missing data in the corrosion pit measurement database. Osman et al. (2018) conducted a comparative study on traditional interpolation methods and various machine-learning methods and sorted out the advantages and disadvantages of various methods in the missing data-completion scenario of Water distribution systems (WDSs).

2.4.1.4 Graph-based methods

Graph-based methods have achieved widespread success in different areas of missing data handling, such as transportation, smart power grids, and gene expression (Chan et al., 2023; Kuppannagari et al., 2021; Xiang et al., 2021). Because UU networks have significant topological connections, graph-based methods have received increasing attention in recent years. Belghaddar et al. (2021) conducted a study on a range of prevalent machine-learning techniques, including Support Vector Machine (SVM) (Belghaddar et al., 2021), decision trees (Cortes et al., 1995), feedforward artificial NNs (ANNs) (Safavian & Landgrebe, 1991), and Multilayer Perceptron (MLP) (Rumelhart et al., 1986), as well as graph-based models, such as GCN (Kipf & Welling, 2017), ChebNet (Defferrard et al., 2016), GraphSAGE (Hamilton et al., 2017), and TAGCN (Du et al., 2017). The results showed that graph-based models have significant data-completion advantages, particularly with less available data. Additionally, Joakim et al. (2022) proposed a novel decoder-focused multitask classification architecture termed the cross-task graph neural network (CT-GNN), which can be used for sewer defects and attribute (water level, pipe material, and pipe shape) classification.

However, these methods were only applied to complete the common attributes of

missing data, such as the material, diameter, and age of the pipe. However, the completion of the topological UU relationship must be explored. Topological relationships, as important information for UU management, are more difficult to obtain than general attribute characteristic data, such as diameter, depth, and material, because of their complexity. If topological data are missing, finding them is often costly. To the best of our knowledge, there is a need for research on the completion of missing topology data for an underground pipe network. However, this is a challenging task.

2.4.2 Graph convolution networks

GCNs are generalisations of classical CNNs (LeCun et al., 1998) used to handle graph data. As proposed by Kipf and Welling (2017), this is an effective graph model for semi-supervised learning. Unlike traditional convolutional neural networks (CNNs), GCNs operate directly on graph-structured data, enabling them to capture the relationships between nodes and neighbours. GCNs stack layers of learned first-order spectral filters followed by a non-linear activation function to learn graph representations (Wu et al., 2020). In recent years, GCN and its variants have been applied in various applications and multiple tasks.

With the foundation of GCN, many researchers have begun to study its improvements and variants. Hamilton et al. (2017) proposed GraphSAGE (SAGEGCN), a general inductive framework that leverages node feature information to generate node embeddings for previously unseen data efficiently. To a certain extent, SAGEGCN can be seen as a special case of GCN, because the aggregation method in SAGEGCN can be seen as a form of GCN. The key idea is to aggregate the feature information from a node's local neighbourhood. However, it only considers the information of first-order neighbour nodes and ignores the keyness of higher-order neighbour nodes. A graph attention network (GATGCN) is a graph neural network model based on the attention mechanism first proposed by Veličković et al. (2018). The GATGCN is a variant of the GCN that is more flexible and interpretable for node feature aggregation and interaction than the GCN, especially when dealing with complex graph structures. The

core idea of the GATGCN model is to apply the attention mechanism to calculate the weights between each node and its neighbours to better use the neighbours' information. In the convolution layers, the GATGCN model employs a multi-head attention mechanism to calculate the weights between the nodes. By learning the weights between each node and its neighbours, it can better integrate the neighbours' information. Simultaneously, the GATGCN model uses residual links to prevent information loss. However, it faces issues of high computational complexity and poor interpretability.

In the same year, Du et al. (2017) proposed TAGGCN, which is a GCN defined in the vertex domain. TAGGCN not only inherits the properties of convolutions in CNN for grid-structured data, but is also consistent with convolution, as defined in graph signal processing. It exhibits better performance than existing spectral CNNs on many datasets and is computationally simpler than other recent methods. The TAGGCN increases the flexibility and robustness of the model through adaptive convolutional kernels and adaptive layer selection mechanisms, thereby addressing the challenges of complex graph structures and practical problems. Chen et al. (2018) proposed FastGCN, which accelerates the convolution operation using sampling technology and introduces block technology to improve the training speed. ChebNet (ChebGCN) (Defferrard et al., 2017) is a GCN based on spectral graph theory, which was proposed in 2019. ChebGCN is based on GCN and uses Shebyshev polynomials instead of an adjacency matrix for the convolution operation, thus improving the calculation efficiency and network depth and enhancing the generalisation of the model. The basic idea of ChebGCN is to represent a graph as an eigen decomposition of its Laplacian matrix and utilise Chebyshev polynomials to approximate the Laplacian matrix. However, one drawback of ChebGCN is its weak ability to process high-frequency information in graphic signals, which may be limited by the sampling rate of the waveform signals.

2.4.3 Summary

The review of existing data completion methods for UUs highlights a critical need for

specialized approaches that can address the unique challenges of predicting topology reconstruction issues within these complex systems. Traditional, imputation, machine-learning, and graph-based methods provide a solid foundation of techniques that have enhanced our understanding and capability in managing data incompleteness. However, these methods primarily focus on attribute data completion, such as material, diameter, and age of pipes, without a specific emphasis on the connectivity and topological relationships essential for comprehensive UU network management.

From the literature, it is evident that machine-learning and graph-based methods, particularly those involving Graph Convolutional Networks (GCNs) and their variants offer promising frameworks for addressing non-trivial problems in structured data environments. These methods effectively utilize the relational information between data points, which is crucial for understanding the connectivity in UU networks.

Despite these advances, there remains a substantial gap in applying these methods specifically for predicting and managing the UU topology reconstruction issues. Connectivity in UU networks entail more than just identifying physical links—it also involves comprehending the operational dependencies and resilience of the network against failures or disruptions. The current research lacks focused studies on how these advanced data completion techniques can be precisely tailored to predict and address connectivity failures in UU networks. Traditional methods, such as using GPR and manual inspections, while accurate, are labor-intensive and costly. On the other hand, conventional imputation methods are ill-suited for predicting the complex topological relationships critical for effective UU management. This gap highlights the need for developing accurate, low-cost, and efficient strategies tailored to address these topological challenges in UU networks.

2.5 Chapter Summary

This chapter reviews the current advancements and ongoing challenges in the 3D reconstruction of underground utilities, a field increasingly vital as urban infrastructures become more complex and densely packed. The exploration of the various methodologies, from non-destructive techniques like Ground Penetrating

Radar (GPR) to image-based reconstructions and topological data completion, reveals a landscape of innovation aimed at enhancing the accuracy and efficiency of subsurface utility mapping.

Despite these efforts, the chapter identifies critical limitations in current research that hinder the practical application of 3D reconstruction technologies: 1) Inadequacies in gpr-based localization: GPR, though popular, faces significant challenges in accurately localizing UUs due to its susceptibility to environmental interferences and the inherent complexity of subsurface environments. The subjective nature of interpreting GPR B-scan images, which heavily relies on expert knowledge, adds another layer of complexity. While deep-learning methods have been explored to automate data interpretation, they often break down the problem into sub-tasks (e.g., box detection and hyperbola fitting) that only achieve local optimality without ensuring the best overall solution. 2) Image-based reconstruction under low-light conditions: Image-based 3D reconstruction techniques, while cost-effective compared to laser scanning, struggle in low-light conditions common in underground settings. Current image enhancement algorithms require manual tuning and are heavily influenced by operator experience, which can lead to inconsistent results. Despite advancements in deep learning for image enhancement, the lack of suitable training data (paired low-light and ideal reference images) and the reliance on subjective reference standards severely limit the reliability of reconstructed outputs. 3) Topology Completion for UUs: Efficiently completing missing topology data for UUs remains a significant challenge. Traditional methods like manual manhole inspections, though accurate, are labor-intensive and costly. Machine learning and imputation strategies, successful in predicting some data attributes, fall short in accurately mapping complex topological relationships essential for comprehensive UU management.

In conclusion, this chapter not only comprehensively explains the decisive methods for UU 3D reconstruction at various stages of existing research but also identifies current unresolved issues. The subsequent chapters will each focus on these research issues, aiming to resolve the precision problems in GPR-based UU reconstruction, the

challenges of 3D reconstruction under low-light conditions during the exposure phase of UUs, and the reconstruction of underground pipeline network topology under conditions of missing records.

Chapter 3 : Research methodology

This chapter outlines the research methodology, which comprises four distinct sections, corresponding to the four objectives outlined in Section 1.3. Section 3.1 provides an overview of the research philosophy, while Section 3.2 illustrates the research design and alignment between research methods and objectives. The methods employed to accomplish Objectives 1 to 4 are presented in Sections 3.3 to 3.6, respectively. Finally, Section 3.7 provides a concise summary of this chapter.

3.1 Research paradigm

This research aims to improve the life-cycle management efficiency of as-built UUs by enhancing the 3D reconstruction performance. The positivist research paradigm was applied in this study.

Positivism is a philosophical approach that emphasises the use of scientific methods and empirical data to understand natural and social worlds. Positivists believe that knowledge can only be obtained through observation and measurement and that scientific enquiry is the best way to achieve this. This study uses scientific methods and empirical data to understand the natural and social worlds. Therefore, in this research, the positivist research paradigm, which insists on realism, objectivism, deductive, and quantitative research methods, will be applied as ontology, epistemology, and methodology, respectively.

(1) Ontology

Ontology is a philosophical discipline concerned with the fundamental nature of existence, the interrelationships among entities, and their essential attributes. Ontologies can be classified into two contrasting types, realism, and relativism. Realists contend that a single reality can be objectively measured and discovered by various observers and researchers. Conversely, relativists assert that the 'truth' is subjective and dependent on the observer. Therefore, multiple realities can be constructed based on individual perspectives and experiences, each of which is valid for the respective observer or researcher (Killam, 2013). In this research, the objects

of study are physical entities and their phenomena in the natural sciences. Therefore, only one realism of the ultimate truth was selected as the ontology for this study.

(2) Epistemology

Epistemology is a philosophical discipline dedicated to investigating the fundamental nature of knowledge and its acquisition, justification, and connection to truth. It delves into a range of issues, such as the distinction between knowledge, beliefs, and opinions; methods of determining truth; the influence of perception, reason, and experience on knowledge acquisition; and assessment of the reliability and validity of knowledge claims. The primary objective of epistemology is to understand the sources, limitations, and essence of human knowledge comprehensively. According to Wilson (2001), researchers can hold divergent epistemological positions, namely, objectivism and subjectivism, which are typically informed by their underlying ontological perspectives. A researcher who adheres to realism typically employs objective techniques to observe phenomena and uncover the singular, objective truth that exists independently of the researcher. Realism ontology is the basis of this research, so objectivist epistemology will be applied as the starting point of the research.

(3) Methodology

Methodology denotes a systematic and structured approach to problem solving that emphasises how research is conducted. Research methodologies, including deductive and inductive approaches, and quantitative and qualitative methods, are determined by a researcher's adherence to either objectivism or subjectivism (Aliyu et al., 2015).

Deductive research starts with a general principle or hypothesis, and then draws specific conclusions based on that principle. However, inductive reasoning starts with specific observations or data, and then uses that information to make broader generalisations or theories. This research began with a theory or hypothesis, and experiments were conducted to test this theory. Therefore, deductive research is applied to the problem solving conducted in this research.

Quantitative research is an empirical research methodology aimed at quantifying and measuring data through statistical analysis. It involves collecting numerical data that can be analysed using mathematical or statistical techniques to describe and explain

phenomena through numerical patterns and relationships. In contrast, qualitative research is an exploratory approach that seeks to understand social phenomena by gathering data through observation, interviews, and other non-numerical methods. The main objective of qualitative research is to gain an in-depth understanding of a phenomenon and to explore its complexity, nuances, and underlying meanings. In this study, quantitative methods and experiments were applied to the analysis and explained the observed phenomena.

(4) Axiology

Axiology is a philosophy that studies how people determine the value of different things. Those who work in this field examine the nature and different types of value, including ethical, moral, religious, and aesthetic values. Axiologists study how people compare and value things, and the impact of those values on reality. In this study, the core value consideration is a practical promotion value for UU project management.

3.2 Overview of the proposed method

An overview of the adopted research methods is shown in Figure 3-1. Each approach can be used to achieve at least one objective. As shown in Figure 3-1, this study includes four parts: a literature review (Objective 1) and the development of three specific models (Objectives 2, 3, and 4). The development of three key models is used to solve the limitations of UU 3D reconstruction in the non-destructive and exposed stages and the problem of topological relationship reconstruction after obtaining the surface reconstruction model. The outputs of Objectives 2 and 3 are part of the inputs of Objective 4. The flow of the research design was structured around four main objectives, each contributing to the overarching goal of advancing the field of UU reconstruction.

Objective 1: Literature Review

The research begins with a thorough examination of existing knowledge and identifies gaps in the current research related to UUs. The literature review encompasses diverse sources including academic journals, books, published standards, electronic databases, and government websites. Critical issues such as limited research attention, inefficient localisation precision in GPR interpretation, challenges in low-light image-based

reconstruction, and inaccuracies in UU topology completion were identified.

Objective 2: GPR Localisation

Building on the insights gained from the literature review, the second objective was to enhance the precision of localising UUs using GPR. The process involves data collection by gathering raw GPR B-scan data, followed by data processing using the RADAN 7 software and Gaussian processing. A localisation model was developed to improve the anti-interference capabilities and accurately predict the UU coordinates. The performance of the model was rigorously validated in terms of its precision, speed, and robustness.

Objective 3: Low-Light Enhancement

To address the challenges posed by low-light conditions, the third objective was to enhance the images of UUs. The method involves image collection under varied illumination, the development of an enhancement mechanism to improve low-light image quality, and integration into 3D reconstruction using COLMAP. The outcome is an improved 3D reconstruction model for UUs under low-light conditions, validated through experiments that focus on the reconstruction amount, accuracy, and efficiency of the proposed loss-function ablations.

Objective 4: Topology Completion

The fourth objective is to complete the topology of an incomplete UU database. This involves the utilisation of a graph-based convolutional network model to enrich the feature dimensions and classify the node topology. The model was employed to achieve a complete topology of the UU database, and controlled experiments were conducted to validate the accuracy of topology completion.

Throughout the research, advanced methods were employed, including GPR-based localisation, image enhancement techniques for low-light conditions, and GCNs for topology completion. Collectively, these methods contribute to the development of a comprehensive 3D reconstruction model for UUs.

The culmination of this study was the development of a comprehensive UU 3D reconstruction model. This model is expected to provide high spatial accuracy and complete topology information for UUs, addressing the challenges identified in the

literature review. The final output aims to improve the accuracy, efficiency, and reliability of 3D reconstructions, thereby potentially enhancing the life-cycle management of UUs.

This research design is poised to significantly advance the field of UU management by systematically addressing key challenges in localisation, image enhancement, and topology completion. The project's comprehensive approach aims to provide practical solutions that contribute to the overall improvement in accuracy and reliability in the 3D reconstruction of UUs, thereby enhancing their life-cycle management.

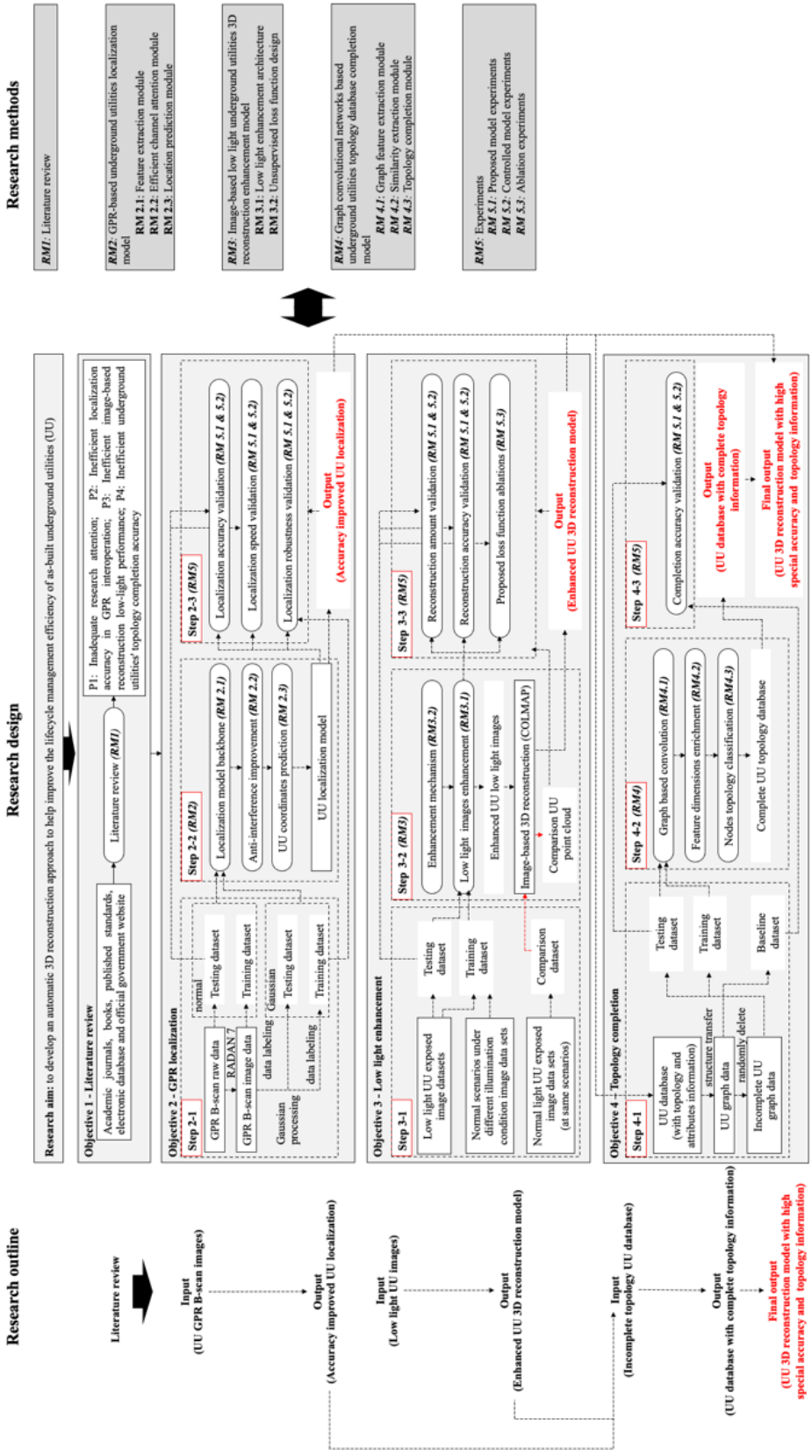

Figure 3-1 Overview of the proposed method

3.3 Literature review method (Objective 1)

This section introduces the research methods and procedures for Objective 1 (literature review). As shown in Figure 3-2, the literature review identified the research topics, trends, and limitations of the automatic 3D reconstruction for as-built UUs and the main research gaps of this thesis by collecting existing research outcomes from academic journals and other sources. The specific steps included scope determination, data collection, and content analysis.

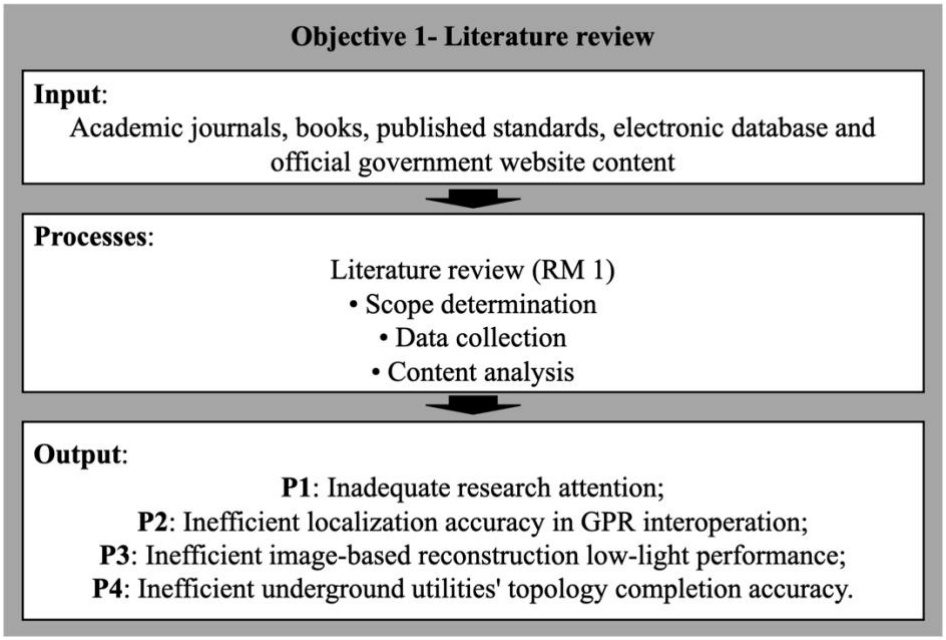

Figure 3-2 Overview of the methodology for Objective 1 (Literature review)

3.3.1 Scope determination

Given the research aim and objectives, the scope of this review includes the following aspects: 1) the advantages, limitations, and application performance of each current 3D reconstruction technique; 2) common challenges and future research directions in the field of 3D reconstruction of UUs; 3) conventional image-processing methods and deep-learning-based UU GPR localisation methods; and 4) image-based 3D reconstruction technology, 3D reconstruction from low-light images, and image-based 3D reconstruction of UUs. 5) Topology completion for UUs and GCN research status.

3.3.2 Data collection

The Web of Science, ASCE databases, and official government websites were selected for data collection in this study because of their wide coverage and high quality. The following keywords were chosen to cover as much of the research area as possible: UU 3D reconstruction/mapping, subsurface utility reconstruction/detection, pipeline/cable detection, GPR interpretation, UU localisation, image-based 3D reconstruction/photogrammetry, low-light image reconstruction, low-light image enhancement, as-built UU records, GCN, and topology completion. To ensure the quality of the articles, they were selected according to the following two criteria: 1) They must be peer-reviewed articles. 2) Check the abstract of the article, which meets the scope of this thesis.

3.3.3 Content analysis

To systematically process and analyse the content of the selected studies. To perform the content analysis, the textual data were systematically deconstructed and categorised through coding. The categories and codes used for the content analysis are listed in Table 3-1.

Table 3-1 Analysing codes of the selected contents

Categories	Codes
UU 3D reconstruction	(1) UU reconstruction technologies, (2) UU reconstruction applications, (3) best UU reconstruction performance, (4) implementation challenges
GPR UU localisation	(1) GPR technology, (2) GPR B-scan interpretation, (3) Deep-learning objects detection models, (4) Image processing for GPR B-scan
Exposed low-light UU reconstruction	(1) Image-based 3D reconstruction (photogrammetry), (2) Low-light 3D reconstruction enhancement, (3) Image enhancement, (4) Unsupervised deep learning, (5) Multi-

Categories	Codes
	view stereo
GCN-based UU topology completion	(1) Graph Convolutional Network, (2) Database completion, (3) Topology prediction, (4) GCN-based database completion

The review addresses the questions that guide the research: 1) What are the prevailing 3D reconstruction technologies extensively employed in the domain of UUs? 2) What are the underlying principles and classification attributes of these technologies? 3) What are the notable advantages, disadvantages, and practical effects of these technologies? 4) What are the primary challenges and limitations encountered in UU 3D reconstruction? 5) What is the current research status of UU 3D reconstruction based on GPR, and what are the key issues to be addressed? 6) What factors contribute to the difficulty in improving the precision of the existing GPR-based UU 3D reconstruction research? 7) What are the underlying principles and research progress in image-based 3D reconstruction technology? 8) What are the conventional methods for enhancing low-light images, and how effective are they? 9) Which deep-learning models have been utilised for low-light image enhancement, and what principles can be derived from their application? 10) What are the specific characteristics of image-based 3D reconstructions in UU scenarios? 11) What is the current development status of the GCN model? 12) In the absence of a comprehensive UU database, what methods can be employed to effectively and scientifically complete the missing data?

3.4 GPR-based UUs localisation model development (Objective 2)

An end-to-end deep-learning model (EUUL) using GPR B-scan data was proposed in this study to improve the precision of UU localisation. As shown in Figure 3-3, the EUUL model first extracts the information features in the GPR B-scan image and then directly establishes the mapping relationship between the features and the UU coordinate point position to reduce the precision loss caused by the step-by-step localisation mode.

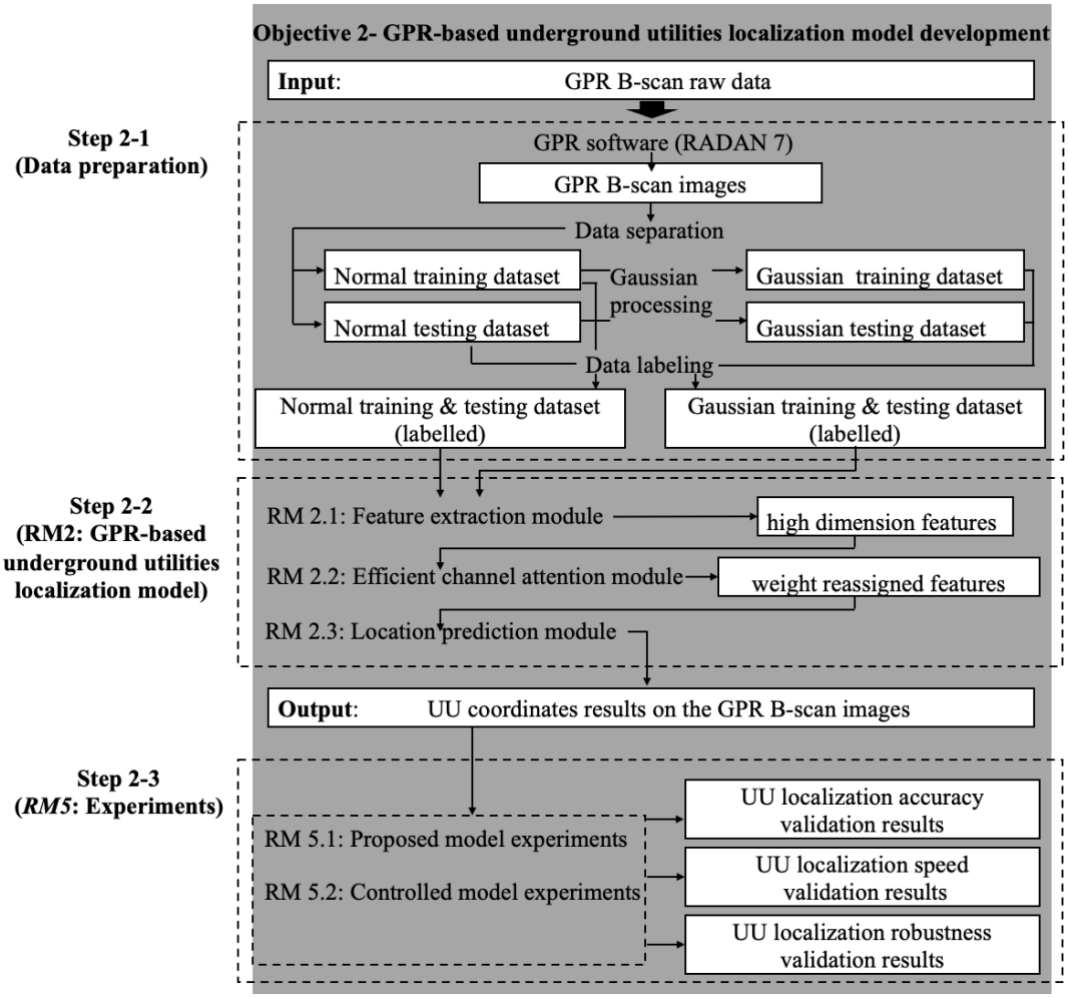

Figure 3-3 Overview of the methodology for Objective 2 (GPR localisation)

3.4.1 Inputs and outputs

EUUL's input data were GPR B-scan data collected by GPR equipment in real municipal road areas and processed using specific software (RADAN (Geophysical Survey Systems, Inc., 2011)). In this study, GPR B-scan data were saved as a JPEG file, which is commonly used in the object-recognition field. EUUL's output data consist of two items: a GPR B-scan image (in jpeg) with the UU position marked and the pixel coordinates of the target apex position in that image.

3.4.2 Data preparation

To emulate the actual data acquisition scene to the greatest extent possible, all data in this study were obtained using GPR equipment instead of virtually generated using

signal simulation software (e.g. GPRmax (De Coster et al., 2019; Pham et al., 2018; Ko et al., 2019)). A GSSI SIR4000 GPR device and a 400 MHz antenna were used for data acquisition in this study.

Over 8 km of municipal roads were scanned to generate the GPR B-scan data. The pipes in the area where data were collected were concrete, and metal pipes with a diameter of 500 mm to 1200 mm, and the depth of these pipes was 1.0 to 3.0 m from the surface, as shown in Figure 9.

Subsequently, the raw data were transferred to B-scan images using RADAN software (Geophysical Survey Systems, Inc., 2011) after removing all data that did not satisfy the requirements, such as data that did not include the pipeline target or data that were severely affected by environmental noise (primarily from the steel mesh placed under the road surface). Finally, 400 GPR B-scan images were filtered for this experimental study, as shown in Figure 3-4. In addition, to measure the robustness of the model, B-scan images in the test set were processed using a Gaussian blur operation (Youn et al., 2002; Feng et al., 2021b; Pasolli et al., 2010). A new blur dataset for robustness testing was generated using the Python Imaging Library, and the radius was set to 2 to simulate the typical noise scenario when the features faded, as shown in Figure 3-5. The GPR B-scan dataset was segregated into training, verification, and test sets for all studies at a ratio of 6:3:1. The details are presented in Table 3-2.

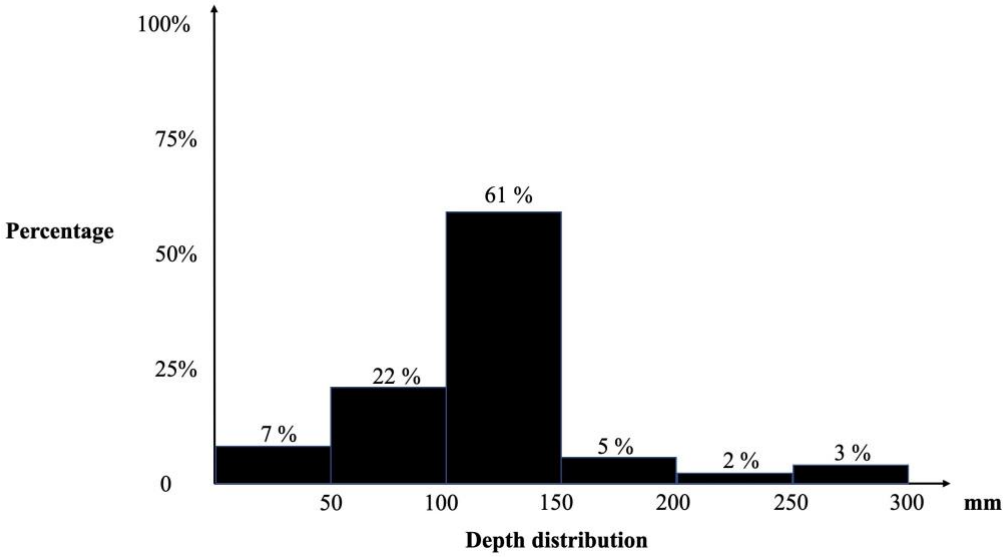

Figure 3-4 Depth distribution of the UUs

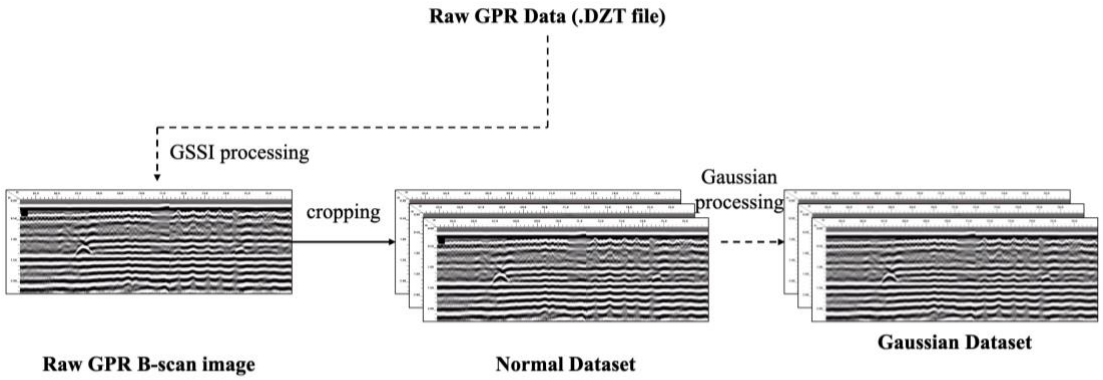

Figure 3-5 Dataset generation process

Table 3-2 Details of training and experimental data

Data type		**Number of images**
Normal dataset	Original data	400
	Training data	240
	Validation data	120
	Test data	40
Gaussian dataset	Test data	40

3.4.3 Overall design of EUUL model

In the existing research, B-scan target positioning of GPR is performed using the ‘box-fitting’ mode, which divides the target positioning problem of UUs into two sub-problems: regional detection and hyperbolic fitting. The ‘box-fitting’ splitting mode seems to simplify the problem; however, it results in possible error accumulation and fails to give full play to the autonomous learning potential of the deep-learning model. The EUUL model proposed in this thesis uses a 'key point-regression' mode to link the entire task in an end-to-end form, which avoids error accumulation and maximally releases the optimisation potential of the deep-learning model. A detailed model design is introduced in Section 4.2.

3.4.4 Model experiments

To validate the model and improvements proposed herein, the EUUL model was separated into three branches with different improvement features for comparison: EUULori, using ResNet50 as the backbone; $EUUL_{csp}$, using CSPDarknet53 as the backbone; and $EUUL_{cspeca}$, which embeds the ECA module based on $EUUL_{csp}$ (the EUUL model). Two models published in 2019, the one-stage UU localisation model based on YOLOv3 (Zong et al., 2019) and the two-stage UU localisation model based on the Faster R-CNN for the same task (Lei et al., 2019; Amaral et al., 2022), were selected as comparison models to verify the effectiveness of the EUUL model.

Therefore, $EUUL_{ori}$, $EUUL_{csp}$, $EUUL_{cspeca}$, YOLOv3, and Faster R-CNN were trained and tested in terms of precision, operating speed, and robustness. To ensure comparability among the models, all the training and testing datasets were rendered identical. In addition, the same environment (NVIDIA RTX 3090, GPU-based computer) was used during the model training and verification to ensure the effectiveness of the experiments.

3.4.4.1 Model evaluation metrics

The EUUL model detects the position of the UU target based on a GPR B-scan image. Therefore, precision, recall, and F1 were applied to measure the ability of the model

to locate the region where UU was located. The point precision metric was applied to measure the ability of the EUUL model to accurately determine the points representing UU.

3.4.4.1.1 Precision, recall, and F1

Precision: In the context of UU localisation, precision is important because it measures the accuracy of positive predictions. High precision means fewer false positives, which is critical for avoiding unnecessary excavations or disturbances in areas where utilities might not exist. Recall: In the context of utility localisation, recall is important because it measures the ability of the model to correctly identify all relevant instances of UUs. A high recall means fewer false negatives, reducing the chances of missing actual utilities, which is crucial for safety in applications, such as GPR. F1-Score: F1 combines precision and recall, providing a balance between false positives and false negatives. Achieving balance in utility localisation is essential. The F1-score is particularly useful when there is an imbalance between the positive and negative classes, ensuring that the model performs well in both aspects of utility detection.

In this thesis, precision, recall, and the F1-score collectively provide a well-rounded evaluation, emphasising the importance of both precision and recall in the detection of UUs, as shown in Eq. 3-1, Eq. 3-2, and Eq. 3-3. Other metrics commonly used in object detection problems, such as accuracy, ROC, and IoU, were not selected because of specific considerations of the problem domain. The accuracy may be skewed by imbalanced training data. The ROC curve may not provide a clear assessment in scenarios where the focus is on correctly identifying the positive class (utilities). Additionally, metrics such as intersection over union (IoU) are more suitable for image segmentation, which involves precise region delineation. The chosen metrics of precision, recall, and F1 were deemed more appropriate for emphasising the correct identification of utilities while balancing the training data in the context of the research object. The three indicators were calculated as follows: *TP*, FP, and false negative (FN) represent the number of correctly identified, overlooked, and mistakenly discovered targets, respectively.

$$Precision = \frac{TP}{TP+FP} \quad \text{Eq. 3-1}$$

$$Recall = \frac{TP}{TP+FN} \quad \text{Eq. 3-2}$$

$$F1 = \frac{2*Recall*Precision}{Recall+Precision} \quad \text{Eq. 3-3}$$

3.4.4.1.2 Point precision

As shown in Figure 3-6, obtaining the bounding box can only provide an approximation of the hyperbolic range in the B-scan image. In contrast, a hyperbola that represents the location of the UUs pipeline and the corresponding apex may exist in multiple potential hyperbolas within the bounding box range. Different fitting processing methods yielded different hyperbolic results. If the localisation ability of a model is evaluated based only on the precision indicator (see Section 3.4.1), the localisation error caused by the fitting process is not considered.

Therefore, *point precision* was utilised to evaluate the model in this thesis as an index for evaluating precision. *Point precision* refers to the ratio between the difference in the apex-predicted coordinate output by the model and that between the actual field-measured coordinates (Eq. 3-4 and Eq. 3-5).

$$Point\ precision_x = \frac{X_{predict}-X_{truth}}{X_{truth}} \quad \text{Eq. 3-4}$$

$$Point\ precision_y = \frac{Y_{predict}-Y_{truth}}{Y_{truth}} \quad \text{Eq. 3-5}$$

Here, the *point precision*$_x$ and *point precision*$_y$ represent the abscissa and ordinate accuracies of the model on the B-scan image, respectively; $X_{predict}$ and $Y_{predict}$ represent the apex abscissa and ordinate predicted by the model, respectively; and X_{truth} and Y_{truth} represent the actual apex coordinates of the UU in the GPR B-scan image.

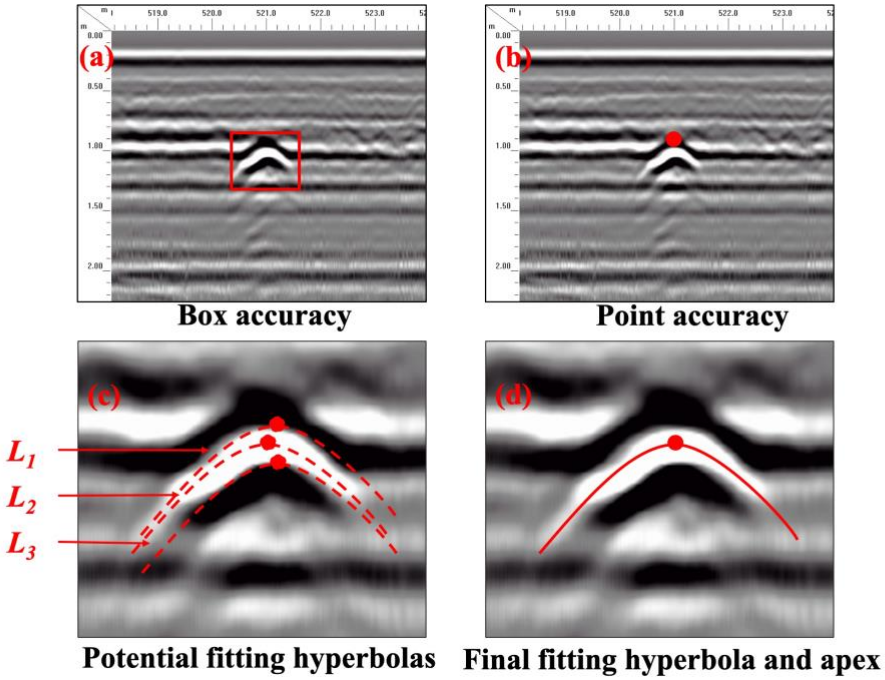

Figure 3-6 Comparison between point precision and box precision

3.4.4.1.3 Speed

In this study, *Fps* was used to measure the operating speed of the model. It is expressed in Eq. 3-6, where *F* represents the number of all B-scan images (frames) input into the model, and *T* represents the length of time from the beginning of the operation instruction to the moment all operation results are output.

$$Fps = \frac{F}{T} \qquad \text{Eq. 3-6}$$

3.5 Image-based low-light utilities localisation reconstruction model development (Objective 3)

An unsupervised deep-learning model (ZDE3D) was proposed in this study to enhance the 3D reconstruction performance of UUs in low-light environments. The proposed ZDE3D model first extracts the pixel features in low-light images and uses different loss functions to highlight the hidden spatial feature information from five aspects to improve the matching success rate of the same position between multiple images and realise UU 3D improvements to the reconstruction effects. Figure 3-7 illustrates the research flow for this objective.

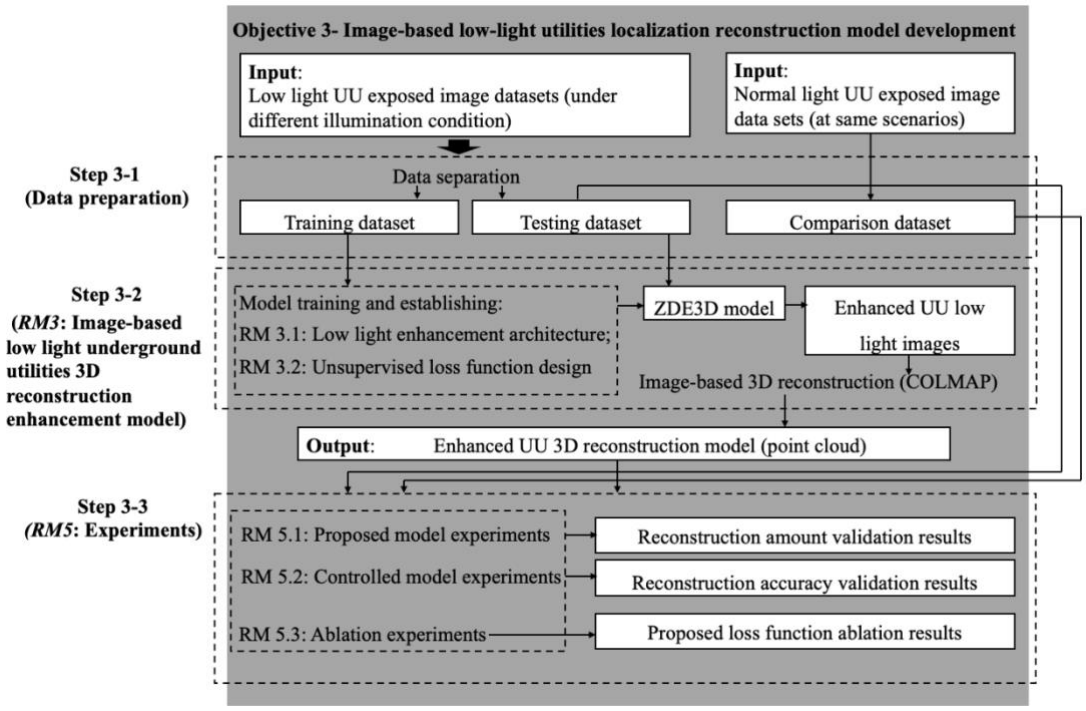

Figure 3-7 Overview of the methodology for Objective 3 (low-light enhancement)

3.5.1 Inputs and outputs

The input of the ZDE3D model was low-light images of exposed UUs captured from real construction sites. Input image data were obtained using consumer smartphones. The output data of the model were low-light image data after the effect was improved. After the output data were processed using MVS, point-cloud 3D-reconstruction models in ply format can be generated.

3.5.2 Data collection

To train the ZDE3D model, the image enhancement dataset from zero-DCE (Guo et al., 2020a) containing 2002 images was used. The training dataset comprises multiple groups of images of the same scene under different lighting conditions. See Figure 3-8 for details.

Figure 3-8 Training data samples

To verify the capability of the proposed ZDE3D model to improve the 3D reconstruction performance of the as-built UUs in the low-light actual construction site environment, ten sets of data were collected from a housing construction site in Perth, Western Australia. The 3D reconstruction target in the validation experiment was the domestic sewage drainage pipes installed, which still needed to be completely buried. It is noteworthy that the low-light data environment in the experiment only retained the lighting conditions of the construction site in a completely dark outdoor environment (after 7:00 pm). For a better representation, the pipeline video data under three different buried depths (300, 500, and 700 mm) for two types of pipe-laying methods (one pipe in the trench and two pipes in the trench) subject to different lighting conditions (normal and low light) were collected. The data samples are shown in Figure 3-9. The device used for data collection was an iPhone 12 (1080p, 60 FPS, with all intelligent optimisations turned off).

Figure 3-9 Data-collection samples

3.5.3 Data processing

To improve the efficiency of field data collection and work convenience, the original data acquired in the experiment were video-format data (mp4). The video data were then extracted using a Python script every 50 frames into a multi-view image dataset.

Thereafter, the multi-view images were imported into the COLMAP software (https://colmap.github.io/) for sparse and dense reconstruction to obtain the final point-cloud files. The pipe size was measured manually using Compare software (https://www.danielgm.net/cc/). All the data processing flows are shown in Figure 3-10.

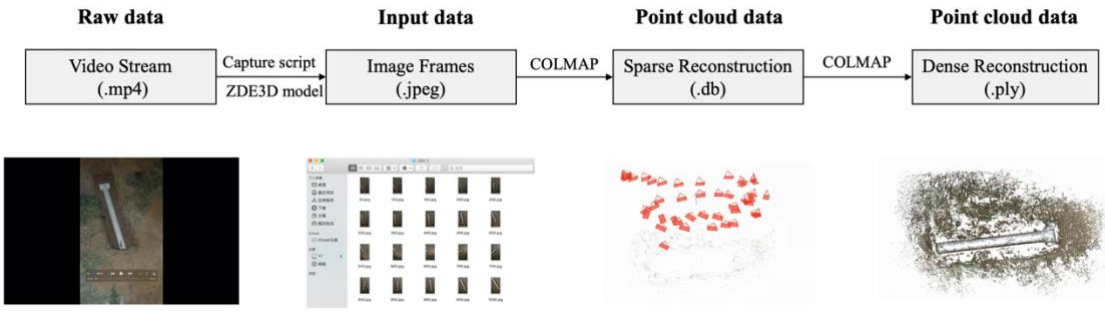

Figure 3-10 Data processing steps

3.5.4 Overall design of the ZDE3D model

In traditional or deep learning, the essence of a low-light image enhancement task is to adjust the image features (such as local brightness and contrast) at the pixel level. The deep-learning model can establish mapping from a low-light image to an optimised image, and the effect of this process depends on the reference image used in the model training. However, in low-light three-dimensional reconstruction scenes, there needs to be a reference image that can be determined by research, and it is more difficult to identify the most appropriate reference image for supervision and training under different UU construction scenes. Therefore, this thesis proposes an unsupervised deep-learning model without reference images. Through the design of the loss function, the prior knowledge of low-light three-dimensional reconstruction and the UU engineering scene is solidified into the deep-learning model. Thus, low-light image enhancement at the pixel level was implemented to generate a better UU three-dimensional point-cloud model.

3.5.5 Model experiments

3.5.5.1 Model evaluation metrics

The purpose of the ZDE3D model is to optimise low-light images at the pixel level to achieve a better 3D reconstruction performance. To measure the performance of the point-cloud model generated from images processed by the model, three metrics were adopted in this study for evaluation: point-cloud quantity, enhanced ratio, and record accuracy.

3.5.5.1.1 Point-cloud quantity

The point-cloud quantity refers to the number of point clouds generated during the sparse 3D reconstruction phase. In a 3D reconstruction task, the number of point clouds generated by sparse reconstruction is the basis for the subsequent dense reconstruction of the point clouds, which determines the performance quality of the point clouds. If the number of point clouds is too small, the spatial information of the target scene cannot be fully expressed, particularly the enlarged local details. Therefore, this study adopted the point-cloud quantity as one of the measurement indicators of model performance. The larger its value, the better the 3D reconstruction performance of the target UU scene.

3.5.5.1.2 Enhanced ratio

The enhanced ratio refers to the ratio of the reconstruction performance between the low-light image enhanced by the ZDE3D model and original input data. This metric was used to quantify the 3D reconstruction effect of the optimised discriminant model, as shown in Eq. 3-7, where Q_r represents the number of sparse point clouds generated by the 3D reconstruction of the original low-light image, and Q_e represents the number of sparse point clouds generated by the 3D reconstruction of the image enhanced by ZDE3D.

$$Enhanced\ ratio = \frac{Q_e - Q_r}{Q_r} \times 100\% \qquad \text{Eq. 3-7}$$

3.5.5.1.3 Record accuracy

Record accuracy refers to the difference between the spatial information expressed by the point cloud from the 3D reconstruction and size information from the actual

construction site. The core scenario of this study was the as-built UU; therefore, the pipe diameter was used as a representative value in the experimental record, as shown in Eq. 3-8. Where D_r represents the pipe diameter of the point-cloud model generated by 3D reconstruction, and D represents the pipe diameter size obtained from actual measurements at the construction site.

$$Record\ accuracy = 1 - \frac{|D - D_r|}{D} \times 100\% \quad \text{Eq. 3-8}$$

3.5.5.2 Experiment design

To verify the practicability of the ZDE3D model, two parts were designed: an experimental and construction environment. Three embedment depths and two pipeline arrangement modes were designed for the experimental environment. Under the condition of lack of a light source, the acquisition was carried out, and then the effects of 3D reconstruction after the acquisition of the original low-light image and the model-enhanced image were compared. In addition, the influence of different loss functions on the reconstruction results proposed by ablation experiments was investigated. In the construction environment section, three low-light images from different UU scenarios at different construction sites are collected, and the point clouds generated by the original low-light images are compared with those generated by the enhanced images to illustrate the effectiveness of the model. Simultaneously, traditional, and mainstream unsupervised deep-learning method models were applied to the same dataset for comparative experiments to verify the superiority of the proposed ZDE3D model.

3.6 Graph-based UU topology-completion model development (Objective 4)

In this study, a GCN-based deep-learning model (UUTC) was proposed for an UU topology information completion task. The UUTC model first converts the table database into graph-structured data, then extracts the correlation information between each observed node through the GCN architecture, and finally predicts the missing topological relationship by combining multi-dimensional information, such as node attribute characteristics and similarity. Figure 3-11 illustrates the research flow for

achieving this objective.

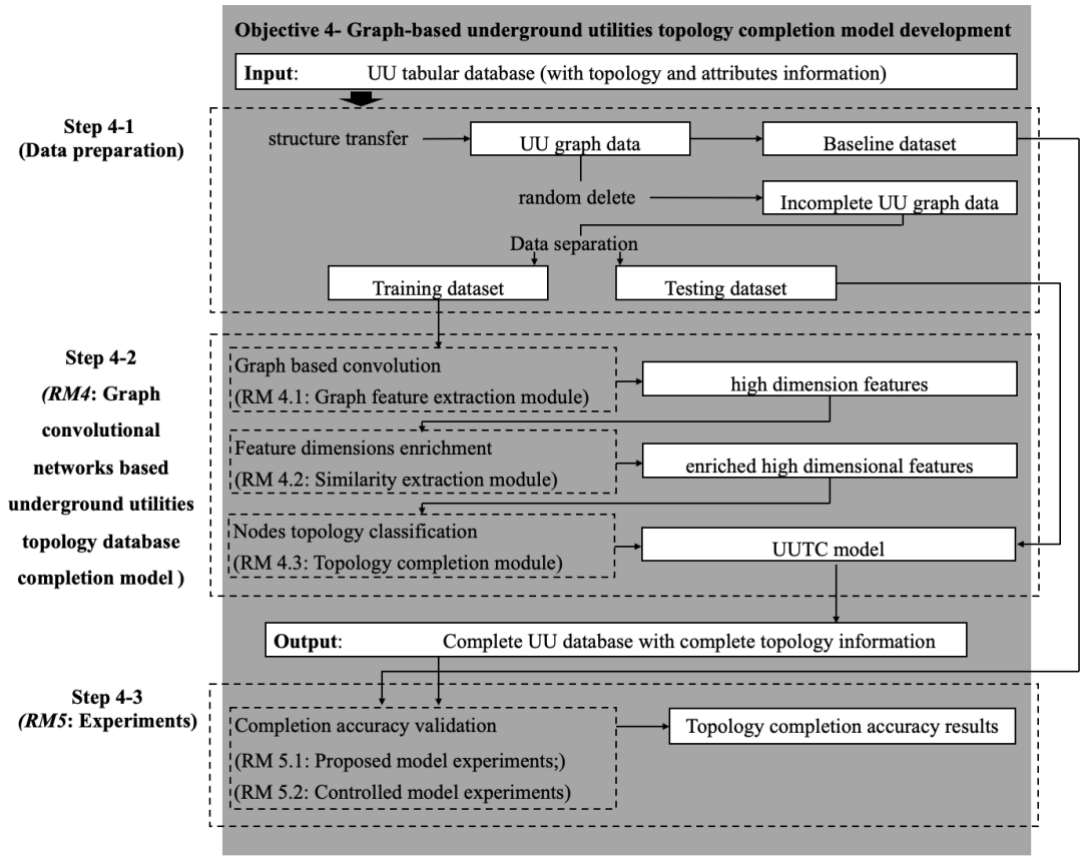

Figure 3-11 Overview of the methodology for Objective 4 (Topology completion)

3.6.1 Inputs and outputs

The input data of the UUTC model were graph data with different proportions of missing topological relationships. The model's output data were the graph data after completing all topological relationships.

3.6.2 Data collection

Data source. All the UU data used in this thesis are collected from the real wastewater network official data of Angers Metropolis City, France, and are available through the French Government's open access (https://www.data.gouv.fr/ (accessed on 1 May 2023)). Three groups of real UU data from different scales of buildings in different locations and periods were selected to ensure the repeatability of the experimental results and normalisation ability of the model. The three sets of experimental data included 26,627, 10,227, and 1,059 UU nodes, and 32,379, 12,369, and 1,031 pairs of

UU topological relationships, respectively. Each set of data was divided into training, verification, and test sets. The division ratio is determined according to the missing rate setting, where the proportion of the test set equals the missing rate, the proportion of the verification set is constant (10%), and the rest of the data is the training set.

Data processing. Figure 3-12 shows the processing flow of the raw data. First, the raw data file, in .shp format, was processed into a commonly used graph data format (CSV) using professional software (ArcGIS) to ensure that the model correctly read the data. Second, the obtained data attributes were filtered. The main consideration was to retain a few attribute features (material, depth, length, and diameter) that were closely related to the UU topology. The remaining features were not closely related to the topology of the UU network; therefore, they were excluded from the study. In addition, keeping materials and other attributes that reflect UU characteristics as small as possible can maximise the possibility of model promotion in other types of UU fields, because information such as laying date and gravity type is not recorded in all UU scenarios. Third, the material was a typical discrete attribute among the four selected attribute characteristics. To facilitate the deep-learning calculation and avoid the data interference problem caused by the assignment of the scalar form, this thesis adopted the one-hot (Shen et al., 2022) encoding form for processing. Each material was recorded as a unique representation vector. Fourth, in machine learning, different evaluation indicators (i.e. different features in the feature vector are different evaluation indicators) often have different dimensions and dimensional units, which will affect the results of data analysis. Therefore, to eliminate the dimensional influence between indicators, this study normalised the data to solve the comparability problem between data indicators.

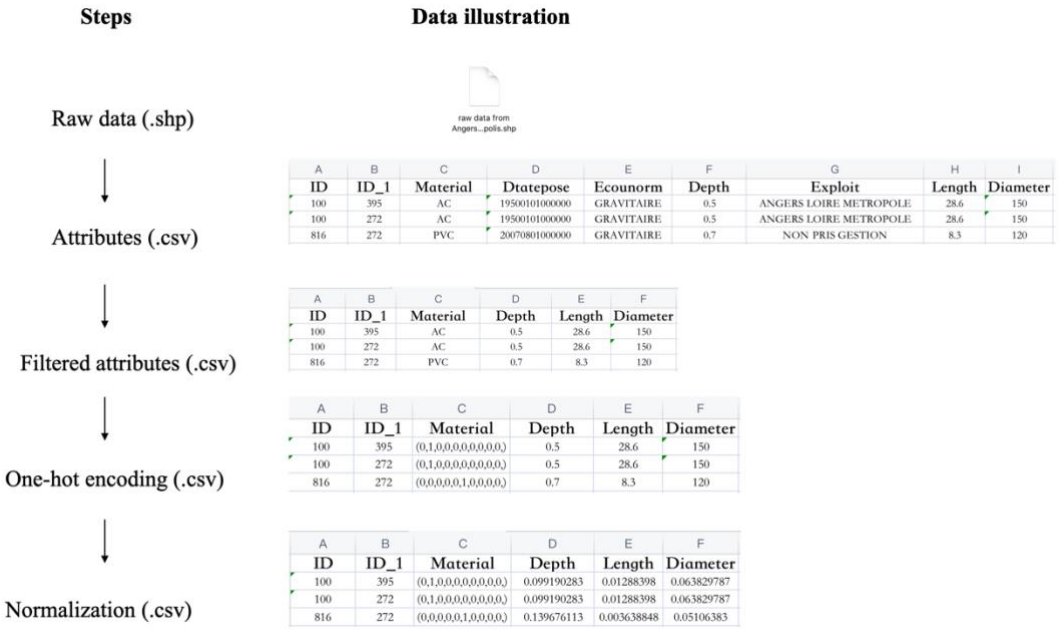

A	B	C	D	E	F	G	H	I
ID	ID_1	Material	Dtatepose	Ecounorm	Depth	Exploit	Length	Diameter
100	395	AC	19500101000000	GRAVITAIRE	0.5	ANGERS LOIRE METROPOLE	28.6	150
100	272	AC	19500101000000	GRAVITAIRE	0.5	ANGERS LOIRE METROPOLE	28.6	150
816	272	PVC	20070801000000	GRAVITAIRE	0.7	NON PRIS GESTION	8.3	120

A	B	C	D	E	F
ID	ID_1	Material	Depth	Length	Diameter
100	395	AC	0.5	28.6	150
100	272	AC	0.5	28.6	150
816	272	PVC	0.7	8.3	120

A	B	C	D	E	F
ID	ID_1	Material	Depth	Length	Diameter
100	395	(0,1,0,0,0,0,0,0,0,0)	0.5	28.6	150
100	272	(0,1,0,0,0,0,0,0,0,0)	0.5	28.6	150
816	272	(0,0,0,0,0,1,0,0,0,0)	0.7	8.3	120

A	B	C	D	E	F
ID	ID_1	Material	Depth	Length	Diameter
100	395	(0,1,0,0,0,0,0,0,0,0)	0.099190283	0.01288398	0.063829787
100	272	(0,1,0,0,0,0,0,0,0,0)	0.099190283	0.01288398	0.063829787
816	272	(0,0,0,0,0,1,0,0,0,0)	0.139676113	0.003638848	0.05106383

Figure 3-12 Data processing steps and illustrations

3.6.3 Overall design of UUTC model

In this study, topological relationship completion among UUs was transformed into an edge prediction of the graph structure. Each pipe target corresponds to a node in the graph data, the attribute characteristics of the pipe itself correspond to node attributes, and the connection relationship (topology) between pipes corresponds to the edge. If there is a topological connection between the pipelines, an undirected edge exists between the corresponding nodes; otherwise, the nodes are independent. The UUTC model comprises of four main modules: input, SEM, convolution, and link prediction. The model takes the observed topological relationships and node attribute information of the UU network as input and aims to generate completed network topology relationship data as output. To improve the accuracy of topological relationship completion, this thesis constructs a SEM combined with professional knowledge in the field of UU to help a deep-learning network identify the connection possibilities between pipeline nodes. A detailed model design is introduced in Section 6.2.

3.6.4 Model experiments

3.6.4.1 Model evaluation metrics

To evaluate the effectiveness of the proposed UUTC model in the UU topological relationship completion scenario, the following four mainstream model evaluation metrics in the field of machine learning were applied. The definitions of TP (True Positive), TN (True Negative), FP (False Positive) and FN are listed in Table 3-3.

Table 3-3 Definition of TP, TN, FP, and FN

	Model predicted as true	**Model predicted as false**
Actual true	TP (True positive)	FN (False negative)
Actual false	FP (False positive)	TN (True negative)

3.6.4.1.1 Accuracy

Accuracy (ACC) indicates the proportion of the number of samples predicted by the model to the total number of samples. The ACC calculation equation is given by Eq. 3-9.

$$ACC = \frac{TP+TN}{TP+FP+TN+FN} \qquad \text{Eq. 3-9}$$

3.6.4.1.2 Area Under Curve

The area under curve (AUC) is the area under the receiver operating characteristic (ROC) curve, which is typically used for binary-classification problems. The ROC curve is a curve with the False-Positive Rate (FPR) as the abscissa and the True Positive Rate (TPR) as the ordinate, as shown in Figure 3-13 Eq. 3-10, and Eq. 3-11. The closer the AUC is to 1, the better the performance of the model. The calculation equation for AUC is shown in Figure 3-13.

$$TPR = \frac{TP}{TP+FN} \qquad \text{Eq. 3-10}$$

$$FPR = \frac{FP}{FP+TN} \qquad \text{Eq. 3-11}$$

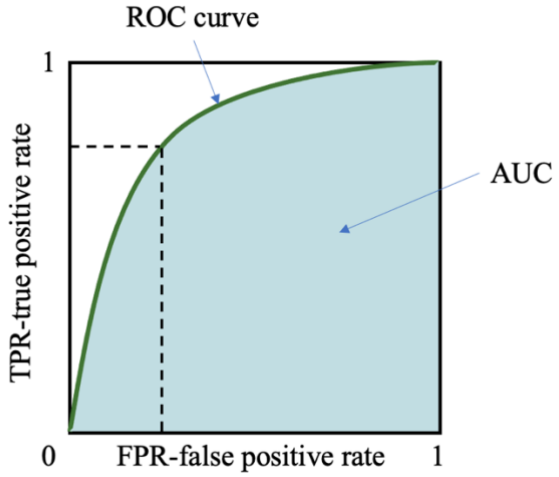

Figure 3-13 Area under curve (*AUC*) and receiver operating characteristic (ROC) curve

3.6.4.1.3 F1

$F1$ is the harmonic mean of Precision and Recall. The precision rate indicates the proportion of predicted positive samples that are positive samples, and the recall rate indicates the proportion of actual positive samples that are correctly predicted as positive samples. The $F1$ value can comprehensively consider the impact of precision and recall. This is a commonly used indicator in binary-classification problems. See the equation Eq. 3-12 for the calculations.

$$F1 = \frac{2TP}{2TP+FP+FN} \qquad \text{Eq. 3-12}$$

3.6.4.1.4 average precision

The average precision (*AP*) is the area under the curve of the precision and recall rate (P-R curve), as shown in Figure 3-14. Compared with other indicators, *the AP* can better reflect the performance of the algorithm in practical applications, and it considers the ranking order of the prediction results and the importance of related targets, not just the accuracy of the classification results. See Eq. 3-13 and Eq. 3-14 for the calculation details.

$$Precision = \frac{TP}{TP+FP} \qquad \text{Eq. 3-13}$$

$$Recall = \frac{TP}{TP+FN} \qquad \text{Eq. 3-14}$$

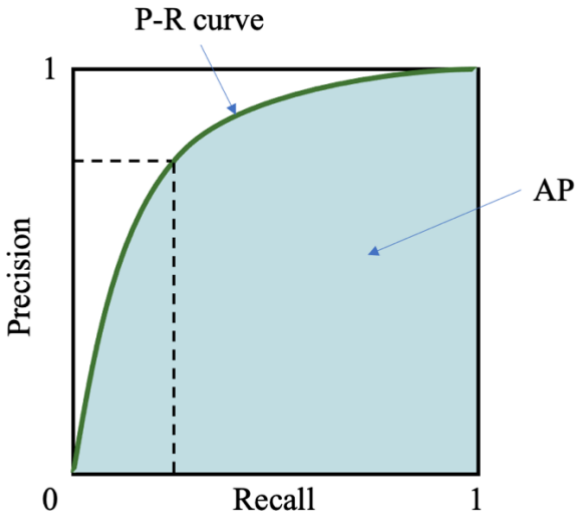

Figure 3-14 P-R Curve (AUC) and AP

3.6.4.2 Model experiments design

The model was verified using the data officially recorded from a real wastewater network. The verification is divided into two steps: 1) The experimental data are randomly removed according to different missing proportions, and then the defective data are imported into the UUTC model for completion. Finally, the topological relationships before and after completion were recorded and compared to verify the effectiveness of the proposed UUTC model. 2) Import the same incomplete dataset from 1) into the mainstream data-completion baseline models in existing studies for comparison, and then record the experimental results and perform a comparative analysis with the experimental data in 1) to illustrate the superiority of the UUTC model over the existing models.

3.7 Chapter summary

This chapter summarises the research methodology. First, research philosophy is introduced as the foundation of this thesis. This study is based on a positivist paradigm. The research methodology was deductive and quantitative, based on objectivist epistemology and realist ontology. Sections 3.4-3.6 introduce specific research

methods. In summary, the EUUL model was utilised to localise the positions of UUs under non-destructive conditions. The ZDE3D model was developed to enhance the 3D reconstruction performance of the exposed UUs. Finally, the UUTC model was proposed to complete the missing topological relationship of the UU nodes. By applying these three components, a 3D model of the UUs can be effectively, automatically, and accurately reconstructed.

Chapter 4 : Developing GPR-based automatic UU localisation model

4.1 Chapter introduction

This chapter presents the detailed design of the GPR-based automatic UU localisation model (EUUL) in Section 4.2. Cross-comparison results are demonstrated to prove the usefulness of the model, and the contributions of the EUUL model are discussed in Section 4.3. All models were developed using a NVIDIA RTX 3090, GPU-based computer, and a Pytorch environment.

4.2 Detailed design of the EUUL model

4.2.1 Framework of EUUL model

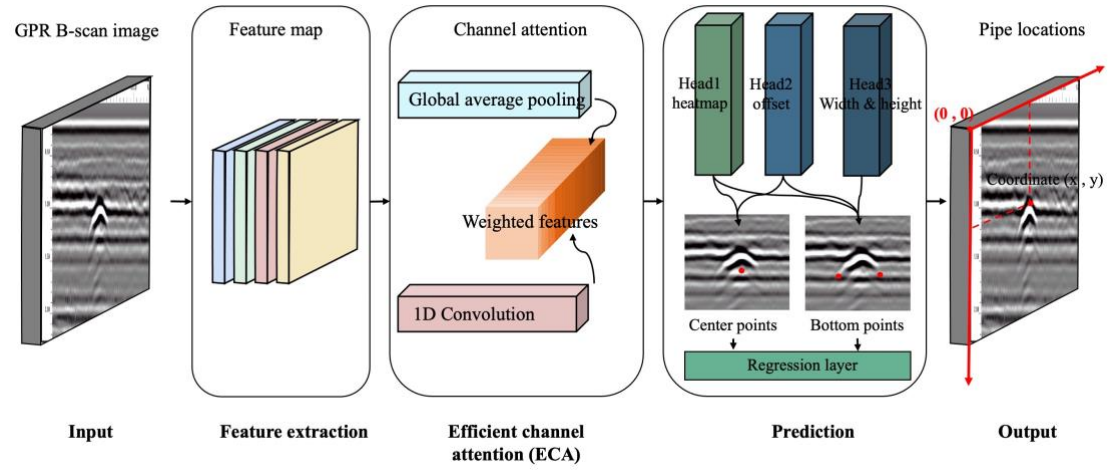

Figure 4-1 Overview of EUUL model

Inspired by CenterNet (Zhou et al., 2019), the EUUL framework was designed to feature three main components: feature extraction, ECA, and prediction, as described in detail in Sections 3.2, 3.3, and 3.4, respectively (see Figure 4-1).

Feature extraction. The CSPDarknet53 backbone (Bochkovskiy et al., 2020) was applied to the EUUL model to extract features from the B-scan image data. To achieve higher deep learning, too large backbone structure will seriously affect the model's speed, whereas too small will reduce the extraction effect of target features. In this thesis, a CSPDarknet53 network with a cross-stage partial (CSP) structure was applied. The addition of the CSP structure can solve the problem of information duplication in

the backbone network, particularly in the neural network gradient optimisation process, which can significantly reduce the number of parameters and floating-point operations of the model, thus improving the reasoning speed of the final model. This operation significantly reduces the overall number of parameters in the model and is conducive to solving the issue of a large data volume in UU localisation. Further details are presented in Section 3.2.

ECA. After switching the lightweight backbone model during the test for improvement, the localisation precision of the model decreased significantly. Therefore, an ECA module was embedded into the EUUL model to ensure precision from lightweight modifications and to manage noise interference in the UU localisation. Compared with other attention mechanisms, the ECA mechanism has higher computational efficiency and less influence on network processing speed, which is suitable for this research scenario. Studies on many other image recognition tasks have confirmed that the ECA mechanism can significantly improve the performance by adding only a few parameters. The ECA module weights the feature channels and ensures that the model focuses on key features. Details regarding the ECA module are provided in Section 3.3.

Prediction. Based on the high-dimensional image features obtained from the above steps, the prediction component was classified into three branches to obtain the heat map, object width and height, and offsets of the UUs target. Subsequently, a regression structure was used to generate the offsets, object size (hyperbola width and height), and point coordinates that represent the UU location as the model's output. The details are presented in Section 3.4.

4.2.2 Feature extraction

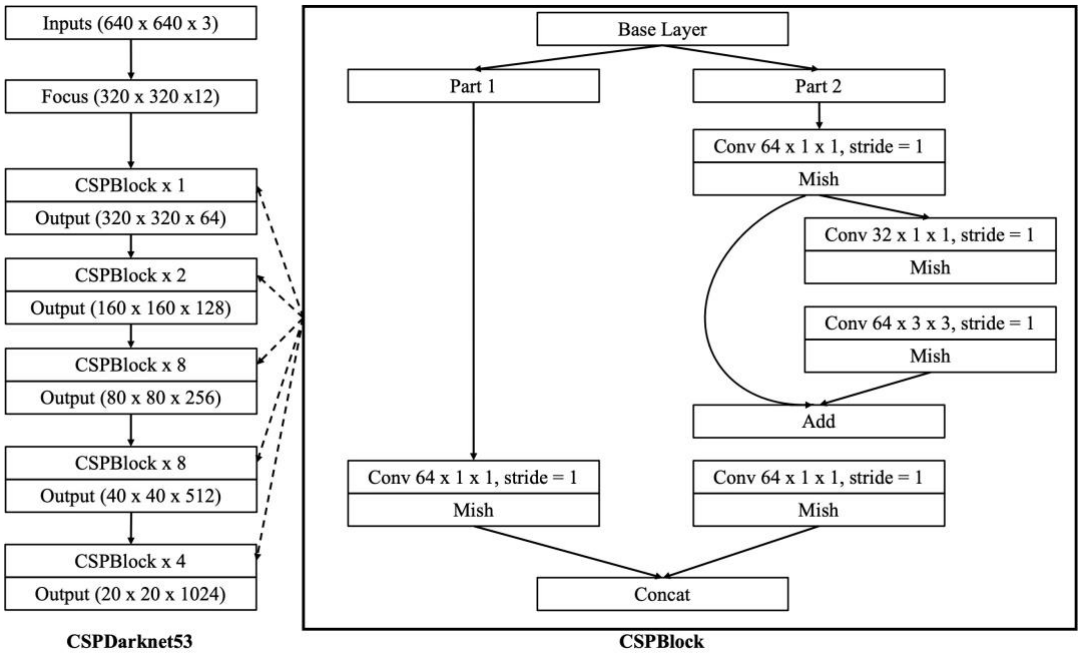

Figure 4-2 Architecture of EUUL backbone

CSPDarknet53 (Bochkovskiy et al., 2020), a deep-learning backbone for object detection, was used for feature extraction. A CSPNet strategy was applied to segment the feature map into two regions and merge them into a cross-stage hierarchy. Figure 4-2 shows details of the CSPDarknet53 structure.

The main features of CSPDarkNet53 include the addition of a CSP (Bochkovskiy et al., 2020) structure to each residual block and the removal of the bottleneck structure. From the standpoint of network structure design, CSP is primarily utilised to solve problems that require extensive calculations. The problem of high inference calculation is caused by the repetition of gradient information in network optimisation. The CSP structure reduces the computational effort while ensuring precision by integrating gradient changes into the feature map from beginning to end. Consequently, the number of model parameters and floating-point operations per second were reduced, which ensured both the speed and precision of inference and reduced the model size. The training was simplified by removing the bottleneck structure, and the number of parameters was reduced.

4.2.3 ECA module

GPR B-scan data often contain noise owing to the complexity of the underground environment. These noise and interference factors include the electrical installations, tree roots, and devices. The complete removal of all these interference factors in engineering practice is unrealistic. Therefore, an ECA (Wang et al., 2020a) module was added to the EUUL model to enhance the operational robustness. The principle of the ECA module is as follows:

When the model processes the input B-scan images, different features are captured by different channels; however, the importance of each channel feature differs. As shown in Figure 4-3, the ECA module allows the model to focus on the key feature channels by assigning different weight evaluations to each channel's information. The first step is to perform a global average pooling operation on the input feature map, which involves calculating and transforming the pixel value of each feature layer into a mean output to create a one-dimensional (1D) vector. Second, 1D convolution with convolution kernel size k is performed on the 1D vector to realise local cross-channel interactions and extract the dependencies between channels, where k is determined by the input characteristic channel C. To obtain the weight w of each channel, the vector obtained after the 1D convolution is passed through the sigmoid activation function (Eq. 4-1 to Eq. 4-5). After performing the above steps, more computing power is directed toward the effective channel information, and noise interference in the input is effectively mitigated. The experiments are detailed in Section 4.3.

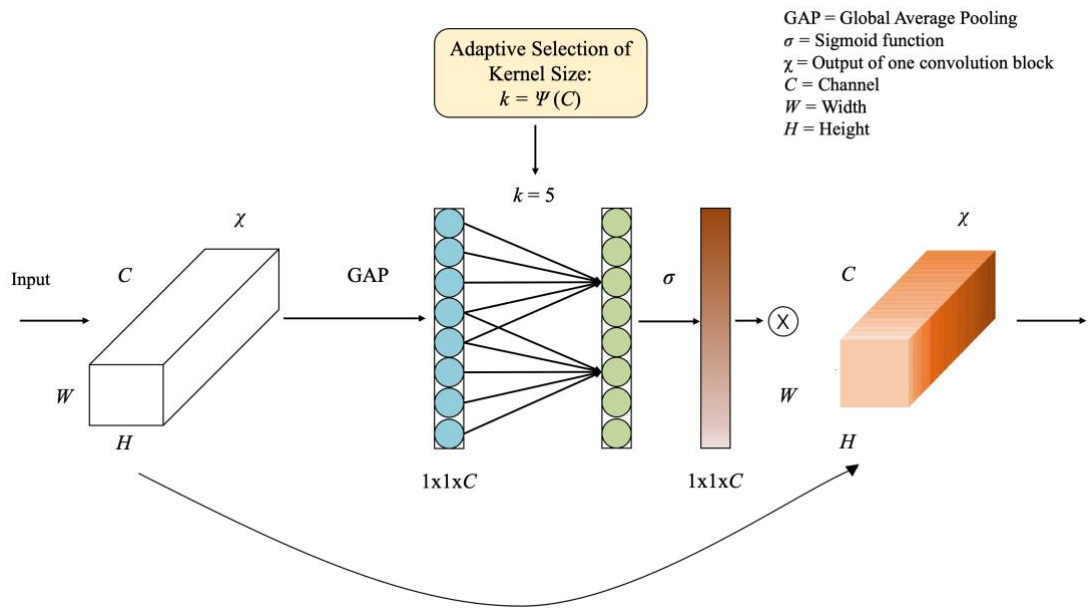

Figure 4-3 Framework of ECA

The weight of each channel w is calculated as follows:

$$w = \sigma(C1D_k(y)), \quad \text{Eq. 4-1}$$

$$C=\Phi(k), \quad \text{Eq. 4-2}$$

$$\Phi(k) = \gamma * k - b, \quad \text{Eq. 4-3}$$

$$C=\Phi(k)=2^{(\gamma*k-b)}, \quad \text{Eq. 4-4}$$

$$k = \Psi(C) = \left|\frac{log_2(C)}{\gamma} + \frac{b}{\gamma}\right|_{odd}. \quad \text{Eq. 4-5}$$

Here, $C1D$ represents a 1D convolution known as the ECA module, and k is the size of the convolution kernel, which is a parameter related only to C.

Therefore, a solution is to extend the linear function (Eq. 4-3) to a non-linear function (Eq. 4-4). Subsequently, for channel dimension C, kernel size k can be adaptively determined using Eq. 4-5.

The approximate range of the channel interaction information must be established because the ECA module seeks to accurately capture the local cross-channel information interaction (convolution kernel size k of 1D convolution). The kernel size k of the 1D convolution is directly proportional to the channel dimension C with

respect to the coverage of cross-channel information exchange. In other words, mapping exists between k and C, as expressed in Eq. 4-2. The most straightforward mapping is a linear function, as shown in Eq. 4-3. However, linear-function-based relationships are overly constrained. A power of two is specified for channel dimension C (i.e. the number of filters) (Wang et al., 2020). Hence, a potential solution was obtained by converting a linear function (Eq. 4-3) to a non-linear function (Eq. 4-4). The kernel size k can be expressed based on C, as shown in Eq. 4-5.

4.2.4 Prediction module

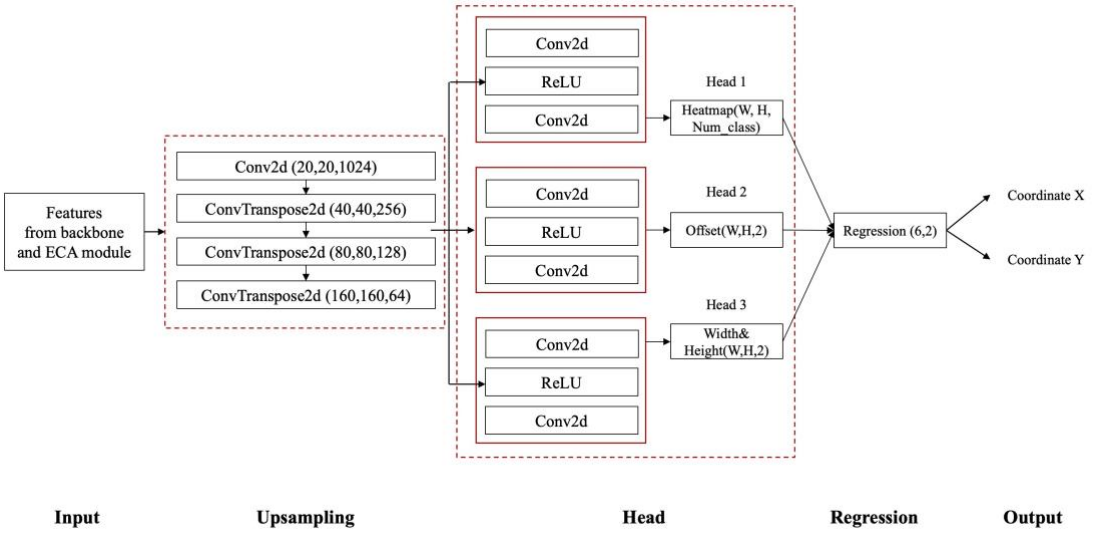

Figure 4-4 Prediction architecture

The prediction comprises up-sampling, head, and regression. It was used to predict the apex coordinates that represented the position of the top of the pipelines on a B-scan image. The prediction architecture is shown in Figure 4-4.

First, three up-samplings (ConvTranspose2d layers) were employed to avoid resolution degradation after restoring the image to its original size. After a complex series of convolution operations, the higher-dimensional features of the input image were extracted. This feature of CNN is particularly beneficial for classification and detection. However, because the resolution of the input image decreases significantly, the precision of the model in performing UU localisation also decreases. Therefore, to achieve greater localisation precision, the spatial dimension of the object in the original

image should be effectively restored using up-sampling operations.

Second, three branch heads were applied to predict the heat map, i.e., ‘offset’, ‘width’, and ‘height’. As shown in Figure 4-4, Head 1 generates the approximate centre position of the target object in the image. Head 2 was used to predict the correction offset of the target centre position to correct the precision loss caused by the model in the down-sampling process. The pixel width and height of the target were predicted using Head 3.

Finally, the coordinates of the UU objects were obtained via regression processing using the output information of the prediction heads, as illustrated in Figure 4-5. The left- and right-bottom-point pixel coordinates can first be calculated based on the coordinates of the heat map, offset, and object size (width and height). Subsequently, the predicted coordinates of the apex can be obtained by the regression of the coordinates of the abovementioned three points.

Through the operations above, the EUUL model circumvented the box-fitting mode in previous studies, in which hyperbola targets were searched first, and apex coordinates were searched via fitting steps. Moreover, the EUUL model directly searches for the apex coordinates on the input image. In this key point-regression mode, global optimisation results were obtained rather than the superposition of two local optimisations (box and fitting results). Under the new key point-regression-end-to-end framework, the UU localisation task model yielded a larger parameter optimisation space and more convenient operation process.

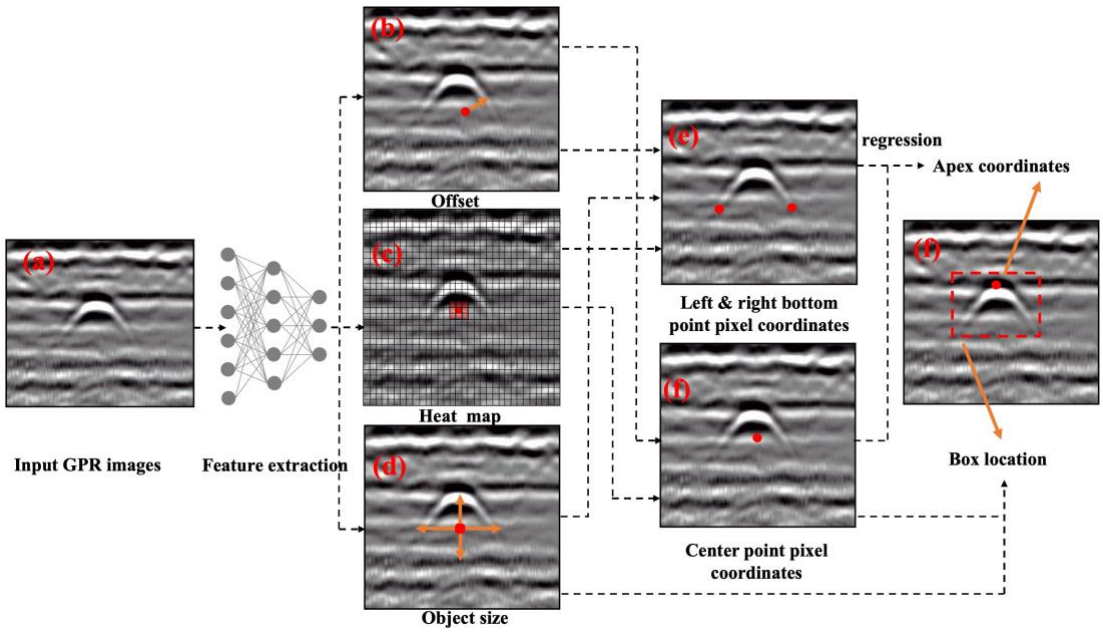

Figure 4-5 Regression processing

4.3 Experiment results and discussions

4.3.1 Experiment to verify precision

An experiment was performed to verify the localisation precision of the proposed EUUL model and the effects of the lightweight improvement and the ECA module on the model function. Therefore, all EUUL searer and composition models were tested based on the same normal dataset in the experiment, and the *parameters, precision, point precision, recall,* and *F1* values were recorded to evaluate the model performance.

As shown in Table 4-1 and Figure 4-6, the accuracies of the $EUUL_{ori}$ (96.49%), $EUUL_{csp}$ (93.10%), and $EUUL_{cspeca}$ (97.01%) models based on the key point-regression mode were significantly higher than those of the one-stage model YOLOv3 (91.67%) and two-stage model Faster R-CNN (65.52%). A comparison of the *F1* values showed the superiority of the proposed EUUL model. Although the *parameters* of the modified $EUUL_{csp}$ model reduced significantly after replacing the backbone (from 136.0 M to 37.0 M), the precision decreased (93.10%), the *recall* decreased significantly (36.00%), and the *F1* value was only 0.52. This indicates that the lightweight transformation deteriorates the recognition ability of the model. However, after embedding the effective channel attention module, the $EUUL_{cspeca}$ model

demonstrated high precision (97.01%) and achieved the highest *F1* value (0.92) among all the models. This shows that the ECA mechanism effectively improves the model's recognition precision and ensures its localisation performance after lightweight transformation. In addition, the point precision verification results of the model support the conclusions above.

Table 4-1 Results of precision based on experiments

Model	Parameter	Test number	Precision	Recall	F1	Point $precision_x$	Point $precision_y$	Point recall
$EUUL_{ori}$	136.0 M	40	96.49%	76.39%	0.85	97%	98%	**100%**
$EUUL_{csp}$	37.0 M	40	93.10%	36.00%	0.52	**99%**	**99%**	70%
$EUUL_{cspeca}$	37.0 M	40	**97.01%**	**86.67%**	**0.92**	98%	98%	**100%**
YOLOv3	237.0 M	40	91.67%	27.50%	0.42	/	/	/
Faster R-CNN	113.4 M	40	65.52%	95.00%	0.78	/	/	/

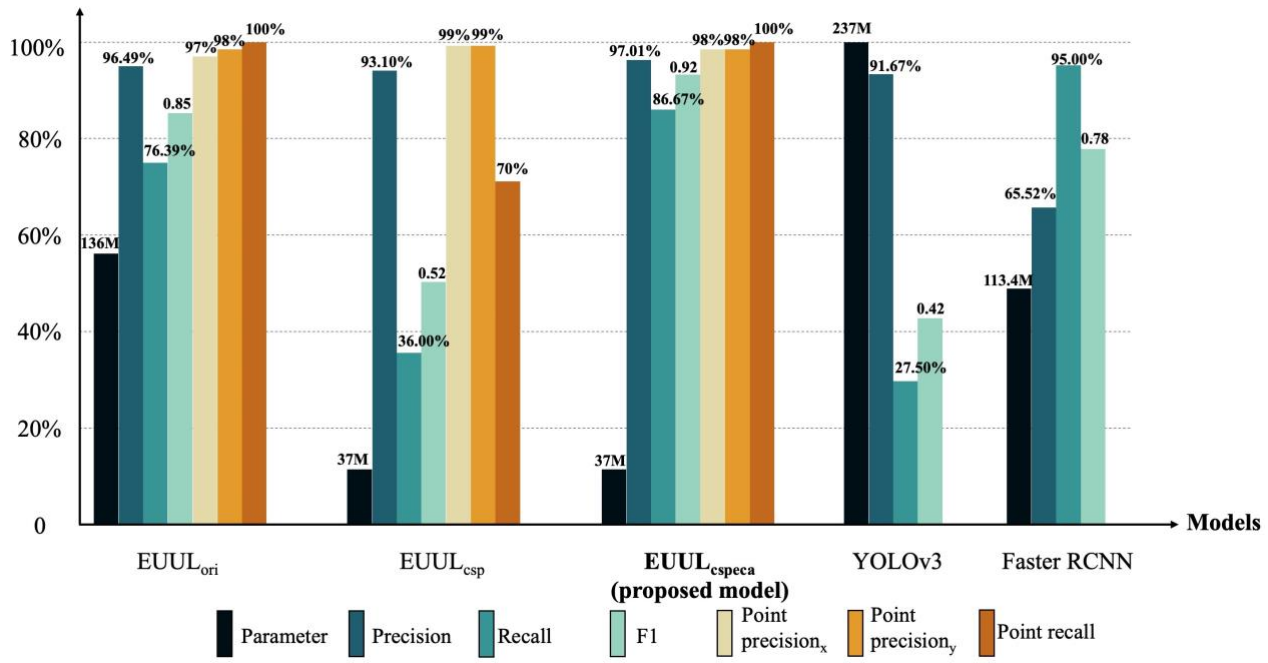

Figure 4-6 Comparison of precision results based on experiments

4.3.2 Experiment to verify robustness

An experiment was performed to determine whether the proposed EUUL model ($EUUL_{cspeca}$) performs better than other existing models in terms of robustness, and to verify the effects of the lightweight model and ECA improvements on the robustness of the model. Therefore, the B-scan image data in the test set were subjected to Gaussian blur processing, as shown in Figure 4-7, to improve the difficulty of model localisation. Subsequently, the processed test images were imported into $EUUL_{ori}$, $EUUL_{csp}$, $EUUL_{cspeca}$, YOLOv3, and Faster R-CNN for testing.

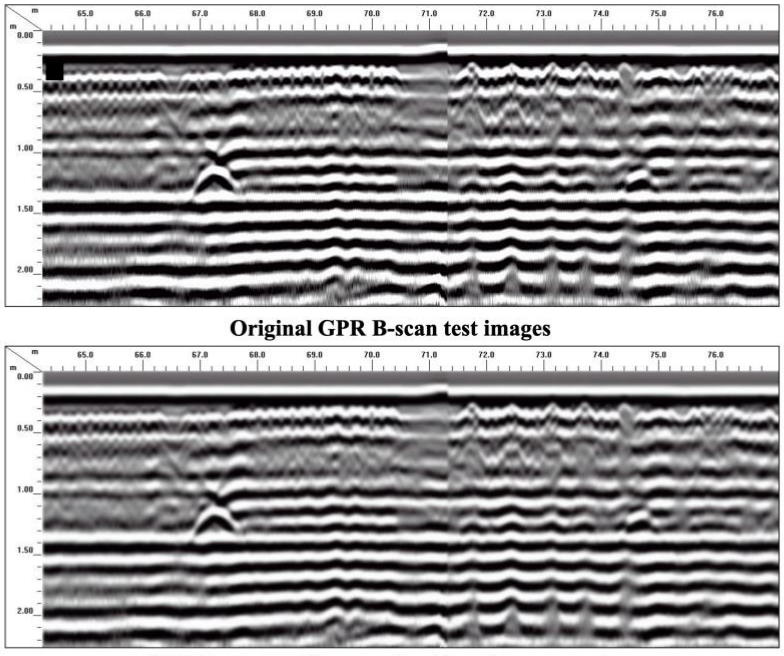

Figure 4-7 Sample of normal and Gaussian test set data

For comparison, Table 4-2 shows the test performance of each model for the normal and Gaussian datasets. The results presented in Figure 4-8 provide a better visualisation of the comparison.

First, the *precision* of the $EUUL_{cspeca}$ model decreased, whereas the performances of $EUUL_{ori}$ and YOLOv3 on the Gaussian test set improved. Meanwhile, the *precision* of $EUUL_{csp}$ and Fast R-CNN did not change. This shows that the noise produced by the Gaussian blur processing affected the performance of the models; however, it was not reflected by the *precision* index alone. Second, regarding *recall*, except for the

$EUUL_{csp}$ and Faster R-CNN models, the *recall* of all other models decreased significantly. The *recall* values of the $EUUL_{ori}$, $EUUL_{cspeca,}$ and YOLOv3 models decreased by 11.11%, 8%, and 7.5%, respectively. This shows that when noise interference occurred, the retrieval ability of the $EUUL_{ori}$, $EUUL_{cspeca}$, and YOLOv3 models for UUs targets in the B-scan images deteriorated. Additionally, this indicates that the increase in the *precision* of $EUUL_{ori}$ and YOLOv3 on the Gaussian test set was due to a significant decrease in the number of UUs targets retrieved by the models. Third, considering the changes in *precision* and *recall* in the two datasets, the *F1* values of models other than the $EUUL_{csp}$ and Faster R-CNN models decreased significantly, and the $EUUL_{cspeca}$ model (0.87) indicated the highest *F1* value. This shows that, when subjected to the same noise interference, the $EUUL_{cspeca}$ model was the best-performing model among all the experimental models. A comparison between $EUUL_{cspeca}$ and $EUUL_{csp}$ indicates that the ECA module improves the robustness of the EUUL model. Finally, the point precision of the models supported this statement.

Table 4-2 Results of robustness based on experiments

Model	**Parameter**	**Test number**	**Precision**	**Recall**	**F1**	**Point precision$_x$**	**Point precision$_y$**	**Point recall**
Normal test data set								
$EUUL_{ori}$	136.0 M	40	96.49%	76.39%	0.85	97%	98%	**100%**
$EUUL_{csp}$	37.0 M	40	93.10%	36.00%	0.52	**99%**	**99%**	70%
$EUUL_{cspeca}$	37.0 M	40	**97.01%**	86.67%	**0.92**	98%	98%	**100%**
YOLOv3	237.0 M	40	91.67%	27.50%	0.42	/	/	/
Faster R-CNN	113.4 M	40	65.52%	**95.00%**	0.78	/	/	/
Gaussian test data set								
$EUUL_{ori}$	136.0 M	40	97.92% ↑	65.28% ↓	0.78 ↓	**99%**↑	**98%-**	90%↓
$EUUL_{csp}$	37.0 M	40	93.10% -	36.00% -	0.52 -	95%↓	96%↓	42.5%↓
$EUUL_{cspeca}$	37.0 M	40	96.72% ↓	78.67% ↓	**0.87** ↓	98% -	**98% -**	**100% -**

Model	Parameter	Test number	Precision	Recall	F1	Point $precision_x$	Point $precision_y$	Point recall
YOLOv3	237.0 M	40	**100.00%↑**	20.00% ↓	0.33 ↓	/	/	/
Faster R-CNN	113.4 M	40	65.52% -	**95.00% -**	0.78 -	/	/	/

Note: In this table, ↑ implies a value increase, ↓ implies a value decrease, and - implies unchanged compared to the value in the normal test dataset.

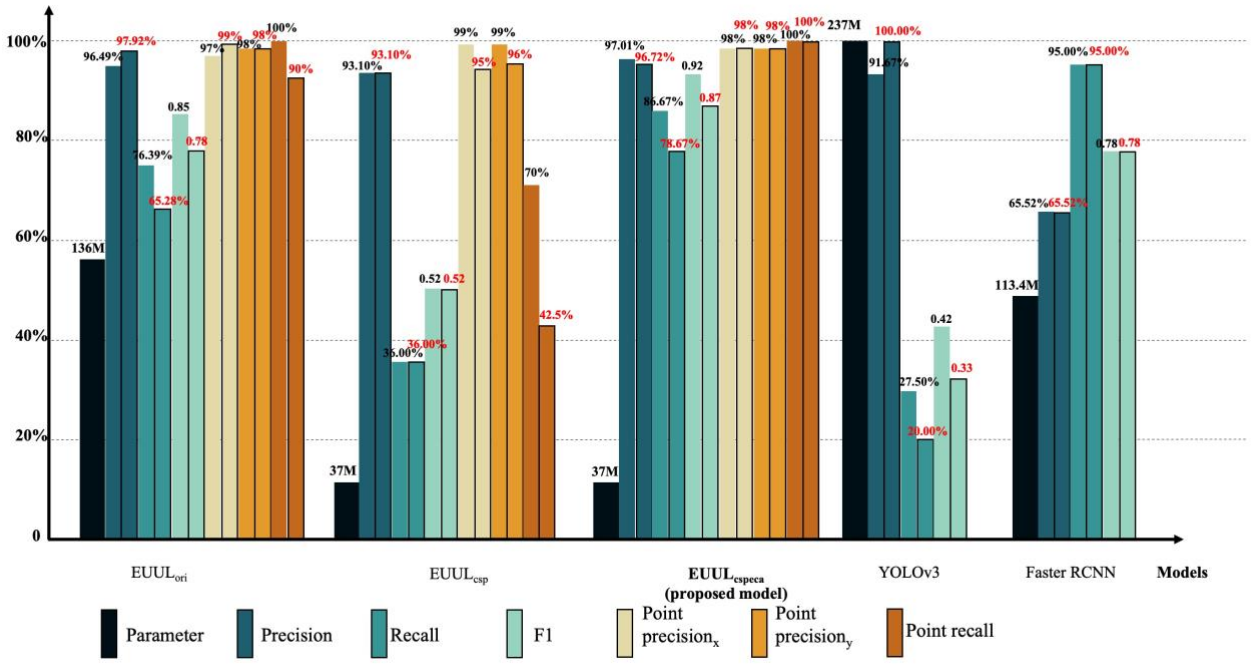

Figure 4-8 Comparison of robustness based on experiments. (Percentages indicated in black and red represent results based on normal and Gaussian test datasets, respectively)

4.3.3 Experiment to verify speed

An experiment was performed to validate whether the proposed anchor-free models (EUUL series) offered a significant advantage over the comparative models in terms of operating speed. Another purpose of this experiment was to verify that the lightweight improvement proposed herein can enhance the operating speed (EUUL$_{csp}$

and $EUUL_{cspeca}$). Therefore, in this experiment, the same test dataset was used to record the processing speed (fps) and parameter quantity for each model.

As shown in Table 4-3, the *fps* of the $EUUL_{ori}$, $EUUL_{csp}$, $EUUL_{cspeca}$, YOLOv3, and Faster R-CNN models under the normal test dataset were 105, 125, 125, 82, and 20, respectively. Among them, the lightweight-improved $EUUL_{csp}$ and $EUUL_{cspeca}$ models indicated the highest operating speeds, which satisfied engineering requirements for real-time applications. However, the operating speed of $EUUL_{ori}$ without lightweight improvement was slightly lower than those of the two aforementioned models, although its *fps* reached 105. Therefore, compared with the comparison models YOLOv3 and Faster R-CNN, the EUUL series models offered a significant advantage in terms of operating speed, which was five to six times that of the Faster R-CNN. In addition, the number of parameters in the lightweight-improved $EUUL_{csp}$ and $EUUL_{cspeca}$ models (37.0 M) was significantly less than those in the comparison models YOLOv3 (237.0 M) and Fast R-CNN (113.4 M). This shows that the GPR B-scan localisation models based on the key point-regression mode proposed herein can eliminate the dependence on expensive hardware under the same conditions more effectively to better adapt to the harsh engineering practice environment.

Table 4-3 Results of speed based on experiments

Model	**Test number**	**Parameter**	***fps***
$EUUL_{ori}$	40	136.0 M	105
$EUUL_{csp}$	40	37.0 M	**125**
$EUUL_{cspeca}$	40	37.0 M	**125**
YOLOv3	40	237.0 M	82
Faster R-CNN	40	113.4 M	20

Note: Experiments were conducted using a NVDIA RTX 3090, GPU-based computer.

4.4 Experiments based on different soil types

To verify the localisation performance of the proposed models under different soil conditions, pipeline data from two different areas (Areas 1 and 2) were obtained by using the same GPR equipment with the same operating frequency (400 MHz). In total, 450 frames were obtained. For each area, 185 and 40 of 225 frames were used for

training and testing, respectively.

The geological conditions in Area 1 were relatively complex, featuring a backfilled soil layer containing large pieces of gravel and holes in the working sections. In Area 2, the backfill soil layer was more uniform; however, the pipelines were densely distributed, and the signals between the pipelines interfered. Sample data from Areas 1 and 2 are shown in Figure 4-9.

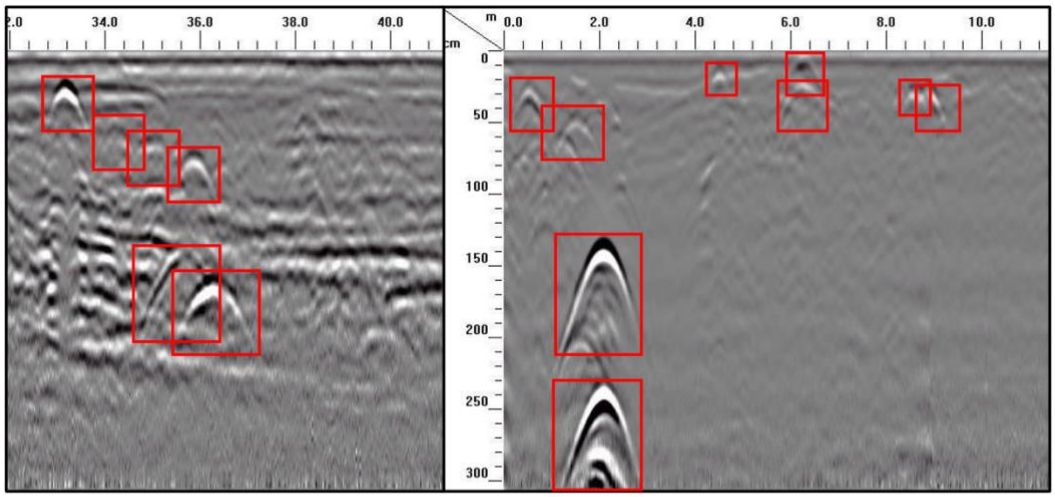

Area 1 (complex soil type with large pieces of gravel and holes)

Area2 (simple soil type with congested pipelines)

Figure 4-9 Sample data from Areas 1 and 2

Five models ($EUUL_{csp}$, $EUUL_{cspeca}$, $EUUL_{ori}$, YOLOv3, and Faster R-CNN) were trained and tested on the same dataset. The experimental results are presented in Table 4-4 and Figure 4-10. The proposed $EUUL_{cspeca}$ model exhibited promising performance in *terms of precision*, *recall*, and *F1*.

Regarding *precision*, $EUUL_{csp}$ performed the best on both test datasets for Areas 1 and 2 (94.64% and 92.75%, respectively). However, the *recalls* of the proposed $EUUL_{cspeca}$ model in these two datasets were 2.35% and 3.61% higher than that of the $EUUL_{csp}$ model. This indicates that the $EUUL_{cspeca}$ model cloud obtained more detection targets. Regarding *F1*, the proposed $EUUL_{cspeca}$ model (0.87 and 0.85) exhibited the best performance compared with the other models.

Table 4-4 Experimental results based on different soil types

Model	Parameter	Test number	Precision	Recall	F1
Area 1					
$EUUL_{ori}$	136.0 M	40	92.00%	72.63%	0.81
$EUUL_{csp}$	37.0 M	40	**94.64%**	76.70%	0.85
$EUUL_{cspeca}$	37.0 M	40	90.59%	83.05%	**0.87**
YOLOv3	237.0 M	40	90.14%	67.37%	0.77
Faster R-CNN	113.4 M	40	58.26%	**95.49%**	0.72
Area 2					
$EUUL_{ori}$	136.0 M	40	90.91%	72.29%	0.81
$EUUL_{csp}$	37.0 M	40	**92.75%**	77.11%	0.84
$EUUL_{cspeca}$	37.0 M	40	89.33%	80.72%	**0.85**
YOLOv3	237.0 M	40	89.23%	69.88%	0.78
Faster R-CNN	113.4 M	40	59.23%	**92.77%**	0.72

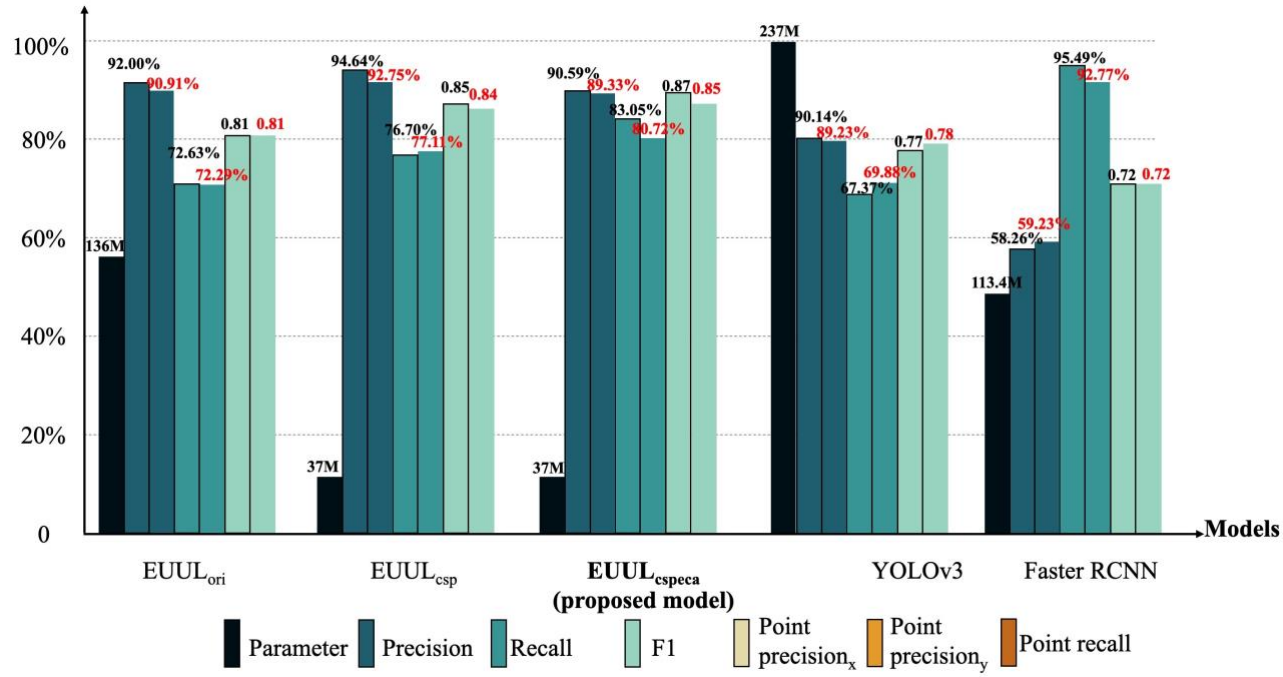

Figure 4-10 Comparison of experimental results based on different soil types. (Percentages in black and red represent results based on test datasets of Areas 1 and 2, respectively.)

4.5 Chapter summary

In this section, an EUUL model is developed using the GPR B-scan images. Three experiments were conducted to validate the proposed model and its improvements on an actual site. The experimental results showed that the *precision* of the proposed EUUL model was 97.01%, operating speed was 125 fps, and precision was 96.72% in a noisy environment. The EUUL model was superior to the existing mainstream models in terms of precision, operating speed, and robustness. The model satisfied the requirements of UU localisation in engineering practice and promotes the development of automatic GPR-based UU localisation.

Chapter 5 : Developing image-based UU 3D reconstruction model

5.1 Chapter introduction

This chapter presents a detailed design of the ZDE3D model for low-light enhancement of the UU 3D reconstruction task. An unsupervised architecture and five loss functions were proposed based on the UU domain knowledge and image-based 3D reconstruction principles. Cross-comparison experiment results using real-site datasets are introduced to demonstrate the effect of 3D reconstruction by measuring the sparse reconstruction quality and the resulting point-cloud model precision. The ablation experiment results were also introduced to demonstrate the usefulness of each loss function in practice. The ZDE3D model was developed using Python and Pytorch deep-learning frameworks for model training, validation, and testing on the Google Colab cloud-computing platform.

5.2 Detailed design of the ZDE3D model

5.2.1 Framework and architecture

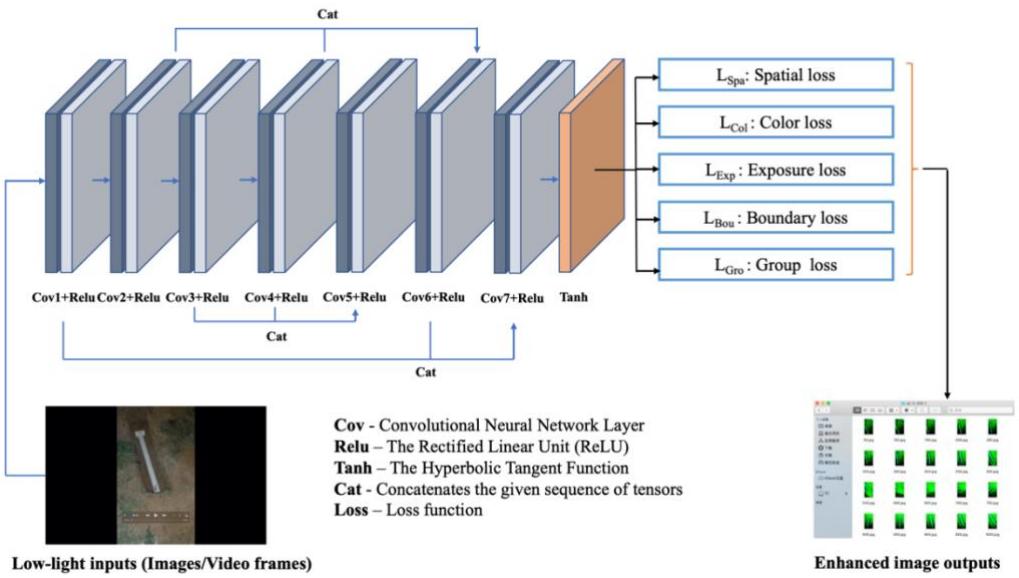

Figure 5-1 Framework of the ZDE3D model

Inspired by zero-DCE (Guo et al., 2020a), ZDE3D adopts a deep-learning method to establish a pixel-wise mapping relationship between the input low-light image and output-enhanced image to improve the 3D reconstruction performance. As shown in

Figure 5-1, the ZDE3D model employed a CNN with seven convolutional layers with symmetrical concatenation. Each layer consisted of 32 convolutional kernels of size 3×3 and stride 1, followed by the ReLU activation function. Because the up-sampling and pooling layers could interfere with the interpixel relationship of the input image and lead to the loss of important information, these layers were completely discarded in the model. The last convolutional layer was followed by the Tanh activation function, which produced 24 parameter maps for eight iterations (n = 8), where each iteration required three curve parameter maps for the three channels.

To improve the 3D reconstruction performance of the input low-light images, the overall goal of ZDE3D was primarily achieved through the following five loss functions: L_{Spa} (spatial loss), L_{Col} (colour loss), L_{Exp} (exposure loss), L_{Bou} (boundary loss), and L_{Gro} (group loss). L_{Spa} was used to improve the image contrast, L_{Col} was used to improve the image brightness reasonably, L_{Exp} was used to adjust the image exposure, L_{Bou} was used to generate a boundary penalty mechanism, and L_{Gro} was used to control the direct difference of the same group of images. The working principle and details of the loss function are described in Section 3.2. By optimising the ZDE3D model, the image data collected in a low-light environment automatically learn how to better generate the mapping relationship of 3D point-cloud images without any paired or unpaired data.

5.2.2 Loss-function design

Because no paired or unpaired reference data were used in the learning process of the ZDE3D model, the effect of the optimisation task depended completely on the design of the loss functions. In the design process of the following loss functions, the requirements of feature point extraction and matching in the 3D reconstruction process are considered. By designing different loss-function features, the enhanced images could reflect as many pixel-level features as possible without losing the original information to improve the 3D reconstruction performance in a low-light environment. Therefore, we designed the following loss functions:

5.2.2.1 Spatial loss

Spatial loss (L_{Spa}) stimulates the pixel difference features in low-light images. By comparing the pixel values of the corresponding positions before and after mapping in some pixel areas (the 4×4 area was adopted in this study following the experience of zero-DCE (Guo et al., 2020a)), the original areas that may contain feature points were enhanced, as shown in Eq. 5-1, where K is the number of local regions and $\Omega(i)$ is the four neighbourhoods centred around region i (upper, lower, left, and right). I represents the pixel value in the input picture, and E represents the pixel value after mapping optimisation. C is a small normal number that avoids inoperable problems without affecting the equation.

$$L_{Spa} = \frac{1}{K}\sum_{i=1}^{k}\sum_{j\in\Omega(i)}\frac{(I_i-I_j)^2+C}{(E_i-E_j)^2+C} \qquad \text{Eq. 5-1}$$

5.2.2.2 Colour loss

Colour loss (L_{Col}) is used to reasonably improve the brightness of pixels in low-light images. Extensive studies have shown that image feature degradation is closely related to the pixel intensity (i.e. image brightness). From the perspective of the pixel value distribution, the pixel values of low-light images are densely distributed in the range of low-brightness areas, which leads to insufficient utilisation of the brightness space. Much effective information is crowded within a narrow range and cannot be used by 3D reconstruction algorithms. Therefore, based on the colour balance algorithm (Pascale et al., 2022), the ZDE3D model adopts L_{Col} to effectively expand the pixel representation space of low-light images, as shown in Eq. 5-2. K represents the number of pixels in each channel and R, G, and B represent the red, green, and blue channels of the colour image, respectively. E_i represents the pixel value of the enhanced image at position i, and j is the channel where the pixel resides. E_{max} represents the maximum pixel value of the enhanced image on a given channel. By adjusting L_{Col}, the pixel values of low-light images in the input model are evenly distributed in the brightness space of 0-255, to obtain better reconstruction performance.

$$L_{Col} = \frac{1}{K}\sum_{i=1}^{k}\sum_{j\in(R,G,B)}(E_i - \frac{E_i}{E_{max}})^2 \qquad \text{Eq. 5-2}$$

5.2.2.3 Exposure loss

The exposure loss (L_{Exp}) was used to prevent abnormal exposure to low-light images after adjustment. Pictures that are too bright or too dark cannot effectively show the characteristics of the target object. This feature is also important for 3D reconstruction. Therefore, the ZDE3D model retains the loss function used by the zero-DCE model to control the exposure (see Eq. 5-3). *M* represents the number of non-overlapping local regions of size 16×16, and *E* represents the average intensity value of local regions in the enhanced image. Based on the experimental results of zero-DCE, *B* was set as a constant value (0.6) in the model (Guo et al., 2020a).

$$L_{Exp} = \frac{1}{M}\sum_{k=1}^{M}|E_k - B| \qquad \text{Eq. 5-3}$$

5.2.2.4 Boundary loss

Boundary loss (L_{Bou}) implements a linear boundary penalty mechanism in as-built UU scenarios. Linear features appear frequently in the image data used for the UU 3D reconstruction. The main reason for this is that the boundary between the underground pipelines and background is linear when mapped to a two-dimensional plane. Based on this feature, the ZDE3D model adds L_{Bou} based on the above loss functions to increase the prominence of the UU target in the scenarios. L_{Bou} is implemented by adjusting the gradient relationship between the pixels, as shown in Eq. 5-4. Here, *N* is the number of iterations, and *j* denotes the different channel positions. ∇X and ∇Y represent the horizontal and vertical gradient operations, respectively. At the boundary position, ∇X and ∇Y are encouraged to lift the gradient to obtain more prominent features.

$$L_{Bou} = \sum_{i=1}^{N}\sum_{j\in(R,G,B)}\frac{N}{(\nabla X+\nabla Y)+C} \qquad \text{Eq. 5-4}$$

5.2.2.5 Group loss

Group loss (L_{Gro}) balances the pixel difference features between adjacent low-light image inputs. The image 3D reconstruction based on SFM does not input image data in order but inputs the same batch of images used to reconstruct a certain scene together (Jiang et al., 2020). Therefore, important matching features may be missed if the difference between the adjacent low-light images is too large. Based on this, L_{Gro} in

the ZDE3D model balances images from different angles in a unified scene in terms of adjacent similarity to obtain better 3D reconstruction effects, as shown in Eq. 5-5. Where N represents the number of pictures in the same group, E_{ave} represents the average pixel value of the pictures, i represents the serial number of images in the group, and j represents the channel information.

$$L_{Gro} = \sum_{i=1}^{N} \sum_{j \in (R,G,B)} (E_{ave(i)} - E_{ave(i+1)})^2 \qquad \text{Eq. 5-5}$$

5.2.2.6 Total loss

In summary, the total loss of the model can be expressed as Eq. 5-6. W represents the weight of L_{Spa}, the function of which ensures that each loss is of the same order of magnitude to avoid the problem of decreasing the training effect caused by the imbalance between them.

$$L_{Total} = W L_{Spa} + L_{Col} + L_{Exp} + L_{Bou} + L_{Gro} \qquad \text{Eq. 5-6}$$

5.3 Experiments results

5.3.1 Laboratory environment experiment results

First, 3D reconstruction experiments were conducted on UU scenes with different arrangements and buried depths under different illumination conditions in a laboratory environment under controlled conditions. Table 5-1 illustrates all parameters and results of the experiments. Under the different experimental environmental conditions mentioned above, the 3D reconstruction effect of the pipeline shows different degrees of quality improvement compared to the original low-light inputs. Simultaneously, the UU point-cloud 3D model generated after enhancement still has high record accuracy.

Table 5-1 Experiment results

Depth	**Categories**	**Input frames**	**Point cloud quantity**	**Enhanced ratio**	**Utility size**	**Point-cloud size**	**Record accuracy**
One pipe in trench							
300 mm	Normal	47	23,217	/	90 mm	88 mm	97.78%

Depth	Categories	Input frames	Point cloud quantity	Enhanced ratio	Utility size	Point-cloud size	Record accuracy
	Low light	47	3,162	/	90 mm	91 mm	98.89%
	Enhanced	47	3,804	20.30 %	90 mm	92 mm	97.78%
500 mm	Normal	45	22,122	/	90 mm	87 mm	96.67%
	Low light	45	4,137	/	90 mm	89 mm	98.89%
	Enhanced	45	4,724	14.19 %	90 mm	91 mm	98.89%
700 mm	Normal	43	26,530	/	90 mm	90 mm	100.00%
	Low light	43	36,99	/	90 mm	92 mm	97.78%
	Enhanced	43	4,024	8.79 %	90 mm	92 mm	97.78%
Two pipes in trench							
300 mm	Normal	49	22,736	/	90 mm	90 mm	100.00%
	Low light	49	4,069	/	90 mm	89 mm	98.89%
	Enhanced	49	4,553	11.40 %	90 mm	88 mm	97.78%
500 mm	Normal	42	20,655	/	90 mm	91 mm	98.89%
	Low light	42	2,949	/	90 mm	92 mm	97.78%
	Enhanced	42	3,115	5.63 %	90 mm	90 mm	100.00%
700 mm	Normal	43	25,946	/	90 mm	89 mm	98.89%
	Low light	43	6,934	/	90 mm	91 mm	98.89%
	Enhanced	43	8,240	18.83 %	90 mm	91 mm	98.89%
Average				13.19 %			98.58%

5.3.2 On-site validations

To further verify that the proposed ZDE3D model is suitable for various real UU construction scenarios, three verification experiments with different reconstruction targets were conducted at three construction sites. Section 4.4.1 describes the background of the three experiments. Section 4.3.2 shows the experimental results. Section 4.3.3 analyses the experimental results.

5.3.2.1 Background

Three group images (248 frames total) were collected from the UU projects in Jiangxi Province, China, where Groups 1 and 3 were bridge-supporting engineering projects, and Group 2 was a civil housing project. In these verification experiments, the data collection and processing procedures were the same as those described in Section 4.2. Moreover, 46, 34, and 45 low-light image frames were obtained, respectively.

During the data-collection process, the real construction site process was restored to the greatest extent, and the datasets were captured using a personal smartphone. Notably, the data collection in these validation experiments involved all frontline construction personnel without professional training. Details of the experimental objectives are listed in Table 5-2.

Table 5-2 Validation scenario details

Group	Frames	Category	Depth	Diameter	Description
Group 1	92	Weak Electricity	1.5 m	200 mm	Change of Plan
Group 2	68	Sewer Pipeline	1.8 m	500 mm	Pipeline Connection
Group 3	88	Strong Electricity	2.0 m	400 mm	Set Arrangement

Figure 5-2 shows sample images of the three groups of field-verification experiments.

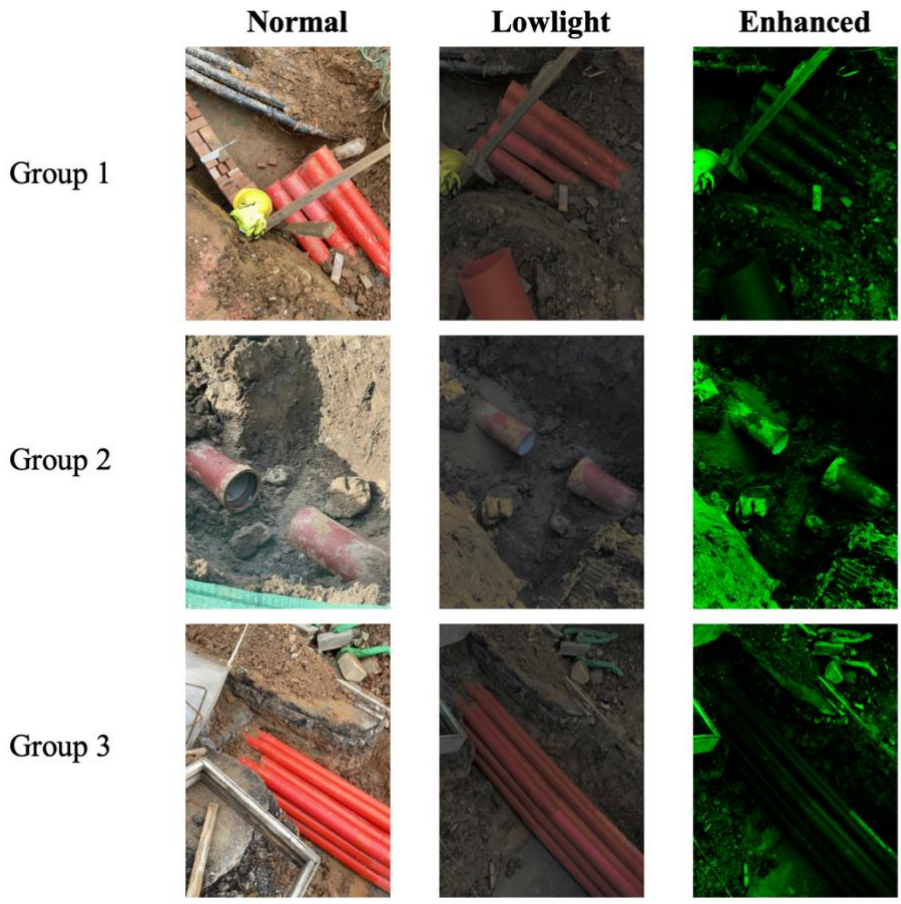

Figure 5-2 Samples images of the on-site validation experiments

5.3.2.2 Validation results

Table 5-3 illustrates the 3D reconstruction performance of the above three groups of scenarios under normal and low-light conditions, and the proposed model enhances the conditions.

Table 5-3 Experiment results

Categories	**Input frames**	**Point-cloud quantity**	**Enhanced ratio**	**Utility size**	**Point-cloud size**	**Record accuracy**
			Group 1			
Normal	46	54,040	/	200 mm	205 mm	97.52%
Low light	46	38,372	/	200 mm	203 mm	98.55%

Categories	Input frames	Point-cloud quantity	Enhanced ratio	Utility size	Point-cloud size	Record accuracy
Enhanced	46	53,519	39.47 %	200 mm	205 mm	97.53%
			Group 2			
Normal	34	19,639	/	500 mm	502 mm	99.63%
Low light	34	12,566	/	500 mm	510 mm	98.01%
Enhanced	34	16,984	35.16%	500 mm	508 mm	98.41%
			Group 3			
Normal	45	44,378	/	400 mm	406 mm	98.53%
Low light	45	28,596	/	400 mm	406 mm	98.57%
Enhanced	45	37,195	30.07 %	400 mm	408 mm	98.08%

5.4 Discussion on image-based UU 3D reconstruction model (Objective 3)

The effectiveness of the proposed ZDE3D model for 3D reconstruction under low-light conditions was evaluated through three sets of on-site validation experiments. In the first experiment, the quantity of 3D reconstructed point clouds increased by 39.47% after applying the unsupervised optimisation model. The Group 1 scene showed the most significant improvement, and the number of point clouds after optimisation was very close to the number obtained under normal lighting conditions. The Group 2 and 3 experiments resulted in 35.16% and 30.07% increases in the quantity of reconstructed point clouds, respectively. Moreover, all three experiments achieved an accuracy rate of over 30.00% for the reconstruction record.

5.4.1 Loss-function ablations

The aim of the ablation study was to assess the contribution of each proposed loss function. In our study, one of the five proposed loss functions was removed while maintaining all the other conditions constant. We then compared the 3D reconstruction results to evaluate the impact of each loss function on the overall performance, as intended in our experimental design. The optimisation performance of different

combinations of the loss functions on the same sample image is shown in Figure 5-3, and Table 5-4 illustrates the ablation experiment results.

The contrast of the low-light images decreases when the spatial control loss L_{Spa} is removed. The pipe position can be recognised; however, 3D point clouds cannot be generated. This indicates that the influence of L_{Spa} is primarily reflected in the contrast constraint.

The result without brightness distribution loss, L_{Col}, lost colour features, whereas the 3D model could not be generated. This indicates that L_{Col} significantly affects the distribution of pixel values in each channel (RGB) of the image.

There was no significant degradation in the image quality, and the original pixel features were retained even more when the exposure control loss L_{Exp} was discarded. However, the 3D reconstruction results indicated that the absence of L_{Exp} reduced the number of sparse point clouds. This indicates that L_{Exp} is still necessary for low-light enhancement, although it may be counterintuitive.

The ablation results of the boundary penalty loss L_{Bou} show that all boundaries of the pipe targets and the background disappear. In this case, 3D reconstruction was impossible. This differs from the assumption that only the pipeline boundary is affected when the L_{Bou} is designed, as expected. However, this also showed that the restriction of the horizontal and vertical gradient operations by L_{Bou} affected the improvement in the low-light boundary.

The average enhancement ratio (15.63%) after L_{Gro} removal was higher than the total loss ratio (11.52%). However, the performances of some groups decreased (500 mm and two pipes). This finding suggests the following. 1) The ZDE3D model still has the potential to continue improving the 3D reconstruction performance under low-light conditions. 2) Removing L_{Gro} affects the robustness of the model. The current study primarily considered the stability performance of the model to be more suitable for the complex environment at the construction site; therefore, L_{Gro} was retained. If others value the enhanced capability of the model for low-light 3D reconstruction, they can

choose to remove it.

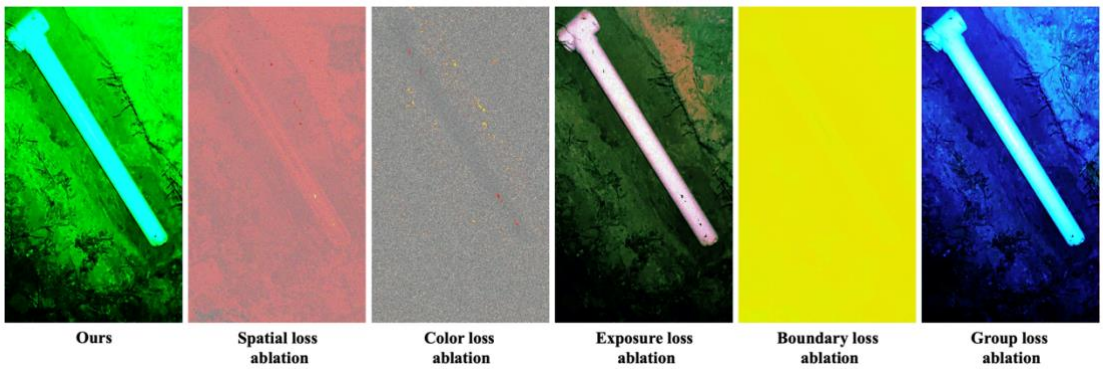

Figure 5-3 Enhanced output samples under difference loss functions

Table 5-4 Loss-function ablation experiment results (This table only shows the results of removing the L_{Exp} loss or L_{Gro} loss; the other three types of loss (L_{Spa}, L_{Col}, and L_{Bou}) are not listed because they are critical to the success of the final 3D point-cloud generation. If remove any one of them, the generation process will fail.)

Categories	**Point-cloud quantity (low light)**	**Point-cloud quantity (total loss enhanced)**	**Point-cloud quantity (partial loss enhanced)**	**Enhanced ratio**	**Record accuracy**
Exposure loss (L_{Exp}) ablation					
300 mm & One pipe	3162	**3804**	1284	- 59.39%	100.00%
300 mm & Two pipes	4069	**4553**	2033	- 50.03%	97.78%
500 mm & One pipe	4137	**4724**	2967	- 28.28%	98.89%
500 mm & Two pipes	2949	**3115**	1792	- 39.23%	96.67%
700 mm &	3699	**4024**	1880	- 49.17%	97.78%

Categories	Point-cloud quantity (low light)	Point-cloud quantity (total loss enhanced)	Point-cloud quantity (partial loss enhanced)	Enhanced ratio	Record accuracy
One pipe 700 mm & Two pipes	6934	**8240**	3962	- 42.36%	98.89%
Average	/	/	/	- 44.74%	98.34%
Group loss (L_{Gro}) ablation					
300 mm & One pipe	3162	3804	**4101**	29.69%	97.78%
300 mm & Two pipes	4069	4553	**4908**	20.61%	100.00%
500 mm & One pipe	4137	**4724**	4167	0.72%	98.89%
500 mm & Two pipes	2949	**3115**	2730	- 7.42%	97.78%
700 mm & One pipe	3699	4024	**4437**	19.95%	98.89%
700 mm & Two pipes	6934	8240	**9032**	30.25%	97.78%
Average	/	/	/	15.63%	98.52%

5.4.2 Comparison experiments with existing methods

To verify whether the proposed ZDE3D model has significant advantages over existing methods, three groups of actual construction site datasets mentioned in Section 4.4 (Group 1, Group 2, and Group 3) were used to verify the effects of different models.

To be representative, the brightness, contrast, supervised deep learning (LLNet), zero-DCE (unsupervised deep learning), and ZDE3D (this study) were tested. The experimental results are presented in Table 5-5.

Table 5-5 Comparison experiments results

Categories	**Point-cloud quantity (low light)**	**Point-cloud quantity (ours)**	**Point-cloud quantity (compare method)**	**Enhanced ratio**	**Record accuracy**
Brightness					
Group 1	38,372	**53,519**	44,551	16.10%	96.78%
Group 2	12,566	**16,984**	15,768	25.48%	97.06%
Group 3	28,596	**37,195**	35,885	25.60%	97.34%
Average	/	/	/	22.39%	97.06%
Contrast					
Group 1	38,372	**53,519**	46,164	20.30%	99.30%
Group 2	12,566	**16,984**	16,714	33.00%	96.89%
Group 3	28,596	**37,195**	36,805	28.71%	97.17%
Average	/	/	/	27.33%	97.79%
RetinexNet (Supervised Deep learning)					
Group 1	38,372	**53,519**	48,210	25.64%	97.73%
Group 2	12,566	**16,984**	5,773	-54.06%	98.01%
Group 3	28,596	**37,195**	31,121	8.83%	98.29%
Average	/	/	/	-6.53%	98.01%
Zero-DCE (Unsupervised deep learning)					
Group 1	38,372	**53,519**	41,091	7.09%	98.85%
Group 2	12,566	**16,984**	10,544	-16.09%	99.13%
Group 3	28,596	37,195	**37,431**	**30.90%**	99.41%

Categories	Point-cloud quantity (low light)	Point-cloud quantity (ours)	Point-cloud quantity (compare method)	Enhanced ratio	Record accuracy
Average	/	/	/	7.30%	99.13%
ZDE3D (Ours)					
Group 1	38,372	**53,519**	/	**39.47 %**	97.53%
Group 2	12,566	**16,984**	/	**35.16%**	98.41%
Group 3	28,596	**37,195**	/	30.07 %	98.08%
Average	/	/	/	**34.90%**	98.01%

The comparison experiments showed that the proposed ZDE3D model had the best UU 3D reconstruction enhancement performance among all tested models. Among them, the parameters of traditional methods (Brightness, Contrast) are prior set manually respectively (brightness: (G1:0.4, G2:0.4, G3:0.3) and contrast: (G1:0.4, G2:0.5, G3:0.4)). Other models applied optimal weights, which have been verified in previous studies. Except for the zero-DCE method in Group 3 (only 0.83% higher than ours), the enhanced ratios of the comparison methods were lower than that of the proposed ZDE3D model.

5.5 Chapter summary

To improve the 3D reconstruction performance of the as-built UU in low-light environments, a zero-reference (unsupervised) deep-learning model for low-light image enhancement in UU 3D reconstruction is proposed (ZDE3D) in this thesis. The main innovations are as follows: (1) A new unsupervised learning model is proposed that can effectively improve the 3D reconstruction effect of UU in a low-light environment. (2) Filling the gap in the image-based UU documentation implementation field in low-light environments. (3) This thesis attempts to use a deep-learning method to learn mapping from the perspective of the relationship between

pixels to achieve a better 3D reconstruction effect.

Real construction site experiments showed a promising result that the ZDE3D model could effectively improve the image-based 3D reconstruction performance in a low-light environment. The number of sparse reconstruction point clouds was improved by 13.19 % on average, and the average reconstruction accuracy was 98.58%. The improvement in 3D reconstruction in a low-light environment can expand the 3D recording efficiency and feasibility of image-based as-built UU projects. The O&M of the UU project cloud also benefits from the as-built 3D information collected on-site in the future.

Chapter 6 : Developing GCN-based UU topology information completion model

6.1 Chapter introduction

This section presents the details of the UUTC. Comparative experiments with different missing data ratios (from 5% to 80%) in real-world datasets are introduced. Five mainstream GCN models (GCN (Kipf & Welling, 2017), ChebGCN (Defferrard et al., 2017), SAGEGCN (Hamilton et al., 2017), GATGCN (Veličković et al., 2018), and TAGCN (Du et al., 2017)) were used as control groups to verify the effectiveness of the UUTC model by completing the UU topological information. The Discussion section compares the effects of the proposed UUTC and GATGCN models and analyses the misjudgement scenarios. All experimental work in this study was completed in a Python 3.8 environment with a Deep Graph Library (DGL (https://www.dgl.ai/)).

6.2 Detailed design of the UUTC model

6.2.1 Overview of the UUTC model

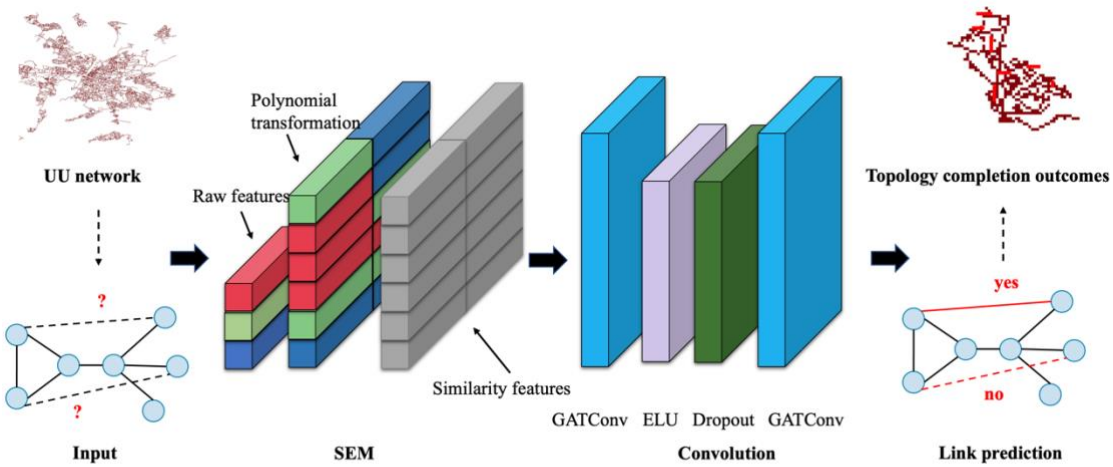

Abbreviations: UU: Underground Utilities; SEM: Similarity Extraction Module; GATConv: Graph Attention-based Convolution layer; ELU: Exponential Linear Unit

Figure 6-1 Framework of UUTC model

The UUTC model comprises four main modules: input, SEM, convolution, and link prediction, as shown in Figure 6-1. The model takes the observed topological relationships and node attribute information of the UU network as input and aims to

generate completed network topology relationship data as output. The input module plays a crucial role in converting the UU network information into graph structure data that the GCN model can effectively recognise. Subsequently, the SEM module leverages the attribute features of each node from the input data to create additional feature attributes, enrich the node features, and provide essential information for subsequent topological completion prediction tasks. The convolution module serves as the central functional component of the UUTC model. Inspired by the working principles of CNNs, it facilitates network operations compatible with graph structures, enabling the learning and updating of weight parameters. Furthermore, drawing inspiration from the GATGCN model, the convolution module incorporates a multi-head self-attention mechanism to enhance information interaction and feature aggregation between nodes more effectively. Finally, the link prediction module quantitatively assesses the potential connection likelihood between each node and delivers comprehensive UU network topology connection information after completion. By integrating these four modules, the UUTC model demonstrates the capability of completing missing topological relations in the UU network, thereby contributing to improving the network management and decision-making processes.

6.2.2 Input module

To enable the prediction of topological relationships among UUs, this model initially converts historical data, presented in tabular form, into a graph structure data format comprising nodes, edges, and attributes. As illustrated in Figure 6-2, each pipe in the original incomplete tabular data corresponds to a node, with the characteristics of the pipe serving as attributes of the node. The graph represents any connection between two pipes as an undirected edge. This graph-based representation facilitates the analysis and modelling of the UU network, enabling the prediction of interconnected relationships among utilities for more effective management and decision-making processes.

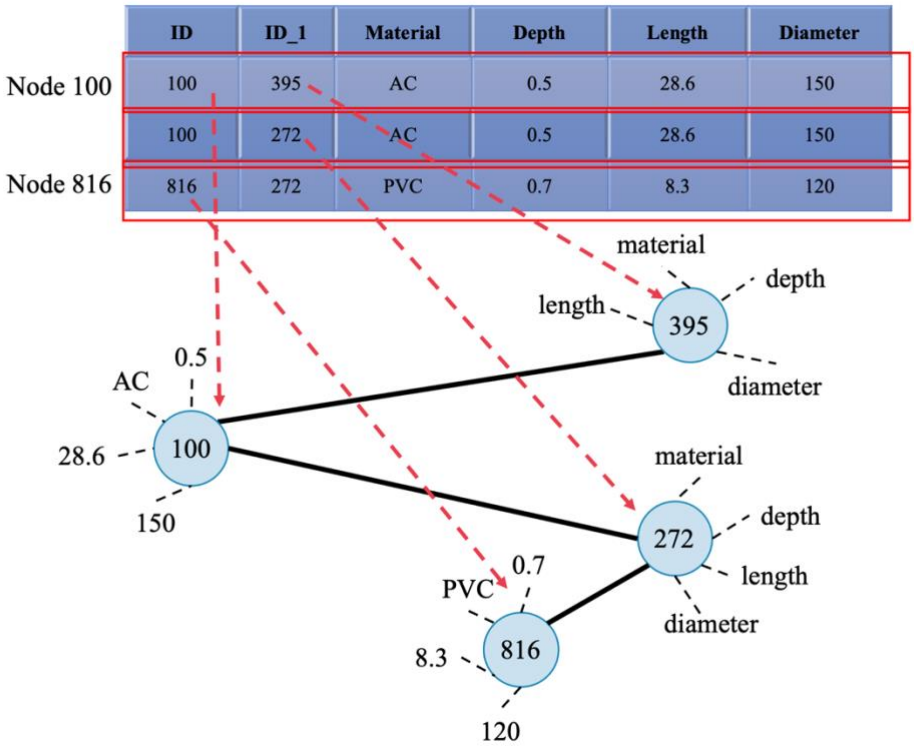

Figure 6-2 An illustration of converting tabular data into graph data

6.2.3 SEM module

The essence of predicting the missing topology lies in predicting the connection relationships among pipeline nodes in the target area. In practical UU engineering, nodes with similar attributes exhibit a significantly higher likelihood of being interconnected than those with substantial differences do. For example, pipelines that share similar attribute characteristics are more likely to form topological connections in a given target area. By contrast, pipelines within different attribute clusters are less likely to exhibit such relationships. Drawing from this domain knowledge, the UUTC model introduces a SEM to assess the similarity between pipeline nodes, thereby enhancing the accuracy of the model in predicting topological relationships. This module leverages attribute clustering to identify nodes with shared characteristics, thereby facilitating precise and informed predictions of the UU network's interconnectedness. As a result, in incorporating the SEM enhances the UUTC model's performance in effectively completing missing topology data, contributing to the improvement of UUs management and decision-making processes. The SEM

module primarily includes the following three components: Polynomial transformation, Similarity calculation, and feature fusion:

1) Polynomial transformation. Polynomial transformation is a data transformation technique that is commonly used in machine learning. By introducing power combinations of the original features, polynomial transformations can capture the non-linear relationships in the data. The various node attributes in the graph input formed by the UU data are combined in a higher-dimensional space to form new valuable features, as shown in Eq. 6-1. Each item in $P\ (x_1, x_2, \ldots, x_n)$ represents a new attribute feature and *n* represents the total number of input graph features. x_i, x_j and x_k denote the different node characteristics. To avoid the over-fitting phenomenon due to excessively high dimensionality and high data calculation, the complexity degree was selected as 3 in this study. Each term in the Eq. 6-1 was then entered into the model as a new attribute of the node. This operation enables the model to improve the available data characteristics without increasing the external data input, thereby improving the prediction performance of the node topology-completion task.

$$P\ (x_1, x_2, \ldots, x_n) = \sum_{i=1}^{n} x_i + \sum_{i,j=1}^{n} x_i x_j + \sum_{i,j,k=1}^{n} x_i x_j x_k \qquad \text{Eq. 6-1}$$

2) Similarity calculation. A polynomial transformation improves the expressive ability of node features through a combination of different attribute features. On this basis, the similarity calculation uses all the characteristic attributes of each node (including initial characteristic attributes and polynomial characteristic attributes) as the overall representation vector of node attributes and uses Euclidean distance to calculate the overall similarity S. Among them, A_i and B_i represent the values of the two node vectors participating in the calculation in the *i*-th dimension. Subsequently, the similarity index S_c between each node in different attribute combination dimensions is calculated, as shown in Eqs. 6-2 and 6-3. Among them, A_j and $B_j$respectively, represent the values of the two node vectors participating in the calculation in the *j*-th dimension, and M represents different combinations of attributes.

$$S = \sqrt{\sum (A_i - B_i)(A_i - B_i)} \qquad \text{Eq. 6-2}$$

$$S_c = \sqrt{\sum(A_j - B_j)(A_j - B_j)} \ (j \subset \{M\}) \qquad \text{Eq. 6-3}$$

Based on polynomial transformation, the similarity calculation creates a new attribute feature expression to improve the possibility of successful topological link prediction. As shown in Figure 6-3, the similarity relationship between the nodes after the similarity calculation operation of the original graph input is embedded in the proximity relationship in Euclidean space. In other words, the more similar the nodes, the closer the similarity index. This echoes prior knowledge that, in UU engineering practice, the possibility of a connection relationship between pipeline nodes with similar attributes is significantly greater than that of pipelines with large differences.

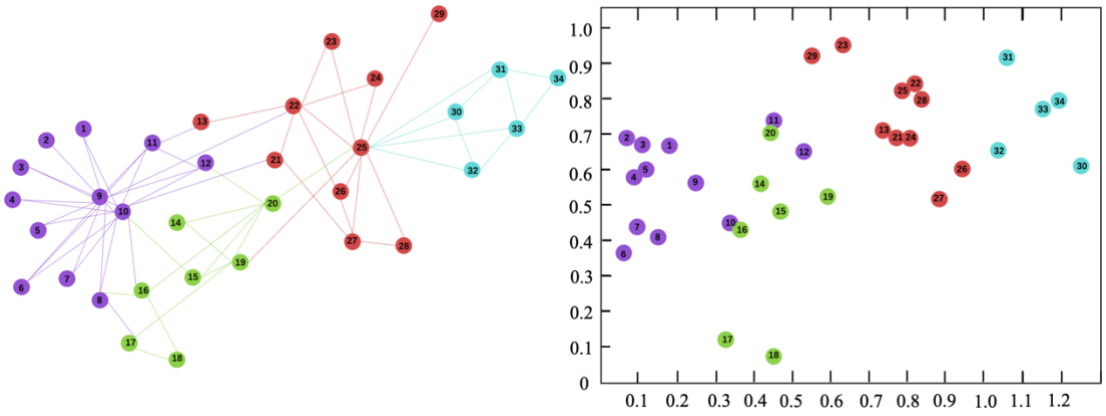

Figure 6-3 An illustration of similarity calculation in two dimensions

3) Feature fusion. After the above two steps, each UU node creates a set of new meaningful attribute features without any external data input, based on the original attribute feature. Feature fusion allows each node to have the same calculation dimension, which is important for subsequent calculation tasks and processing, thereby ensuring the consistency and comparability of features between nodes. Completing this step means that the original attribute features and newly generated meaningful attribute features are integrated, providing a consistent and complete node feature representation for the next analysis and application.

6.2.4 Convolution module

The convolution module primarily includes two key parts: graph convolution and

multi-head attention. As shown in Figure 6-4, graph convolution is an operation for the feature propagation and aggregation of graph-structured data. It updates the feature representation of the node based on its neighbour's information. The convolution module uses two graph volume base layers with a multi-head self-attention mechanism, dropout layer, and ELU activation function to use the connection relationship in the graph structure to propagate information to achieve a convolution effect similar to Euclidean structure data. For the node-update equations, Eqs. 6-4, 6-5, and 6-6; A represents the adjacency matrix input by the graph; I represents the identity matrix; $\widetilde{D}$ represents the degree matrix of $\tilde{A}$; σ represents the activation function, namely ELU; $W^{(l)}$ represents the weight parameter; and $H^{(l)}$ and $H^{(l+1)}$ represent the features of the input layer and the updated features in the next layer, respectively. Thus, the model only needs to learn to update the weight $W^{(l)}$ through back-propagation to achieve convolutional feature extraction, thereby providing the basis for implementing the subsequent link prediction module.

$$\tilde{A} = A + I \qquad \text{Eq. 6-4}$$

$$\widetilde{D}_{ii} = \sum_j \tilde{A}_{ij} \qquad \text{Eq. 6-5}$$

$$H^{(l+1)} = \sigma(\widetilde{D}^{-\frac{1}{2}}\tilde{A}\widetilde{D}^{-\frac{1}{2}}H^{(l)}W^{(l)}) \qquad \text{Eq. 6-6}$$

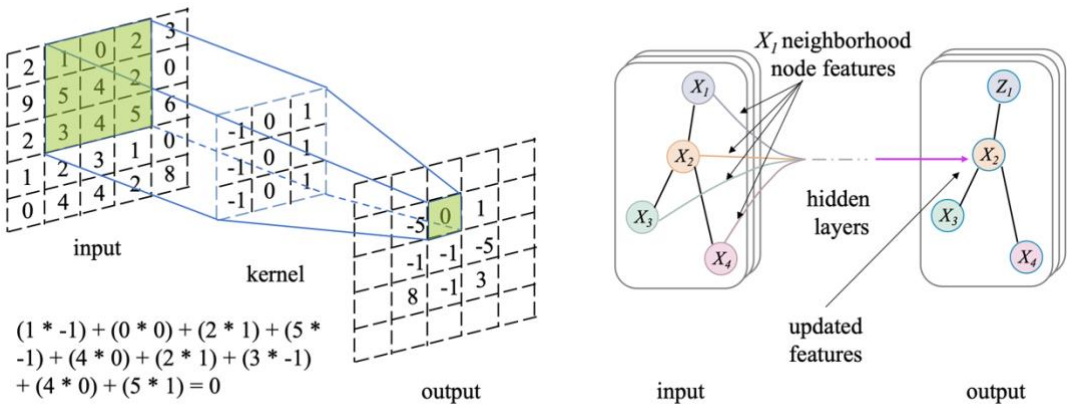

Figure 6-4 An illustration of CNN (Euclid structure) and GCN (graph structure) convolution operation

Multi-head self-attention is an extension of the attention mechanism that can capture

complex node relationships and dependencies. The GATConv layer in the convolution module incorporates a multi-head attention mechanism to model the relationship between the nodes. By introducing multiple attention heads, each of them can focus on different feature subspaces and learn different attention weights. This can improve the expressiveness and generalisation ability of the model, allowing nodes to carry out information transfer and interaction on different feature subspaces. As shown in Figure 6-5, h_1 and h'_1 represent the characteristics of the nodes before and after updating, respectively, and w_1, w_2, ..., and w_6 represent the update weights between nodes. When updating nodes, if only the traditional GCN convolution is used for learning, the difference in the influence of different nodes on the target node cannot be realised. Therefore, by adding a multi-head self-attention mechanism, adding a judgement operation to the influence of information transfer between nodes can effectively help the model mine the utilisation potential of node information. In Figure 6-5, different arrow styles and colours denote independent attention computations. The aggregated features from each head were concatenated or averaged to obtain h'_1.

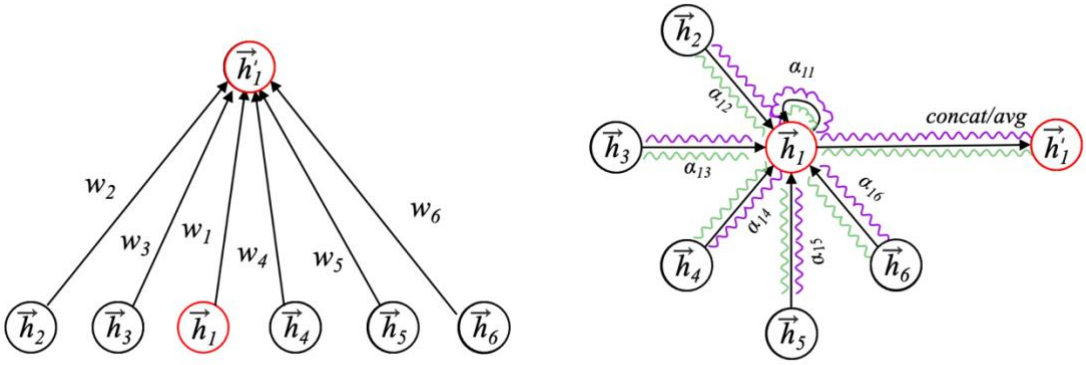

Figure 6-5 Multi-head attention (in GATConv)

6.2.5 Link prediction module

The essence of UU topology completion is the link prediction task in the graph data. After the operation of these modules, many features with abstract information were extracted. The link prediction module uses these features to calculate the possibility score $y_{u,v}$ for any pair of nodes between them (e.g. $h_u$and h_v) (see Eq. 6-7). Among

them, ∅ represents the dot production predictor. The topological information of the UU nodes is obtained by sorting all connection possibility scores to select node pairs that are trusted to have a connection relationship.

$$y_{u,v} = \emptyset\ (h_u, h_v) \qquad \text{Eq. 6-7}$$

6.3 Experiment results

6.3.1 Experiment results under different missing rate conditions

To validate the effect of the proposed UUTC model in the UU topology-completion task, comparative experiments were conducted under different missing data ratios (from 5% to 80%) in the real dataset. In the experiment, the UUTC model and five mainstream GCN models (GCN (Kipf & Welling, 2017), ChebGCN (Defferrard et al., 2017), SAGEGCN (Hamilton et al., 2017), GATGCN (Veličković et al., 2017), and TAGCN (Du et al., 2017)) were used as control groups to verify the effectiveness of the model by completing the UU topological relationship. Table 6-1 and Figure 6-6 shows the UU topology-completion metrics for all experimental conditions. The following conclusions can support the experimental results: 1) Except for the Group 3 experiment with the least number of nodes, the index of the comparison model is better than that of the proposed model, and the remaining indices show that the UUTC model can obtain better UU topology-completion accuracy under the same conditions. The average completion accuracy (*AP*) of the UUTC model in the three experiments reached 85.33%, surpassing the performance of the existing mainstream methods (GCN 76.78%, ChebGCN 76.37%, SAGEGCN 79.37%, GTAGCN 80.85%, and TAGCN 79.44%). 2) As the proportion of missing data increased, the accuracy of completion also decreased. This feature was present in all the experiments, including the control and proposed models. However, it is worth noting that the proposed model maintains high completion accuracy without a large amount of data. 3) When the UU network was small in scale and the missing data ratio was low, it was not significantly better than the control model. However, the UUTC model gradually showed its accuracy advantages when the proportion of missing data was further increased.

Table 6-1 Experiment results under different missing rate conditions

Area 1 (26,627 nodes)						
	GCN	**ChebGCN**	**SAGEGCN**	**GATGCN**	**TAGCN**	**ours**
missing data 5%						
ACC	0.75	0.78	0.75	0.77	0.76	**0.80**
AUC	0.86	0.83	0.85	0.88	0.87	**0.91**
F1	0.80	0.81	0.79	0.81	0.80	**0.83**
AP	0.84	0.80	0.83	0.87	0.86	**0.90**
missing data 10%						
ACC	0.75	0.76	0.75	0.77	0.75	**0.80**
AUC	0.85	0.83	0.84	0.88	0.87	**0.91**
F1	0.79	0.80	0.79	0.80	0.80	**0.83**
AP	0.83	0.79	0.83	0.86	0.85	**0.90**
missing data 20%						
ACC	0.75	0.76	0.75	0.76	0.75	**0.79**
AUC	0.85	0.82	0.83	0.86	0.86	**0.91**
F1	0.79	0.80	0.79	0.80	0.79	**0.82**
AP	0.83	0.78	0.81	0.85	0.84	**0.89**
missing data 30%						
ACC	0.74	0.75	0.73	0.75	0.74	**0.79**
AUC	0.84	0.81	0.81	0.86	0.85	**0.90**
F1	0.79	0.79	0.73	0.79	0.78	**0.82**
AP	0.82	0.77	0.79	0.83	0.84	**0.88**
missing data 40%						
ACC	0.73	0.74	0.74	0.75	0.74	**0.78**
AUC	0.82	0.81	0.81	0.84	0.83	**0.88**
F1	0.78	0.78	0.78	0.79	0.77	**0.81**
AP	0.80	0.77	0.78	0.82	0.82	**0.87**

Area 1 (26,627 nodes)						
	GCN	**ChebGCN**	**SAGEGCN**	**GATGCN**	**TAGCN**	**ours**
missing data 50%						
ACC	0.73	0.73	0.73	0.74	0.73	**0.76**
AUC	0.81	0.80	0.80	0.83	0.82	**0.87**
F1	0.77	0.77	0.78	0.78	0.76	**0.80**
AP	0.79	0.76	0.77	0.81	0.81	**0.86**
missing data 60%						
ACC	0.72	0.73	0.73	0.73	0.72	**0.76**
AUC	0.80	0.79	0.79	0.82	0.80	**0.87**
F1	0.77	0.77	0.77	0.77	0.75	**0.80**
AP	0.78	0.75	0.77	0.80	0.79	**0.85**
missing data 70%						
ACC	0.72	0.72	0.72	0.72	0.71	**0.76**
AUC	0.79	0.78	0.78	0.80	0.79	**0.86**
F1	0.76	0.76	0.77	0.77	0.74	**0.79**
AP	0.76	0.74	0.75	0.78	0.77	**0.85**
missing data 80%						
ACC	0.71	0.72	0.71	0.71	0.71	**0.75**
AUC	0.78	0.77	0.76	0.79	0.78	**0.84**
F1	0.76	0.76	0.76	0.76	0.75	**0.78**
AP	0.75	0.73	0.72	0.77	0.75	**0.83**

Area 2 (10,227 nodes)						
	GCN	**ChebGCN**	**SAGEGCN**	**GATGCN**	**TAGCN**	**ours**
missing data 5%						
ACC	0.76	0.77	0.75	0.77	0.76	**0.79**
AUC	0.87	0.85	0.87	0.89	0.89	**0.92**

Area 2 (10,227 nodes)						
	GCN	**ChebGCN**	**SAGEGCN**	**GATGCN**	**TAGCN**	**ours**
F1	0.80	0.81	0.80	0.81	0.81	**0.82**
AP	0.85	0.82	0.85	0.87	0.88	**0.91**
missing data 10%						
ACC	0.76	0.77	0.76	0.76	0.76	**0.79**
AUC	0.86	0.84	0.86	0.88	0.88	**0.92**
F1	0.80	0.81	0.80	0.80	0.80	**0.82**
AP	0.84	0.81	0.84	0.86	0.87	**0.91**
missing data 20%						
ACC	0.75	0.76	0.75	0.75	0.75	**0.78**
AUC	0.85	0.83	0.84	0.87	0.87	**0.91**
F1	0.80	0.80	0.79	0.79	0.79	**0.82**
AP	0.84	0.79	0.83	0.85	0.85	**0.90**
missing data 30%						
ACC	0.75	0.75	0.74	0.75	0.75	**0.78**
AUC	0.84	0.83	0.83	0.85	0.86	**0.90**
F1	0.79	0.79	0.79	0.79	0.79	**0.82**
AP	0.82	0.79	0.82	0.83	0.84	**0.89**
missing data 40%						
ACC	0.75	0.75	0.74	0.75	0.74	**0.78**
AUC	0.84	0.82	0.82	0.85	0.84	**0.89**
F1	0.79	0.79	0.78	0.79	0.78	**0.81**
AP	0.82	0.78	0.80	0.83	0.83	**0.88**
missing data 50%						
ACC	0.74	0.74	0.73	0.73	0.73	**0.78**
AUC	0.83	0.81	0.81	0.84	0.83	**0.88**
F1	0.78	0.78	0.78	0.78	0.77	**0.81**

Area 2 (10,227 nodes)						
	GCN	**ChebGCN**	**SAGEGCN**	**GATGCN**	**TAGCN**	**ours**
AP	0.81	0.78	**0.88**	0.82	0.82	**0.88**
missing data 60%						
ACC	0.74	0.74	0.73	0.73	0.73	**0.77**
AUC	0.82	0.81	0.80	0.82	0.81	**0.87**
F1	0.78	0.78	0.78	0.77	0.77	**0.80**
AP	0.80	0.78	0.78	0.81	0.80	**0.86**
missing data 70%						
ACC	0.72	0.73	0.73	0.73	0.72	**0.76**
AUC	0.80	0.80	0.80	0.81	0.81	**0.86**
F1	0.77	0.77	0.77	0.77	0.76	**0.80**
AP	0.78	0.77	0.76	0.79	0.79	**0.85**
missing data 80%						
ACC	0.71	0.72	0.71	0.72	0.72	**0.76**
AUC	0.79	0.79	0.77	0.79	0.79	**0.84**
F1	0.76	0.76	0.76	0.76	0.76	**0.79**
AP	0.76	0.75	0.74	0.77	0.76	**0.83**

Area 3 (1,059 nodes)						
	GCN	**ChebGCN**	**SAGEGCN**	**GATGCN**	**TAGCN**	**ours**
missing data 5%						
ACC	0.70	0.70	**0.72**	**0.72**	0.71	0.71
AUC	0.79	0.76	0.81	**0.86**	0.83	**0.86**
F1	0.76	0.76	**0.78**	0.77	0.77	0.76
AP	0.80	0.75	0.82	**0.86**	0.83	**0.86**
missing data 10%						
ACC	**0.72**	**0.72**	**0.72**	0.71	0.70	**0.72**

Area 3 (1,059 nodes)						
	GCN	**ChebGCN**	**SAGEGCN**	**GATGCN**	**TAGCN**	**ours**
AUC	0.81	0.77	0.81	**0.84**	0.82	**0.84**
F1	**0.78**	0.77	0.77	0.76	0.76	0.77
AP	0.81	0.76	0.81	**0.85**	0.81	**0.85**
missing data 20%						
ACC	0.71	0.72	0.71	0.71	0.70	**0.72**
AUC	0.83	0.77	0.80	**0.85**	0.81	**0.85**
F1	0.77	0.78	0.76	0.76	0.76	**0.77**
AP	0.82	0.75	0.80	**0.85**	0.81	0.83
missing data 30%						
ACC	0.70	0.71	**0.72**	0.71	0.70	**0.72**
AUC	0.81	0.78	0.79	0.82	0.80	**0.82**
F1	0.76	0.76	0.76	**0.77**	0.75	**0.77**
AP	0.80	0.76	0.79	**0.82**	0.79	**0.82**
missing data 40%						
ACC	0.69	0.69	**0.71**	0.69	0.69	**0.71**
AUC	0.80	0.77	0.78	0.80	0.79	**0.81**
F1	**0.76**	0.75	0.75	0.75	0.73	**0.76**
AP	0.79	0.74	0.77	0.79	0.78	**0.81**
missing data 50%						
ACC	0.68	0.69	**0.71**	0.69	0.69	**0.71**
AUC	**0.80**	0.77	0.78	**0.80**	0.78	**0.80**
F1	0.75	0.75	0.75	0.75	0.73	**0.76**
AP	0.79	0.75	0.78	**0.80**	0.77	**0.80**
missing data 60%						
ACC	0.68	0.68	0.68	0.68	**0.69**	**0.69**
AUC	0.78	0.76	0.76	0.79	0.79	**0.80**

Area 3 (1,059 nodes)						
	GCN	**ChebGCN**	**SAGEGCN**	**GATGCN**	**TAGCN**	**ours**
F1	**0.75**	0.74	0.73	0.75	0.74	**0.75**
AP	0.78	0.75	0.75	0.78	0.77	**0.80**
missing data 70%						
ACC	0.67	0.67	0.67	0.68	0.68	**0.69**
AUC	0.76	0.75	0.75	0.76	0.75	**0.77**
F1	0.74	0.73	0.73	0.74	0.73	**0.75**
AP	0.76	0.73	0.74	0.76	0.74	**0.78**
missing data 80%						
ACC	0.67	0.66	0.66	0.66	0.65	**0.68**
AUC	0.76	0.73	0.73	0.74	0.71	**0.77**
F1	**0.74**	0.73	0.72	0.73	0.71	**0.74**
AP	0.76	0.70	0.72	0.74	0.71	**0.77**

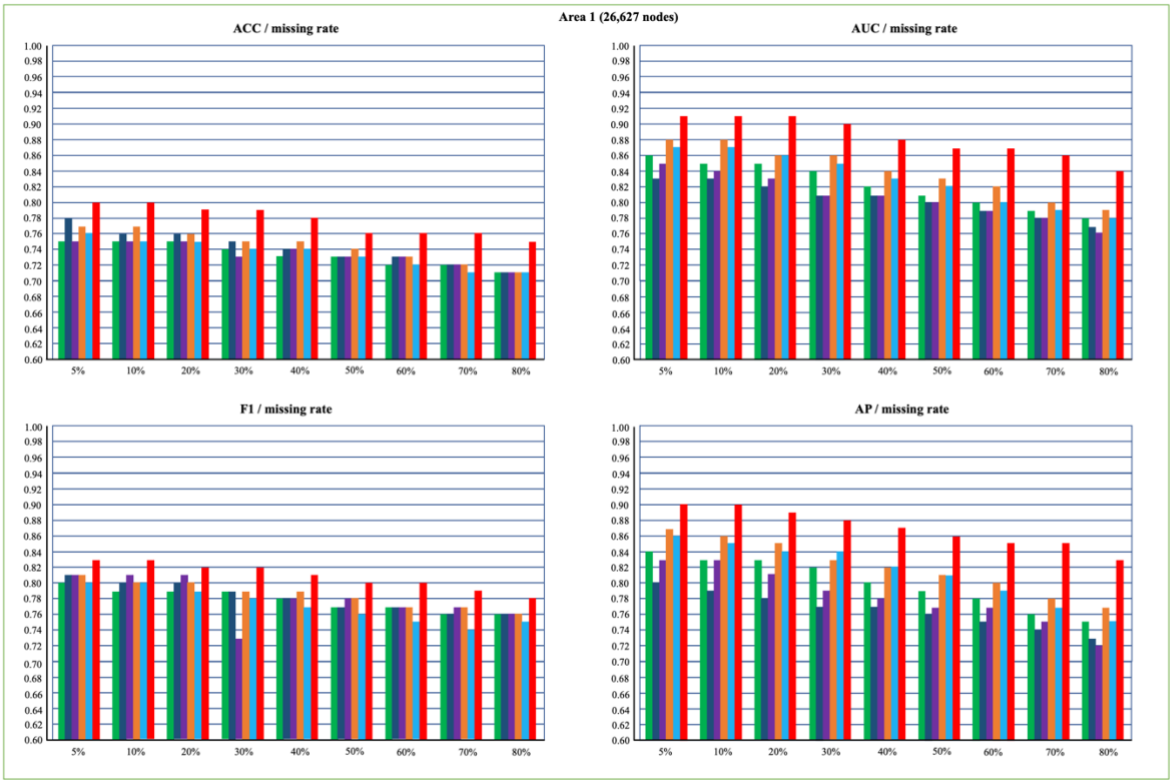

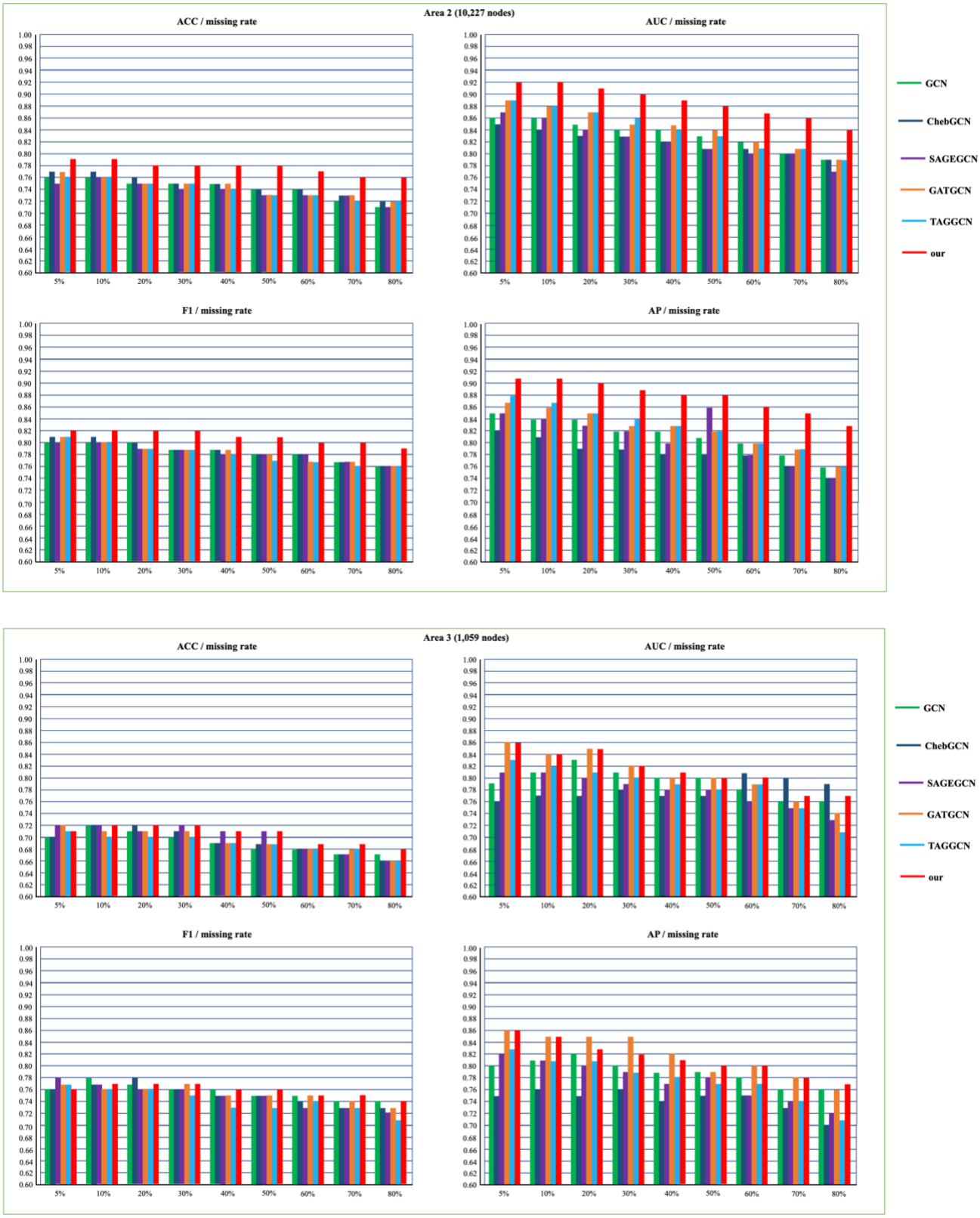

Figure 6-6 Completion experiment results under different missing conditions

6.4 Discussion on GCN-based UU topology information completion model (Objective 4)

6.4.1 Comparison of GATGCN and proposed model

The proposed UUTC model was inspired by the GATGCN model, and both the models used the GCN fusion GAT framework. To make the GATGCN and UUTC models comparable, both models used the same feature extraction structure, self-attention mechanism, and activation function. The main difference between the two is that the UUTC model adds SEM based on prior knowledge of the UU field to improve the data-expression ability of the input graph under the condition of limited attribute characteristics. From the perspective of the experimental data, the UUTC model, after adding the SEM module, obtains better UU topology-completion capabilities, and the completion accuracy is improved to varying degrees, as shown in Figure 6-7. It is worth noting that in the Group 3 experiment, at some missing rates (20%, 30%, and 40%), GATGCN had better completion accuracy, which may be affected by the amount of input data. During the training process, the SEM mapping of attribute features caused a decrease in model accuracy. This leads to an unstable performance of the UUTC model when the observed sample size is small, but the UUTC model can achieve the highest accuracy in the rest of the cases. Overall, the proposed model significantly outperformed other models in most cases.

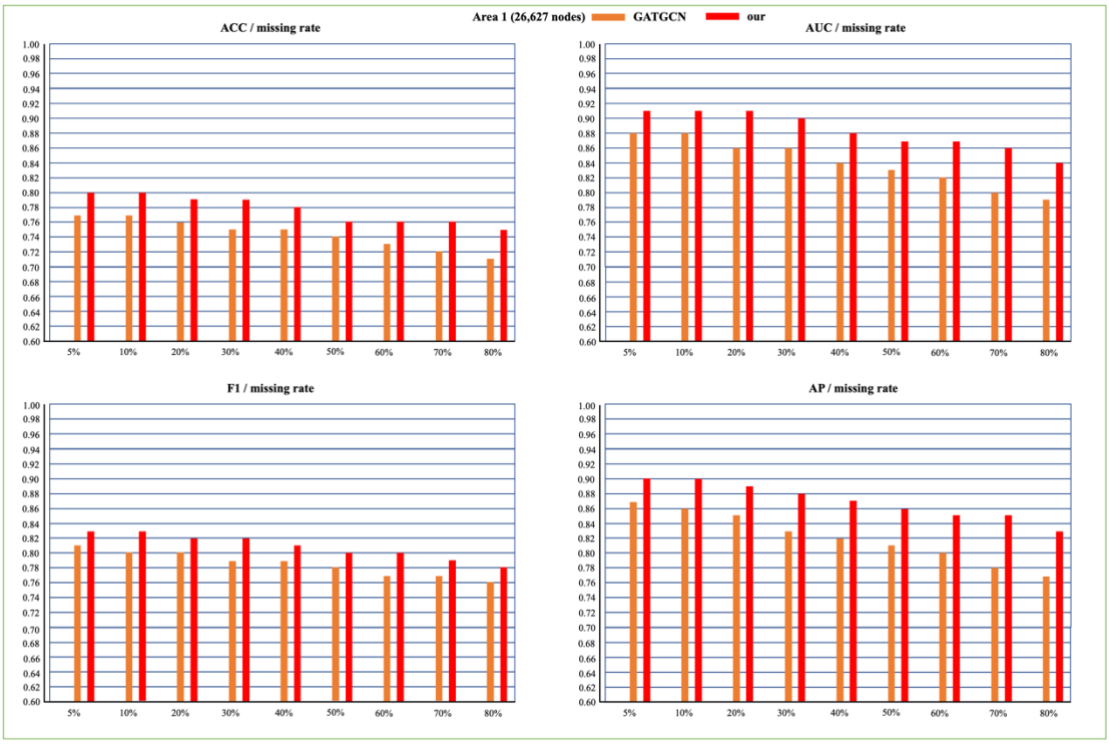
Area 1 (26,627 nodes)
GATGCN
our
ACC / missing rate
AUC / missing rate
F1 / missing rate
AP / missing rate
1.00 0.98 0.96 0.94 0.92 0.90 0.88 0.86 0.84 0.82 0.80 0.78 0.76 0.74 0.72 0.70 0.68 0.66 0.64 0.62 0.60
5% 10% 20% 30% 40% 50% 60% 70% 80%

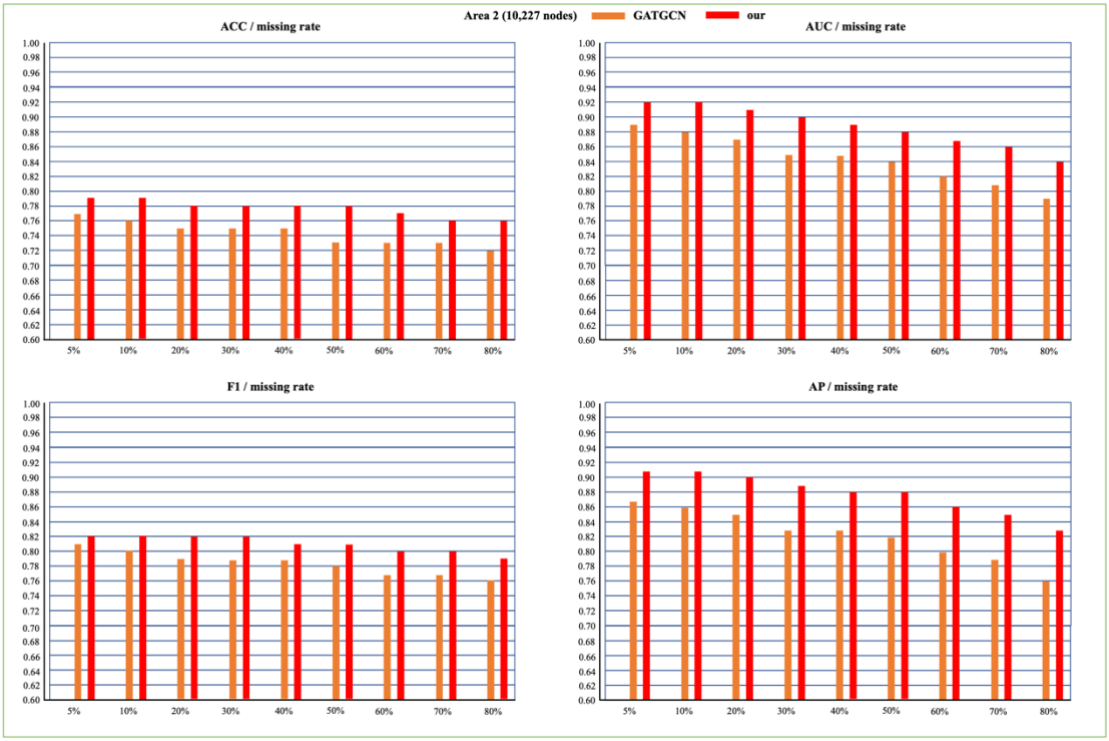
Area 2 (10,227 nodes)
GATGCN
our
ACC / missing rate
AUC / missing rate
F1 / missing rate
AP / missing rate
1.00 0.98 0.96 0.94 0.92 0.90 0.88 0.86 0.84 0.82 0.80 0.78 0.76 0.74 0.72 0.70 0.68 0.66 0.64 0.62 0.60
5% 10% 20% 30% 40% 50% 60% 70% 80%

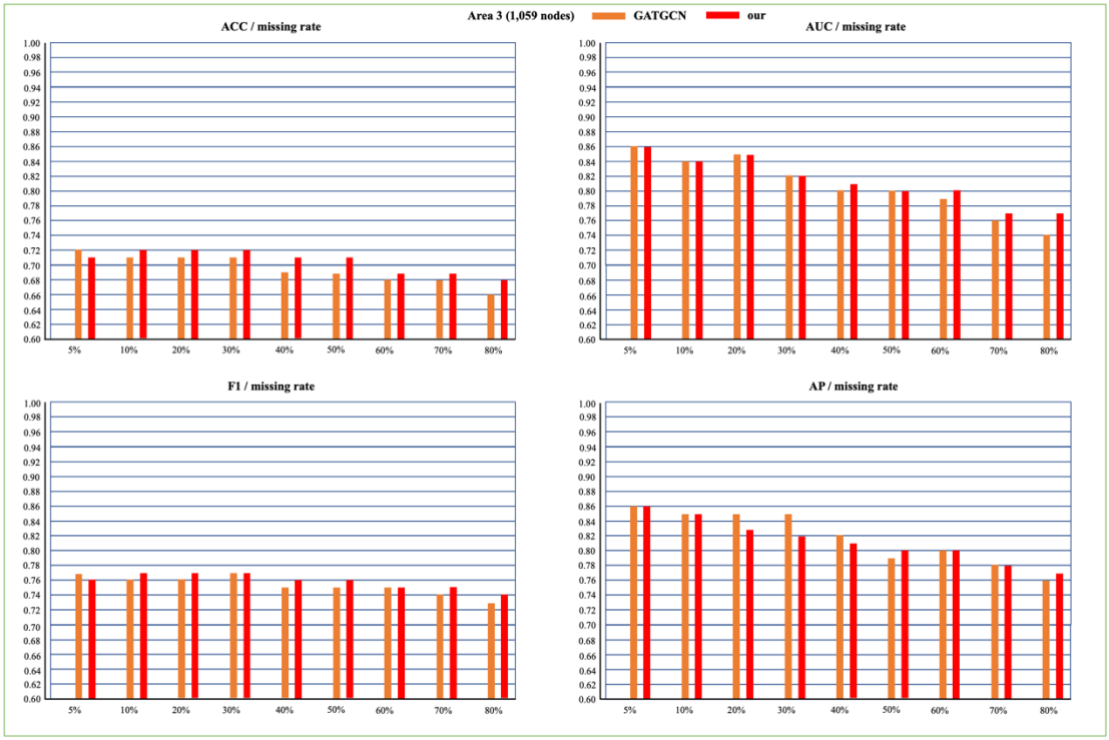

Figure 6-7 Comparison of GATGCN and proposed model

6.4.2 Incorrect predictions

The findings presented in Section 6.3, comprising three sets of experimental data, demonstrate that the proposed UUTC model achieves a commendable average accuracy of up to 85.33% in completing the network topology. Although these outcomes are promising, they also underscore the untapped potential of enhancing the precision of topological relationship predictions among UU nodes. To gain deeper insights into the underlying causes of inaccuracies in the UUTC model predictions, this section strategically identifies two instances of judgement errors from the experiments. An in-depth analysis of these cases was conducted.

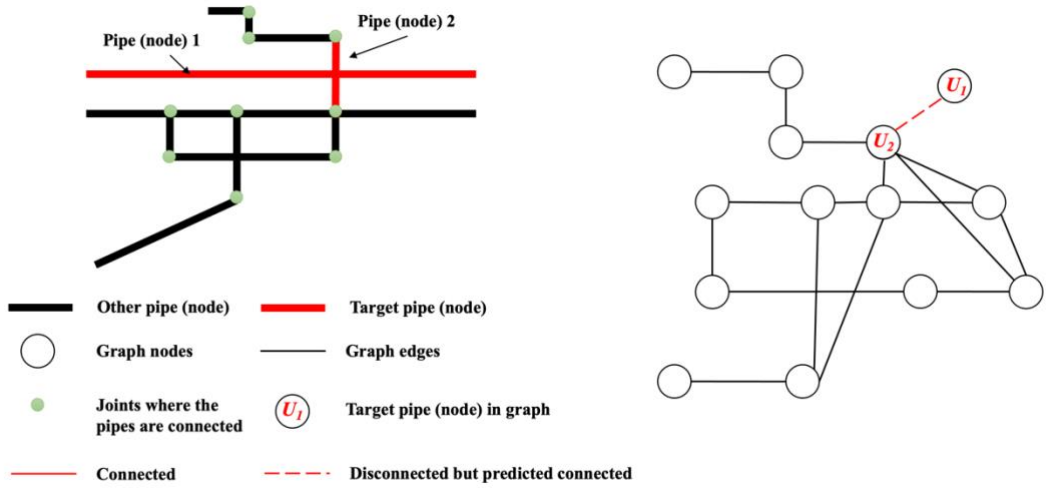

Figure 6-8 Incorrect predictions Position 1

As shown in Figure 6-8, the UUTC model determines the existence of a topological link between the two pipelines, whereas the empirical data contradict this prediction by revealing their non-connectedness. Several underlying factors may account for this discrepancy: 1) network complexity. The core principle underlying the utilisation of GCN for topological relationship completion is to summarise and evaluate the distribution of topological configurations within a pipe network. Throughout this process, as the complexity of the UU network escalates, certain patterns may emerge at a higher frequency than others. This discrepancy in pattern occurrence could induce a bias within the model's learning, potentially leading to an overemphasis on specific types of topological connection patterns, culminating in misjudgements. 2) Temporal information deficiency: As highlighted above, Conventional GCN models predominantly operate on a static graph structure and consequently neglect the dynamic evolution of temporal information. Given the intricate nature of underground pipe networks, the establishment and disruption of connections can be influenced by temporal factors and other dynamic variables. Disregarding this temporal context can result in inaccurate connection forecasts. 3) Edge-weight considerations. While the connection relationships of the UU network are abstracted into undirected edges, the intrinsic significance of these edges and their potential impact on the topological relationship inference should be considered. Neglecting this facet may contribute to

misaligned judgements regarding the topological connections. These considerations underscore the multifaceted nature of the observed instances of misjudgement and emphasise the need for comprehensive enhancements in the UUTC model. Addressing these limitations, particularly by incorporating temporal dynamics, accounting for edge weights, and refining model training on complex networks, may contribute to refining the accuracy of topological relationship predictions within the UU domain.

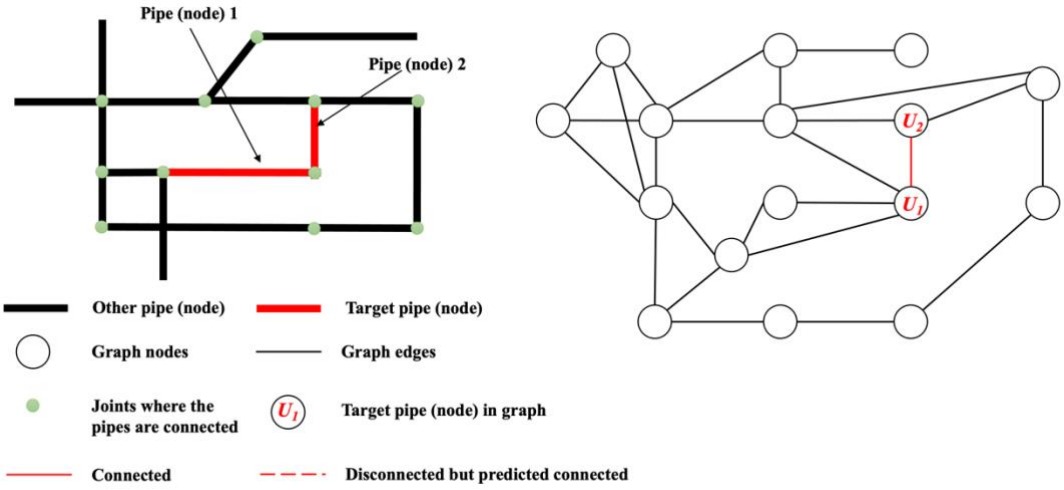

Figure 6-9 Incorrect predictions Position 2

As shown in Figure 6-9, the UUTC model prediction indicates that no topological linkage exists between two specific pipes; however, empirical evidence confirms the presence of such a connection. The following factors potentially underlie this misjudgement: 1) Spatial information deficiency. The approach in this study involves integrating the original linear pipeline structure into graph nodes endowed with attribute information. However, this abstraction results in the loss of intricate spatial relationships at both ends of the pipeline. This spatial information gap is a key contributor to observed misclassifications. 2) Feature gaps. Underground-pipeline network data may encompass critical attributes that must be accurately extracted or adequately represented. Consequently, the model can be used to effectively discern the interconnections between the pipelines. To widen the model's applicability, this thesis focused solely on the four most prevalent attributes for decision making, potentially rendering the model insufficiently equipped to discern connections between pipelines

that are genuinely linked within certain contextual scenarios.

Furthermore, potential data inaccuracies, such as erroneous connection markers, flawed measurement values, or data entry discrepancies, could also contribute to the aforementioned judgement errors. The data entry process for the original database entails meticulous and repetitive work, susceptible to the influence of uncontrollable factors that may introduce inaccuracies into the UU network data. These inaccuracies might become part of the learning process for the GCN models during training, leading to erroneous connection predictions.

6.5 Chapter summary

A UU pipeline network is one of the most important infrastructures for guaranteeing the basic functions of a city. However, for long-term reasons, the lack of a UU topology relationship often requires expensive manual inspection methods. To solve this problem, this study proposes a deep-learning model based on a GCN by abstracting UU pipe network information into graph nodes and attributes to use the observed data to complete missing topological relationships. The experimental results show that the proposed model can effectively complete the UU topological relations (*AP* of 85.33%) for different proportions of missing topological relations. This study explored a new UU data-completion method. The model proposed in this study effectively improves the accuracy of the data-driven UU topological relationship completion method. The proposed UUTC model potentially provides a low-cost decision-making tool for stakeholders in UU facility management.

Chapter 7 : Discussions

7.1 Knowledge area in UUs 3D reconstruction

Accurate mapping and modelling of UUs are critical for urban planning, construction, and maintenance, helping to avoid costly and dangerous mistakes (Underground-Pipeline Committee of the China Planning Association, 2020; Pipeline and Hazardous Materials Safety Administration, 2021; Tanoli et al., 2019). Historically, the field has evolved from rudimentary manual detection methods and 2D records to sophisticated 3D reconstruction technologies, driven by the need for precision, safety, and efficiency. Initially, UU 3D reconstruction relied on physical records and manual probing, which were often inaccurate and incomplete (University of Birmingham et al., 2012; Wang & Yin, 2022b). The advent of geophysical surveying methods in the mid-20th century marked a significant advancement, offering non-invasive methods to detect subsurface objects. The last two decades have seen rapid advancements in 3D reconstruction techniques, driven by improvements in sensor technology, data processing algorithms, and computational power. Techniques such as laser scanning (Bosché et al., 2015), photogrammetry (Javadnejad et al., 2017), and the integration of deep learning (Zong et al., 2019; Jaufer et al., 2021) have become crucial for creating detailed 3D models of underground infrastructure. The development history of the 3D reconstruction of UUs reflects a field that has continually evolved to meet the demands of urban development and infrastructure management. From basic manual methods to advanced digital technologies, progress in this field has significantly reduced the risks and improved the efficiency of construction and maintenance activities.

However, although new technologies have improved the efficiency of UU 3D reconstruction, they have also created new problems. Through a literature review of existing research, this thesis found the following three key problems that affect the 3D reconstruction effect of UU at different life-cycle stages.

1) Environmental noise problem in GPR-based non-destructive UU 3D reconstruction. The environmental noise problem in the GPR-based non-destructive

3D reconstruction of UUs (scenarios where existing utilities are covered by soil layers) is a critical issue that affects the precision and reliability of the reconstruction process (Zhang et al., 2016; Šarlah et al., 2020). GPR serves as a cornerstone technology in the field of UU 3D reconstruction, owing to its ability to penetrate subsurface layers and detect buried objects. Despite its widespread use, GPR encounters challenges stemming from various sources of environmental noise. These include high-voltage electricity, rock mass, and complex soil conditions (Lei et al., 2019; Singh et al., 2013; Adouane et al., 2021), which can obscure important features and degrade the quality of reconstructed 3D models. Addressing these noise-related issues is paramount for improving the effectiveness and precision of GPR-based reconstruction, thus enabling better urban planning, construction, and maintenance practices.

2) Low-light illumination problem in image-based exposed UU 3D reconstruction. Owing to tight construction schedules or requirements to avoid social impacts (e.g. traffic congestion (Broere et al., 2016)), it is a commonly performed UU 3D reconstruction under low-light conditions (Nguyen et al., 2014a; Nguyen et al., 2014b). The low-light illumination problem presents a significant obstacle in image-based exposed UU 3D reconstruction (such as new installation, maintenance, and repair scenarios), particularly in scenarios where lighting conditions are suboptimal or insufficient. Numerous studies have shown that lighting conditions significantly affect the quality of image-based 3D reconstructions, such as Bruno et al. (2021), Kanellakis et al. (2019), and Tang et al. (2019). Low-light conditions, such as those encountered during night-time operations or in poorly lit environments, pose challenges in obtaining high-quality images with sufficient contrast and detail. Overcoming the low-light illumination problem requires innovative techniques and technologies that enhance image clarity, reduce noise, and improve the overall quality of the reconstructed 3D models. Effective solutions in this area are essential for advancing UU management practices and for ensuring the safety and efficiency of infrastructure development projects.

3) Missing information in the UU topology structure reconstruction. For a long time, UU information has been recorded on paper files (Pickering et al., 1993; Wang et al., 2019), and it is not uncommon for records to be lost because of incomplete records or recording errors due to the passage of time (Li et al., 2015; Al-Bayati et al., 2019; Beck et al., 2009). The absence of utility data, particularly topological information, poses a significant obstacle to the comprehensive reconstruction and effective management of UUs. The lack of this information hampers the decision-making processes related to infrastructure planning, maintenance, and emergency response.

To address the above issues, this thesis aims to improve the data-collection process and accuracy of the data used in the 3D reconstruction of the as-built UU. By obtaining better data and more accurate 3D reconstructions, the management decision making of UU operation maintenance rehabilitation and renewal can be potentially improved. To achieve the aim of having more accurate and reliable 3D reconstructions, this thesis proposed a unified framework to solve the 3D reconstruction problem of UU in all stages of its life-cycle, which include the following three aspects.

1) Develop a novel GPR-based as-built UU-localised deep-learning model for non-destructive scenarios. This thesis developed a novel GPR-based as-built UU localisation deep-learning model, resulting in the creation of the EUUL model, validated through three experiments in real-world settings. The findings indicate that the EUUL model's precision reached 97.01%, operating speed was 125 fps, and precision was 96.72%, even in noisy environments, surpassing existing models in terms of precision, operating speed, and robustness. The architecture of the EUUL model integrates a 'key point-regression' mode and an innovative anchor-free structure, supported by a lightweight CSPDarknet53 backbone, and enhanced by the ECA module. This configuration significantly improves precision and performance, while also increasing adaptability across diverse soil conditions. The anchor-free structure simplifies the model, reduces computational demands, and enhances the detection

accuracy of underground utilities in noisy environments. By eliminating the constraints of predefined anchor boxes, the anchor-free structure allows for direct localization of keypoints, enabling the model to dynamically adjust to varying object scales and densities in real-time, thus improving detection reliability. These improvements make the EUUL model highly effective for accurate, non-destructive location detection in various engineering applications, promising faster and more reliable results. The EUUL model incorporates an anchor-free structure and a lightweight CSPDarknet53 backbone which simplifies the computational demands. This structure eliminates the need for computationally expensive anchor boxes, thereby reducing the model's overall computational complexity. The key point-regression mode enables efficient feature extraction and localization directly from the raw data, further streamlining processing. Due to its lightweight architecture and the dynamic nature of the anchor-free approach, the EUUL model scales well across different scenarios and soil types. Its ability to operate effectively in noisy environments and maintain high precision and speed (125 fps) showcases its capability to handle large-scale deployments and real-time applications in various engineering settings.

2) Develop a novel unsupervised image-based 3D reconstruction model for the low-light 3D reconstruction of as-built UUs for exposed scenarios. In this study, an unsupervised deep-learning model, ZDE3D, was developed to enhance the low-light images in UU 3D reconstruction. The ZDE3D model yielded promising results in terms of improving the sparse reconstruction point-cloud quantity by an average of 13.19% and achieving an average reconstruction accuracy of 98.58%. The unsupervised nature of the deep-learning method eliminates the need for pairs of training data, and the proposed five loss functions effectively enhance low-light UU images, outperforming traditional adjustment methods and existing deep-learning models in terms of UU 3D reconstruction enhancement performance. The unsupervised nature of the ZDE3D model reduces the computational burden typically

associated with supervised learning, as it does not require paired training data. The use of five specialized loss functions to enhance low-light images ensures that the model remains computationally efficient while focusing on feature enhancement and noise reduction, crucial for sparse reconstruction in low-light conditions. The ZDE3D model demonstrates an ability to improve the quantity of reconstruction point clouds by an average of 13.19% and achieve a high reconstruction accuracy of 98.58%. This indicates that the model can be effectively scaled to handle larger datasets and more complex 3D reconstruction tasks, particularly beneficial in real-world engineering applications where lighting conditions can vary significantly.

3) Development of a novel GCN-based topology-completion model for as-built UUs. This thesis aimed to develop a GCN-based topology-completion model for as-built UUs. The UUTC model outperformed the baseline models with an average completion accuracy of 85.33% across various missing topology rates. The proposed SEM proved effective in enhancing prediction accuracy by identifying nodes with shared attributes, which facilitated precise predictions of the UU network's interconnectedness. The UUTC model utilizes a Graph Convolutional Network (GCN) which is particularly suited for handling relational data like network topologies. The model's complexity is moderated by the efficient processing of GCNs, which leverage the inherent sparsity of graph data, reducing the computational load compared to fully connected network approaches. The SEM (Shared-attributes Enhancement Module) within the UUTC model enhances its scalability by identifying nodes with shared attributes, which helps in accurate prediction across different sizes and complexities of UU networks. This ability ensures that the model can be scaled up to handle larger and more complex network topologies with varying degrees of missing data, proving its effectiveness in expansive urban planning and infrastructure management.

7.2 Theoretical contribution to the knowledge areas

The novelty of the proposed unified framework lies in its comprehensive and integrated approach to the 3D reconstruction of UUs, which addresses the limitations

and challenges of existing methods while leveraging emerging technologies and best practices. It represents a paradigm shift towards a more collaborative, data-driven, and sustainable approach to managing UUs in urban environments.

For a long time, researchers have been pursuing more accurate 3D reconstruction of UU. For example, in 1988, Caldecott proposed a combined system using an impulse radar to map buried underground pipelines (Caldecott et al., 1988). In 2012, the UK conducted a project called MTU, which involved relatively comprehensive 3D reconstruction research on existing UUs of various materials and functions (University of Birmingham et al., 2012). In 2017, the Singapore Land Authority, in collaboration with the Singapore-ETH Centre, launched a system called Imagining a digitally enabled future (Yan et al., 2021) for digital twins of UUs to complement the 3D maps of the country and facilitate integrated planning and development.

However, these existing studies have not established a unified reconstruction framework to cover the 3D reconstruction demands for the entire UU life-cycle. Conventional frameworks for UU 3D reconstruction have distinct limitations. First, these frameworks were unidimensional. Previous UU 3D reconstruction frameworks emphasised the geometric restoration of existing utilities, overlooking the incorporation of significant semantic data attainable during the new installation and maintenance phase, as well as the vital reconstruction of topological relationships crucial for expressing the functional dynamics of the utility network. For example, Bilal, Van, and Feng only considered data collection from the existing UU and ignored the topology information reconstruction crucial for the functional expression of the UU network (Bilal et al., 2018; Van et al., 2018; Feng et al., 2021a). Second, the conventional UU 3D reconstruction frameworks are inaccurate. The bulk of the data employed in traditional UU 3D reconstruction predominantly stems from existing utilities, thereby neglecting the new installation phase, which provides much useful information. Multiple studies (Bureau of Transportation Statistics, 2016; Van et al., 2019; Wang et al., 2022b; Yan et al., 2019) have shown that exposed scenarios (e.g. new installation stage) are the best opportunity to conduct UU 3D reconstruction,

particularly semantic information. Consequently, this shortfall engenders a pervasive issue of suboptimal accuracy in the reconstruction models, as the opportune and optimal phase for achieving precision is inadequately noticed. Third, conventional frameworks for UU 3D reconstruction tend to incur substantial resource demand. Whether involving geometric or topological reconstruction, traditional frameworks heavily rely on field-based detections, such as GPR detection (De Coster et al., 2019; Özkaya et al., 2021). For example, Cazzaniga et al. (2013) and Dou et al. (2020) showed that performing a survey on the UU reconstruction of a large area is an expensive solution. This reliance necessitates significant investment in human resources and equipment costs, particularly when confronted with intricate and extensive urban infrastructure configurations. When faced with more complex and larger city-level situations, the cost disadvantage of traditional 3D reconstruction frameworks becomes more prominent.

The proposed framework considers the entire life-cycle of UU projects, including the new installation, existing, maintenance, and repair stages, as well as the topology reconstruction stage. The unified framework for UU 3D reconstruction presented in this thesis offers distinct advantages over conventional frameworks. 1) User-friendly: The unified framework incorporates a highly automated 3D information collection method tailored to existing utilities and those associated with new construction projects. For example, the EUUL model eliminates the dependence on experts by solidifying domain knowledge into deep-learning models. This process can be realised using a readily available consumer-level smartphone, particularly in new construction settings. For example, in an image-based 3D reconstruction process performed in stages, such as a new installation, all process operations are based on an ordinary smartphone terminal. In addition, the topology reconstruction process employs a data-driven approach, which significantly enhances the automation level and overall efficiency of the UU 3D reconstruction pipeline. 2) Enhanced precision: Many studies have reported a reconstruction accuracy of over 90% (Hou et al., 2021a; Xiao et al., 2021; Lei et al., 2019). However, the framework proposed in this thesis, based on dealing with data noise, also incorporates the full life-cycle of the UU 3D

reconstruction process to obtain better reconstruction results. The average localisation precision for the invisible existing UU reached 97.01%, and the reconstruction precision for the directly visible exposed UU reached 98.58%. 3) Transferability: The proposed unified framework exhibits notable versatility and can be extended beyond UU 3D reconstruction scenarios. It can be readily applied to diverse contexts, such as the 3D reconstruction of rebar networks within extensive structural health monitoring, large building foundations, bridges, and tunnels. It can also be applied to fields outside the construction industry, such as the abyssal ocean and archaeological exploration.

Based on these contributions, specific innovations are evidenced by the following three aspects.

7.2.1 Novel model for automatic UU localisation based on GPR data

To automatically reconstruct invisible UUs under non-destructive scenarios, this study proposed a deep-learning model (EUUL) to interpret UU coordinates from B-scan images.

In previous research, the GPR-based UU localisation problem was decomposed into two sub-problems: box detection and hyperbola fitting for GPR B-scan images (Figure 2-2). For instance, in Hou et al. (2021a), Xiao et al. (2021), and Lei et al. (2019), the area containing UU features was first determined in the box detection stage. Subsequently, various fitting algorithms were used to determine the hyperbola representing the UU position and finally use it. As a result, the fixed points are output. However, the ‘box-fitting’ mode solves the problem solely from the local optimal solutions of the sub-problems, rather than from the global optimal solution. This step-by-step solution results in greater error accumulation, which affects the UU localisation precision (Alhnaity et al., 2021; Wu et al., 2020).

Unlike existing deep-learning methods that handle each step individually (Xie et al., 2021; Singh et al., 2013), the EUUL model was designed to comprehend the entire process, from raw GPR B-scan images to the final interpretation of UU coordinates. Numerous studies have reported the importance of the ‘end-to-end’ mode for deep learning (Wu et al., 2018; Geng et al., 2023; Chen et al., 2017). This thesis contributes

by solving the problem ‘end-to-end’ to maximise the advantage of machine-learning models in UU localisation (Wang et al., 2022b; Oguntoye et al., 2023). The term ‘end-to-end’ in this context signifies that the proposed EUUL model tackles the entire problem of UU localisation in a unified manner without breaking it down into separate sub-problems (box detection and hyperbola fitting (Lei et al., 2019; Harkart et al., 2019; Hou et al., 2021b) in previous research. This holistic approach eliminates error accumulation during the steps, providing a direct comprehensive mapping from the GPR images to the UU localisation coordinates.

To achieve end-to-end learning, the EUUL model proposed a novel ‘key point-regression’ mode, indicating a method that identifies crucial points in the GPR data and directly regresses them to obtain UU coordinates. In this ‘key point-regression’ mode, the global optimisation results were obtained rather than the superposition of two local optimisations (results of box and fitting, separately). Under the new ‘key point-regression’ end-to-end framework, the EUUL model yielded a larger parameter optimisation space and a more convenient operation process. Simultaneously, improving the feature extraction architecture (CSPDarknet53) and channel attention mechanism (ECA module) increases the localisation speed and robustness to environmental noise.

The experimental findings demonstrate that the proposed methodology exhibits superior performance compared with the prevailing models in terms of localisation precision (97.01%) and inference speed (125 frames per second) on the platform (NVIDIA RTX 3090 GPU). The precision result obtained in this thesis is significantly improved compared to previous studies; for example, Jaufer et al. (2021) (89.8%), Xiao et al. (2021) (89%), and Lei et al. (2019) (95.66%).

7.2.2 Novel unsupervised model for low-light automatic UU image-based reconstruction enhancement

To improve the performance of image-based 3D reconstruction of UU in low-light environments, this study proposes a novel unsupervised deep-learning model (ZDE3D).

Previous studies have predominantly employed supervised-learning techniques to improve low-light images, often neglecting the correlation between image enhancement and 3D reconstruction principles. For example, previous studies (Li et al., 2022; Lv et al., 2021) have applied a supervised-learning mode to improve the images captured from low-light scenarios. The specific method involves manually selecting pairs of input and reference data and then inputting them into the deep-learning model for supervised learning. However, methods based on supervised-learning models typically have the following limitations. First, the acquisition of paired training data is a cumbersome task that often requires extensive resources and time (Li et al., 2022; Triantafyllidou et al., 2020; Lv et al., 2021). Second, supervised-learning methods are prone to subjective limitations. Specifically, the process of selecting appropriate reference training data for model training makes the performance of the model heavily dependent on the quality of the data selection (Wei et al., 2018; Lore et al., 2017). Simultaneously, the quality of data selection depended on the subjective experience of the experts who built the model.

This thesis addresses these limitations by proposing a ZDE3D model that seamlessly integrates the principles of image-based 3D reconstruction and domain knowledge specific to UUs, by leveraging an unsupervised learning paradigm. This integration allows the model to optimise the input data at the pixel level, providing an effective solution for enhancing low-light images. By enhancing the low-light image inputs, the originally degraded matching features are revealed, thereby obtaining more key points for the 3D reconstructed point-cloud model. Simultaneously, the enhancement learning mode changed from learning the mapping based on pre-set paired training data to autonomous learning based on the UU scenario features and 3D reconstruction theory.

Field data implementation of the ZDE3D model validated its capabilities, and ablation experiments were performed to verify the contribution of the proposed loss functions. The results demonstrate a remarkable improvement, with an average increase of 13.19% in the quantity of sparse reconstruction point clouds and an 98.58% reconstruction accuracy. Compared with the existing research, the UU 3D reconstruction effect under

low-light conditions has been effectively improved (Kanellakis et al., 2019; Hu et al., 2005). Additionally, ablation experiments were conducted to rigorously assess the contribution of the proposed loss functions, further substantiating the effectiveness and robustness of the ZDE3D model in addressing the challenges associated with low-light image-based 3D reconstruction for UUs.

7.2.3 Novel GCN-based model for the completion of UU topology information

Traditional methods, such as GPR surveys (Tabarro et al., 2017; Sharafat et al., 2021) and manual inspection (Wang et al., 2022b), have long been mainstream for UU topology-completion tasks. However, these methods are costly and require significant labour and equipment resources. Data-driven statistical UU data-completion methods have also been proposed in existing research. Missing data imputation for electric utilities (Sim et al., 2022; Verboven et al., 2007). However, because the UU network topology information is a non-Euclidean space attribute, existing statistical methods are not suitable for topological completion tasks. They can only complete conventional missing attributes such as diameter and material (Bilal et al., 2018; Belghaddar et al., 2021).

Recognising these challenges, the proposed UUTC model introduced a paradigm shift by embracing a deep-learning approach grounded in GCN. This departure from traditional and statistical methods is significant because it transforms the intricate problem of topological relationship completion into a more manageable task of predicting edges within the graph structure. The UUTC model addresses the shortcomings of existing methodologies and pioneers a data-driven approach to UU topological relation completion, thereby filling a critical research gap in this field. Compared with traditional manual inspection methods, the proposed method significantly improves the efficiency of the UU topology reconstruction through a data-driven approach. Thus, the number of complicated on-site investigations can be reduced (Wang et al., 2022b; Costello et al., 2007). Compared with existing statistical methods, such as imputation, the proposed method emphasises the particularity of UU topology attributes and provides promising solutions to such special scenarios.

Topological structures, such as general attributes, can be reconstructed in a data-driven manner (Belghaddar et al., 2021; Hajibabaei et al., 2023).

To further improve the accuracy of the data-driven UUTC model in the topology-completion task, this thesis also proposes an SEM module that utilises domain knowledge. This helps the UUTC model to obtain more high-dimensional information without introducing further input information. This thesis capitalises on domain knowledge, specifically acknowledging the strong correlation between attribute similarities among UU nodes and their connection relationships. By incorporating this additional layer of information, the SEM module acts as a powerful enhancer of the UUTC model, refining predictions and further elevating the model's overall performance. Experiments based on real wastewater databases showed that the proposed UUTC model could effectively identify unknown UU topological relationships, with an average completion accuracy of 85.33%. Compared with existing research, the accuracy of topological completion has exceeded the average accuracy of 61.11% (Belghaddar et al., 2021).

7.3 Potential benefits, implications, and practical applications

7.3.1 Time saving

The use of GPR equipment to collect underground data in the target area to interpret the 3D information of existing utilities is a foundational step for ensuring the smooth progress of the follow-up work of the entire UU project. Traditional manual interpretation methods are time consuming and error prone. The proposed UU 3D reconstruction approach can achieve automatic GPR data interpretation and is more stable than the manual methods. The time required for manual interpretation of a ground-penetrating radar (GPR) B-scan frame can vary widely depending on several factors, such as the complexity of the frame, experience of the interpreter, and study objectives (Zhou et al., 2018; Lei et al., 2019). The industrial normal speed of manual GPR data interpretation is 1 fps (processing one B-scan image frame per second for a length of 0.5 m). The approach proposed in this study can achieve a speed of 125 fps faster than that of the existing mainstream deep-learning-based models YOLOv3 (82

fps) and Faster R-CNN (20 fps).

To illustrate the advantages of this study in terms of time cost more intuitively, the following estimations and comparisons were made based on the real-site experiment results in Section 4.3.3. A real UU network inspection project located in Jiangsu Province, China, as shown in Fig 7-1, is considered as an example to illustrate the time-saving advantages of the proposed approach. The project aims to implement the 3D reconstruction of underground pipelines in the embankment road area on the south side of a river to determine the depth and location information. GPR has been employed to understand the underground comprehensive pipeline situation by coordinating it with other known designs. The project underwent two rounds of testing, and the detailed workloads are listed in Table 7-1.

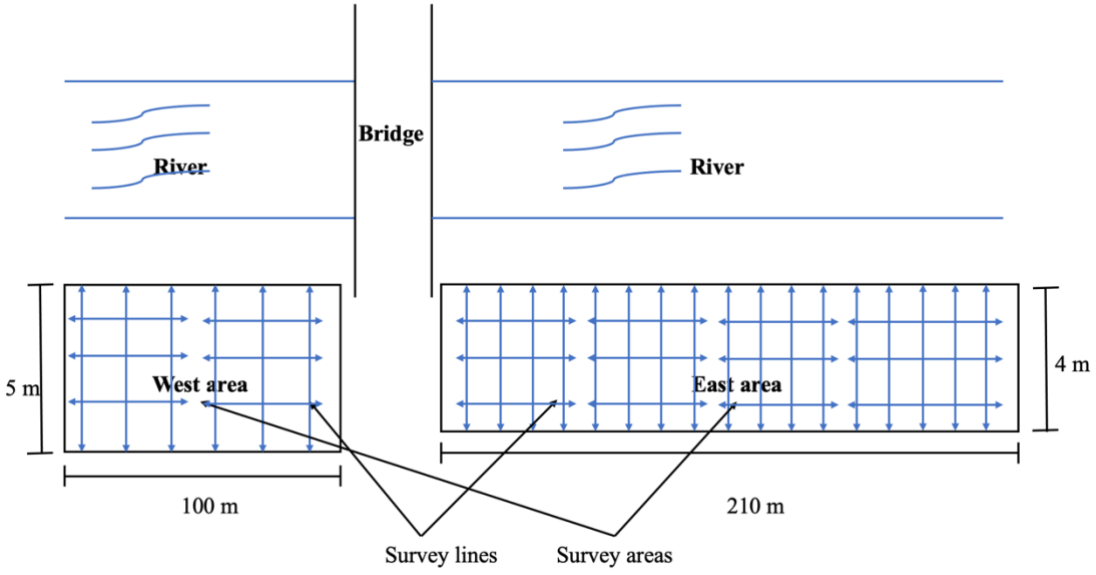

Figure 7-1 UU network inspection project located in China Jiangsu Province

Table 7-1 Workload details of the UU network inspection project in Jiangsu Province. In this table, 'm' means metre

Testing area	GPR frequency	Survey lines amount	Survey lines length	Total Survey line length	Testing personnel
First round test					
West	400 MHz	20	200 m	700 m	4
	900 MHz	6	200 m		
	1600 MHz	14	200 m		
East	900 MHz	20	200 m		
	1600 MHz	10	50 m		
Second round test					
West	100 MHz	20	200 m	900 m	5
	400 MHz	20	200 m		
	900 MHz	6	200 m		
	1600 MHz	14	200 m		
East	100 MHz	10	50 m		
	1600 MHz	10	50 m		

The GPR survey line for the project totals 1,600 m. Table 7-2 illustrates the time cost comparison for project GPR interpretation using different approaches. Under equivalent conditions, manual GPR interpretation, applied in a real project, requires 8,000 s, whereas existing mainstream automated methods, specifically YOLOv3 and Faster R-CNN, require 97.56 s and 400 s, respectively. The approach proposed in this thesis takes only 64 s, which is only 0.8% of the time required by traditional manual methods and is faster than the currently available automated methods. Therefore, the method proposed in this study offers significant time-saving advantages for interpreting the as-built UU 3D information scenarios.

Table 7-2 Time-saving comparison of the existing and proposed approaches. In this table, ‘m’ means metres, ‘min’ means minutes

Categories	**Manual**	**Existing automatic**		**Proposed**
		YOLOv3	Faster R-CNN	**method**
Total length of survey lines (m)	1,600	1,600	1,600	1,600
Length per frame (GPR B-scan data) (m)	0.2	0.2	0.2	0.2
GPR data frame number	8,000	8,000	8,000	8,000
Processing speed (fps)	1	82	20	125
Processing time (seconds)	**8,000**	97.56	400	**64**

The proposed 3D reconstruction approach demonstrated significant time savings in the UU project, as previously shown. However, its potential impact is more pronounced in large-scale projects. In typical infrastructure endeavours covering expansive areas, our method excels at efficiently collecting and interpreting extensive GPR data. In contrast to manual interpretation, which becomes exponentially challenging with increased project size, our automated approach ensures the rapid and reliable acquisition of underground information across the entire project region. The speed and precision enhancements of the proposed approach become particularly crucial as the coverage of underground-pipeline networks extends beyond the scale witnessed in the Jiangsu Province case study. In larger projects, the proposed approach further shortens the data interpretation time by improving the processing speed and reducing the error rates.

7.3.2 Cost saving

Obtaining topological structural information for the UU network in the target area is crucial in various scenarios including project design, daily O&M, and leakage investigation. However, incomplete topological information is common, owing to

factors such as record loss. In typical infrastructure endeavours covering expansive areas, the proposed method efficiently collects and interprets extensive GPR data. The approach proposed in this study can complete the missing topological information of the UU network by leveraging its internal connections and topological information of known part data. Compared with traditional manual inspection methods, the data-driven approach suggested in this study offers a significant cost advantage.

To more intuitively illustrate the cost-saving contribution of this study, estimations were conducted based on real-site experiment results in Section 6.3.1, still using the project from Jiangsu Province as a reference (as mentioned in Section 7.2.2.1). Table 7-4 presents a detailed cost comparison between the traditional method and data-driven approach proposed in this study during the process of reconstructing topological relationships in the target area. The manual cost calculation was based on the Regulations on the Administration of Fees for Engineering Survey and Design issued by the State Planning Commission of China and the Ministry of Construction (2002); the details can be found in Table 7-3. The costs required for the proposed algorithm-based approach primarily include two parts: the existing information collection and algorithm inference (computational resources) which are estimated according to the experimental process discussed in section 4.3.

Table 7-3 Engineering survey and design charging standards (China). The prices in this table are converted from Chinese currency (RMB) into Australian currency (AUD) (State Planning Commission of China and the Ministry of Construction, 2002).

Categories		**Unit**	**Basic price (AUD)**		
UU detection	UUs		Simple	Middle	Difficult
	Cable (electricity and communication, etc.)	km	360	720	1,260
	Metal pipelines		450	900	1,440
	Non-metal pipelines		540	1,080	1,800
	Sewer (with manhole)		270	540	1,080

Categories	Unit	Basic price (AUD)		
Blind detection	m^2	0.2	0.3	0.6

Table 7-4 Cost-saving comparison of the existing and proposed approaches. The costs are expressed in Australian dollars (AUD). In this table, 'm^2' means square metres

Manual inspection approach		Proposed approach	
Target area	1,340 m^2	Target area (m^2)	1,340 m^2
Overall costing equation (including equipment, labour, and experts fee)	0.6 (AUD/ m^2) * Working area (m^2) * 1.22	Existing information collection	200
		Algorithm inference (computation resource)	100
Total cost	980.88 AUD	Total cost	300 AUD

The comparison results show that the proposed approach has a significant cost advantage over the current mainstream manual inspection approach, with a cost of approximately 30% of the latter. Additionally, it is important to note that the cost savings demonstrated in this real project indicate the potential efficiency gains that can be achieved on a larger scale. Owing to the marginal cost-effectiveness of the algorithm, the proposed approach is poised to unlock even greater cost-saving potential in more extensive projects, highlighting its scalability and economic advantages on a broader scale.

7.3.3 Safety enhancement

During construction, the primary safety risks associated with the UU project are closely tied to potential accidental damage to existing utilities (Pipeline and Hazardous Materials Safety Administration, 2021). Traditional construction practices often involve manual inspections, which are prone to human error and may not account for various underground environmental factors. This introduces significant challenges in accurately detecting the 3D spatial information of existing utilities. One specific concern is the accidental damage to high-pressure water pipes, which can lead to burst

accidents. Similarly, the potential damage to oil and gas pipelines poses a more severe threat, with the risk of explosion and fire accidents (Chinese Association of Surveying and Mapping Underground Pipeline Professional Committee, 2023). The complex and unpredictable nature of underground environments increases these risks.

The approach proposed in this study addresses these challenges and contributes to practical solutions in three key methods: First, it eliminates the need for manual inspection, thereby significantly reducing the likelihood of human error that could lead to accidents. By leveraging advanced technologies, the proposed method ensures a more accurate and reliable detection of existing utilities. Second, the implementation of this approach results in fewer instances of striking gas lines. The frequency of such incidents is critical to prevent gas leaks, which can have serious consequences. The improved precision of the proposed method directly translates into a reduction in the number of accidental strikes on gas lines, thus mitigating the potential for hazardous situations. Third, the proposed approach contributes to a reduction in the overall time spent on-site during construction activities. This not only enhances operational efficiency, but also minimises the exposure of construction workers to potential hazards. Less time spent on-site correlates with a decreased risk of serious injuries, thereby promoting a safer working environment for all personnel involved in the construction process.

In summary, the practical contribution of this study lies in its ability to enhance safety during the construction of a UU project by reducing the need for manual inspection, decreasing the frequency of gas line strikes, and minimising the time spent on-site, consequently lowering the risk of serious injuries. The 5.43% improvement in the precision of locating existing utilities is a significant advancement that directly translates into tangible safety benefits for construction workers and helps safeguard against personal and property losses.

7.3.4 Implications and practical applications

This thesis presents a unified practical application framework designed to address critical challenges in the life-cycle management of UUs. This framework not only

streamlines the reconstruction of UU, but also ensures their sustainable management throughout their typical life-cycle, which includes planning and design, construction (new installation), operation (existing UU), maintenance (including repair and upgrade), and decommissioning stages (Soni et al., 2017; University of Birmingham et al., 2012). The proposed framework has practical value in all stages of the UU life-cycle, except for decommissioning. This framework is underpinned by three innovative components: 1) EUUL model for construction (new installation) and operation (existing UU) stage: Utilising GPR B-scan data, the EUUL model incorporates a key point-regression approach, an anchor-free structure, and a channel attention mechanism to significantly enhance localisation precision and processing speed for UU positioning. 2) The zero-reference deep-learning model for low-light image enhancement (ZDE3D) was primarily used in the construction (new installation) stage. Tailored for low-light conditions, ZDE3D improves the 3D reconstruction performance by utilising an unsupervised loss-function design that does not rely on paired or unpaired training datasets. 3) UUTC model for the planning, design, and maintenance stages, The UUTC model employs GCN techniques to accurately complete missing topological data and is essential for the functionality of UU network expression.

7.3.4.1 Contribution towards life-cycle management of UU

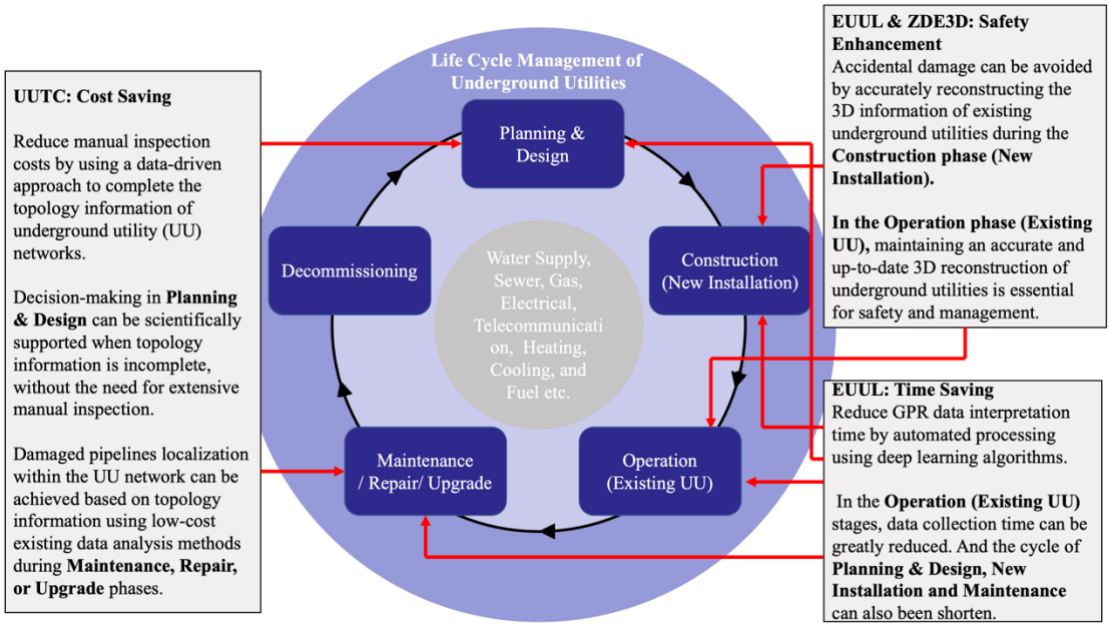

Figure 7-2 Application scenarios of the unified UU 3D reconstruction framework

The application processes involved deploying these models at different stages of the UU project life-cycle, as shown in Figure 7-2:

Planning and Design: During this initial stage, the framework supports the decision-making process by providing a data-driven approach (UUTC) to fill in the incomplete topology information of the UU networks. This approach helps avoid extensive manual inspections and optimises the process for designing underground infrastructure. The planning and design cycle can also be shortened using an automated deep-learning approach (EUUL) to reduce GPR data interpretation time.

Construction (New Installation): In this stage, the application of the framework ensures safety by facilitating the accurate 3D reconstruction of existing UUs. ZDE3D can help obtain the most accurate UU reconstruction, especially when night construction is required owing to tight construction schedules. EUUL can ensure that the accurate 3D information of all existing UU in the construction area is established before the excavation of new utilities. This helps to avoid any accidental damage that might occur during the installation of new utilities. For example, it can serve as an invaluable guide for machinery, mitigate the risk of inadvertent damage to pipelines, and guarantee the safety of construction equipment. The processing time of new installations can also be shortened when the existing UU data-collection time is significantly reduced.

Operation (Existing UU): Once the utilities are in place and operational, the framework emphasises the importance of maintaining an accurate and current 3D reconstruction of UUs (EUUL and ZDE3D). This continuous update is crucial for efficient management and ongoing safety of UU networks.

Maintenance/Repair/Upgrade: At this stage, the framework assists in localising the damaged pipes within the UU network. It utilises topology information and low-cost data-analysis methods (UUTC), which are instrumental during routine maintenance, necessary repairs, or upgrades to utility systems. Damaged pipeline localisation within

a UU network can be achieved based on topology information using low-cost existing data-analysis methods during the maintenance, repair, or upgrade phases. By reducing the GPR data interpretation time, EUUL makes the operation stage more efficient. This allows quicker responses to maintenance, repair, or upgrade needs within the utility network.

Throughout these stages, the framework's integration of innovative technology and methodology represents a shift towards more advanced, efficient, and safer UU management. The practical application framework developed in this thesis streamlines the management, construction, and maintenance of UUs by integrating state-of-the-art technological models and domain knowledge, thereby significantly enhancing efficiency, reducing costs, and improving safety across the entire UU life-cycle.

7.3.4.2 Practical relevance with life-cycle management tasks of UU

This section introduces the critical integration of the proposed unified practical application framework into the life-cycle management tasks of the UU. This integration is pivotal for enhancing the efficiency, safety, and sustainability throughout the life-cycle of UUs, which encompasses the planning and design, construction (new installation), operation (existing UUs), maintenance (including repair and upgrade), and decommissioning stages. Each stage gains distinct benefits from the framework, leveraging its innovative components to address the specific challenges inherent in the management of UUs.

Planning and Design: The initial stage benefits immensely from the UUTC and EUUL models. Thorough site surveys and risk assessments help identify utility needs and scope (Yan et al., 2021; Lai & Sham, 2023; Oguntoye et al., 2023). The environmental impact was also assessed (Plati et al., 2015), contributing to sustainable design, while budgeting and sourcing financing round out the planning stage (Salim et al., 2022; Wang et al., 2022b). The UUTC model aids in accurately filling incomplete topological data, thereby facilitating informed decision making and optimising the design of underground infrastructure (Wang et al., 2019; Gilbert et al., 2021). Simultaneously, the EUUL model reduces the GPR data interpretation time (Feng et

al., 2021a), expediting the planning and design process by providing a rapid and accurate localisation of existing UUs.

Construction (new installation): Safety and efficiency are of paramount importance during this stage. Site preparation and excavation, including the installation of protection for existing UUs and laying new utility lines, are critical steps (Goel et al., 2012; Tanoli et al., 2019). The zero-reference deep-learning model for low-light image enhancement (ZDE3D) enables the accurate 3D reconstruction of UU under low-light conditions, which is crucial for night construction scenarios (Nguyen et al., 2014a; Patel et al., 2010a). Meanwhile, the EUUL model ensures the precise localisation of existing utilities and prevents accidental damage during excavation in new installation stages (Tanoli et al., 2019; Al-Bayati et al., 2019). This dual application of ZDE3D and EUUL not only improves the safety of construction personnel and equipment but also streamlines the construction process by significantly reducing the data collection and processing times (Hansen et al., 2021b; Hu et al., 2005; Tulloch et al., 2006). Additionally, testing for integrity and safety, followed by backfilling and site restoration with proper documentation of the utility installation, completes this stage.

Operation (existing UU): During the operational stage, maintaining an accurate and current 3D reconstruction of the UU is essential for efficient management and ongoing safety. Routine monitoring of utility performance (Wallace, 2021), safety inspections (Yadav et al., 2022), and regulatory compliance (Yan et al., 2018) are ongoing tasks that are critical to this stage. The continuous update capability provided by both the EUUL and ZDE3D models can support this need, ensuring that utility managers have the most current data for effective decision making (Wang et al., 2019; Sharafat et al., 2021) and emergency response (Sharafat et al., 2021) planning and management operations of the UU network.

Maintenance/Repair/Upgrade: The framework application during the maintenance stage incorporates the UUTC model to support the low-cost analysis of topology-related tasks, such as damage positioning (Yu et al., 2019; Lacroix et al., 2015; Wang et al., 2021b). This data-driven approach avoids expensive manual inspection times

and labour costs (Goel et al., 2012; Wang et al., 2021a), particularly in scenarios where rapid maintenance feedback is required. Routine inspections, identifying and diagnosing issues, repairing faults or leaks (Maree et al., 2021; Wu et al., 2021), and record-keeping (Maree et al., 2021) of maintenance and repairs can also benefit from the UUTC and ELLU. The reduction in the GPR data interpretation time through the EUUL model further enhances the efficiency of maintenance operations (Esekhaigbe et al., 2020), enabling quicker responses to repair or upgrade requirements within the utility network.

Decommissioning: The proposed unified application framework has no direct application significance during the UU decommissioning stage. These methodologies and technologies offer foundational insights that can be adapted to inform the process of decommissioning. By understanding detailed 3D reconstructions and topological data, stakeholders can approach decommissioning tasks with a higher degree of precision and safety (Bumby et al., 2010; Sueri et al., 2022), potentially leveraging aspects of the technology to ensure minimal environmental impact and resource optimisation.

In summary, the practical application framework developed in this thesis is instrumental to the entire life-cycle of UUs. Integrating advanced technological models and leveraging domain knowledge significantly enhances the efficiency, cost-effectiveness, and safety of UU management. This unified framework not only addresses current challenges in the field, but also sets a foundation for future innovations in UU life-cycle management.

7.4 Summary

In the context of modern urban development, the demand for the 3D reconstruction of UUs is increasingly urgent, fundamentally aimed at the safe, efficient, and economical utilisation of urban subsurface resources. As urbanisation accelerates, UUs, such as water pipes, electrical cables, and gas pipelines, have become critical infrastructures essential for maintaining the basic functions of a city. However, if the locations of these facilities are unclear, construction activities can easily cause damage, leading to

disruptions in water and electricity supply, gas leaks, and even more severe accidents. Through precise 3D reconstruction, these risks can be significantly reduced, thereby providing strong support for urban planning and management. It helps planners and managers to better understand the structure of underground spaces, enabling the rational planning of underground facility layouts, thereby enhancing the efficiency of city operations. Moreover, 3D models are crucial for maintaining and updating underground facilities, reducing excavation costs and time, responding to emergencies, and improving the quality of public service.

This section presents and discusses the key findings of the established objectives. Objective 1 delves into the significance of accurate 3D reconstruction for UU life-cycle management, favouring GPR technology. However, the identified limitations prompted the proposition of an integrated approach that introduced a decision-making framework to guide the selection of optimal reconstruction technology. Objective 2 introduced the EUUL model for UU localisation, which demonstrated remarkable precision and speed across diverse soil types. Objective 3 introduces the ZDE3D model for low-light 3D reconstruction, showing significant enhancements and outperforming existing methods. Ablation studies underscored the effectiveness of the proposed loss function. In Objective 4, the UUTC model for topology completion outperformed the baseline models, particularly when integrating the SEM. The discussions within the chapter dissect model intricacies, identify instances of misjudgement, and highlight theoretical contributions, emphasising the 'key point-regression' mode in EUUL, the unsupervised approach in ZDE3D, and the UUTC model's graph-based topology completion. The practical implications of these advancements are underscored, addressing challenges in different stages of the UU life-cycle, and providing practical solutions for UU management and construction site challenges.

Chapter 8 : Conclusions, contributions, and future work

8.1 Main findings

8.1.1 Research findings for Objective 1

Objective 1: To identify research topics, trends, and limitations of automatic 3D reconstruction for as-built UUs.

Main findings: Peer-reviewed journal articles from the Web of Science and ASCE databases on various aspects of relevant technological developments were reviewed, including key technologies for 3D UU reconstruction, current applications of 3D reconstruction methods, and potential future research directions. The main findings are:

- Accurate, up-to-date, and comprehensive 3D reconstruction of as-built UUs is important for the life-cycle management of UUs. This section analyses the advantages, limitations, and best performance of each of the widely used 3D reconstruction techniques. Finally, the limitations of the UU's existing 3D reconstruction techniques and future work in this field are also investigated.
- GPR is the best non-destructive UU 3D reconstruction technology, with the widest application range and the best comprehensive outcome. However, conventional image-processing methods are time consuming and susceptible to noise. Deep-learning-based methods cannot optimise parameters globally because of their box-fitting mode, which requires the separation of a task into region detection and hyperbolic fitting problems. Thus, the precision and robustness of the localisation task were reduced.
- Image-based 3D reconstruction has become one of the most promising as-built UU 3D reconstruction methods during the exposed stages, owing to its cost efficiency and outstanding performance. However, the quality performance of image-based 3D reconstruction is highly sensitive to illumination conditions. To date, image-based 3D reconstruction in a low-light environment has mainly been optimised by traditional approaches that are time consuming and require manual

parameters. In addition, supervised deep-learning methods require suitable paired image data (low-light images and paired reference images), which limits their capability to enhance the performance of UU 3D reconstruction.

- The limited availability of UU data, particularly topological information, is a major issue in UU management. Current research primarily concentrates on conventional properties such as pipe diameter and material, and not on topological data completion.
- Owing to the above limitations, an automatic 3D reconstruction approach that can enhance GPR-based localisation, low-light environment 3D reconstruction, and UU network topology completion is required for UU projects.

8.1.2 Research findings for Objective 2

Objective 2: To develop a novel GPR-based as-built UU localisation deep-learning model for non-destructive scenarios.

Main findings: An end-to-end UU localisation deep-learning model (EUUL) was developed using GPR B-scan images as inputs. Three experiments were conducted to validate the proposed model and its improvements on an actual site. Based on the experimental results, the following conclusions were drawn.

- The experimental results showed that the precision of the proposed EUUL model was 97.01%, operating speed was 125 fps, and precision was 96.72% in a noisy environment.
- The EUUL model was superior to the existing mainstream models in terms of precision (Figure 4-6), operating speed (Table 4-3), and robustness (Figure 4-8).
- The proposed EUUL model architecture with a 'key point-regression' mode had increased precision and enhanced performance when compared to the most popular 'Box-fitting' mode (region detection first and then fitting the hyperbolas for apex localisation).
- The application of an anchor-free structure with a lightweight backbone

(CSPDarknet53) increased the calculation speed of the UU localisation model and reduced model deployment costs.

- The added ECA module can help the EUUL model focus on key features that contain more position information to manage the noise interference of the UU positioning data to ensure precision.
- By conducting experiments based on different soil types, the results showed that the EUUL model can be used in engineering practice for the accurate non-destructive position detection of various UUs.

8.1.3 Research findings for Objective 3

Objective 3: To develop a novel unsupervised image-based 3D reconstruction model for the low-light 3D reconstruction of as-built UUs for exposed scenarios.

Main findings: This objective proposes an unsupervised deep-learning model for low-light image enhancement in UU 3D reconstruction (ZDE3D). Field experiment results showed that the proposed model could effectively improve the UU object point-cloud effect based on image generation under low-light conditions. The specific findings are as follows:

- The experiments on-site showed a promising result: the quantity of sparse reconstruction point clouds was improved by 13.19 % on average, and the average reconstruction accuracy reached 98.58% when comparing image datasets collected in normal light and the low-light datasets enhanced by the ZDE3D model.
- The unsupervised deep-learning method can help achieve the low-light enhancement task through the loss-function design based on image-based 3D reconstruction principles, where pairs of training data (low-light image and expected reference image) are not required.
- By conducting five ablation experiments, the five proposed loss functions, L_{Spa} (spatial loss), L_{Col} (colour loss), L_{Exp} (exposure loss), L_{Bou} (boundary loss), and L_{Gro} (group loss), were effective in enhancing low-light UU images.

- The comparison experiments showed that the proposed ZDE3D model had the best UU 3D reconstruction enhancement performance compared with traditional brightness, contrast adjustment methods, and existing popular deep-learning low-light enhancement models.

8.1.4 Research findings for Objective 4

Objective 4: To develop a GCN-based topology-completion model for as-built UUs.

Main findings: A GCN-based deep-learning model was developed for the UU topology-completion task. Five mainstream models were applied as control group experiments, and the results indicated that the UUTC model outperformed the baseline models, particularly in terms of effectively completing topological relationships. The specific findings are as follows:

- The experimental results demonstrated that the proposed UUTC model achieved an average completion accuracy of 85.33% under various topology missing rates, ranging from 5% to 80%.
- The SEM was validated to be effective in enhancing the model's accuracy in predicting topological relationships by leveraging attribute clustering to identify nodes with shared characteristics, consequently facilitating more precise and informed predictions of the UU network's interconnectedness.
- Using each pipeline in the UU network as a graph node and the connection relationship between pipelines as graph edges, the UU topology-completion problem can be transformed into an edge prediction problem in the graph. The GCN technology can effectively solve this problem, although there is still room for improvement in completion accuracy.

8.2 Summary of theoretical contribution

This thesis is motivated by the increasing challenges faced by project planners, managers, and stakeholders in managing different UU construction stages. The theoretical contributions outlined in this section address the challenges of 3D

reconstruction in UU environments by presenting a unified framework that surpasses the limitations of the conventional approaches. Existing frameworks are critiqued for their unidimensional focus, inaccuracy stemming from a lack of attention to new installation stages, and substantial resource demands associated with field-based detection. In contrast, the proposed unified framework stands out for its user-friendliness, enhanced precision, and transferability to diverse contexts beyond UU reconstruction. The three main theoretical contributions of this study are as follows:

(1) Novel model for automatic UU localisation (EUUL)

A deep-learning model, EUUL, was introduced for the automatic reconstruction of UUs based on GPR data.

- The model adopts an 'end-to-end' approach, addressing the limitations of existing methods that separate the problem into sub-problems, such as box detection and hyperbola fitting.
- The key point-regression mode in EUUL minimises error accumulation and maximises machine-learning strengths in pattern recognition and relationship modelling.
- The experimental results showed superior performance in terms of localisation accuracy, inference speed, and robustness.

Unsupervised model for low-light UU image-based reconstruction enhancement (ZDE3D):

(2) ZDE3D was proposed to enhance the performance of image-based 3D reconstructions in low-light environments.

- Unlike previous supervised approaches, ZDE3D leverages unsupervised learning by integrating the principles of image-based 3D reconstruction and the domain knowledge specific to UUs.
- Field data implementation validated the model, demonstrating a significant increase in the quantity of sparsely reconstructed point clouds and impressive

reconstruction accuracy.

(3) GCN-Based Model for UU Topology Completion (UUTC):

- UUTC introduces a deep-learning approach based on GCN to complete the missing topological information in UU areas.
- Departing from traditional and statistical methods, UUTC transforms a complex task into edge prediction within a graph structure, pioneering a data-driven approach.
- The proposed SEM module leverages domain knowledge and further enhances the accuracy of the UUTC model by considering the strong correlation between the attribute similarity among UU nodes and their connection relationships.
- Experiments based on real wastewater databases confirmed the effectiveness of UUTC in identifying unknown UU topological relationships, with an average completion accuracy of 85.33%. The effectiveness of the SEM module is validated through comparative experiments.

In summary, the theoretical contributions of this thesis present a unified framework that addresses the limitations of the existing UU 3D reconstruction frameworks. The proposed models (EUUL, ZDE3D, and UUTC) show advancements in UU localisation, low-light image-based reconstruction enhancement, and topological information completion, collectively offering a comprehensive and innovative approach to the challenges in the field.

8.3 Summary of practical contribution

The practical contributions of this study revolve around time-saving techniques, cost-effective strategies, and safety enhancements in UU projects.

(1) Time saving:

Traditional manual interpretation methods for GPR data are time consuming and prone to errors. The proposed UU 3D reconstruction approach automates GPR data

interpretation and significantly expedites the process. Real-site experiments showcased substantial time savings. Whereas manual interpretation typically requires 8,000 s, the proposed method only requires 64 s, achieving a remarkable 0.8% of the traditional manual method's time consumption. Moreover, the proposed approach outperforms existing automated methods, such as YOLOv3 and Faster R-CNN, in terms of processing speed, further emphasising its efficiency.

(2) Cost savings:

This study highlights the cost-effectiveness of the proposed approach in comparison with traditional manual inspection methods. Based on real-site experimental results, the proposed method offers significant cost advantages, amounting to approximately 30% of the cost incurred by manual inspection. These cost savings are crucial for large-scale projects and underscore the scalability and economic benefits of the proposed approach.

(3) Safety Enhancement:

Safety concerns in UU projects, including accidental damage to existing utilities, pose significant risk during construction. The proposed approach addresses these challenges by eliminating manual inspections and minimising on-site exposure of construction workers. By leveraging advanced technologies and reducing human error, the proposed method enhances safety standards and promotes a safer working environment.

In summary, this study significantly contributes to improving the efficiency and safety of UU projects. The proposed approach offers tangible benefits to construction workers and project stakeholders by streamlining processes, reducing costs, and enhancing safety. These findings underscore the importance of technological advancements for enhancing the overall effectiveness and safety of infrastructure projects.

8.4 Limitations and future work

(1) Limitations of the EUUL model

The limitations of this thesis are as follows: 1) There are few comparative models. Because an open model code does not exist, determining the specific details of the model based on the framework and reproducing the model based on other studies is challenging. Therefore, the YOLOv3 and Faster R-CNN models were selected to perform comparative experiments under several conditions, such as different publication times and dataset sizes. 2) The experimental conditions were limited. Only a 400 MHz antenna was used for data acquisition. In contrast, the B-scan images obtained under different antenna frequency conditions were not considered.

The following are planned for future studies: 1) A public GPR dataset for UU, including radar manufacturers, different antenna frequencies, different geological environments, and other factors, will be developed such that this research area can be investigated more effectively in the future. 2) Using the acquired B-scan dataset, more features of UU can be analysed to achieve more intelligent and scientific management of UU networks.

(2) Limitations of the ZDE3D model

The ZDE3D model proposed in this paper can not only be applied in the UU project record field but can also be extended to other scenarios requiring 3D reconstruction of low-light environments, such as underground mines, tunnel exploration, and cave sites.

However, the ZDE3D model proposed in this paper still has the following limitations: 1) The ZDE3D model improves the 3D reconstruction effect in a low-light environment; however, it fails to maintain the colour information of the original reconstruction target well. 2) The robustness verification of the ZDE3D model must be implemented under more complex environmental conditions to ensure that it can be applied to various complex scenarios. 3) At present, the image datasets used in the ZDE3D model experiments are all close-range construction site images, which could be better suited for long-range construction.

In the future, the following three directions may achieve better performance in UU low-light 3D reconstruction tasks: 1) Transformer. A transformer is an attention-based model that has been extensively used in language and image-processing tasks. The attention mechanism can help the model better capture long-term dependencies and relationships between different parts of the input sequence, which is important in low-light enhancement tasks. 2) Multimodal learning. With multimodal learning, multiple sources, or modalities, such as text and images from the UU project, can be used together for the training process, which may increase the robustness and accuracy. 3) Optical flow. Optical flow is a computer-vision technique that can track the movement of pixels between consecutive frames. In UU 3D reconstruction scenarios, capturing the same pixels in different frames is the foundation of image-based 3D reconstruction. Combining the deep-learning method with optical flow may increase the feature extraction ability of the model. Based on the research proposed in this study, the low-light 3D reconstruction model will be further tested and improved under more complex environmental conditions. In addition, a deep-learning model without reference data will also help in the design and application of more deep-learning models and provide more scientific solutions for more complex and realistic reconstruction problems, or even be combined with AR or VR techniques.

(3) Limitations of the UUTC model

While the proposed UUTC model demonstrates commendable performance in completing UUs' topological information data, certain limitations persist within this thesis: 1) Spatial and temporal dimensions. The integration of temporal and spatial information is important for understanding UU network topology. However, owing to the need for comprehensive historical data, the execution of dynamic time-series analyses of pipeline networks remains unfeasible. Regrettably, this constraint considers the spatial distribution factors within the UU network and their interactions with the surrounding environment. Instances such as the positioning of sewage treatment stations and the dispersion of final sewage discharge points still need to be accounted for. 2) Edge information usage. This study's treatment of edge information

is confined to a criterion for adjudicating the existence of topological relationships among UU nodes. This approach does not effectively harness the inherent potential of edge data within the framework of graph data structures. Beyond its role in signifying topological links, edge information possesses distinct attributes, akin to node and graph attributes. Each edge theoretically assumes a unique character across diverse graphs. Furthermore, it establishes a foundation for the enriched representation of intricate network attributes by systematically exploring the structural intricacies of graphs. The untapped potential in this regard could enhance the topology prediction accuracy, particularly when confronted with scenarios with few observed features. 3) Limited verification scope. The current model validation is confined exclusively to a singular category of the UU context, namely wastewater networks. However, the expansive spectrum of UU scenarios encompasses diverse domains, such as water and sewer pipelines, gas and oil conduits, electrical cables, and telecommunication lines. These domains exhibit distinct topological distribution characteristics. Therefore, the efficacy of the proposed model may fluctuate across diverse UU scenarios, necessitating meticulous examination and validation.

In future work, there are several promising research directions that can further promote the development of the UU 3D reconstruction field.

(1) Scalability and computational complexity

As UU projects often entail large-scale datasets, particularly in complex urban environments, ensuring that the proposed deep-learning models can scale effectively without exorbitant computational costs is essential. In future studies, it will be important to focus on optimizing the architecture of deep-learning models like EUUL and ZDE3D to handle larger and more complex datasets efficiently. One approach could be to incorporate more efficient neural network architectures that require less computational power. Techniques such as pruning, quantization, and the use of knowledge distillation could be explored to reduce the model size and speed up inference times without sacrificing accuracy. Additionally, leveraging more advanced forms of transfer learning could enable these models to adapt more quickly to new data,

reducing the need for extensive retraining and thus lowering computational costs. For the topology completion models like UUTC, methods to reduce graph complexity, such as graph sparsification or the use of hierarchical graph neural networks, could be investigated to manage the computational burden while maintaining or even improving the accuracy of topological predictions.

Moreover, it could be beneficial to explore hybrid approaches that combine traditional computational methods with machine learning enhancements to strike a balance between computational demand and reconstruction performance. These methods might prioritize machine learning interventions for the most complex or error-prone segments of data while handling more straightforward tasks with less computationally intensive algorithms. By pursuing these avenues, the scalability and computational efficiency of the models can be enhanced, making them more practical for widespread implementation in real-world UU management scenarios.

(2) Data impact factors

For the accuracy of the underground utilities topology completion (UUTC) model, future research should focus on a comprehensive analysis of both data sources and environmental influences. This includes evaluating the quality and origin of the data used, as well as assessing how external factors such as soil type, weather conditions, and urban development might affect the efficacy of data collection methods like ground-penetrating radar. Additionally, human factors should not be overlooked; investigating operator experience and data entry processes could uncover potential biases that compromise data accuracy.

Implementing advanced statistical analyses and robustness testing under varied conditions will further enhance the understanding of the impact of these factors on the UUTC model's performance. By intentionally testing the model with corrupted or incomplete data sets, researchers can identify vulnerabilities and areas for improvement. Moreover, exploring technological advancements in sensor technology and data processing algorithms can lead to significant enhancements in data reliability. This holistic approach will provide valuable insights into the multifaceted challenges

of data accuracy in underground utility management, ultimately contributing to more effective modelling and decision-making processes for underground utilities.

(3) Life cycle management

Future research should specifically address the relationship between these improvements and their impact on life-cycle management processes. While the current research demonstrates enhanced accuracy and reliability in 3D reconstructions, it does not directly establish how these advancements contribute to better life-cycle management of UUs.

To bridge this gap, future studies could focus on empirical testing that examines the correlation between accurate UU location data and key performance indicators in life-cycle management, such as maintenance scheduling, cost reduction, and risk mitigation. By conducting case studies or field experiments that link improved reconstruction outcomes to tangible enhancements in life-cycle management practices, researchers can provide a clearer understanding of this relationship. Additionally, integrating stakeholder feedback and decision-making frameworks into the research will help elucidate how precise 3D reconstructions can inform and optimize management strategies throughout the UU life cycle. Such investigations will not only validate the claims made in this research but also contribute valuable insights into the practical applications of advanced 3D reconstruction technologies in the field of underground utility management.

Reference

Adouane, K., Boujon, F., & Domer, B. (2021). Digital modelling of underground volumes, including the visualization of confidence levels for the positioning of subsurface objects. *Applied Sciences, 11*(8), pp. 3483. https://doi.org/10.3390/app11083483.

Agustsson, E., & Timofte, R. (2017). Ntire 2017 challenge on single image super-resolution: Dataset and study. *In Proceedings of the IEEE conference on computer vision and pattern recognition workshops*, pp. 126-135. https://doi.org/10.1109/cvprw.2017.150.

Ahmadi, R., & Fathianpour, N. (2017). Estimating geometrical parameters of cylindrical targets detected by ground-penetrating radar using template matching algorithm. *Arabian Journal of Geosciences, 10*(6). https://doi.org/10.1007/s12517-017-2901-8.

Ahmed, H., La, H. M., & Tran, K. (2020). Rebar detection and localization for bridge deck inspection and evaluation using deep residual networks. *Automation in Construction, 120*, pp. 103393. https://doi.org/10.1016/j.autcon.2020.103393.

Al-Bayati, A. J., & Panzer, L. (2019). Reducing damage to underground utilities: Lessons learned from damage data and excavators in North Carolina. *Journal of Construction Engineering and Management, 145(12),* 04019078. https://doi.org/10.1061/(ASCE)CO.1943-7862.0001724.

Al-Nuaimy, W., Huang, Y., Nakhkash, M., Fang, M. T. C., Nguyen, V. T., & Eriksen, A. (2000). Automatic detection of buried utilities and solid objects with GPR using neural networks and pattern recognition. *Journal of applied Geophysics*, 43(2-4), 157-165. https://doi.org/10.1016/S0926-9851(99)00055-5.

Alasal, S. A., Alsmirat, M., Baker, Q. B., & Jararweh, Y. (2018). Improving passive 3d model reconstruction using image enhancement. *In 2018 6th International Conference on Multimedia Computing and Systems (ICMCS).* 1-7. https://doi.org/10.1109/icmcs.2018.8525977.

Aldeeb, N. H., & Hellwich, O. (2018). Reconstructing textureless objects-image enhancement for 3d reconstruction of weakly-textured surfaces. *International Joint Conference on Computer Vision, Imaging and Computer Graphics Theory and Applications*, pp. 572-580. https://doi.org/10.5220/0006628805720580.

Alejo, D., Caballero, F., & Merino, L. (2019). A robust localization system for inspection robots in sewer networks. *Sensors*, 19(22), 4946. https://doi.org/10.3390/s19224946.

Alhnaity, B., Kollias, S., Leontidis, G., Jiang, S., Schamp, B., & Pearson, S. (2021). An autoencoder wavelet based deep neural network with attention mechanism for multi-step prediction of plant growth. *Information Sciences*, 560, pp. 35-50. https://doi.org/10.1016/j.ins.2021.01.037.

Ali, H., Ideris, N. S. M., Ahmad Zaidi, A. F., Zanar Azalan, M. S., Tengku Amran, T. S., Ahmad, M. R., Abdul Rahim, N., & Abdul Shukor, S. A. (2021). Ground penetrating radar for buried utilities detection and mapping: a review. *Journal of*

Physics: Conference Series, 2107(1), pp. 012056. https://doi.org/10.1088/1742-6596/2107/1/012056.

Aliyu, A., Singhry, I. M., Adamu, H., & Abubakar, M. M. (2015). Ontology, epistemology and axiology in quantitative and qualitative research: Elucidation of the research philophical misconception. *In the Academic Conference: Mediterranean Publications & Research International on New Direction and Uncommon*, 2, (1) 1-26. https://www.researchgate.net/profile/Aliyu-Aliyu-2/publication/318721927_ONTOLOGY_EPISTEMOLOGY_AND_AXIOLOGY_IN_QUANTITATIVE_AND_QUALITATIVE_RESEARCH_ELUCIDATION_OF_THE_RESEARCH_PHILOSOPHICAL_MISCONCEPTION/links/59798097aca27203ecc63de3/ONTOLOGY-EPISTEMOLOGY-AND-AXIOLOGY-IN-QUANTITATIVE-AND-QUALITATIVE-RESEARCH-ELUCIDATION-OF-THE-RESEARCH-PHILOSOPHICAL-MISCONCEPTION.pdf.

Amaral, L. C. M., Roshan, A., & Bayat, A. (2022). Review of machine learning algorithms for automatic detection of underground objects in GPR images. *Journal of Pipeline Systems Engineering and Practice, 13*(2). https://doi.org/10.1061/(asce)ps.1949-1204.0000632.

Ancuti, C., De Vleeschouwer, C., & Bekaert, P. (2018). Color balance and fusion for underwater image enhancement. *IEEE Transactions on Image Processing*, *27*(1), pp. 379–393. https://doi.org/10.1109/tip.2017.2759252.

Ardekani, S. (2006). Automatic and fast detection of buried utilities positions and estimation of soil permittivity using GPR. *The 11th International Conference on Ground Penetrating Radar*. https://www.researchgate.net/publication/236901846.

Azinovic, D., Martin-Brualla, R., Goldman, D. B., Nießner, M., & Thies, J. (2021). Neural RGB-D Surface Reconstruction. *ArXiv (Cornell University)*. https://doi.org/10.1109/cvpr52688.2022.00619.

Azzam, R., Taha, T., Huang, S., & Zweiri, Y. (2020). Feature-based visual simultaneous localization and mapping: A survey. *SN Applied Sciences, 2(2),* pp. 1-24. https://doi.org/10.1007/s42452-020-2001-3.

Bach, P. M., & Kodikara, J. K. (2017). Reliability of infrared thermography in detecting leaks in buried water reticulation pipes. *IEEE Journal of Selected Topics in Applied Earth Observations and Remote Sensing*, 10(9), 4210-4224. https://doi.org/10.1109/JSTARS.2017.2708817.

Bai, H., & Sinfield, J. V. (2020). Improved background and clutter reduction for pipe detection under pavement using Ground Penetrating Radar (GPR). *Journal of Applied Geophysics*, *172*, 103918. https://doi.org/10.1016/j.jappgeo.2019.103918.

Ballabeni, A., Apollonio, F. I., Gaiani, M., & Remondino, F. (2015). Advances in image pre-processing to improve automated 3d reconstruction. *The International Archives of the Photogrammetry, Remote Sensing and Spatial Information Sciences*, pp. 315–323. https://doi.org/10.5194/isprsarchives-xl-5-w4-315-2015.

Barros, R. C., Basgalupp, M. P., de Carvalho, A. C. P. L. F., & Freitas, A. A. (2012). A survey of evolutionary algorithms for decision-tree induction. *In IEEE Transactions on Systems Man and Cybernetics Part C (Applications and Reviews)*, 42(3), 291–312. https://www.cs.kent.ac.uk/people/staff/aaf/pub_papers.dir/IEEE-SMC-C-2012-Barros-pre-print.pdf.

Batista, G.E., & Monard, M.C. (2002). A study of k-nearest neighbour as an imputation method. *International Conference on Health Information Science*, https://api.semanticscholar.org/CorpusID:37493644.

Bay, H., Tuytelaars, T., & Van Gool, L. (2006). SURF: Speeded up robust features. *Lecture Notes in Computer Science*, pp. 404–417. https://doi.org/10.1007/11744023_32.

Becka, R. A., Cohna, A. G., Parkerb, J., Boukhelifaa, N., & Fua, G. (2009). Seeing the unseen: delivering integrated underground utility. *In Proceedings of the GeoWeb Conference. https://www.isprs.org/proceedings/XXXVIII/3_4-C3/Paper_GeoW09/paper07_beck.pdf.*

Belghaddar, Y., Chahinian, N., Seriai, A., Begdouri, A., Abdou, R., & Delenne, C. (2021). Graph convolutional networks: Application to database completion of wastewater networks. *Water*, 13(12), 1681. https://doi.org/10.3390/w13121681.

Biersteker, E., Koppenjan, J., & Van Marrewijk, A. (2021). Translating the invisible: Governing underground utilities in the Amsterdam airport Schiphol terminal project. *International Journal of Project Management*, *39*(6), 581–593. https://doi.org/10.1016/j.ijproman.2021.04.003.

Bilal, M., Khan, W., Muggleton, J. M., Rustighi, E., Jenks, H., Pennock, S. R., Atkins, P., & Cohn, A. G. (2018). Inferring the most probable maps of underground utilities using Bayesian mapping model. *Journal of Applied Geophysics*, *150*, 52–66. https://doi.org/10.1016/j.jappgeo.2018.01.006.

Bochkovskiy, A., Wang, C., & Liao, H. M. (2020). YOLOv4: Optimal speed and accuracy of object detection. *ArXiv: Computer Vision and Pattern Recognition*. https://arxiv.org/pdf/2004.10934v1.

Bosché, F., Ahmed, M., Turkan, Y., Haas, C. T., & Haas, R. (2015). The value of integrating Scan-to-BIM and Scan-vs-BIM techniques for construction monitoring using laser scanning and BIM: The case of cylindrical MEP components. *Automation in Construction*, *49*, pp. 201–213. https://doi.org/10.1016/j.autcon.2014.05.014.

Birkenfeld, S. (2010). Automatic detection of reflexion hyperbolas in GPR data with neural networks. *In 2010 World Automation Congress*. 1-6. https://ieeexplore.ieee.org/abstract/document/5665328.

Bishop, C. M. (1995). Neural networks for pattern recognition. *Oxford Academic*. https://doi.org/10.1093/oso/9780198538493.001.0001.

Broere, W. (2016). Urban underground space: Solving the problems of today's cities. *Tunnelling and Underground Space Technology*, 55, 245-248. https://doi.org/10.1016/j.tust.2015.11.012.

Bureau of Transportation Statistics. (2016). As-built utility surveys: a tale of two state transportation departments. united states. *Federal Highway Administration*. https://rosap.ntl.bts.gov/view/dot/63379.

Bruno, N., A. Giacomini, R., Roncella, K., & Thoeni. (2021). Influence of illumination changes on image-based 3d surface reconstruction. *The International Archives of the Photogrammetry, Remote Sensing and Spatial Information Sciences*, 43, 701-708. http://dx.doi.org/10.5194/isprs-archives-xliii-b2-2021-701-2021.

Bugarinović, E., Pajewski, L., Ristić, A., Vrtunski, M., Govedarica, M., & Borisov, M. (2020). On the introduction of canny operator in an advanced imaging algorithm for real-time detection of hyperbolas in ground-penetrating radar data. *Electronics, 9*(3), pp. 541. https://doi.org/10.3390/electronics9030541.

Bumby, S., Druzhinina, E., Feraldi, R., Werthmann, D., Geyer, R., & Sahl, J. (2010). Life cycle assessment of overhead and underground primary power distribution. *Environmental science & technology*, 44(14), 5587-5593. https://doi.org/10.1021/es9037879.

Burdziakowski, P., & Bobkowska, K. (2021). UAV Photogrammetry under poor lighting conditions—accuracy considerations. *Sensors, 21*(10), pp. 3531. https://doi.org/10.3390/s21103531.

Cai, J., Jeon, J., Cai, H., & Li, S. (2020). Fusing heterogeneous information for underground utility map generation based on Dempster-Shafer theory. *Journal of Computing in Civil Engineering*, 34(3), 04020013. https://doi.org/10.1061/(ASCE)CP.1943-5487.0000892.

Caldecott, D., Poirier, M., Scofea, D., Svoboda, D.E., & Terzuoli, A.J. (1988). Underground mapping of utility lines using impulse radar. *In IEEE Proceedings F (Communications, Radar and Signal Processing)*, 135(4), 343-353. https://doi.org/10.1049/ip-f-1.1988.0041.

Calonder, M., Lepetit, V., Strecha, C., & Fua, P. (2010). BRIEF: Binary robust independent elementary features. *Springer EBooks*, pp. 778–792. https://doi.org/10.1007/978-3-642-15561-1_56.

Capineri, L., Grande, P., & Temple, J. A. G. (1998). Advanced Image-processing Technique for Real-time Interpretation of Ground-penetrating Radar Images. *International Journal of Imaging Systems and Technology, 9*(1), pp. 51–59. https://doi.org/10.1002/(sici)1098-1098(1998)9:1.

Capozzoli, L., & Rizzo, E. (2017). Combined NDT techniques in civil engineering applications: Laboratory and real test. *Construction and Building Materials*, *154*, 1139–1150. https://doi.org/10.1016/j.conbuildmat.2017.07.147.

Cazzaniga, N. E., D. Carrion, F. Migliaccio & R. Barzaghi. (2013). A shared database of underground utility lines for 3D mapping and GIS applications. *The International Archives of the Photogrammetry, Remote Sensing and Spatial Information Sciences*, 40, 105-108. https://doi.org/10.5194/ISPRSARCHIVES-XL-4-W1-105-2013.

Chan. R. K. C., Lim, J. M. Y., & Parthiban, R. (2023). Missing traffic data imputation for artificial intelligence in intelligent transportation systems: review of methods,

limitations, and challenges. *IEEE Access*, 11, 34080-34093. https://doi.org/10.1109/ACCESS.2023.3264216.

Chen, C. S., & Jeng, Y. (2021). Improving gpr imaging of the buried water utility infrastructure by integrating the multidimensional nonlinear data decomposition technique into the edge detection. *Water, 13*(21), pp. 3148. https://doi.org/10.3390/w13213148.

Chen, J., Ma, T., Xiao, C. (2018). FastGCN: Fast learning with graph convolutional networks via importance sampling. Arxiv. https://doi.org/10.48550/arXiv.1801.10247.

Chen. Z & Huang, X. (2017). End-to-end learning for lane keeping of self-driving cars. *In 2017 IEEE intelligent vehicles symposium*, 1856-1860. https://doi.org/10.1109/IVS.2017.7995975.

Cheng, L., Wei, Z., Sun, M., Xin, S., Sharf, A., Li, Y., Chen, B., & Tu, C. (2020). DeepPipes: Learning 3D pipelines reconstruction from point clouds. *Graphical Models /Graphical Models and Image Processing /Computer Vision, Graphics, and Image Processing*, *111*, 101079. https://doi.org/10.1016/j.gmod.2020.101079.

Childs, J., Orfeo, D., Burns, D., Huston, D., & Xia, T. (2020). Enhancing ground penetrating radar with augmented reality systems for underground utility management. *Proc. SPIE 11426, Virtual, Augmented, and Mixed Reality (XR) Technology for Multi-Domain Operations*, 1142608. https://doi.org/10.1117/12.2561042.

Chinese Association of Surveying and Mapping Underground Pipeline Professional Committee. (2023). Statistical Analysis Report of National Underground Pipeline Accidents in 2022 (January 2022 - December 2022). http://www.lingpiankeji.com/newsinfo/5655377.html. (Access date: 28/ 12/2023).

Chowdhury, M. S., & Abdel-Hafez, M. F. (2016). Pipeline inspection gauge position estimation using inertial measurement unit, odometer, and a set of reference stations. *ASCE-ASME journal of risk and uncertainty in engineering systems, Part B. Mechanical engineering, (2)*. https://doi.org/10.1115/1.4030945.

Choy, C., Xu, D., Gwak, J., Chen, K. J., & Savarese, S. (2016). 3D-R2N2: A unified approach for single and multi-view 3D object reconstruction. *Springer EBooks*, pp. 628–644. https://doi.org/10.1007/978-3-319-46484-8_38.

Chrysostomou, D., Dimitriou, A., Kokkinos, N. D., & Charalambous, C. A. (2020). Short-term electromagnetic interference on a buried gas pipeline caused by critical fault events of a wind park: A realistic case study. *IEEE Transactions on Industry Applications, 56(2),* pp. 1162-1170. https://doi.org/10.1109/TIA.2020.2965494.

Cloete, C., Germishuys, L., & Cook, L. (2020). Utility detection in property development. *International Journal of Science and Research*, 77(3). https://doi.org/10.21506/j.ponte.2021.3.10.

Coltuc, D., Bolon, P., & Chassery, J. (2006). Exact histogram specification. *IEEE Transactions on Image Processing*, *15*(5), pp. 1143–1152.

https://doi.org/10.1109/tip.2005.864170.
Cortes, C., & Vapnik, V. (2004). Support-vector networks. *Machine Language*, 20(3), 273-297. https://doi.org/10.1023/A:1022627411411.
Costello, S. B., Chapman, D. N., Rogers, C. D. F., & Metje, N. (2007). Underground asset location and condition assessment technologies. *Tunnelling and Underground Space Technology*, 22(5-6), 524-542. https://doi.org/10.1016/j.tust.2007.06.001.
Davey, A., J. Savla. (2009). Statistical power analysis with missing data: A structural equation modeling approach. https://doi.org/10.4324/9780203866955.
De Coster, A., Medina, J. P., Nottebaere, M., Alkhalifeh, K., Neyt, X., Vanderdonckt, J., & Lambot, S. (2019). Towards an improvement of GPR-based detection of pipes and leaks in water distribution networks. *Journal of Applied Geophysics, 162*, 138–151. https://doi.org/10.1016/j.jappgeo.2019.02.001.
Defferrard, M., Bressen, X., & Vandergheynst, P. (2016). Convolutional neural networks on graphs with fast localized spectral filtering. *In Proceedings of the 30th International Conference on Neural Information Processing Systems*, 3844–3852. https://api.semanticscholar.org/CorpusID:3016223.
Deng, S., Ma, S., Zhang, X., & Zhang, S. (2020). Integrated detection of a complex underground water supply pipeline system in an old urban community in China. *Sustainability, 12(4)*, pp. 1670. https://doi.org/10.3390/su12041670.
Dou, Q., Lin, Z., Magee, D. R., & Cohn, A. G. (2020). 3D mapping from partial observations: An application to utility mapping. *Automation in Construction*, 117, 103229. https://doi.org/10.1016/j.autcon.2020.103229.
Döner, F., Thompson, R., Stoter, J., Lemmen, C., Ploeger, H., Van Oosterom, P., & Zlatanova, S. (2011). Solutions for 4D cadastre – with a case study on utility networks. *International Journal of Geographical Information Science*, *25*(7), pp. 1173–1189. https://doi.org/10.1080/13658816.2010.520272.
Du, J., S. Zhang, G. Wu, J. M. F. Moura & S. Kar. (2017). Topology adaptive graph convolutional networks. *Arxiv*. https://api.semanticscholar.org/CorpusID:27731709.
Duda, R. O., & Hart, P. E. (1972). Use of the Hough transformation to detect lines and curves in pictures. *Communications of the Association for Computing Machinery (ACM), 15*(1), pp. 11–15. https://doi.org/10.1145/361237.361242.
Duran, O., Althoefer, K., & Seneviratne, L. (2003). Pipe inspection using a laser-based transducer and automated analysis techniques. *IEEE-ASME Transactions on Mechatronics, 8*(3), 401–409. https://doi.org/10.1109/tmech.2003.816809.
Eigen, D., Puhrsch, C., & Fergus, R. (2014). Depth map prediction from a single image using a multi-scale deep network. *Neural Information Processing Systems, 27*, pp. 2366–2374. https://arxiv.org/pdf/1406.2283.
Elkhrachy, I. (2021). Accuracy assessment of low-cost unmanned aerial vehicle (UAV) photogrammetry. *Alexandria Engineering Journal*, 60(6), 5579-5590. https://doi.org/10.1016/j.aej.2021.04.011.
Esekhaigbe, E., Kazan, E., & Usmen, M. (2020). Integration of digital technologies

into underground utility asset management. *Open Journal of Civil Engineering,* 10(4), 403-428. https://doi.org/ 10.4236/ojce.2020.104030.

Fan, C., Sun, F., & Yang, L. (2005). Investigation on nondestructive evaluation of pipelines using infrared thermography. *International Conference on Infrared, Millimeter, and Terahertz Waves*. https://doi.org/10.1109/icimw.2005.1572551.

Fenais, A., Ariaratnam, S. T., & Smilovsky, N. (2020). Assessing the Accuracy of an Outdoor Augmented Reality Solution for Mapping Underground Utilities. *Journal of Pipeline Systems Engineering and Practice*, *11*(3). https://doi.org/10.1061/(asce)ps.1949-1204.0000474.

Feng, J., Yang, L., Hoxha, E., & Xiao, J. (2022). Improving 3D metric GPR imaging using automated data collection and learning-based processing. IEEE Sensors Journal. https://doi.org/10.1109/JSEN.2022.3164707.

Feng, J., Yang, L., Hoxha, E., Sanakov, D., Sotnikov, S., & Xiao, J. (2021a). GPR-based model reconstruction system for underground utilities using GPRNet. *In 2021 IEEE International Conference on Robotics and Automation (ICRA)*, pp. 845-851. https://doi.org/10.1109/ICRA48506.2021.9561355.

Feng, W., Li, J., Cai, H., Luo, X., & Zhang, J. (2021b). Neural Points: Point cloud representation with neural fields. *ArXiv: Computer Vision and Pattern Recognition*. https://doi.org/10.48550/arXiv.2112.04148.

Furukawa, Y., & Hernández, C. F. G. (2015). Multi-view stereo: A tutorial. *Foundations and Trends in Computer Graphics and Vision*, *9*(1–2), pp. 1–148. https://doi.org/10.1561/0600000052.

Furukawa, Y., Curless, B., Seitz, S. M., & Szeliski, R. (2010). Towards internet-scale multi-view stereo. *In 2010 IEEE computer society conference on computer vision and pattern recognition.* pp. 1434-1441. https://doi.org/10.1109/cvpr.2010.5539802.

Gamba, P., & Belotti, V. (2003). Two fast buried pipe detection schemes in Ground Penetrating Radar images. *International Journal of Remote Sensing, 24*(12), pp. 2467–2484. https://doi.org/10.1080/0143116021000050673.

Gangopadhyay, S., Das Gupta, A., & Nachabe, M. H. (2005). Evaluation of ground water monitoring network by principal component analysis. *Groundwater*, 39(2), 181-191. https://doi.org/10.1111/j.1745-6584.2001.tb02299.x.

Geng, Y., B. An, H. Geng, Y. Chen, Y. Yang & H. Dong. (2023). Rlafford: End-to-end affordance learning for robotic manipulation. *In 2023 IEEE International Conference on Robotics and Automation (ICRA)*, 5880-5886. https://doi.org/10.1109/ICRA48891.2023.10161571.

Geophysical Survey Systems, Inc. (2011). RADAN (Version 7). [Software]. Geophysical Survey Systems, Inc. https://www.geophysical.com/software. (Last accessed in October 10th, 2022).

Gilbert, T., James, P., Smith, L., Barr, S., & Morley, J. (2021). Topological integration of BIM and geospatial water utility networks across the building envelope. Computers, *Environment and Urban Systems*, 86, 101570. https://doi.org/10.1016/j.compenvurbsys.2020.101570.

Girshick, R. (2015). Fast R-CNN. *2015 Institute of Electrical and Electronics Engineers (IEEE) International Conference on Computer Vision (ICCV)*. https://doi.org/10.1109/iccv.2015.169.

Girshick, R., Donahue, J., Darrell, T., & Malik, J. (2014). Rich feature hierarchies for accurate object detection and semantic segmentation. In *2014 Institute of Electrical and Electronics Engineers (IEEE) Conference on Computer Vision and Pattern Recognition*. https://doi.org/10.1109/cvpr.2014.81.

Glass, E., & Glass, V. (2019). Underground power lines can be the least cost option when study biases are corrected. *The Electricity Journal*, *32*(2), 7–12. https://doi.org/10.1016/j.tej.2019.01.015.

Goel, R. K., Singh, B., & Zhao, J. (2012). Underground infrastructures: planning, design, and construction. butterworth-heinemann. https://shop.elsevier.com/books/underground-infrastructures/goel/978-0-12-397168-5.

Graham, J. W. (2012). Missing data: Analysis and design. New York, NY: Springer Science & Business Media. https://link.springer.com/content/pdf/bfm:978-1-4614-4018-5/1.pdf.

Grundland, M., & Dodgson, N. A. (2007). Decolorize: Fast, contrast enhancing, color to grayscale conversion. *Pattern Recognition*, *40*(11), pp. 2891–2896. https://doi.org/10.1016/j.patcog.2006.11.003.

Guidi, G., Gonizzi, S., & Micoli, L. L. (2014). Image pre-processing for optimizing automated photogrammetry performances. *ISPRS Annals of the Photogrammetry, Remote Sensing and Spatial Information Sciences*, *II–5*, pp. 145–152. https://doi.org/10.5194/isprsannals-ii-5-145-2014.

Gunatilake, A., Piyathilaka, L., Tran, A., Vishwanathan, V. K., Thiyagarajan, K., & Kodagoda, S. (2020). Stereo vision combined with laser profiling for mapping of pipeline internal defects. *IEEE Sensors Journal, 21(10).* https://doi.org/11926-11934. 10.1109/JSEN.2020.3040396.

Guo, C., Li, C., Guo, J., Loy, C. C., Hou, J., Kwong, S., & Cong, R. (2020a). Zero-reference deep curve estimation for low-light image enhancement. *In Proceedings of the IEEE/CVF Conference on Computer Vision and Pattern Recognition.* pp. 1780-1789. https://doi.org/10.1109/cvpr42600.2020.00185.

Guo, J., Wang, Q., & Park, J. (2020b). Geometric quality inspection of prefabricated MEP modules with 3D laser scanning. *Automation in Construction*, *111*, 103053. https://doi.org/10.1016/j.autcon.2019.103053.

Guo, W., Soibelman, L., & Garrett, J. (2009). Automated defect detection for sewer pipeline inspection and condition assessment. *Automation in Construction, 18*(5), 587–596. https://doi.org/10.1016/j.autcon.2008.12.003.

Hajibabaei, M., Hesarkazzazi, S., Dastgir, A., Minaei, A., & Sitzenfrei, R. Reconstruction of missing information in water distribution networks based on graph theory. *In World Environmental and Water Resources Congress 2023*, 1015-1026. https://doi.org/10.1061/9780784484852.093.

Hamilton, W. L., Ying, P., & Leskovec, J. (2017). Inductive representation learning on large graphs. *In Proceedings of the 31st International Conference on Neural Information Processing Systems*, 1025–1035. https://dl.acm.org/doi/pdf/10.5555/3294771.3294869.

Hansen, L., Pedersen, T. O., Kjems, E., & Wyke, S. C. S. (2021a). Smartphone-based reality capture for subsurface utilities: experiences from water utility companies in denmark. *The International Archives of the Photogrammetry, Remote Sensing and Spatial Information Sciences*, *XLVI-4/W4-2021*, pp. 25–31. https://doi.org/10.5194/isprs-archives-xlvi-4-w4-2021-25-2021.

Hansen, L., Van Son, R., Weiser, A., & Kjems, E. (2021b). Addressing the elephant in the underground: an argument for the integration of heterogeneous data sources for reconciliation of subsurface utility data. *The International Archives of the Photogrammetry, Remote Sensing and Spatial Information Sciences*, *XLVI-4/W4-2021*, pp. 43–48. https://doi.org/10.5194/isprs-archives-xlvi-4-w4-2021-43-2021.

Hao, T., Burd, H. J., Edwards, D., & Stevens, C. W. (2008). Enhanced detection of buried assets. *Loughborough Antennas and Propagation Conference*. https://doi.org/10.1109/lapc.2008.4516913

Hao, T., Rogers, C. D. F., Metje, N., Chapman, D. M. F., Muggleton, J. M., Foo, K. K., Wang, P., Pennock, S. R., Atkins, P. R., Swingler, S., Parker, J. W., Costello, S. B., Burrow, M. F., Anspach, J., Armitage, R. J., Cohn, A. G., Goddard, K. F., Lewin, P., Orlando, G., . . . Saul, A. J. (2012). Condition assessment of the buried utility service infrastructure. *Tunnelling and Underground Space Technology*, *28*, 331–344. https://doi.org/10.1016/j.tust.2011.10.011.

Harbin, K. B. (2016). Data collection techniques for subsurface utility planning on a university campus: a case study. *In Pipelines 2016* (pp. 827-837). https://doi.org/10.1061/9780784479957.076.

Harkat, H., Elfakir, Y., Bennani, S. D., Khaissidi, G., & Mrabti, M. (2016). Ground penetrating radar hyperbola detection using scale-invariant feature transform. *2016 International Conference on Electrical and Information Technologies (ICEIT)*. https://doi.org/10.1109/eitech.2016.7519626.

Harkat, H., Ruano, A., Ruano, M., & Bennani, S. (2018). Classifier design by a multi-objective genetic algorithm approach for GPR automatic target detection. *IFAC-PapersOnLine, 51*(10), pp. 187–192. https://doi.org/10.1016/j.ifacol.2018.06.260.

Harkart, H., Ruano, A., Ruano, M., & Bennani, S. (2019). GPR target detection using a neural network classifier designed by a multi-objective genetic algorithm. *Applied Soft Computing, 79*, pp. 310–325. https://doi.org/10.1016/j.asoc.2019.03.030.

Hartley, R., & Zisserman, A. (2003). Multiple view geometry in computer vision (2nd ed). *Cambridge University Press EBooks*. https://digitalcollections.anu.edu.au/handle/1885/52332.

Hartshorn, C. A., Isaacson, S. D., Barrowes, B. E., Perren, L. J., Lozano, D., & Shubitidze, F. (2022). Analysis of the feasibility of UAS-based EMI sensing for

underground utilities detection and mapping. *Remote sensing*, 14(16), 3973. https://doi.org/10.3390/rs14163973.

Hashemi, B., Iseley, T., & Raulston, J. (2011). Water pipeline renewal evaluation using AWWA class IV CIPP, pipe bursting, and open-cut. *In ICPTT 2011: Sustainable Solutions for Water, Sewer, Gas, And Oil Pipelines*, pp. 1257-1266. https://doi.org/10.1061/41202(423)133.

He, K., Zhang, X., Ren, S., & Sun, J. (2015). Spatial pyramid pooling in deep convolutional networks for visual recognition. *Institute of Electrical and Electronics Engineers (IEEE) Transactions on Pattern Analysis and Machine Intelligence, 37*(9), pp. 1904–1916. https://doi.org/10.1109/tpami.2015.2389824.

Hebsur, A. V., Muniappan, N., Rao, E. P., & Venkatachalam, G. (2013). Simulation of close-range remote sensing of subsurface features using GPR for urban utility information system development. *In Earth Resources and Environmental Remote Sensing/GIS Applications IV, 8893*. pp. 39-47. https://doi.org/10.1117/12.2028957.

Honaker. J., King, G., & Blackwell, M. (2011). Amelia II: A program for missing data. *Journal of Statistical Software*, 45(7), 1–47. https://doi.org/10.18637/jss.v045.i07.

Hou, F., Lei, W., Li, S., & Xi, J. (2021a). Deep learning-based subsurface target detection from GPR scans. *Institute of Electrical and Electronics Engineers (IEEE) Sensors Journal, 21*(6), pp. 8161-8171. https://doi.org/10.1109/JSEN.2021.3050262.

Hou, F., Lei, W., Li, S., Xi, J., Xu, M., & Luo, J. (2021b). Improved mask r-cnn with distance guided intersection over union for GPR signature detection and segmentation. *Automation in Construction, 121*, 103414. https://doi.org/10.1016/j.autcon.2020.103414.

Hu, W. (2005). 3D reconstruction of exposed underground utilities using photogrammetric methods. *Ann Arbor*, 1050, pp. 48106-1346. ISBN: 9798617084827. https://www.proquest.com/docview/305345077?pq-origsite=primo.

Huang, M., Ninić, J., & Zhang, Q. (2021). BIM, machine learning and computer vision techniques in underground construction: Current status and future perspectives. *Tunnelling and Underground Space Technology, 108*, 103677. https://doi.org/10.1016/j.tust.2020.103677.

Hyun, D., Yang, H. K., Park, H., & Kim, H. (2010). Dead-reckoning sensor system and tracking algorithm for 3-D pipeline mapping. *Mechatronics*, *20*(2), 213–223. https://doi.org/10.1016/j.mechatronics.2009.11.009.

Ibrahim, H., & Kong, N. (2007). Brightness preserving dynamic histogram equalization for image contrast enhancement. *IEEE Transactions on Consumer Electronics*, *53*(4), pp. 1752–1758. https://doi.org/10.1109/tce.2007.4429280.

Jaufer, R., Ihamouten, A., Guilbert, D., Todkar, S., Yaram, T., & Derobert, X. (2021). Deep learning based automatic hyperbola detection on GPR data for buried utility pipes mapping. *In 2021 11th International Workshop on Advanced Ground*

Penetrating Radar (IWAGPR), 1-6. https://doi.org/10.1109/IWAGPR50767.2021.9843151.

Javadnejad, F., Simpson, C., Gillins, D. T., Claxton, T., & Olsen, M. H. (2017). An assessment of uas-based photogrammetry for civil integrated management (CIM) modeling of pipes. *Pipelines 2017*. https://doi.org/10.1061/9780784480885.012.

Jaw, S. W., & Hashim, M. (2013). Locational accuracy of underground utility mapping using ground penetrating radar. *Tunnelling and Underground Space Technology*, *35*, 20–29. https://doi.org/10.1016/j.tust.2012.11.007.

Jeong, H. M., & Abraham, D. M. (2004). A decision tool for the selection of imaging technologies to detect underground infrastructure. *Tunnelling and Underground Space Technology*, *19*(2), 175–191. https://doi.org/10.1016/j.tust.2003.09.001

Jiang, G., Zhou, X., Li, J., & Chen, H. (2019). A cable-mapping algorithm based on ground-penetrating radar. *IEEE Geoscience and Remote Sensing Letters*, 16(10), 1630-1634. https://doi.org/10.1109/LGRS.2019.2902890.

Jiang, S. P., Jiang, C., & Jiang, W. (2020). Efficient structure from motion for large-scale UAV images: A review and a comparison of SfM tools. *ISPRS Journal of Photogrammetry and Remote Sensing*, 167, pp. 230–251. https://doi.org/10.1016/j.isprsjprs.2020.04.016.

Jiang, Y., Gong, X., Liu, D., Cheng, Y., Fang, C., Shen, X., Yang, J., Zhou, P., & Wang, Z. (2021). EnlightenGAN: Deep light enhancement without paired supervision. *IEEE Transactions on Image Processing*, *30*, pp. 2340–2349. https://doi.org/10.1109/tip.2021.3051462.

Joakim, B. H., Madadi, M., Escalera, S., & Moeslund, T. B. (2022). Multi-task classification of sewer pipe defects and properties using a cross-task graph neural network decoder. *In 2022 IEEE/CVF Winter Conference on Applications of Computer Vision (WACV)*. https://ieeexplore.ieee.org/stamp/stamp.jsp?arnumber=9706846.

Kanellakis, C., Karvelis, P., & Nikolakopoulos, G. (2019). On image-based enhancement for 3d dense reconstruction of low light aerial visual inspected environments. *In Science and Information Conference.* pp. 265-279. https://doi.org/10.1007/978-3-030-17798-0_23.

Karaa, F. A., Katz, A., & Niver, E. (2014). Decision analysis of preferred methods for locating underground conduits. *Journal of Pipeline Systems Engineering and Practice*, *5*(2). https://doi.org/10.1061/(asce)ps.1949-1204.0000162

Karsznia, K. R., Onyszko, K., & Borkowska, S. (2021). Accuracy tests and precision assessment of localizing underground utilities using GPR detection. *Sensors*, 21(20), pp. 6765. https://doi.org/10.3390/s21206765.

Kaur, P., Dana, K. J., Romero, F. A., & Gucunski, N. (2016). Automated GPR rebar analysis for robotic bridge deck evaluation. *Institute of Electrical and Electronics Engineers* (*IEEE) Transactions on Cybernetics, 46*(10), pp. 2265–2276. https://doi.org/10.1109/tcyb.2015.2474747.

Khan, A., Qureshi, A. S., Wahab, N., Hussain, M., & Hamza, M. Y. (2021). A recent survey on the applications of genetic programming in image processing.

Computational Intelligence, 37(4), pp. 1745-1778. https://doi.org/10.1111/coin.12459.

Khan, M. A., Al-Nuaimy, W., & El-Samie, F. E. A. (2010). Detection of landmines and underground utilities from acoustic and GPR images with a cepstral approach. *Journal of Visual Communication and Image Representation*, *21*(7), 731–740. https://doi.org/10.1016/j.jvcir.2010.05.007.

Killam, L. (2013). Research terminology simplified: Paradigms, axiology, ontology, epistemology and methodology. Ontario, Canada, Laura Killam. 0993622801.

Kim, G., Kwon, D., & Kwon, J. (2019a). Low-lightgan: Low-light enhancement via advanced generative adversarial network with task-driven training. *In 2019 IEEE International Conference on Image Processing (ICIP)*. pp. 2811-2815. https://doi.org/10.1109/icip.2019.8803328.

Kim, N., Kim, S., An, Y. K., & Lee, J. J. (2019b). A novel 3D GPR image arrangement for deep learning-based underground object classification. *International Journal of Pavement Engineering, 22*(6), pp. 740–751. https://doi.org/10.1080/10298436.2019.1645846.

Ko, H., & Kim, N. (2019). Performance analysis of Detecting buried pipelines in GPR images using Faster R-CNN. *Journal of Convergence Information Technology, 9*(5), pp. 21–26. https://doi.org/10.22156/cs4smb.2019.9.5.021.

Kipf, T, N & Welling, M. (2017). Semi-supervised classification with graph convolutional networks. *Arxiv*. https://doi.org/10.48550/arXiv.1609.02907.

Kropp, C., Koch, C., & König, M. (2018). Interior construction state recognition with 4D BIM registered image sequences. *Automation in Construction*, *86*, pp. 11–32. https://doi.org/10.1016/j.autcon.2017.10.027.

Kumar, B., & Sommerville, J. (2012). A model for RFID-based 3D location of buried assets. *Automation in Construction, 21,* 121–131. https://doi.org/10.1016/j.autcon.2011.05.020.

Kuppannagari, S., Fu, Y., Cheung, C, M., & Prasanna, V. K. (2021). Spatio-temporal missing data imputation for smart power grids. *In proceedings of the Twelfth ACM International Conference on Future Energy Systems*. https://doi.org/10.1145/3447555.3466586.

Lacroix, M. (2015). Dealing with topological relations in underground networks. *In Proceedings of Int. Conf*, 21, pp. 12-14. http://intercarto.msu.ru/jour/data/v7/article217.pdf.

Lagüela, S., Solla, M., Puente, I., & Prego, F. (2018). Joint use of GPR, IRT and TLS techniques for the integral damage detection in paving. *Construction and Building Materials, 174,* 749–760. https://doi.org/10.1016/j.conbuildmat.2018.04.159.

Lai, T. T., Chen, Y. H., Huang, P., & Chu, H. H. (2010). PipeProbe: a mobile sensor droplet for mapping hidden pipeline. *In Proceedings of the 8th ACM Conference on Embedded Networked Sensor Systems,* 113-126. https://doi.org/10.1145/1869983.1869996.

Lai, W. W., & Sham, J. F. (2023). Standardizing non-destructive underground utility

survey methods. *Tunnelling and Underground Space Technology*, 134, 104933. https://doi.org/10.1016/j.tust.2022.104933.

Lai, W. W., Derobert, X., & Annan, P. (2017). A review of Ground Penetrating Radar application in civil engineering: A 30-year journey from locating and testing to imaging and diagnosis. *NDT & E International*, *96*, 58–78. https://doi.org/10.1016/j.ndteint.2017.04.002.

Lau, P. C. K., Cheung, B. W., Lai, W. W., & Sham, J. F. (2021). Characterizing pipe leakage with a combination of GPR wave velocity algorithms. *Tunnelling and Underground Space Technology*, *109*, 103740. https://doi.org/10.1016/j.tust.2020.103740.

Lecun, Y., Bottou, L., Bengio, Y., Haffner, P. (1998). Gradient-based learning applied to document recognition. *In Proceedings of the IEEE*, 86, 11, 2278-2324. https://doi.org/10.1109/5.726791.

Lee, E., W, Lee & P. K. Tae. (2011). Availability analysis of IMU system for underground facility surveying. *Korean Cadastre Inf. Assoc*, 13(2), 63–69. https://www.dbpia.co.kr/journal/articleDetail?nodeId=NODE01770417&language=ko_KR&hasTopBanner=true.

Lee, J., Son, H., & Kim, C. (2013). Skeleton-based 3D reconstruction of as-built pipelines from laser-scan data. *Automation in Construction*, *35*, 199–207. https://doi.org/10.1016/j.autcon.2013.05.009.

Lee, M., Choi, S., Jeon, H., & Kim, S. W. (2020). Development of 3D underground utilities processing and partial update automation technology - focused on 3D underground geospatial map. *Journal of the Korean Association of Geographic Information Studies*, 23(4), 1–15. https://doi.org/10.11108/kagis.2020.23.4.001.

Lei, W., Hou, F., Xi, J., Tan, Q., Xu, M., Jiang, X., Liu, G., & Gu, Q. (2019). Automatic hyperbola detection and fitting in GPR B-scan image. *Automation in Construction, 106*, pp. 102839. https://doi.org/10.1016/j.autcon.2019.102839.

Leinov, E., Lowe, M. J., & Cawley, P. (2015). Investigation of guided wave propagation and attenuation in pipe buried in sand. *Journal of Sound and Vibration, 347, 96*-114. https://doi.org/10.1016/j.jsv.2015.02.036.

Lhuillier, M., & Lin, P. (2005). A quasi-dense approach to surface reconstruction from uncalibrated images. *IEEE Transactions on Pattern Analysis and Machine Intelligence*, *27*(3), pp. 418–433. https://doi.org/10.1109/tpami.2005.44.

Li, C., Guo, C., Han, L., Jiang, J., Cheng, M. M., Gu, J., & Loy, C. C. (2022). Low-light image and video enhancement using deep learning: A survey. *IEEE transactions on pattern analysis and machine intelligence*, 44(12), 9396-9416. https://doi.org/10.1109/TPAMI.2021.3126387.

Li, C., Guo, J., Porikli, F., & Li, X. (2018a). LightenNet: A convolutional neural network for weakly illuminated image enhancement. *Pattern Recognition Letters*, *104*, pp. 15–22. https://doi.org/10.1016/j.patrec.2018.01.010.

Li, H., Chou, C. J., Fan, L., Li, B., Wang, D., & Song, D. (2020a). Toward automatic subsurface pipeline mapping by fusing a ground-penetrating radar and a camera.

IEEE Transactions on Automation Science and Engineering, *17*(2), 722–734. https://doi.org/10.1109/tase.2019.2941848.

Li, H., Li, N., Wu, R., Wang, H., Gui, Z., & Song, D. (2021). GPR-RCNN: An algorithm of subsurface defect detection for airport runway based on GPR. *Institute of Electrical and Electronics Engineers (IEEE) Robotics and Automation Letters, 6*(2), pp. 3001–3008. https://doi.org/10.1109/lra.2021.3062599.

Li, S., Cai, H., Abraham, D. M., & Mao, P. (2016). Estimating features of underground utilities: hybrid GPR/GPS approach. *Journal of Computing in Civil Engineering, 30*(1). https://doi.org/10.1061/(asce)cp.1943-5487.0000443.

Li, S., Cai, H., & Kamat, V. R. (2015). Uncertainty-aware geospatial system for mapping and visualizing underground utilities. *Automation in Construction*, 53, 105-119. https://doi.org/10.1016/J.AUTCON.2015.03.011.

Li, W., Zhou, H., & Wan, X. (2012). Generalized Hough transform and ANN for subsurface cylindrical object location and parameters inversion from GPR data. *In 2012 14th International Conference on Ground Penetrating Radar (GPR) IEEE.* pp. 281-285. https://doi.org/10.1109/ICGPR.2012.6254874.

Li, X., Yi, W., Chi, H. L., Wang, X., & Chan, A. P. (2018b). A critical review of virtual and augmented reality (VR/AR) applications in construction safety. *Automation in Construction*, 86, 150-162. https://doi.org/10.1016/j.autcon.2017.11.003.

Li, Y., Zhao, Z., Luo, Y., & Qiu, Z. (2020b). Real-time pattern-recognition of gpr images with yolo v3 implemented by Tensorflow. *Sensors, 20*(22), pp. 6476. https://doi.org/10.3390/s20226476.

Lin, J., Zheng, C., Xu, W., & Zhang, F. (2021). R2LIVE: A robust, real-time, lidar-inertial-visual tightly-coupled state estimator and mapping. *ArXiv (Cornell University)*. https://doi.org/10.48550/arxiv.2102.12400.

Lin, T. Y., Goyal, P., Girshick, R., He, K., & Dollar, P. (2017). Focal loss for dense object detection. In *2017 Institute of Electrical and Electronics Engineers (IEEE) International Conference on Computer Vision (ICCV)*. https://doi.org/10.1109/iccv.2017.324.

Little, R. J., & Rubin, D. B. (2019). Statistical analysis with missing data (Third edition). New York, NY: John Wiley & Sons. https://doi.org/10.1002/9781119482260.

Liu, H., Lin, C., Cui, J., Fan, L., Xie, X., & Spencer, B. F. (2020). Detection and localization of rebar in concrete by deep learning using ground penetrating radar. *Automation in Construction, 118*, pp. 103279. https://doi.org/10.1016/j.autcon.2020.103279.

Liu, H., Yue, Y., Liu, C., Spencer Jr, B. F., & Cui, J. (2023). Automatic recognition and localization of underground pipelines in GPR B-scans using a deep learning model. *Tunnelling and Underground Space Technology*, 134, 104861. https://doi.org/10.1016/j.tust.2022.104861.

Liu, R., & Issa, R. R. A. (2012). 3D Visualization of sub-surface pipelines in connection with the building utilities: integrating GIS and BIM for facility

management. *Computing in Civil Engineering (2012)*. https://doi.org/10.1061/9780784412343.0043

Liu, W. D., Erhan, D., Szegedy, C., Reed, S., Fu, C., & Berg, A. C. (2016). SSD: Single Shot MultiBox Detector. *European Conference on Computer Vision (ECCV) 2016. Lecture Notes in Computer Science*. pp. 9905. https://doi.org/10.1007/978-3-319-46448-0_2.

Liu, Y., Chan, W., & Chen, Y. (1995). Automatic white balance for digital still camera. *IEEE Transactions on Consumer Electronics*, *41*(3), pp. 460–466. https://doi.org/10.1109/30.468045.

Liu, Z., & Kleiner, Y. (2013). State of the art review of inspection technologies for condition assessment of water pipes. *Measurement, 46(1),* 1-15. https://doi.org/10.1016/j.measurement.2012.05.032.

Lore, K. G., Akintayo, A., & Sarkar, S. (2017). LLNet: A deep autoencoder approach to natural low-light image enhancement. *Pattern Recognition*, *61*, pp. 650–662. https://doi.org/10.1016/j.patcog.2016.06.008.

Lowe, D. G. (1999). Object recognition from local scale-invariant features. *International Conference on Computer Vision*. https://doi.org/10.1109/iccv.1999.790410.

Lowe, D. J. (2004). Distinctive Image Features from Scale-Invariant Keypoints. *International Journal of Computer Vision*, *60*(2), pp. 91–110. https://doi.org/10.1023/b:visi.0000029664.99615.94.

Lu, C., Xu, L., & Jia, J. (2012). Contrast preserving decolorization. *In 2012 IEEE international conference on computational photography (ICCP).* pp. 1-7. https://doi.org/10.1109/iccphot.2012.6215215.

Lueke, J. S., Pinghe, S., & Ariaratnam, S. T. (2011). Application of digital photogrammetry in trenchless engineering. In *International Conference on Pipelines and Trenchless Technology 2011American Society of Civil EngineersChina University of GeosciencesUniversity of Texas, ArlingtonChina University of GeosciencesChina Ministry of EducationChina Petroleum Pipeline Bureau Wuhan Deawon Trenchless Technology Company Limited*. https://doi.org/10.1061/41202(423)230.

Lv, F., Y. Li & F. Lu. (2021). Attention guided low-light image enhancement with a large scale low-light simulation dataset. *International Journal of Computer Vision*, 129(7), 2175-2193. https://doi.org/10.48550/arXiv.1908.00682.

Ma, L., Ma, T., Liu, R., Fan, X., & Luo, Z. (2022). Toward fast, flexible, and robust low-light image enhancement. *In Proceedings of the IEEE/CVF Conference on Computer Vision and Pattern Recognition.* pp. 5637-5646. https://doi.org/10.1109/cvpr52688.2022.00555.

Ma, Z., & Liu, S. (2018). A review of 3D reconstruction techniques in civil engineering and their applications. *Advanced Engineering Informatics*, *37*, pp. 163–174. https://doi.org/10.1016/j.aei.2018.05.005.

Maalek, R., Lichti, D. D., & Maalek, S. (2021). Towards automatic digital documentation and progress reporting of mechanical construction pipes using

smartphones. *Automation in Construction*, *127*, 103735. https://doi.org/10.1016/j.autcon.2021.103735.

Maalek, R., Lichti, D. D., & Ruwanpura, J. Y. (2018). Robust segmentation of planar and linear features of terrestrial laser scanner point clouds acquired from construction sites. *Sensors*, *18*(3), 819. https://doi.org/10.3390/s18030819.

Maas, C., & Schmalzl, J. (2013). Using pattern recognition to automatically localize reflection hyperbolas in data from ground penetrating radar. *Computers & Geosciences*, *58*, 116–125. https://doi.org/10.1016/j.cageo.2013.04.012.

MacDonald, L., Hindmarch, J., Robson, S., & Terras, M. (2014). Modelling the appearance of heritage metallic surfaces. *The International Archives of Photogrammetry, Remote Sensing and Spatial Information Sciences, 40(5)*, pp. 371. https://doi.org/10.5194/isprsarchives-xl-5-371-2014.

Manataki, M., Vafidis, A., & Sarris, A. (2021). GPR data interpretation approaches in archaeological prospection. *Applied Sciences*, 11(16), 7531. https://doi.org/10.3390/app11167531.

Maree, S., Rotimi, F. E., & Rotimi, J. O. B. (2021). The primacy of as-built drawings in the management of underground utility operations: A New Zealand study. *Buildings*, 11(9), 399. https://doi.org/10.3390/buildings11090399.

Mark, S. (2010). Unique Autonomous Pipeline Mapping System: An Overview. *In the 18th Pipeline Technology Conference in BERLIN*. https://www.pipeline-conference.com/abstracts/unique-autonomous-pipeline-mapping-system.

Mat Junoh, M. S. A., Sulaiman, S. A. H., Natnan, S. R., & Purwanto, H. (2022). Estimation diameter of buried pipe using principle of ground penetrating radar and electromagnetic locator. *International Journal of Geoinformatics*, 18(4). https://doi.org/10.52939/ijg.v18i4.2261.

Metcalf, M. D., Hui, K., Hoffman, D. J., Castellanos, V., Thorstenson, M., Skipper, G., & Tarkenton, G. M. (2020). Acoustic-based underground utility mapping at the annacis island WWTP. *Pipelines 2020*. https://doi.org/10.1061/9780784483213.039.

Meijer, D., Korving, H., & Clemens-Meyer, F. (2022). A topological characterisation of looped drainage networks. *Structure and Infrastructure Engineering*, 1-14. https://doi.org/10.1080/15732479.2022.2152464.

Metje, N., Atkins, P. R., Brennan, M. J., Chapman, D. F., Lim, H. S., Machell, J., Muggleton, J. M., Pennock, S. R., Ratcliffe, J. G., Redfern, M. S., Rogers, C. D. F., Saul, A. J., Qi, S., Swingler, S., & Thomas, A. W. (2007). Mapping the Underworld-State-of-the-art review. *Tunnelling and Underground Space Technology*, *22*(5–6), 568–586. https://doi.org/10.1016/j.tust.2007.04.002

Metje, N., Hojjati, A., Beck, A., & Rogers, C. D. (2020). Improved underground utilities asset management–assessing the impact of the UK utility survey standard (PAS128). *In Proceedings of the Institution of Civil Engineers-Municipal Engineer. 173, 4.* pp. 218-236.

Molyneaux, T., Millard, S., Bungey, J., & Zhou, J. (1995). Radar assessment of structural concrete using neural networks. *Nondestructive Testing and Evaluation*

(NDT & E) International, 28(5), pp. 281–288. https://doi.org/10.1016/0963-8695(95)00027-u.

Mooney, J. P., Ciampa, J. D., Young, G. N., Kressner, A. R., & Carbonara, J. (2010). GPR mapping to avoid utility conflicts prior to construction of the M-29 transmission line. *In IEEE PES T&D 2010 (pp. 1-8). IEEE.* https://doi.org/10.1109/TDC.2010.5484564.

Muggleton, J. M., & Brennan, M. J. (2002). Axisymmetric wave propagation in buried, fluid-filled pipes: effects of the surrounding medium. *Proceedings of the Institute of Acoustics, 24*(2). http://eprints.soton.ac.uk/id/eprint/10050.

Naghshbandi, S. N., Varga, L., & Hu, Y. (2021). Technologies for safe and resilient earthmoving operations: A systematic literature review. *Automation in Construction, 125,* 103632. https://doi.org/10.1016/j.autcon.2021.103632

Nguyen, L. D., Nguyen, T. K., Tran, D. Q., & Villiers, C. (2014a). Productivity in daytime and nighttime construction of urban sewer systems. *Journal of construction engineering and management*, 140(7), 04014021. https://doi.org/10.1061/(ASCE)CO.1943-7862.00008.

Nguyen, L. D., Nguyen, T. K. N., & Tran, D. Q. (2014b). Shift work and labor productivity in urban sewer construction. *In Construction Research Congress 2014: Construction in a Global Network,* 877-886. https://doi.org/10.1061/9780784413517.090.

North, D. (2010). Buried treasure: A transportation department leads utilities in deploying radio-based marking technology. *Public Works*, *141*(1). https://trid.trb.org/view/920635

Oguntoye, K. S., Laflamme, S., Sturgill, R., & Eisenmann, D. J. (2023). Review of artificial intelligence applications for virtual sensing of underground utilities. *Sensors*, 23(9), 4367. https://doi.org/10.3390/s23094367.

Oliver, L., Khadijah., S. Ainon., O. Hezri, R., Nafisah, K. (2020). Accuracy assessment on underground utility equipment. *Built Environment Journal*, 17(3):57. https://ir.uitm.edu.my/id/eprint/41997.

Onyszko, K., & Fryśkowska-Skibniewska, A. (2021). A new methodology for the detection and extraction of hyperbolas in GPR images. *Remote Sensing, 13*(23), pp. 4892. https://doi.org/10.3390/rs13234892.

Ortega, S., Wendel, J., Santana, J. C. C., Murshed, S. M., Boates, I., Trujillo, A., Nichersu, A., & Suárez, J. A. (2019). Making the invisible visible—strategies for visualizing underground infrastructures in immersive environments. *ISPRS International Journal of Geo-Information, 8*(3), 152. https://doi.org/10.3390/ijgi8030152.

Osman, M. S., Abu-Mahfouz, A., & Page, P. (2018). A survey on data imputation techniques: water distribution system as a use case. *IEEE Access*, 6, 63279-63291. https://doi.org/10.1109/ACCESS.2018.2877269.

Özkaya, U., Öztürk, A., Melgani, F., & Seyfi, L. (2021). Residual CNN + Bi-LSTM model to analyze GPR B scan images. *Automation in Construction, 123*, pp. 103525. https://doi.org/10.1016/j.autcon.2020.103525.

Pascale, D. (2006). RGB coordinates of the macbeth colour checker. *The Babel Colour Company: Montreal, Canada*, pp. 1–16. https://www.xrite.com/service-support/new_color_specifications_for_colorchecker_sg_and_classic_charts. (Accessed on 10 November 2022).

Pasolli, E., Melgani, F., & Donelli, M. (2010). Gaussian process approach to buried object size estimation in GPR Images. *Institute of Electrical and Electronics Engineers (IEEE) Geoscience and Remote Sensing Letters, 7(1),* pp. 141–145. https://doi.org/10.1109/lgrs.2009.2028697.

Patel, A. A., & Chasey, A. D. (2010a). Integrating GPS and laser technology to map underground utilities installed using open trench method. *Construction Research Congress 2010. Innovation for Reshaping Construction Practice American Society of Civil Engineers*. https://doi.org/10.1061/41109(373)63.

Patel, A., Chasey, A. D., & Ariaratnam, S. T. (2010b). Integrating global positioning system with laser technology to capture as-built information during open-cut construction. *Journal of Pipeline Systems Engineering and Practice*, *1*(4), 147–155. https://doi.org/10.1061/(asce)ps.1949-1204.0000065.

Pătrăucean, V., Armeni, I., Nahangi, M., Yeung, J., Brilakis, I., & Haas, C. (2015). State of research in automatic as-built modelling. *Advanced Engineering Informatics, 29(2)*, pp. 162-171. https://doi.org/10.1016/j.aei.2015.01.001.

Pennock, S. R., Chapman, D. N., Rogers, C. D. F., Royal, A. C. D., Naji, A., & Redfern, M. A. (2010). Effects of iron pipe corrosion on GPR detection. *In Proceedings of the XIII Internarional Conference on Ground Penetrating Radar IEEE.* (pp. 1-5). https://doi.org/10.1109/ICGPR.2010.5550072.

Pham, M. T., & Lefevre, S. (2018). Buried object detection from b-scan ground penetrating radar data using Faster-RCNN. *2018 - 2018 Institute of Electrical and Electronics Engineers (IEEE) International Geoscience and Remote Sensing Symposium*. https://doi.org/10.1109/igarss.2018.8517683.

Pickering, D., Park, J. M., & Bannister, D. H. (1993). Utility mapping and record keeping for infrastructure. *Urban Management Programme*. 0821324268.

Pipeline and Hazardous Materials Safety Administration (PHMSA). (2021). *All Reported Pipeline Incidents by Cause*. https://portal.phmsa.dot.gov/analytics/saw.dll?Portalpages&PortalPath=%2Fshared%2FPDM%20Public%20Website%2F_portal%2FSC%20Incident%20Trend&Page=All%20Reported. (Access date: 04/05/2023).

Plati, C., & Dérobert, X. (2015). Inspection procedures for effective GPR sensing and mapping of underground utilities and voids, with a focus to urban areas. *In Civil engineering applications of ground penetrating radar*, pp. 125-145. https://link.springer.com/content/pdf/10.1007/978-3-319-04813-0.pdf.

Pozo, D., Jaramillo, K., Ponce, D., Torres, A., & Morales, L. (2019). 3D reconstruction technologies for using in dangerous environments with lack of light: a comparative analysis. *Revista Ibérica de Sistemas e Tecnologias de Informação, (E19)*, pp. 507-518. ISSN: 1646-9895.

Prego, F., Solla, M., Puente, I., & Arias, P. (2017). Efficient GPR data acquisition to

detect underground pipes. *NDT & E International*, 91, 22–31. https://doi.org/10.1016/j.ndteint.2017.06.002.

Rachev, R. K., Wilcox, P. D., Velichko, A., McAughey, K., & Giese, J. (2018). Ultrasonic immersion testing for crack detection and depth sizing in large diameter pipes. *In Proc. ECNDT. pp. 1-8*. https://www.ndt.net/article/ecndt2018/papers/ecndt-0084-2018.pdf.

Rajiv, K., Chandra, G. R., & Rao, B. B. (2017). GPR objects hyperbola region feature extraction. *Advances in Computational Sciences and Technology, 10*(5), pp. 789-804. https://www.researchgate.net/publication/317577717_GPR_Objects_Hyperbola_Region_Feature_Extraction.

Rashed, M., & Atef, A. (2015). Mapping underground utilities within conductive soil using multi-frequency electromagnetic induction and ground penetrating radar. *Arabian Journal of Geosciences*, 8, 2341-2346. https://doi.org/10.1007/s12517-014-1358-2.

Redmon, J., & Farhadi, A. (2018). YOLOv3: An incremental improvement. *ArXiv: Computer Vision and Pattern Recognition*. https://arxiv.org/pdf/1804.02767.

Redmon, J., Divvala, S., Girshick, R., & Farhadi, A. (2016). You Only Look Once: Unified, real-time object detection. *2016 Institute of Electrical and Electronics Engineers (IEEE) Conference on Computer Vision and Pattern Recognition (CVPR)*. https://doi.org/10.1109/cvpr.2016.91.

Ren, H., Zhao, Y., Xiao, W., & Hu, Z. (2019). A review of UAV monitoring in mining areas: current status and future perspectives. *International Journal of Coal Science & Technology*, *6*(3), pp. 320–333. https://doi.org/10.1007/s40789-019-00264-5.

Ren, S., He, K., Girshick, R., & Sun, J. (2017). Faster R-CNN: Towards real-time object detection with region proposal networks. *Institute of Electrical and Electronics Engineers (IEEE) Transactions on Pattern Analysis and Machine Intelligence, 39*(6), pp. 1137–1149. https://doi.org/10.1109/tpami.2016.2577031.

Reyes-Acosta, A., Lopez-Juarez, I., Osorio-Comparan, R., & Lefranc, G. (2019). 3D pipe reconstruction employing video information from mobile robots. *Applied Soft Computing, 75*, 562–574. https://doi.org/10.1016/j.asoc.2018.11.016.

Richard H., Canberra, Z. (2003). Multiple view geometry in computer vision. *Cambridge University Press*. https://doi.org/10.1017/CBO9780511811685.

Riegler, G., Ulusoy, A. O., Bischof, H., & Geiger, A. (2017). Octnetfusion: Learning depth fusion from data. *In 2017 International Conference on 3D Vision (3DV).* pp. 57-66. https://doi.org/10.1109/3dv.2017.00017.

Ristić, A. J., Govedarica, M., Vrtunski, M., & Pctrovacki, D. (2014). Application of GPR for creating underground structure model of specific areas of interest. *Ground Penetrating Radar (GPR), 2014 15th International Conference On*. https://doi.org/10.1109/icgpr.2014.6970464.

Rogage, K., Mahamedi, E., Brilakis, I., & Kassem, M. (2022). Beyond digital shadows: Digital Twin used for monitoring earthwork operation in large infrastructure

projects. *AI in Civil Engineering*, 1(1), 7. https://doi.org/10.1007/s43503-022-00009-5.

Roncella, R., Bruno, N., Diotri, F., Thoeni, K., & Giacomini, A. (2021). Photogrammetric digital surface model reconstruction in extreme low-light environments. *Remote Sensing*, *13*(7), pp. 1261. https://doi.org/10.3390/rs13071261.

Rosten, E., & Drummond, T. (2006). Machine learning for high-speed corner detection. *Lecture Notes in Computer Science, 3951*, pp. 430–443. https://findanexpert.unimelb.edu.au/scholarlywork/1596023-machine-learning-for-high-speed-corner-detection.

Rublee, E., Rabaud, V., Konolige, K., & Bradski, G. (2011). ORB: An efficient alternative to SIFT or SURF. *In 2011 International conference on computer vision.* pp. 2564-2571. https://doi.org/10.1109/iccv.2011.6126544.

Rumelhart, D., Hinton, G., & Williams, R. (2019). Learning representations by back-propagating errors. *Nature,* 323, 533–536. https://doi.org/10.1038/323533a0.

Saeed, N., Alouini, M. S., & Al-Naffouri, T. Y. (2019). Toward the internet of underground things: A systematic survey. *IEEE Communications Surveys & Tutorials, 21*(4), 3443-3466. https://doi.org/10.1109/COMST.2019.2934365.

Safavian, S. R & Landgrebe, D. (1991). A survey of decision tree classifier methodology. *In IEEE Transactions on Systems, Man, and Cybernetics,* 21(3), 660-674. https://doi.org/10.1109/21.97458.

Sagnard, F., & Tarel, J. P. (2016). Template-matching based detection of hyperbolas in ground-penetrating radargrams for buried utilities. *Journal of Geophysics and Engineering, 13*(4), pp. 491–504. https://doi.org/10.1088/1742-2132/13/4/491.

Salim, S. I. S., Zakaria, A., Nordin, N. A., & Mohamed, S. (2022). Implementation of EML and GPR technology for underground utilities detection. Engineering, Agriculture, *Science and Technology Journal (EAST-J)*, 1(1), 75-80. https://doi.org/10.37698/eastj.v1i1.129.

Samuelsson. O., Björk, A., Zambrano, J., & Carlsson, B. (2017). Gaussian process regression for monitoring and fault detection of wastewater treatment processes. *Water science and technology*, 75 12, 2952-2963. https://api.semanticscholar.org/CorpusID:11825445.

Santise, M., Thoeni, K., Roncella, R., Diotri, F., & Giacomini, A. (2018). Analysis of low-light and night-time stereo-pair images for photogrammetric reconstruction. *The International Archives of the Photogrammetry, Remote Sensing and Spatial Information Sciences, XLII–2*, pp. 1015–1022. https://doi.org/10.5194/isprs-archives-xlii-2-1015-2018.

Šarlah, N., Podobnikar, T., Ambrožič, T., & Mušič, B. (2020). Application of Kinematic GPR-TPS model with high 3D georeference accuracy for underground utility infrastructure mapping: a case study from urban sites in Celje, Slovenia. *Remote Sensing, 12*(8), 1228. https://doi.org/10.3390/rs12081228.

Schonberger, J. L., & Frahm, J. M. (2016). Structure-from-motion revisited. *In Proceedings of the IEEE conference on computer vision and pattern recognition.*

pp. 4104-4113. https://doi.org/10.1109/cvpr.2016.445.

Sen, D., Sen, P., & Das, A. M. (2009). *RFID for energy & utility industries*. Pennwell Books. ISSN: 0196-6006. https://www.proquest.com/docview/200145930?accountid=10382&forcedol=true&pq-origsite=primo.

Sharafat, A., Khan, M. S., Latif, K., Tanoli, W. A., Park, W., & Seo, J. (2021). BIM-GIS-based integrated framework for underground utility management system for earthwork operations. *Applied Sciences*, 11(12), 5721. https://doi.org/10.3390/app11125721.

Shen, C., Wang, Q., & Priebe, C. E. (2022). One-Hot graph encoder embedding. *IEEE Transactions on Pattern Analysis and Machine Intelligence*. https://arxiv.org/pdf/2109.13098.pdf.

Shokri, N. H., Amin, Z. M., & Seli, V. A. (2020). Non-destruction method for detecting corroded underground pipe using ground penetrating radar. *In IOP Conference Series: Earth and Environmental Science (Vol. 540, No. 1,* p. 012027). https://doi.org/10.1088/1755-1315/540/1/012027.

Singh, N. P., & Nene, M. J. (2013). Buried object detection and analysis of GPR images: Using neural network and curve fitting. *In 2013 Annual International Conference on Emerging Research Areas and 2013 International Conference on Microelectronics, Communications and Renewable Energy*. pp. 1-6. https://doi.org/10.1109/AICERA-ICMiCR.2013.6576024.

Sim, Y. S., J. S. Hwang, S. D. Mun, T. J. Kim & S. J. Chang. (2022). Missing data imputation algorithm for transmission systems based on multivariate imputation with principal component analysis. *IEEE Access*, 10, 83195-83203. https://doi.org/10.1109/ACCESS.2022.3194545.

Siu, K., & Lai, W. W. (2019). A lab study of coupling effects of electromagnetic induction on underground utilities. *Journal of Applied Geophysics, 164,* 26–39. https://doi.org/10.1016/j.jappgeo.2019.02.002.

Skartados, E., Kargakos, A., Tsiogas, E., Kostavelis, I., Giakoumis, D., & Tzovaras, D. (2019). GPR Antenna localization based on A-scans. *In 2019 27th European Signal Processing Conference,* 1-5. https://doi.org/10.23919/EUSIPCO.2019.8902528.

Smith, A., Moore, I. D., & Dixon, N. (2019). Acoustic emission sensing of pipe–soil interaction: full-scale pipelines subjected to differential ground movements. *Journal of Geotechnical and Geoenvironmental Engineering, 145*(12). https://doi.org/10.1061/(asce)gt.1943-5606.0002185.

Sobbahi, R. A., & Tekli, J. (2022). Comparing deep learning models for low-light natural scene image enhancement and their impact on object detection and classification: Overview, empirical evaluation, and challenges. *Signal Processing-Image Communication, 109,* pp. 116848. https://doi.org/10.1016/j.image.2022.116848.

Sohaib, M., Ahmed, N., & Minallah, N. (2013). Image enhancement for the 3-d reconstruction in the uncontrolled environment using shape from silhouette.

International Journal of Computer Applications. pp.*975,* 8887. https://www.researchgate.net/profile/Nasir-Ahmad-13/publication/259235145_Image_Enhancement_for_the_3-D_Reconstruction_in_the_Uncontrolled_Environment_using_Shape_from_Silhouette/links/00b4952a9a9f846748000000/Image-Enhancement-for-the-3-D-Reconstruction-in-the-Uncontrolled-Environment-using-Shape-from-Silhouette.pdf.

Solla, M., Asorey-Cacheda, R., Núñez-Nieto, X., & Conde-Carnero, B. (2016). Evaluation of historical bridges through recreation of GPR models with the FDTD algorithm. *Ndt & E International, 77,* 19-27. https://doi.org/10.1016/j.ndteint.2015.09.003.

Son, H., & Kim, C. (2016). Automatic segmentation and 3D modeling of pipelines into constituent parts from laser-scan data of the built environment. *Automation in Construction*, *68*, 203–211. https://doi.org/10.1016/j.autcon.2016.05.010.

Son, H., Kim, C., & Kim, C. (2015). Fully automated as-built 3D pipeline extraction method from laser-scanned data based on curvature computation. *Journal of Computing in Civil Engineering, 29(4),* B4014003. https://doi.org/10.1061/(ASCE)CP.1943-5487.0000401.

Son, J. W., Moon, G. S., & Kim, Y. (2021). Automatic detection system of underground pipe using 3d gpr exploration data and deep convolutional neural networks. *Journal of the Korea Society of Computer and Information*, 26(2), 27-37. https://doi.org/10.9708/jksci.2021.26.02.027.

Soni, A. K. (2017). Underground utilities: Constructing a sustainable future. *Indian Mining & Engineering Journal*, 56(10), 25-29. http://cimfr.csircentral.net/id/eprint/1852.

Srebotnjak. T., Carr, G., Sherbinin, A., & Rickwood, C. (2012). A global water quality index and hot-deck imputation of missing data. *Ecological Indicators*, 17, 108-119. https://doi.org/10.1016/j.ecolind.2011.04.023.

State Planning Commission of China and Ministry of Construction of China. (2002). Regulations on the administration of fees for engineering survey and design. http://www.dzwzjsoft.com/update/other/%E5%B7%A5%E7%A8%8B%E5%8B%98%E5%AF%9F%E8%AE%BE%E8%AE%A1%E6%94%B6%E8%B4%B9%E6%A0%87%E5%87%86(2002%E5%B9%B4%E4%BF%AE%E8%AE%A2%E6%9C%AC)%E5%AE%8C%E6%95%B4%E7%89%88.pdf. (Access date: 28/ 12/2023).

Stanić, N., Lepot, M., Catieau, M., Langeveld, J., & Clemens, F. (2017). A technology for sewer pipe inspection (part 1): Design, calibration, corrections and potential application of a laser profiler. *Automation in Construction, 75,* 91–107. https://doi.org/10.1016/j.autcon.2016.12.005.

Sterling, R. L., State and Local Government Committee of America. (2000). Utility locating technologies. Federal Laboratory Consortium. https://agris.fao.org/agris-search/search.do?recordID=US201300068375.

Stylianidis, E., Valari, E., Pagani, A., Carrillo, I., Kounoudes, A., Michail, K., &

Smagas, K. (2020). Augmented reality geovisualisation for underground utilities. *Pfg – Journal of Photogrammetry, Remote Sensing and Geoinformation Science*, *88*(2), 173–185. https://doi.org/10.1007/s41064-020-00108-x.

Sueri, M., & Erdal, M. Ü. R. S. E. L. (2022). Early estimation of sewerage line costs with regression analysis. *Gazi University Journal of Science*, 35(3), 822-832. https://doi.org/10.35378/gujs.949726.

Syambas, N. R. (2012). An approach for predicting the shape and size of a buried basic object on surface ground penetrating radar system. *International Journal of Antennas and Propagation, 2012*, pp. 1–13. https://doi.org/10.1155/2012/919741.

Tabarro, P. G., Pouliot, J., Fortier, R., & Losier, L. M. (2017). A WebGIS to support GPR 3D data acquisition: A first step for the integration of underground utility networks in 3D city models. *The International Archives of the Photogrammetry, Remote Sensing and Spatial Information Sciences*, 42, 43-48. https://doi.org/10.5194/ISPRS-ARCHIVES-XLII-4-W7-43-2017.

Talmaki, S. A. (2012). Real-time hybrid virtuality for prevention of excavation related utility strikes (Doctoral dissertation). https://doi.org/10.1061/(ASCE)CP.1943-5487.0000269.

Talmaki, S., Kamat, V. R., & Cai, H. (2013). Geometric modeling of geospatial data for visualization-assisted excavation. *Advanced Engineering Informatics*, *27*(2), 283–298. https://doi.org/10.1016/j.aei.2013.01.004

Tang, R., Zhang, G., & Liu, X. (2019). A stereo matching with reconstruction network for low-light stereo vision. *In Proceedings of the 2019 2nd International Conference on Signal Processing and Machine Learning.* pp. 98-102. https://doi.org/10.1145/3372806.3372821.

Tanoli, W. A., Sharafat, A., Park, J., & Seo, J. J. (2019). Damage prevention for underground utilities using machine guidance. *Automation in Construction*, *107*, pp. 102893. https://doi.org/10.1016/j.autcon.2019.102893.

Templ, M., Kowarik, A., & Filzmoser, P. (2011). Iterative stepwise regression imputation using standard and robust methods. *Computational Statistics & Data Analysis*, 55 (10), 2793–2806. https://doi.org/10.1016/j.csda.2011.04.012.

Terrasse, G., Nicolas, J. M., Trouve, E., & Drouet, E. (2016). Automatic localization of gas pipes from GPR imagery. *2016 24th European Signal Processing Conference (EUSIPCO)*. https://doi.org/10.1109/eusipco.2016.7760678.

Tosti, F., Benedetto, A., Ciampoli, L. B., Lambot, S., Patriarca, C., & Slob, E. (2016). GPR analysis of clayey soil behaviour in unsaturated conditions for pavement engineering and geoscience applications. *Near Surface Geophysics*, *14*(2), 127–144. https://doi.org/10.3997/1873-0604.2016011.

Triantafyllidou, D., Moran, S., McDonagh, S., Parisot, S., & Slabaugh, G. (2020). Low light video enhancement using synthetic data produced with an intermediate domain mapping. *In Computer Vision–ECCV 2020: 16th European Conference, Glasgow*, 23–28, 103-119. https://doi.org/10.1007/978-3-030-58601-0_7.

Tulloch, M., Hu, W., & Chapman, M. (2006). Mapping underground infrastructure using photogrammetric methods. *In Masters Abstracts International*. Vol. 47, pp. 04. https://www.asprs.org/a/publications/proceedings/reno2006/0157.pdf.

Underground Pipeline Professional Committee of Urban Planning Association of China. (2020). *The 2020 national underground pipeline accident analysis report (Underground Pipeline Professional Committee of Urban Planning Association of China)*. Lingpiankeji. http://www.lingpiankeji.com/newsitem/278381568. (Access date: 04/05/2023).

University of Birmingham., University of Bath., The University of Sheffield & University of Leeds. (2012). Mapping the underworld (MTU). http://www.mappingtheunderworld.ac.uk/MTU%20Brochure%20Final%20Version.pdf. (Access date: 04/05/2023).

Van Son, R. J., Jaw, S. W., & Wieser, A. (2019). A data capture framework for improving the quality of subsurface utility information. *The International Archives of the Photogrammetry, Remote Sensing and Spatial Information Sciences*. https://doi.org/10.5194/isprs-archives-xlii-4-w15-97-2019.

Van Son, R., Jaw, S. W., Yan, J., Khoo, V., Loo, R., Teo, S., & Schrotter, G. (2018). A framework for reliable three-dimensional underground utility mapping for urban planning. *The International Archives of the Photogrammetry, Remote Sensing and Spatial Information Sciences*, 42, 209-214. https://doi.org/10.5194/isprs-archives-XLII-4-W10-209-2018.

Vedaldi, A., & Fulkerson, B. (2010). VLFeat: An open and portable library of computer vision algorithms. *In Proceedings of the 18th ACM international conference on Multimedia.* pp. 1469-1472. https://doi.org/10.1145/1873951.1874249.

Veličković, P., Cucurull, G., Casanova, A., Romero, A., Lio, P., & Bengio, Y. (2018). Graph Attention Networks. *ArXiv*. https://api.semanticscholar.org/CorpusID:3292002.

Veldhuis, H., & Vosselman, G. (1998). The 3D reconstruction of straight and curved pipes using digital line photogrammetry. *Isprs Journal of Photogrammetry and Remote Sensing*, *53*(1), 6–16. https://doi.org/10.1016/s0924-2716(97)00031-2.

Verboven. S., Branden, K. V., & Goos, P. (2007). Sequential imputation for missing values. computational biology and chemistry, 31(5), 320–327. https://doi.org/10.1016/j.compbiolchem.2007.07.001.

Viola, P., & Jones, M. J. (2004). Robust real-time face detection. *International Journal of Computer Vision, 57*(2), pp. 137–154. https://doi.org/10.1023/b:visi.0000013087.49260.fb.

Volker, A., & Van Zon, T. (2013). Ultrasonic multi-skip tomography for pipe inspection. *AIP Conference Proceedings*. https://doi.org/10.1063/1.4789117.

Von H. P. T. (2004). Biases in SPSS 12.0 missing value analysis. *The American Statistician,* 58(2), 160–164. https://doi.org/10.1198/0003130043204.

Wallace. W. L. (2021). Underground utilities imaging and diagnosis. Urban Informatics, 415-438. https://doi.org/10.1007/978-981-15-8983-6_24.

Wang, B., Wang, Q., Cheng, J. C., Song, C., & Yin, C. (2022a). Vision-assisted BIM

reconstruction from 3D LiDAR point clouds for MEP scenes. *Automation in Construction, 133*, 103997. https://doi.org/10.1016/j.autcon.2021.103997.

Wang, B., Yin, C., Luo, H., Cheng, J. C. Y., & Wang, Q. (2021a). Fully automated generation of parametric BIM for MEP scenes based on terrestrial laser scanning data. *Automation in Construction*, *125*, 103615. https://doi.org/10.1016/j.autcon.2021.103615.

Wang, M. (2021b). Ontology-based modelling of lifecycle underground utility information to support operation and maintenance. *Automation in Construction, 132*, pp. 103933. https://doi.org/10.1016/j.autcon.2021.103933.

Wang, M., & Yin, X. (2022b). Construction and maintenance of urban underground infrastructure with digital technologies. *Automation in Construction, 141*, pp. 104464. https://doi.org/10.1016/j.autcon.2022.104464.

Wang, M., Deng, Y., Won, J., & Cheng, J. C. (2019). An integrated underground utility management and decision support based on BIM and GIS. *Automation in Construction*, 107, 102931. https://doi.org/10.1016/j.autcon.2019.102931.

Wang, Q., Wu, B., Zhu, P., Li, P., Zuo, W., & Hu, Q. (2020a). ECA-Net: Efficient channel attention for deep convolutional neural networks. *2020 Institute of Electrical and Electronics Engineers (IEEE) Conference on Computer Vision and Pattern Recognition (CVPR)*. https://doi.org/10.1109/cvpr42600.2020.01155.

Wang, X., & Song, H. (2012). The inertial technology based 3-dimensional information measurement system for underground pipeline. *Measurement, 45*(3), 604–614. https://doi.org/10.1016/j.measurement.2011.08.016.

Wang, Y., Cui, G., & Xu, J. (2020b). Semi-automatic detection of buried rebar in GPR data using a genetic algorithm. *Automation in Construction, 114*, pp. 103186. https://doi.org/10.1016/j.autcon.2020.103186.

Weder, S., Schonberger, J., Pollefeys, M., & Oswald, M. R. (2020). Routedfusion: Learning real-time depth map fusion. *In Proceedings of the IEEE/CVF Conference on Computer Vision and Pattern Recognition.* pp. 4887-4897. https://doi.org/10.1109/cvpr42600.2020.00494.

Wei, C., Wang, W., Yang, W., & Liu, J. (2018). Deep retinex decomposition for low-light enhancement. *British Machine Vision Conference*. pp. 155. https://arxiv.org/pdf/1808.04560.pdf.

Weng, C. C., Chen, H., & Fuh, C. S. (2005). A novel automatic white balance method for digital still cameras. *In 2005 IEEE International Symposium on Circuits and Systems (ISCAS).* pp. 3801-3804. https://doi.org/10.1109/iscas.2005.1465458

Widya, A. R., Monno, Y., Okutomi, M., Suzuki, S., Gotoda, T., & Miki, K. (2021). Stomach 3d reconstruction using virtual chromoendoscopic images. *IEEE Journal of Translational Engineering in Health and Medicine*, *9*, pp. 1–11. https://doi.org/10.1109/jtehm.2021.3062226.

Wilson, S. (2001). What is an indigenous research methodology? *Canadian journal of native education*, 25(2), 175-179. https://www.researchgate.net/profile/Shawn-Wilson-3/publication/234754037_What_Is_an_Indigenous_Research_Methodology/link

s/0a85e5320f48b8d0a3000000/What-Is-an-Indigenous-Research-Methodology.pdf.

Woldesellasse, H., & Tesfamariam, S. (2021). Handling incomplete and missing data in corrosion pit measurement database using imputation methods: model development using artificial neural network. *Journal of Pipeline Systems Engineering and Practice*, 12(3), 04021033. https://doi.org/10.1061/(ASCE)PS.1949-1204.0000572.

Wu, C., Wang, X., Chen, M., & Kim, M. J. (2019). Differential received signal strength-based RFID positioning for construction equipment tracking. Advanced Engineering Informatics, 42, 100960. https://doi.org/10.1016/j.aei.2019.100960.

Wu, F., Zhang, T., Holanda, A., Fifty, C., Yu, T., & Weinberger, K. Q. (2020). Simplifying graph convolutional networks. *Arxiv*. https://doi.org/10.48550/arXiv.1902.07153.

Wu, H., Zheng, S., Zhang, J., & Huang, K. (2018). Fast end-to-end trainable guided filter. *In Proceedings of the IEEE Conference on Computer Vision and Pattern Recognition*, 1838-1847. https://doi.org/10.1109/CVPR.2018.00197.

Wu, J., Bai, Y., Fang, W., Zhou, R., Reniers, G., & Khakzad, N. (2021). An integrated quantitative risk assessment method for urban underground utility tunnels. *Reliability Engineering & System Safety*, 213, 107792. https://doi.org/10.1016/j.ress.2021.107792.

Wu, T., Yeung, S., Jia, J., & Tang, C. (2010). Quasi-dense 3D reconstruction using tensor-based multiview stereo. *Computer Vision and Pattern Recognition*. https://doi.org/10.1109/cvpr.2010.5539796.

Wu, Z., Zhou, Y., & Wang, H. (2020). Real-time prediction of the water accumulation process of urban stormy accumulation points based on deep learning. *IEEE Access*, 8, 151938-151951. https://doi.org/10.1109/ACCESS.2020.3017277.

Xiang, M., Hou, J., Luo, W., Tao, W., & Wang, D. (2021). Impute gene expression missing values via biological networks: Optimal fusion of data and knowledge. *In 2021 International Joint Conference on Neural Networks (IJCNN)*, 1-8. https://doi.org/10.1109/IJCNN52387.2021.9533355.

Xiao, J., Gao, Q., Ling, Y., Yan, J., & Liu, B. (2021). Research on hyperbola detection and fitting in GPR B-scan image. *2021 International Conference on Communications, Information System and Computer Engineering (CISCE), 2021*, pp. 266-270. https://doi.org/10.1109/CISCE52179.2021.9445915.

Xie, F., Lai, W. W., & Dérobert, X. (2021). GPR-based depth measurement of buried objects based on constrained least-square (CLS) fitting method of reflections. *Measurement, 168*, pp. 108330. https://doi.org/10.1016/j.measurement.2020.108330.

Xu, H., & Sinha, S. K. (2021). Modeling pipe break data using survival analysis with machine learning imputation methods. *Journal of Performance of Constructed Facilities*, 35(5), 04021071.

Xue, J., Hou, X., & Zeng, Y. (2021). Review of image-based 3d reconstruction of building for automated construction progress monitoring. *Applied Sciences, 11*(17), pp. 7840. https://doi.org/10.3390/app11177840.

Yadav, B. P., Siddiqui, N. A., Jain, S., & Nayar, D. V. (2022). Utility damage prevention measures during excavation: a review. *Advances in Construction Safety: Proceedings of HSFEA 2020*, 41-53. https://doi.org/10.1007/978-981-19-4001-9_4.

Yan, J., Jaw, S. W., Van Son, R. J., Soon, K., & Schrotter, G. (2018). Three-dimensional data modelling for underground utility network mapping. *The International Archives of the Photogrammetry, Remote Sensing and Spatial Information Sciences, XLII–4*, pp. 711–715. https://doi.org/10.5194/isprs-archives-xlii-4-711-2018.

Yan, J., Jaw, S., Soon, K., Wieser, A., & Schrotter, G. (2019). Towards an underground utilities 3d data model for land administration. *Remote Sensing, 11*(17), pp. 1957. https://doi.org/10.3390/rs11171957.

Yan, J., Van Son, R., & Soon, K. H. (2021). From underground utility survey to land administration: An underground utility 3D data model. *Land use policy, 102*, 105267. https://doi.org/10.1016/j.landusepol.2020.105267.

Yang, Y., Xu, J., Elkhuizen, W. S., & Song, Y. (2021). The development of a low-cost photogrammetry-based 3D hand scanner. *HardwareX*, 10, e00212. https://doi.org/10.1016/j.ohx.2021.e00212.

Ye, H., Chen, Y., & Li, M. (2019). Tightly coupled 3d lidar inertial odometry and mapping. *ArXiv (Cornell University)*. https://doi.org/10.1109/icra.2019.8793511.

Yeh, C., & Lin, M. (2021). Robust 3D reconstruction using HDR-based SLAM. *IEEE Access, 9*, 16568–16581. https://doi.org/10.1109/access.2021.3051257.

Yılmaztürk, F., Kulur, S., & Terzi, N. (2010). Measurement of deflections in buried flexible pipes by close range digital photogrammetry. *Measurement*, *43*(6), 857–865. https://doi.org/10.1016/j.measurement.2010.03.005.

Youn, H. S., & Chen, C. C. (2002). Automatic GPR target detection and clutter reduction using neural network. *In Ninth International Conference on Ground Penetrating Radar. 4758*, pp. 579-582. https://doi.org/10.1117/12.462229.

Yu, G., Mao, Z., Hu, M., Li, Z., & Sugumaran, V. (2019). BIM+ topology diagram-driven multiutility tunnel emergency response method. *Journal of Computing in Civil Engineering*, 33(6), 04019038. https://doi.org/10.1061/(ASCE)CP.1943-5487.0000851.

Yu, Y., Safari, A., Niu, X., Drinkwater, B. W., & Horoshenkov, K. V. (2021). Acoustic and ultrasonic techniques for defect detection and condition monitoring in water and sewerage pipes: A review. *Applied Acoustics*, *183*, 108282. https://doi.org/10.1016/j.apacoust.2021.108282.

Yuen, R. Z. M., & Boehm, J. (2022). Potential of consumer-grade cameras and photogrammetric guidelines for subsurface utility mapping. *The International Archives of the Photogrammetry, Remote Sensing and Spatial Information*

Sciences, XLVIII-2/W1-2022, pp. 243–250. https://doi.org/10.5194/isprs-archives-xlviii-2-w1-2022-243-2022.

Zanfei. A., Manapace, A., Brentan, B. M., & Righetti, M. (2022). How does missing data imputation affect the forecasting of urban water demand? *Journal of Water Resources Planning and Management,* 148(11). https://doi.org/10.1061/(ASCE)WR.1943-5452.0001624.

Zeng. X & McMechan, A. (1997). GPR characterization of buried tanks and pipes. *Geophysics*, (1997) 62 (3): 797–806. https://doi.org/10.1190/1.1444189.

Zhang, P., Guo, X., Muhammat, N., & Wang, X. (2016). Research on probing and predicting the diameter of an underground pipeline by GPR during an operation period. *Tunnelling and Underground Space Technology, 58,* 99-108. https://doi.org/10.1016/j.tust.2016.04.005.

Zhang, P., Hancock, C. M., Lau, L., Roberts, G. W., & De Ligt, H. (2019a). Low-cost IMU and odometer tightly coupled integration with Robust Kalman filter for underground 3-D pipeline mapping. *Measurement, 137,* pp. 454-463. https://doi.org/10.1016/j.measurement.2019.01.068.

Zhang, W., Hao, T., Chang, Y. H., & Zhao, Y. B. (2017). Time-frequency analysis of enhanced GPR detection of RF tagged buried plastic pipes. *NDT & E International*, *92*, 88–96. https://doi.org/10.1016/j.ndteint.2017.07.013

Zhang, X., Han, L., Robinson, M., & Gallagher, A. (2021). A GANs-based deep learning framework for automatic subsurface object recognition from ground penetrating radar data. *Institute of Electrical and Electronics Engineers (IEEE) Access, 9*, pp. 39009–39018. https://doi.org/10.1109/access.2021.3064205.

Zhang, X., Li, Y., & Wu, D. (2020a). Developing an underground utility occupation index for efficient urban utilities planning. *Journal of Construction Engineering and Management, 146(5)*, 04020036. https://doi.org/10.1061/(ASCE)CO.1943-7862.0001810.

Zhang, X., Zhao, P., Hu, Q., Wang, H., Ai, M., & Li, J. (2019b). A 3D reconstruction pipeline of urban drainage pipes based on multi view image matching using low-cost panoramic video cameras. *Water, 11(10),* 2101. https://doi.org/10.3390/w11102101.

Zhang, Y., Di, X., Zhang, B., & Wang, C. (2020b). Self-supervised image enhancement network: training with low light images only. *ArXiv (Cornell University)*. http://arxiv.org/pdf/2002.11300.pdf.

Zhao, S., & Al-Qadi, I. L. (2017). Pavement drainage pipe condition assessment by GPR image reconstruction using FDTD modeling. *Construction and Building Materials*, *154*, 1283–1293. https://doi.org/10.1016/j.conbuildmat.2017.06.103.

Zheng, J., Peng, S. P., & Yang, F. (2014). A novel edge detection for buried target extraction after SVD-2D wavelet processing. *Journal of Applied Geophysics, 106,* pp. 106–113. https://doi.org/10.1016/j.jappgeo.2014.04.016.

Zhou, X., H. Chen & J. Li. (2018). An automatic GPR B-scan image interpreting model. *In IEEE Transactions on Geoscience and Remote Sensing*, 56(6), 3398-3412. https://doi.org/10.1109/TGRS.2018.2799586.

Zhou, X., Chen, Q., Lyu, S., & Chen, H. (2022). Mapping the buried cable by ground penetrating radar and gaussian-process regression. *IEEE Transactions on Geoscience and Remote Sensing*, 60, 1-12. https://doi.org/10.1109/TGRS.2022.3181380.

Zhou, X., Wang, D., & Krähenbühl, P. (2019). Objects as points. *ArXiv: Computer Vision and Pattern Recognition*. https://arxiv.org/pdf/1904.07850.pdf.

Zhu, S., Zhang, R., Zhou, L., Shen, T., Fang, T., Tan, P., & Quan, L. (2018). Very large-scale global SFM by distributed motion averaging. *Computer Vision and Pattern Recognition*. https://doi.org/10.1109/cvpr.2018.00480.

Zollhöfer, M., Stotko, P., Görlitz, A., Theobalt, C., Nießner, M., Klein, R., & Kolb, A. (2018). State of the art on 3d reconstruction with RGB-D cameras. *Computer Graphics Forum*, *37*(2), pp. 625–652. https://doi.org/10.1111/cgf.13386.

Zong, Z., Chen, C., Mi, X., Sun, W., Song, Y., Li, J., ... & Yang, B. (2019). A deep learning approach for urban underground objects detection from vehicle-borne ground penetrating radar data in real-time. *The International Archives of Photogrammetry, Remote Sensing and Spatial Information Sciences*, 42, 293-299. https://doi.org/10.5194/isprs-archives-XLII-2-W16-293-2019.

Appendix

Appendix 1 List of publications

A. Journal paper (* corresponding author)

1. **Su, Y.,** Wang, J*., Li, D., Wang, X., Hu, L., Yao, Y., & Kang, Y. (2023). End-to-end deep learning model for underground utilities localization using GPR. Automation in Construction, 149, 104776.
2. **Su, Y.,** Wang, J*., Wang, X., Hu, L., Yao, Y., Shou, W., & Li, D. (2023). Zero-reference deep learning for low-light image enhancement of underground utilities 3D reconstruction. Automation in Construction, 152, 104930.
3. **Su, Y.,** Wang, J*., Wang, X., Yao, Y., & Shou, W. (2023). 3D reconstruction in underground utilities. Automation in Construction, 156, 105100.
4. **Yang Su,** Jun Wang*, Peng Wu, Chengke Wu, Aobo Yue, Wenchi Shou. (2023). Automatic Completion of Underground Utility Topologies Using Graph Convolutional Networks. Journal of Computing in Civil Engineering. (Under Review)

B. Conference paper (* corresponding author)

1. **Yang, SU.,** Qian, Jia., Yuan Yao., Jun Wang*. (2022). A review of GPR application on underground utilities: limitations and the best performance. World Building Conference 2022 (Melbourne, Australia).

C. Attribution Statement

	Conception and Design	Acquisition of Data and Method	Data Conditioning and Manipulation	Analysis and Statistical Method	Interpretation and Discussion
Paper 1: End-to-end deep learning model for underground utilities localization using GPR. Automation in Construction, 149, 104776.					
Co-Author 1: Yang Su	70%	70%	80%	70%	60%
Co-Author 1 Acknowledgment: I acknowledge that these represent my contribution to the above research output and I have approved the final version. Signed:					
Co-Author 2:	20%	10%	0%	10%	10%

Jun Wang					
Co-Author 2 Acknowledgment: I acknowledge that these represent my contribution to the above research output and I have approved the final version. Signed:					
Co-Author 3: Danqi Li	10%	0%	0%	10%	10%
Co-Author 3 Acknowledgment: I acknowledge that these represent my contribution to the above research output and I have approved the final version. Signed:					
Co-Author 4: Xiangyu Wang	0%	0%	0%	0%	10%
Co-Author 4 Acknowledgment: I acknowledge that these represent my contribution to the above research output and I have approved the final version. Signed:					
Co-Author 5: Lei Hu	0%	10%	0%	10%	0%
Co-Author 1 Acknowledgment: I acknowledge that these represent my contribution to the above research output and I have approved the final version. Signed:					
Co-Author 6: Yuan Yao	0%	0%	0%	0%	10%
Co-Author 6 Acknowledgment: I acknowledge that these represent my contribution to the above research output and I have approved the final version. Signed:					
Co-Author 7: Yuanxin Kang	0%	10%	20%	0%	0%
Co-Author 7 Acknowledgment: I acknowledge that these represent my contribution to the above research output and I have approved the final version. Signed:					
Paper 2: Zero-reference deep learning for low-light image enhancement of underground utilities 3D reconstruction. Automation in Construction, 152, 104930.					
Co-Author 1: Yang Su	70%	70%	70%	70%	70%
Co-Author 1 Acknowledgment: I acknowledge that these represent my contribution to the above research output and I have approved the final version.					

Signed:					
Co-Author 2: Jun Wang	20%	0%	0%	20%	20%
Co-Author 2 Acknowledgment: I acknowledge that these represent my contribution to the above research output and I have approved the final version. Signed:					
Co-Author 3: Xiangyu Wang	0%	10%	0%	0%	0%
Co-Author 3 Acknowledgment: I acknowledge that these represent my contribution to the above research output and I have approved the final version. Signed:					
Co-Author 4: Lei Hu	0%	10%	10%	0%	0%
Co-Author 4 Acknowledgment: I acknowledge that these represent my contribution to the above research output and I have approved the final version. Signed:					
Co-Author 5: Yuan Yao	0%	10%	0%	10%	0%
Co-Author 5 Acknowledgment: I acknowledge that these represent my contribution to the above research output and I have approved the final version. Signed:					
Co-Author 6: Wenchi Shou	0%	0%	10%	0%	10%
Co-Author 6 Acknowledgment: I acknowledge that these represent my contribution to the above research output and I have approved the final version. Signed:					
Co-Author 7: Danqi Li	10%	0%	10%	0%	0%
Co-Author 7 Acknowledgment: I acknowledge that these represent my contribution to the above research output and I have approved the final version. Signed:					
Paper 3: 3D reconstruction in underground utilities. Automation in Construction, 156, 105100.					
Co-Author 1: Yang Su	80%	80%	70%	80%	70%
Co-Author 1 Acknowledgment:					

I acknowledge that these represent my contribution to the above research output and I have approved the final version. Signed:					
Co-Author 2: Jun Wang	20%	0%	10%	10%	10%
Co-Author 2 Acknowledgment: I acknowledge that these represent my contribution to the above research output and I have approved the final version. Signed:					
Co-Author 3: Xiangyu Wang	0%	0%	10%	0%	10%
Co-Author 3 Acknowledgment: I acknowledge that these represent my contribution to the above research output and I have approved the final version. Signed:					
Co-Author 4: Yuan Yao	0%	10%	10%	10%	0%
Co-Author 4 Acknowledgment: I acknowledge that these represent my contribution to the above research output and I have approved the final version. Signed:					
Co-Author 5: Wenchi Shou	0%	10%	0%	0%	10%
Co-Author 5 Acknowledgment: I acknowledge that these represent my contribution to the above research output and I have approved the final version. Signed:					
Paper 4: Automatic Completion of Underground Utility Topologies Using Graph Convolutional Networks. Journal of Computing in Civil Engineering. (Under Review)					
Co-Author 1: Yang Su	80%	70%	80%	70%	70%
Co-Author 1 Acknowledgment: I acknowledge that these represent my contribution to the above research output and I have approved the final version. Signed:					
Co-Author 2: Jun Wang	20%	0%	0%	20%	10%
Co-Author 2 Acknowledgment: I acknowledge that these represent my contribution to the above research output and I have approved the final version. Signed:					
Co-Author 3:	0%	0%	0%	10%	10%

Peng Wu					
Co-Author 3 Acknowledgment: I acknowledge that these represent my contribution to the above research output and I have approved the final version. Signed:					
Co-Author 4: Chengke Wu	0%	20%	10%	0%	0%
Co-Author 4 Acknowledgment: I acknowledge that these represent my contribution to the above research output and I have approved the final version. Signed:					
Co-Author 5: Aobo Yue	0%	10%	10%	0%	0%
Co-Author 5 Acknowledgment: I acknowledge that these represent my contribution to the above research output and I have approved the final version. Signed:					
Co-Author 6: Wenchi Shou	0%	0%	0%	0%	10%
Co-Author 6 Acknowledgment: I acknowledge that these represent my contribution to the above research output and I have approved the final version. Signed:					
Paper 5:					
Co-Author 1: Yang Su	80%	80%	70%	80%	70%
Co-Author 1 Acknowledgment: I acknowledge that these represent my contribution to the above research output and I have approved the final version. Signed:					
Co-Author 2: Qian Jia	10%	20%	20%	10%	10%
Co-Author 2 Acknowledgment: I acknowledge that these represent my contribution to the above research output and I have approved the final version. Signed:					
Co-Author 3: Yuan Yao	0%	0%	10%	0%	10%
Co-Author 3 Acknowledgment: I acknowledge that these represent my contribution to the above research output and I have approved the final version. Signed:					

Co-Author 4: Jun Wang	10%	0%	0%	10%	10%
Co-Author 4 Acknowledgment: I acknowledge that these represent my contribution to the above research output and I have approved the final version. Signed:					